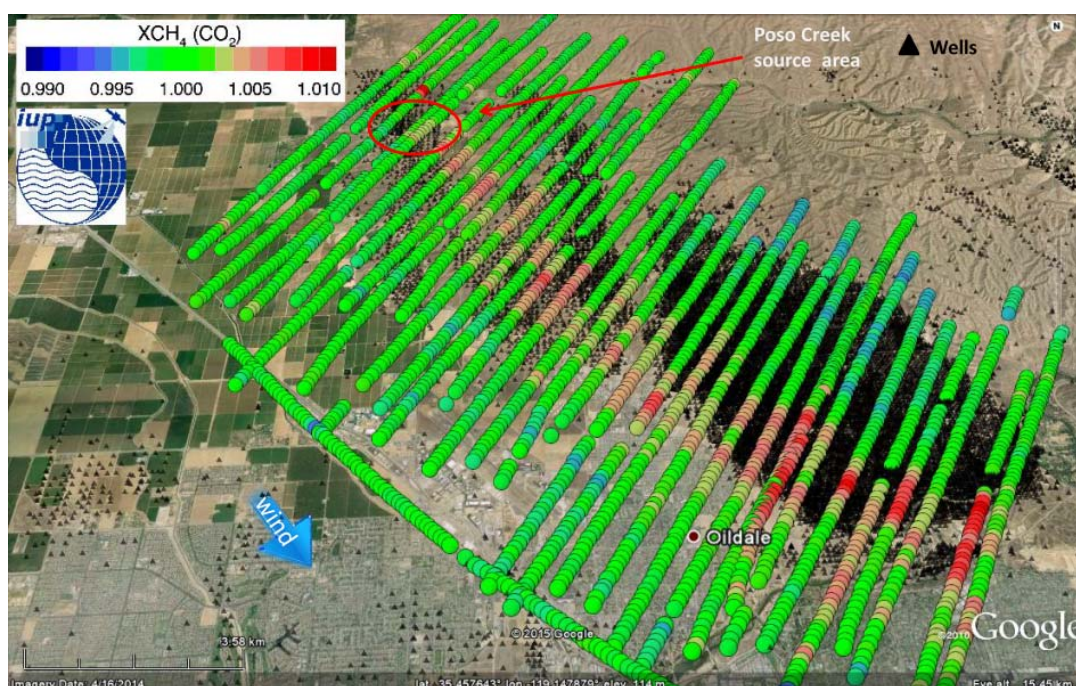
	<p style="text-align: center;"><b>COMEX</b> <b>Final Report</b></p>	<p style="text-align: right;">Version: 2.0 Doc ID: IUP-COMEX-FR Date: 3. July 2016</p>
--	---	--

# COMEX - Final Report

ESA Study

“Scientific and Technical Assistance for the Deployment of a flexible airborne spectrometer system during C-MAPEX and COMEX”

ESTEC Contract No. 4000106993/12/NL/FF/If, CCN#1 (COMEX)



Authors: S. Krautwurst, K. Gerilowski, T. Krings, J. Borchard, H. Bovensmann


Contact: [Heinrich.Bovensmann@iup.physik.uni-bremen.de](mailto:Heinrich.Bovensmann@iup.physik.uni-bremen.de)




Institute of Environmental Physics (IUP), Bremen, Germany

**With contributions from:**

I. Leifer, Bubbleology Research International  
M. Fladeland, R. Kolyer, L. Iraci, B. Luna NASA Ames Research Center  
D. R. Thompson, M. Eastwood, R. Green, Jet Propulsion Laboratory, California Institute of Technology  
H. Jonsson, Center for Interdisciplinary Remotely-Piloted Aircraft Studies  
S. A. Vigil, California Polytechnic State University  
D. Tratt, Aerospace Corporation


	<p><b>COMEX</b></p> <p><b>Final Report</b></p>	<p>Version: 2.0</p> <p>Doc ID: IUP-COMEX-FR</p> <p>Date: 3. July 2016</p>
---	--	---

	<p style="text-align: center;"><b>COMEX</b> <b>Final Report</b></p>	<p style="text-align: right;">Version: 2.0 Doc ID: IUP-COMEX-FR Date: 3. July 2016</p>
--	---	--

## Change log

Version	Date	Status	Authors	Reason for change
Draft 0.0	10.06.2014	To Team	H. Bovensmann	template internal version
Draft 1.0	18.12.2015	To Team	See cover page	Internal review
1.0	02.02.2016	To ESA	See cover page	To ESA
1.9	25.5.2016	Internal review	See cover page	ESA comments and internal review
2.0 draft	3.6.2016	To ESA	See cover page	Comments from internal review
2.0	3.7.2016	To ESA	See cover page	


Important Note: All emission estimates given in this report are preliminary (and may change when further refining the analysis) and for the purpose to demonstrate adequate data quality only. They should not be published or cited without written agreement by the author of the study.

	<b>COMEX</b> <b>Final Report</b>	Version: 2.0 Doc ID: IUP-COMEX-FR Date: 3. July 2016
---	-------------------------------------	--




## Table of Contents

1.	Purpose of Document.....	9
2.	Introduction .....	10
3.	The COMEX campaign objectives and campaign set-up .....	11
4.	Description of main campaign instrumentation.....	13
4.1.	Methane Airborne MAPper (MAMAP) (CIRPAS TO).....	15
4.2.	CIRPAS atmospheric measurements suite (CIRPAS TO) .....	17
4.3.	PICARRO GHG Sensor (CIRPAS TO) .....	18
4.4.	LGR CO2 isotope analyzer (CIRPAS TO) .....	19
4.5.	AVIRIS-C (ER-2) and AVIRIS-NG (TOI).....	19
4.6.	Mako Thermal Infrared Hyperspectral Imaging Spectrometer (TO) .....	22
4.7.	PICARRO GHG sensor (Alpha Jet) .....	24
4.8.	LOS GATOS ICOS Instruments (AMOG Surveyor) .....	25
5.	Summary of campaign as performed .....	27
6.	Examples of Collected Data .....	35
6.1.	Quick look processing.....	36
7.	Processing of campaign data .....	42
7.1.	The MAMAP remote sensing data.....	42
7.1.1.	The MAMAP retrieval algorithm in general .....	42
7.1.2.	The MAMAP retrieval algorithm for the COMEX data set .....	44
7.2.	The CIRPAS in-situ data set.....	47
7.3.	The Picarro in-situ data set.....	49
8.	Data formats and data archive .....	50
8.1.	Data Format MAMAP .....	50
8.2.	Data Format In-situ.....	51
8.3.	Description of Data Archive.....	51
9.	Examples on emissions estimated from COMEX campaign data .....	52
9.1.	Approach .....	52
9.1.1.	The MAMAP remote sensing data.....	52
9.1.2.	The Picarro in-situ data .....	54
9.2.	Example 1: Landfill Olinda Alpha.....	55
9.2.1.	The MAMAP remote sensing data.....	55
9.2.2.	The Picarro in-situ data .....	59

	<p style="text-align: center;"><b>COMEX</b> <b>Final Report</b></p>	<p style="text-align: right;">Version: 2.0 Doc ID: IUP-COMEX-FR Date: 3. July 2016</p>
---	---	--

9.2.3.	Investigation of co-emitted CO <sub>2</sub> induced error on the MAMAP retrieval XCH <sub>4</sub> (CO <sub>2</sub> ) proxy approach for the Olinda Alpha Landfill.....	62
9.3.	Example 2: Poso Creek, Kern River and Kern Front Oil Fields .....	64
9.3.1.	The MAMAP remote sensing data.....	65
9.3.2.	The Picarro in-situ data .....	70
9.3.3.	Investigation and justification of the MAMAP XCH <sub>4</sub> (CO <sub>2</sub> ) proxy retrieval assumption over the Kern Oil Fields.....	74
9.4.	Comparison of MAMAP XCH <sub>4</sub> data with AVIRS-NG methane anomaly maps acquired over Kern River, Kern Front and Poso Creek Oil Fields .....	76
10.	Analysis of Glint data over the Santa Barbara Seeps .....	79
10.1.1.	Coal Oil Point 2014-06-04.....	80
10.1.2.	Coal Oil Point 2014-08-25.....	83
11.	Spatial and spectral tradeoffs and extrapolation to satellite scales .....	87
11.1.1.	Sensitivity comparison between medium and low spectral resolution data .....	87
11.1.2.	Extrapolation of AVIRIS-NG data to HypsIRI and EnMAP satellite scales.....	89
11.1.3.	Extrapolation of MAMAP data to CarbonSat, Sentinel 5p and GOSAT satellite scales .	92
12.	Recommendations and Lessons Learned .....	94
12.1.	Future analysis of the campaign data set.....	94
12.2.	Lessons learned from campaign preparation and execution .....	94
13.	Summary .....	96
14.	References .....	99
Annex 1: Overview of targets.....		102
Annex 2: COMEX Flight Documentation (day-by-day) .....		105

	<p style="text-align: center;"><b>COMEX</b> <b>Final Report</b></p>	<p style="text-align: right;">Version: 2.0 Doc ID: IUP-COMEX-FR Date: 3. July 2016</p>
--	---	--

### Applicable Documents


Id.	Title
AD-1	Technical Assistance for the Deployment of a flexible airborne spectrometer system during COMEX, Statement of Work , Change Request No. for Contract Change Notice No. 1 on Contract No. 4000107496/12/NL/FF/If, ref. PFL-PSO/FF/vb/13.777, 10. Oct. 2013
AD-2	Technical Assistance for the Deployment of a flexible airborne spectrometer system during COMEX, Proposal version 2, dated 18.12.2013
AD-3	Technical Assistance for the Deployment of a flexible airborne spectrometer system during COMEX, Clarification Points dated 18.12.2013
AD-4	Letter agreement of NASA with University of Bremen, final signed 13. May 2014
AD-5	Ira Leifer, Konstantin Gerilowski, Thomas Krings, John Burrows, Chuanmin Hu, Heinrich Bovensmann, Michael Buchwitz, Robert Green, Laura Iraci, Matthew Fladeland, Liane Guild; An ESA/NASA Collaborative Remote Sensing Study in Support of Future Greenhouse Gas Satellite Missions: HyspIRI and CarbonSAT, revised proposal to NASA, dated 25 May 2013.
AD-6	NASA Grant Number NNX13AM07G with Dr. Ira Leifer, Bubbleology Research International, dated 11. Sept. 2013.
AD-7	CarbonSat Mission Requirement Document v1.2

### Reference Documents

Id.	Reference
RD-1	Gerilowski, K., A. Tretner, T. Krings, M. Buchwitz, P. P. Bertagnolio, F. Belemmezov, J. Erzinger, J. P. Burrows, and H. Bovensmann, MAMAP – a new spectrometer system for column-averaged methane and carbon dioxide observations from aircraft: instrument description and performance analysis, Atmos. Meas. Tech., 4, 215-243, 2011.
RD-2	Krings, T., Gerilowski, K., Buchwitz, M., Reuter, M., Tretner, A., Erzinger, J., Heinze, D., Pflüger, U., Burrows, J. P., and Bovensmann, H.: MAMAP – a new spectrometer system for column-averaged methane and carbon dioxide observations from aircraft: retrieval algorithm and first inversions for point source emission rates, Atmos. Meas. Tech., 4, 1735-1758, doi:10.5194/amt-4-1735-2011, 2011.
RD-3	Bovensmann, H., Buchwitz, M., Burrows, J. P., Reuter, M., Krings, T., Gerilowski, K., Schneising, O., Heymann, J., Tretner, A., and Erzinger, J.: A remote sensing technique for global monitoring of power plant CO <sub>2</sub> emissions from space and related applications, Atmos. Meas. Tech., 3, 781-811, 2010.
RD-4	COMEX Campaign Implementation Plan, University of Bremen, Version 2, August 2014
RD-5	Krings, T., K. Gerilowski, M. Buchwitz, J. Hartmann, T. Sachs, J. Erzinger, J. P. Burrows, H. Bovensmann, Quantification of methane emission rates from coal mine ventilation shafts using airborne remote sensing data, Atmos. Meas. Tech., 6, 151–166, 2013.
RD-6	Gerilowski, K., Krings, T., Hartmann, J., Buchwitz, M., Sachs, T., Erzinger, J., Burrows, J.P.; Bovensmann, H.; Methane Remote Sensing Constraints on direct Sea-Air Flux from the 22/4b North Sea Massive Blowout Bubble Plume, Journal of Marine and Petroleum Geology, Volume 68, Part B, December 2015, Pages 824–835, 2015, doi:10.1016/j.marpetgeo.2015.07.011
RD-7	C-MAPExp Data Acquisition Report, University of Bremen, 2013
RD-8	C-MAPExp Final Report, University of Bremen, July 2014
RD-9	COMEX Data Acquisition Report, University of Bremen, Version 1.1, June 2015

### List of acronyms

Acronym	Meaning
AJAX	Alpha Jet Atmospheric eXperiment
AOD	Aerosol Optical Depth
ARC	Ames Research Center
AVIRIS-C	Airborne Visible InfraRed Imaging Spectrometer Classic
AVIRIS-NG	Airborne Visible InfraRed Imaging Spectrometer Next Generation
ATC	Air Traffic Control
BESD	Bremen optimal ESTimation DOAS
CarbonSat	Carbon Monitoring Satellite
CIRPAS	Center for Interdisciplinary Remotely-Piloted Aircraft Studies
DOAS	Differential Optical Absorption Spectroscopy
DWD	Deutscher Wetterdienst
EnMAP	Environmental Mapping and Analysis Program
ENVISAT	Environmental Satellite
ESA	European Space Agency
FLEX	Fluorescence Explorer
GHG	Greenhouse Gas
GRG	Global Reactive Gases
HSI	Hyperspectral Imaging
HyspIRY	Hyperspectral Infrared Imager
GOSAT	Greenhouse Gases Observing Satellite
IGBP	International Geosphere–Biosphere Programme
IUP-UB	Institute of Environmental Physics (Institut für Umweltphysik), University of Bremen, Germany
LFG	LandFill Gas
LGR	Los Gatos Research
MAMAP	Methane Airborne MAPper
mamsl	meters above mean sea level
MRD	Mission Requirements Document
NASA	National Aeronautics and Space Administration
NIR	Near Infrared
RMSE	Root Mean Square Error
SCIAMACHY	Scanning Imaging Absorption Spectrometers for Atmospheric Chartography
SJV	San Joaquin Valley
SNR	Signal to Noise Ratio
SWIR	Short Wave Infrared
SZA	Solar Zenith Angle
TBC	To Be Clarified
TIR	Thermal Infrared
TO	Twin Otter
TOA	Top of atmosphere
TOI	Twin Otter International
VIS	Visible

	<p style="text-align: center;"><b>COMEX</b> <b>Final Report</b></p>	<p style="text-align: right;">Version: 2.0 Doc ID: IUP-COMEX-FR Date: 3. July 2016</p>
--	---	--

## 1. Purpose of Document

This final report describes the COMEX campaign executed between May and September 2014 around Los Angeles, its data processing and quality, a description of the generated data set, preliminary results for selected targets and a summary of the overall achievements.


The document is structured as follows:

In chapter 2 the overall context of the COMEX campaign and its linkage to the CarbonSat mission is described. Chapter 3 summarises the main campaign objectives and provides an overview of the overall campaign set-up. Chapter 4 gives a description of the instrumentation as used in the campaign. In chapter 5 it is summarised how the campaign was performed, which targets were flown, which data set was collected. Examples of the collected data are given in chapter 6.

Chapter 7 contains background information about how the campaign data is processed and chapter 8 gives a summary on the campaign data format and data archive.

Chapter 9 contains the initial analysis of the campaign data to demonstrate that data quality is sufficient to derive emissions from the remote sensing data over land. Chapter 10 contains the analysis of glint data over the Santa Barbara seeps and chapter 11 investigates spatial and spectral trade-offs and evaluates the campaign data on the scales of the CarbonSat mission.

The report closes with recommendations and lessons learned (Chapter 12) and an overall summary (Chapter 13).

	<p style="text-align: center;"><b>COMEX</b> <b>Final Report</b></p>	<p style="text-align: right;">Version: 2.0 Doc ID: IUP-COMEX-FR Date: 3. July 2016</p>
---	---	--

## 2. Introduction

The COMEX campaign supports the mission definition of CarbonSat and HypsIRI by providing representative airborne remote sensing data - MAMAP for CarbonSat; the Airborne Visible InfraRed Imaging Spectrometer (Classic & Next Generation) AVIRIS-C/AVIRIS-NG for HypsIRI - as well as ground-based and airborne in-situ data.

The objectives of the COMEX campaign activities are (see Campaign Implementation Plan (RD-4)):

1. Investigate spatial/spectral resolution trade-offs for CH<sub>4</sub> anomaly detection and flux inversion by comparison of MAMAP-derived emission estimates with AVIRIS/AVIRIS-NG derived data.
2. Evaluate sun-glint observation geometry on CH<sub>4</sub> retrievals for marine sources.
3. Characterize the effect of Surface Spectral Reflectance (SSR) heterogeneity on trace gas retrievals of CO<sub>2</sub> and CH<sub>4</sub> for medium and low-resolution spectrometry.
4. Identify benefits from joint SWIR/TIR data for trace gas detection and retrieval by comparison of MAMAP and AVIRIS/AVIRIS-NG NIR/SWIR data with MAKO TIR data.

The ability to derive emission source strength for a range of strong emitting targets by remote sensing will be evaluated from combined AVIRIS-NG and MAMAP data, adding significant value to the HypsIRI-campaign AVIRIS-NG dataset. The data will be used to quantify anomalies in atmospheric CO<sub>2</sub> and CH<sub>4</sub> from strong local greenhouse gas sources e.g. localized industrial complexes, landfills, etc. and to derive CO<sub>2</sub> and CH<sub>4</sub> emissions estimates from atmospheric gradient measurements.

The original campaign concept was developed by University of Bremen and BRI [AD-05]. The COMEX campaign is funded bilaterally by NASA and ESA. Whereas NASA funds the US part of the project via a contract with Ira Leifer, BRI, [AD-06], the contribution of MAMAP to the COMEX campaign is funded by ESA within the COMEX-E project and NASA w.r.t. a 50% contribution to the flight related costs of flying MAMAP on an US aircraft [AD04].

The Data Acquisition Report (RD-9) describes the instrumentation used, the measurements made by the team during the COMEX campaign in May/June 2014 and August/September 2014 in California, and an initial assessment of the data quality.

### 3. The COMEX campaign objectives and campaign set-up

To address the campaign objective as outlined in chapter 2 above, a set of remote sensing and in-situ data was collected over suitable source areas. The linkage of the campaign objectives with measurement needs, data sets and campaign instrumentation is given in *Figure 1*. The objectives were addressed by a unique combination of VIS/NIR/SWIR hyperspectral remote sensing airborne instrumentation (AVIRIS-C, AVIRIS-NG), TIR hyperspectral remote sensing airborne instrumentation (Mako), NIR/SWIR spectroscopic remote sensing airborne instrumentation (MAMAP) as well as in-situ airborne (Picarro / CIRPAS-Twin Otter & AJAX ) and ground based (Los Gatos / AMOG) measurements for validation and interpretation support. AVIRIS was flown on the NASA ER-2 regularly in 2014 covering large, dedicated flight boxes containing relevant and important terrestrial targets and also off-shore targets in the California target area. COMEX made use of the already planned and funded ER-2 flight with AVIRIS-C.

Campaign Objective	Measurement Needs	Data Sets	Instrument Perform.	Functional Requirements
1. Spatial and spectral resolution tradeoffs and synergies for CH <sub>4</sub> and CO <sub>2</sub> anomaly detection and flux inversion in the context of upcoming hyperspectral (HYPSPRI) and GHG missions (CarbonSat)	From aircraft, obtain measurements of radiances in the NIR and SWIR over land in regions with large sources of CH <sub>4</sub> (CO <sub>2</sub> ) from an imaging spectrometer (high spatial resolution, low spectral resolution) and atmospheric sounding spectrometers (lower spatial resolution, high spectral resolution).	Derived XCH <sub>4</sub> (or XCO <sub>2</sub> ) fields over land from high spectral resolution data and hyperspectral data (CH <sub>4</sub> , CO <sub>2</sub> anomalies) in areas of emission hot spots.  Airborne in-situ trace gases and meteorology parameters. Ground-based in-situ to identify hot spots.	For All goals: Hyperspectral Imager AVIRIS-C on ER-2: 700-2100 nm 20 nm spectral resolution 20 m ground spatial resolution (GSR) Swath: 10 km  For All goals alternative: Hyperspectral Imager AVIRIS-NG on TO: 700-2100 nm 10 nm spectral resolution < 5 m ground spatial resolution (GSR) Swath: < 5 km	All aircraft RS instruments (AVIRIS-C/AVIRIS-NG and MAMAP): Measurements under clear skies (<10% cloud cover).  ALL: In-situ wind field, trace gases and aerosol to support data interpretation
2. Quantify CH <sub>4</sub> (or CO <sub>2</sub> ) emissions over ocean using sun glint mode.	From aircraft, obtain high spectral resolution glint measurements in the NIR-SWIR over ocean areas with high CH <sub>4</sub> (CO <sub>2</sub> ) emissions, complemented by hyperspectral measurements (ideally also under glint conditions).	Derived XCH <sub>4</sub> (or XCO <sub>2</sub> ) fields over ocean in glint mode from high spectral resolution data and hyperspectral data.	For All goals: Atmospheric Sounder MAMAP 750-800 nm 1590-1690 nm 0.5-0.8 nm spectral resolution ~50 m ground spatial resolution (GSR) Swath: 50 m (SWIR) Gyro gimbal for glint	AVIRIS-C/AVIRIS-NG and MAMAP: coordinated data acquisition under similar sun elev. angle.
3. Quantify impact of surface spectral reflectance non-uniformity on trace gas retrievals.	From aircraft, obtain simultaneous measurements of radiance from AVIRIS-C/AVIRIS-NG and MAMAP over areas with surface spectral reflectance non-uniformities.	Derived XCH <sub>4</sub> (or XCO <sub>2</sub> ) fields over land from high spectral resolution data and hyperspectral surface reflectance data in areas of emission hot spots and  Airborne in-situ trace gases and meteorology parameters. Ground-based in-situ to identify hot spots.	Airborne in-situ wind, CO <sub>2</sub> , CH <sub>4</sub> , aerosol - on CIRPAS TO - on Alphalet  Airborne TIR sounder	MAMAP instruments: Measurements in glint geometry over ocean under clear skies (<10% cloud cover). Hyperspectral Instruments: Measurements in swath mode (ideally covering glint over ocean) under clear skies (<10% cloud cover).
4. Provide data to investigate SWIR-TIR synergies.	From aircraft, obtain simultaneous radiance measurements with AVIRIS-C/AVIRIS-NG, MAMAP, TIR over land in areas with strong sources.	Derived XCH <sub>4</sub> (or XCO <sub>2</sub> ) fields over land from high spectral resolution data, hyperspectral and TIR data in areas of emission hot spots.		AVIRIS-C/AVIRIS-NG and MAMAP and TIR: coordinated data acquisition under similar sun elev. angle.
<div style="display: flex; justify-content: space-around; align-items: center;"> <div style="border: 1px solid black; padding: 2px; text-align: center;">Aircraft</div> </div>				
<div style="display: flex; justify-content: space-around; align-items: center;"> <div style="border: 1px solid black; padding: 2px; text-align: center;">On-ground</div> </div>				
	Collect pre-survey and ground truth data.	Concentrations of CH <sub>4</sub> , CO <sub>2</sub> etc., surface winds	Airborne in-situ wind, CO <sub>2</sub> , CH <sub>4</sub> , aerosol etc. by car	In-situ trace gases on-ground for survey and limited ground truth


*Figure 1: COMEX experiment traceability table. The table is linking the campaign objectives with the data needs and the sensors for deployment.*

The experiments on the different platforms are described in chapter 4.

The main focus ESA's contribution to the COMEX campaign was to deploy MAMAP in the US, to perform the campaign coordinated with US activities and to perform limited data analysis to demonstrate that the generated data set is fit for purpose and present examples how the overall goals can be reached.


As the TIR-SWIR is not directly relevant for CarbonSat and the TIR-SWIR synergy is an add-on to COMEX from US perspective, no data analysis at IUP side was planned within this project. Comparison with AVIRIS-NG/C trace gas indicator products will be performed only for targets, where the according AVIRIS data products data has been provided to IUP by the US-teams.



	<p style="text-align: center;"><b>COMEX</b> <b>Final Report</b></p>	<p style="text-align: right;">Version: 2.0 Doc ID: IUP-COMEX-FR Date: 3. July 2016</p>
--	---	--

Results from the campaign will help to support the justification of CarbonSat spectral and spatial resolution trade-offs, will deliver glint data relevant for CarbonSat glint algorithms development, will allow to scale campaign data to the CarbonSat spatial scale for investigations on intra-pixel heterogeneity, will allow to investigate assumptions and limitations of the XCH<sub>4</sub> proxy approach and will provide show-case data for CarbonSat application on small scales.

Details of the campaign implementation are documented in the COMEX campaign implementation plan [RD-4].


	<p style="text-align: center;"><b>COMEX</b></p> <p style="text-align: center;"><b>Final Report</b></p>	<p style="text-align: right;">Version: 2.0 Doc ID: IUP-COMEX-FR Date: 3. July 2016</p>
---	--	--

## 4. Description of main campaign instrumentation

The NASA funded HypsIRI airborne campaign collected vast amounts of AVIRIS (Airborne Visible InfraRed Imaging Spectrometer) data while flying on NASA ER-2 data over California, including many strong CH<sub>4</sub> source areas. COMEX added to the planned HypsIRI campaign CH<sub>4</sub> and CO<sub>2</sub> specific data capabilities:

- The European airborne **MAMAP** (Methane Airborne MAPper) sensor on-board the CIRPAS Twin Otter measured XCH<sub>4</sub> and XCO<sub>2</sub> which can then be inverted to estimate plume source strength and serves as a demonstrator for the ESA Earth Explorer Candidate Mission, CarbonSat. MAMAP was flown on the CIRPAS Twin Otter together with a **Picarro GHG sensor**, a **Los Gatos isotope analyser** and an **atmospheric measurement suite**, including temperature, aerosol, and wind/turbulence measurements to support and validate inversion calculations and provide vertical profile measurements to characterize the boundary layer (height and stability).
- Coordinated flights with **AVIRIS-NG** installed on second Twin Otter were flown over some targets to characterise different source areas and provide high resolution but lower sensitivity CH<sub>4</sub> anomaly maps.
- Under flights below ER-2 with **AVIRIS-C** on-board were performed whenever possible providing lower spatial and spectral resolution CH<sub>4</sub> anomaly maps compared to AVIRIS-NG.
- Alpha Jet (NASA AMES) supported a **Picarro GHG sensor** and was tasked for repeat GHG measurements in California and Nevada. In-situ data that were collected including measurements of CO<sub>2</sub>, CH<sub>4</sub>, and H<sub>2</sub>O at 2Hz or CH<sub>4</sub> and H<sub>2</sub>O at 10Hz with a strategy of characterizing the larger atmospheric structure – marine air, interior air, and vertical profiles to at least 5000 m.
- Ground surface and lower atmosphere validation data was collected using **AMOG Surveyor**, an AutoMObile greenhouse Gas system. AMOG integrated for realtime visualization to AMOG operators at up to highway speeds, winds, meteorology, and three **Los Gatos ICOS instruments** that measured CO<sub>2</sub>, CH<sub>4</sub>, CO<sub>2</sub>, NO<sub>2</sub>, NH<sub>3</sub>, H<sub>2</sub>O, and O<sub>3</sub> at 5 Hz. In addition pre-screening data was collected with the 12-m MACLab vehicle, containing an analytic chemistry laboratory and habitation module. The laboratory has four gas chromatographs for measurements of n-alkanes (C<sub>2</sub>-C<sub>8</sub>), alkanes, alkenes, and alkynes, BTEX, NO<sub>x</sub>, etc., at ambient background levels and a Los Gatos Research ICOS instrument for GHG measurements. MACLab is described in below.
- Aerospace Corp. provided **MAKO TIR** (thermal infrared) imaging spectrometry data to find TIR/SWIR synergies. MAKO (Aerospace, Corp.) is a TIR HSI (hyperspectral imaging) spectrometer that flew on a third Twin Otter over some of the target areas with a time-delay of some weeks (*at no cost to the COMEX project*) to collect high spatial and spectral resolution TIR HSI data.


Table 1 gives an overview about which instrument contributed with which geophysical parameter.

	<b>COMEX</b> <b>Final Report</b>	Version: 2.0 Doc ID: IUP-COMEX-FR Date: 3. July 2016
--	-------------------------------------	--

Instrument	Platform	Type	Measured Parameters
CIRPAS atmospheric measurement suite	CIRPAS TO	In-situ airborne	location (lat, lon, alt)   ground velocity (speed, direction)   attitude (pitch, roll, heading)
			Temperature   dew point temperature   static and total pressure   wind speed and wind direction   aerosol   humidity
PICARRO GHG sensor	CIRPAS TO	In-situ airborne	dry CO <sub>2</sub>   dry CH <sub>4</sub>   and H <sub>2</sub> O
LOS GATOS CO <sub>2</sub> isotope analyser	CIRPAS TO	In-situ airborne	CO <sub>2</sub>   d <sup>13</sup> C, d <sup>18</sup> O, d <sup>17</sup> O from CO <sub>2</sub>
MAMAP	CIRPAS TO	Remote sensing airborne (NIR/SWIR)	XCH <sub>4</sub> (CO <sub>2</sub> )   XCO <sub>2</sub> (CH <sub>4</sub> )   [XCH <sub>4</sub> (O <sub>2</sub> )   XCO <sub>2</sub> (O <sub>2</sub> )]
AVIRIS-C	ER-2	HSI VIS/NIR/SWIR	Reflectance spectra   Methane flag: yes or no – TBC
AVIRIS-NG	TOI	HSI VIS/NIR/SWIR	Reflectance spectra   Methane flag: yes or no
PICARRO GHG analyser	Alpha Jet	In-situ airborne	CO <sub>2</sub>   CH <sub>4</sub>   H <sub>2</sub> O
AMOG / LOS GATOS ICOS instruments	car	In-situ car based	CO <sub>2</sub>   CH <sub>4</sub>   CO <sub>2</sub>   NO <sub>2</sub>   NH <sub>3</sub>   H <sub>2</sub> O   O <sub>3</sub>
MAKO	TO	HSI TIR	CH <sub>4</sub>   NH <sub>3</sub>

Table 1: Summary of geophysical parameters measured during COMEX. TO: Twin Otter; TOI: Twin Otter International.

Details on the campaign instrumentation and their performance during the campaign are summarised in the chapters below.

	<p style="text-align: center;"><b>COMEX</b></p> <p style="text-align: center;"><b>Final Report</b></p>	<p style="text-align: right;">Version: 2.0 Doc ID: IUP-COMEX-FR Date: 3. July 2016</p>
--	--	--


#### 4.1. Methane Airborne MAPper (MAMAP) (CIRPAS TO)

For the remote sensing of the greenhouse gases CO<sub>2</sub> and CH<sub>4</sub> the Methane Airborne MAPper (MAMAP) was flown on CIRPAS Twin Otter above the boundary layer. MAMAP is an airborne 2-channel NIR-SWIR grating spectrometer system for accurate measurements of gradients of column-averaged methane and carbon dioxide concentrations (for details, see RD-1, RD-2).

CH <sub>4</sub> /CO <sub>2</sub> -SWIR-spectrometer	O <sub>2</sub> -NIR-spectrometer
F = 300 mm temperature stabilized grating spectrometer system (f/3.9)	F = 300 mm temperature stabilized grating spectrometer system (f/3.9)
<b>Grating:</b> 600 grooves/mm	<b>Grating:</b> 1200 grooves/mm
<b>Detector:</b> LN cooled 1024 pixel InGaAs FPA	<b>Detector:</b> 512 x 512 pixel CCD Sensor, TE cooled, 6 pixel binned in imaging direction
<b>Spectral range:</b> 1.590 - 1.690 nm	<b>Spectral range:</b> 755 - 785 nm
<b>Spectral resolution:</b> ~0.9 nm FWHM	<b>Spectral resolution:</b> ~0.46 nm FWHM
<b>Spectral sampling:</b> ~8 pix/FWHM	<b>Spectral sampling:</b> ~ 6 pix/FWHM
<b>Detector-SNR:</b> ~ 1000 at ~ 0.6 - 1.0 sec. integration/co-adding time	<b>Detector-SNR:</b> ~ 4000 (1D-binned) at ~ 0.6 - 1.0 sec integration/co-adding time
<b>Detector-Cooling:</b> Liquid Nitrogen (LN) (~ 1.5 l LN / 10h operation)	<b>Detector-Cooling:</b> Thermo-Electric
<b>IFOV:</b> ~ 1.14° across track(CT) x ~ 1.14° along track	<b>IFOV:</b> : ~ 1.14° across track(CT) x ~ 1.14° along track
<b>Spatial resolution:</b> at 3 km flight altitude, ground speed 200 km/h, the co-added ground pixel size is in the order of 55 m along track x 60 m across track (non-imaging)	<b>Spatial resolution:</b> at 3 km flight altitude, ground speed 200 km/h, the co-added ground pixel size is in the order of 55 m along track x 60 m across track (non-imaging)
<b>Precision:</b> ~ 0.3 % XCH <sub>4</sub> (CO <sub>2</sub> ) & XCO <sub>2</sub> (CH <sub>4</sub> ) (1 σ) for 0.6-1 sec co-adding/integration time (precision is defined as the random error of the retrieved XCH <sub>4</sub> and XCO <sub>2</sub> columns due to instrument noise). Slightly degraded precision expected for XCH <sub>4</sub> (O <sub>2</sub> ) & XCO <sub>2</sub> (O <sub>2</sub> ).	
<b>Relative Accuracy:</b> < 0.5 % XCH <sub>4</sub> (CO <sub>2</sub> ) & XCO <sub>2</sub> (CH <sub>4</sub> ) on spatial scales in the range of 20-30 km at clear sky, < 1 % XCH <sub>4</sub> (CO <sub>2</sub> ) & XCO <sub>2</sub> (CH <sub>4</sub> ) on spatial scales in the range of ~ 100 km at clear sky.	
<b>Measurement modes:</b> nadir- (terrestrial targets) or glint- radiance (marine targets) on demand, zenith sky irradiance (optional as reference).	
<b>Size:</b> 2 standard racks, 556 x 650 x 968 mm each.	
<b>Weight:</b> 2 x ~120 kg.	
<b>Power consumption:</b> ~ 600 Watt at nominal operation, < 1000 Watts at warm-up	
<b>Flight record:</b> Cessna Caravan (RWE), Cessna 207 (FU-Berlin), DC3T-BT67 (AWI Polar-5, Transport Canada air worthiness approval)	

Table 2: MAMAP sensor properties and characteristics.

MAMAP was jointly developed by the Institute of Environmental Physics / Remote Sensing (IUP/IFE), University of Bremen (Germany) and the Helmholtz Centre Potsdam, German Research Centre for Geosciences (GFZ). MAMAP has air worthiness approval for operation on the Cessna T207A and AWI – Polar 5 and was already flown successfully in 2008, 2011 and 2012 on that aircraft. Data analysis methods for MAMAP data are well developed to derive the emission strength of strong point sources

	<b>COMEX</b> <b>Final Report</b>	Version: 2.0 Doc ID: IUP-COMEX-FR Date: 3. July 2016
---	-------------------------------------	--

from the gradient measurements (RD-2). The MAMAP sensor can be operated in nadir mode but also in glint mode when a gyro-stabilised platform is used. The latter was successfully tested during a campaign in June 2011 (RD-6). For COMEX, MAMAP was equipped with the CSM130 gyro-stabilised platform to perform sun-glint measurements over ocean. Flight worthiness approval of the instrument for the CIRPAS aircraft was performed by ZIVKO Aeronautics and NASA based on the by IUP prepared and provided instrument documentation.

For MAMAP, it was demonstrated that the instrument is able to detect and retrieve the total dry column of the greenhouse gases CH<sub>4</sub> and CO<sub>2</sub> with a precision of ~ 0.3% (1-sigma) at local scales (several 10th of km), and that MAMAP is an appropriate tool for detection and inversion of localized GHG emissions from aircraft (RD-1, RD-2).

Assuming a wind speed of ~ 2-3 m/sec (min. for Gauss plume inversion), a 0.3% precision translates to a (flight path, pixel size and pointing accuracy dependent) detection limit of this airborne non-imaging instrument of approx. to 1-2kt CH<sub>4</sub>/yr (1-2Mt CO<sub>2</sub>/yr) and a minimum quantifiable (error 50%) source strength of approx. 5 kt CH<sub>4</sub>/yr (5 Mt CO<sub>2</sub>/yr), assuming that on the scale of a plume extension, the precision is dominating the relative accuracy.


Therefore, MAMAP, with its current proven instrument and algorithm performance, is well suited for the detection of strong point sources of CH<sub>4</sub> and CO<sub>2</sub>.

In comparison to CarbonSat, there are some differences to be mentioned:

- Due to the measurement geometry MAMAP has compared to CarbonSat an enhanced sensitivity to the column below the aircraft.
- MAMAP in comparison to CarbonSat did not allow for “absorber free” solar reference measurements, with the consequence that MAMAP delivers no absolute single total column data, but accurate gradients in columns below aircraft.
- As MAMAP on a Twin Otter can only probe gradients on small scales up to 100 km, quantification of larger scale biospheric fluxes is not feasible with MAMAP within the COMEX campaign set-up, in contrast to CarbonSat, where large scales are probed within minutes.
- MAMAP has no 2 µm channel and the spectral resolution in the NIR and SWIR is lower than for CarbonSat. Therefore required relative accuracy can be achieved only in areas exhibiting “clear sky” atmospheric conditions (see RD-1).
- MAMAP has no swath and a higher spatial resolution.

In comparison to previous campaigns (e.g., C-MapExp), a real-time retrieval for the MAMAP instrument was developed for the COMEX project. This retrieval analyses the MAMAP measurements in real-time during the flight and delivers dry-air column averaged mole fractions of CH<sub>4</sub> or CO<sub>2</sub>, which are displayed in Google Earth to the science operator. The science operators can dynamically adapt the flight pattern on basis of the real-time result and identify and follow unknown emissions sources (more details in chapter 3.1). This opportunity is very important, when the source location is not known or the atmospheric conditions are non-stationary, e.g. a change in wind direction occurs in comparison to the forecast from a few hours ago or even during the time period where measurements are taken.

The MAMAP instrument worked well during the whole field campaign, even on most days with high temperatures in LA during August and September 2014. There was only a minor malfunction of the dark current monitoring shutter unit due to the high temperatures in Los Angeles on one day, but the measurements can still be used for further data analysis.

	<p style="text-align: center;"><b>COMEX</b> <b>Final Report</b></p>	<p style="text-align: right;">Version: 2.0 Doc ID: IUP-COMEX-FR Date: 3. July 2016</p>
--	---	--

## 4.2. CIRPAS atmospheric measurements suite (CIRPAS TO)

<http://www.cirpas.org/index.html>

The CIRPAS Twin Otter is an instrumented twin-engine turboprop aircraft. It supports individual scientists as well as teams of scientists from various Universities and Laboratories who are interested in lower-tropospheric phenomena and air/sea interaction. The core payload can be selected from a large suite of state of the art meteorological, aerosol, and cloud particle sensors, while additional equipment of collaborating scientists may wish to include can be integrated as well. Instruments may be installed in racks inside the cabin where a well-characterized community inlet delivers ambient air samples, or in pods either suspended by wing-mounted pylons or mounted on a hard point on the cabin roof. Optical ports and windows are on the aircraft's belly and in the cabin roof. CIRPAS staff calibrates and maintains the facility payload and provides fully reduced, synchronized, and coherent data sets to the collaborating scientists. The Twin Otter is based at the CIRPAS Marina Facility.

The CIRPAS Twin Otter is a non-pressurized turbo-prop, twin-engine aircraft with a **Payload Capacity** of 1500 lbs, **Available Payload Power** of 200 Ampere of 28 VDC, or 5600 Watts, of which up to 4000 watts can be inverted to 120V AC at 60 Hz. **Endurance** is 5-6 hours, fully loaded, with a 12000 ft ceiling without oxygen, 18000 ft. maximum. Twin Otter missions have been sponsored by ONR, NSF, DOE, NOAA, NASA, CARB, and NRL.



Figure 2: CIRPAS Twin Otter

### Standard Instrument Suite

- 1) C-MIGITS-III is the primary GPS/INS System. It provides Location (Lat, Lon, Altitude), Ground velocity (speed and direction), Platform attitude (pitch, roll, and heading).
- 2) NovAtel – backup Lat, Lon, altitude, and ground speed.
- 3) Trimble TANS VECTOR – backup pitch, roll, and heading.

### Meteorological suite:

- 1) Temperature: Retrieved from Total Temperature measurement using Rosemount– platinum wire, fast response sensor. Range: -50 C to + 50 C
- 2) Egdetech chilled mirror Dew Point Temperature – slow, but accurate, not suitable for flux retrievals. Range -50 C to +50 C, but limited to ~20°C dewpoint depression.
- 3) Static pressure: SETRA 270 barometric transducer – Range 1100 to 600 mb.
- 4) Total Pressure: SETRA 270 barometric transducer – Range 1100-600 mbar.
- 5) Winds: Retrieved from differential pressure measurements on a five-hole radome, and synchronized GPS/INS platform motion data.
- 6) Surface temperature (Land or sea surface): Heitronics KT 19.85 IRT.

	<p style="text-align: center;"><b>COMEX</b> <b>Final Report</b></p>	<p style="text-align: right;">Version: 2.0 Doc ID: IUP-COMEX-FR Date: 3. July 2016</p>
--	---	--

#### **Aerosol Instruments:**

1. 2 Condensation Particle counters, TSI 2010, usually operated with different super-saturation, different detection threshold, for indication of fine particles. Thresholds at 10 and about 15 nm particle diameter
2. TSI 2025 Ultrafine particle counter. Threshold at 3 nm.
3. Passive Cavity Aerosol Spectrometer Probe (PCASP-100). Optical particle size spectrometer. Bins particle by size into 20 channels covering the range from about 0.1 to 3  $\mu\text{m}$ .
4. Cloud Aerosol Spectrometer (CAS): Optical particle size spectrometer with range from about 0.5 to 50  $\mu\text{m}$  diameter. Bins by size into 20 channels.
5. 3 Wavelength Nephelometer, TSI – 3550: Measures the scattering and backscattering coefficients in the blue, green and red.
6. 3 Wavelength Soot Photometer (PSAP): Measures the absorption coefficient in the blue, green and red.

#### **Cloud and Precipitation instruments:**

- 1) Forward Scatter Spectrometer probe –FSSP-100: Bins particles by size into 20 bins. Range 3–50  $\mu\text{m}$  diameter.
- 2) Cloud Aerosol Precipitation Probe (CAPS): Three instruments in one:
  - a) CAS – Size spectrometer with range of 0.5 – 50  $\mu\text{m}$  (20 Channels).
  - b) Cloud Imaging Probe (CIP): We run it as a 1-D probe sizing particles in the range of 25–1500  $\mu\text{m}$ , binned into 62 channels.
  - c) Hot Wire Liquid Water Content probe.
- 3) Cloud Droplet Probe (CDP): Size spectrometer in the range of 2-50  $\mu\text{m}$ , bins in 40 channels.
- 4) HVPM-100 (Gerber probe): Measures Liquid water content, and effective radius of cloud droplets.

With the exception of May 30, 2014 (failure of CIRPAS suite during test flight), the CIRPAS suite worked well during the campaign and the collected data is of high quality. This is confirmed by post-flight analysis of the data.

Also installed on the CIRPAS Twin Otter for this campaign was the NASA Ames Research Center cavity ring down spectrometer for the detection of  $\text{CO}_2$ ,  $\text{CH}_4$  and  $\text{H}_2\text{O}$  as well as the Los Gatos Research Isotope analyser.


### **4.3. PICARRO GHG Sensor (CIRPAS TO)**

M. Fladeland/R. Kolyer, NASA Ames Research Center

During the COMEX campaign the 10 Hz Eddy Covariance Flux  $\text{CO}_2/\text{CH}_4/\text{H}_2\text{O}$  Cavity Ring Down Spectroscopy instrument (G2301-f) was operated in a low flow/high precision mode. The sampling rate was  $\sim 3\text{Hz}$ . Automated  $\text{H}_2\text{O}$  vapor corrections for both  $\text{CO}_2$  and  $\text{CH}_4$  allowed measurement of dry gas mixing ratios directly in the wet gas stream. Addition of a GPS antenna dedicated specifically to this instrument allowed for longitude, latitude, and altitude to be added directly to the instrument's data set for each flight thus constraining each data point spatially. This enhancement obviated the need to interface with aircraft provided position information. Post flight analysis of the instrument's engineering parameters indicated that the instrument operated nominally for all flights allowing for full confidence in the collected data set.

Time-lag calibration parameters were provided by NASA-Ames after the campaign.



	<p style="text-align: center;"><b>COMEX</b> <b>Final Report</b></p>	<p style="text-align: right;">Version: 2.0 Doc ID: IUP-COMEX-FR Date: 3. July 2016</p>
--	---	--

#### 4.4. LGR CO<sub>2</sub> isotope analyzer (CIRPAS TO)

Elena Berman Los Gatos Research - LGR

The Los Gatos Research carbon dioxide isotope analyser measures CO<sub>2</sub> concentrations as well as  $\delta^{13}\text{C}$ ,  $\delta^{18}\text{O}$ , and  $\delta^{17}\text{O}$  from CO<sub>2</sub>. During the COMEX campaign, the instrument measured CO<sub>2</sub> concentrations typically around 395 ppm and encountered plumes with concentrations as high as 480 ppm. Isotopic measurements varied in a manner consistent with the source of the plume encountered; for example, measurements over the Kern oil fields show a depletion of  $^{13}\text{C}$  in CO<sub>2</sub> plumes. When sampling above a landfill site, the CO<sub>2</sub> plume had enriched  $^{13}\text{C}$  signal, which is consistent with the literature. Results from the COMEX campaign can help constrain isotopic signatures of CO<sub>2</sub> from a variety of sources, including dairy complexes, landfills, oil fields, etc.

#### 4.5. AVIRIS-C (ER-2) and AVIRIS-NG (TOI)

Michael Eastwood, Robert O. Green, David R. Thompson <http://AVIRIS-NG.jpl.nasa.gov>

Until recently, remote measurement via imaging spectroscopy (100–1000 bands, 5–10 nm) has been inadequate for accurate trace gas column derivation. In recent years, several studies have demonstrated the ability to measure CH<sub>4</sub> from imaging spectroscopy data collected by the original AVIRIS (Green et al., 1998), the “classic” AVIRIS-C imaging spectrometer (Bradley et al. 2011). Recent AVIRIS-C SWIR measurements (Roberts et al. 2010; Bradely et al., 2011), have demonstrated the value of high spatial resolution (sub-decametre) imaging for trace gas anomaly detection and mapping, i.e., plumes, using diagnostic spectral features. The AVIRIS-NG instrument (installed on a second Twin Otter aircraft) contributed to the COMEX campaign in two ways: first, with real-time detection of CH<sub>4</sub> that provided reconnaissance for other remote and in-situ assets during acquisition; and second, by mapping the precise location and extent of sources to sub-decametre accuracy, improving interpretation of data from the other sensors.

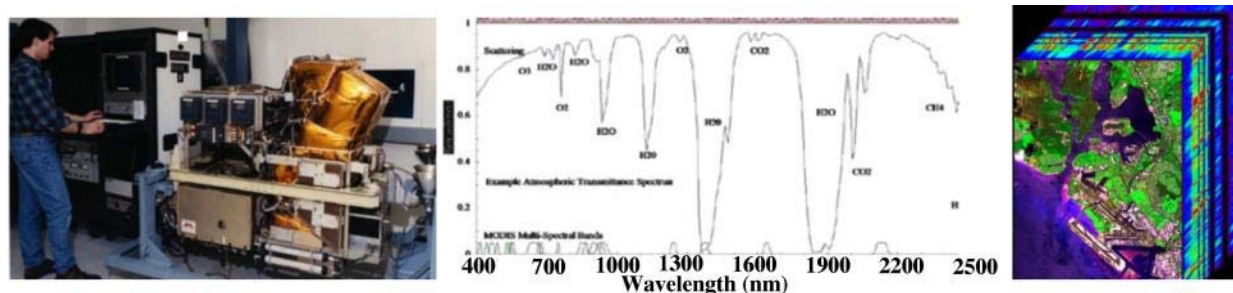



Figure 3: Left: AVIRIS-C in the laboratory at Jet Propulsion Laboratory (photo: Michael Eastwood, JPL). Middle: 224 channel spectrum with key trace gases identified. Right: Example AVIRIS data cube for Pearl Harbour, Hawaii.

Designed at the NASA Jet Propulsion Laboratory as a successor to the Airborne Imaging Spectrometer (AIS) technology demonstrator, the “classic” Airborne Visible / Infrared Imaging Spectrometer (AVIRIS) instrument has been in operation since 1986. AVIRIS-C was designed to measure the complete solar reflected spectrum from 400 to 2500 nm and to capture a significant spatial image domain. Several upgrades over time have kept AVIRIS-C the premier civilian imaging spectrometer in use. Customers work with the NASA Terrestrial Ecology Program Office to schedule flight time with AVIRIS-C. See Figure 3 for a view of the AVIRIS-C instrument in the Lab at Jet Propulsion Laboratory. AVIRIS-C measures the total upwelling spectral radiance in the spectral range from 380 to 2510 nm with approximately 10 nm sampling intervals, and a similar spectral response. These continuous spectral channels enable spectroscopy of features from visible to short wavelength-infrared wavelengths.

	<b>COMEX</b> <b>Final Report</b>	Version: 2.0 Doc ID: IUP-COMEX-FR Date: 3. July 2016
--	-------------------------------------	--

AVIRIS-C data are delivered in an image cube format. High-precision calibration is provided by annual calibration flights over well-characterized sites as well as pre-flight and post-flight calibrations on each day of operations. The science enabled by this high uniformity and high signal-to-noise ratio imaging spectrometer is well established over the past two decades. To date, AVIRIS data have been referenced in more than 600 journal articles in the refereed literature. A broad array of applications regularly utilize AVIRIS-C data include mineral mapping, land use trends, inland / coastal waters, environmental hazards / cleanups, disaster responses. Key characteristics of the AVIRIS-C design include 200  $\mu\text{m}$  detectors and F/1 optics. Other features are listed in Table 3.

	AVIRIS-Next Generation	AVIRIS-Classic
<b>SPECTRAL</b>		
Range	380 to 2510 nm	380 to 2500 nm
Position	5 nm	10 nm
Response	1 to 1.5 X sampling	1 to 1.5 X sampling
Calibration	$\pm 0.1$ nm	$\pm 0.1$ nm
<b>RADIOMETRIC</b>		
Range	0 to max Lambertian	0 to max Lambertian
Precision (SNR)	>2000 @ 600 nm	>1000 @ 600 nm
	>1000 @ 2200 nm	>400 @ 2200 nm
Accuracy	95% (<5% uncertainty)	90% (<10% uncertainty)
Linearity	$\geq 99\%$ characterization	$\geq 99\%$ characterization
<b>SPATIAL</b>		
Range	34° field-of-view	34° field-of-view
Sampling	1 milliradian	1 milliradian
Response	1 to 1.5 X sampling	1 to 1.5 X sampling
Sample Distance	0.3 m to 20 m	4 m to 20 m
Geom Model	Full 3 Axes cosines	Full 3 Axes cosines
<b>UNIFORMITY</b>		
Spectral Cross-Track	>95% across FOV	>98% across FOV
Spectral-IFOV-Variation	>95% Spectral Direction	>98% Spectral Direction

Table 1: AVIRIS Key Measurement Characteristics

<b>Spectral</b>		
Range		370 to 2500 nm
Sampling		9.8 nm
Accuracy		0.5 nm
<b>Radiometric</b>		
Range		0 to Max Labertian
Sampling		12 bits
Accuracy		96 percent
<b>Spatial (ER-2 / Twin Otter aircraft)</b>		
Swath		11/2.2 km ER-2/TO
Sampling		20/4 m ER-2/TO
Accuracy		20/4 m ER-2/TO
Full INU/GPS geo rectification		

Table 3: Right: Comparison of AVIRIS-NG and AVIRS performance parameters. Left: Performance parameters for AVIRIS on ER-2 and on Twin Otter.

AVIRIS-NG (Next Generation) has a 5 nm bandwidth, higher signal to noise and other improvements provided in Table 3. Its high SNR and spectral resolution mean that it is better suited for CH<sub>4</sub> hot spot detection than AVIRIS-C.

AVIRIS-NG data analysis consists of several independent products. First, a real-time display analyzes the methane absorption feature from 2.1-2.5 microns, and applies detection methods such as band ratios or matched filters to map relative concentrations over the flight line. These results are immediately sent to a real-time operator display (Thompson et al., 2015). Later, a similar process on the ground produces maps of methane concentrations for all flight lines. Finally, atmospherically-corrected surface reflectance and H<sub>2</sub>O retrievals are provided using standard atmospheric correction algorithms (Thompson et al., 2015).

Over 40 AVIRIS-NG flight lines were acquired during the COMEX campaign, spanning 13 June and 2-4 September. Data and contact information is provided via the web site at <http://AVIRIS-NG.jpl.nasa.gov>.



# COMEX Final Report

Version: 2.0  
Doc ID: IUP-COMEX-FR  
Date: 3. July 2016



Figure 4: Side view (left) and front view (right) of JPLs AVIRIS-NG instrument installed aboard the Twin Otter International research aircraft. Right picture shows the instrument control units installed in front of the instrument. Credits: Jet Propulsion Laboratory, California Institute of Technology.

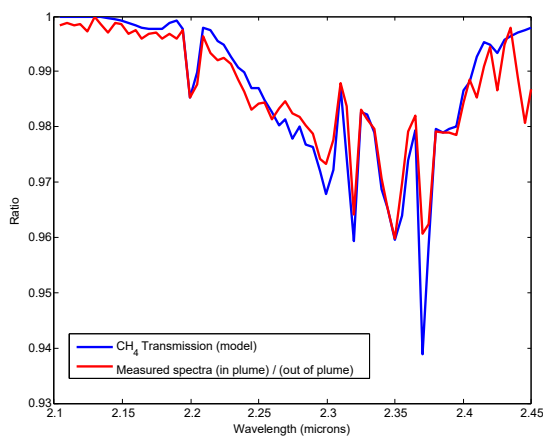
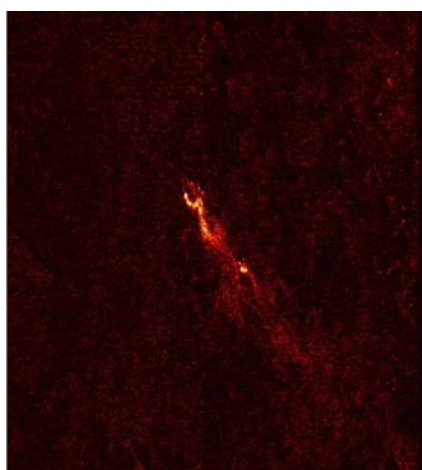


Figure 5: Left: Plume detection in AVIRIS-NG data. Right: comparison of in-plume/out-of-plume radiances (red) and the modeled transmission of methane (blue). The alignment is a confirming indication that methane concentrations are elevated within the plume.

#### 4.6. Mako Thermal Infrared Hyperspectral Imaging Spectrometer (TO)

Dave Tratt, Aerospace Corporation

Mako (Warren *et al.*, 2010; Hall *et al.*, 2011) is a TIR HSI spectrometer that was intended to fly on a third Twin Otter in close coordination with CIRPAS flights to collect high spatial, moderate spectral resolution TIR imagery. Joint data analysis would then help to identify synergies of SWIR/TIR joint datasets for trace gas remote sensing [Leifer *et al.*, 2012].



Figure 6: Mako installed in a DeHavilland DHC-6 Twin Otter aircraft.

Mako has previously demonstrated trace gas mapping at fine spatial scales and its performance against methane in particular was recently described in detail [Tratt *et al.*, 2014]. Built by The Aerospace Corporation (Los Angeles, USA), the sensor features ~50-nm resolution ( $4 \text{ cm}^{-1}$  @  $10 \text{ }\mu\text{m}$ ) across its operating wavelength range and acquires imagery in 128-pixel wide strips. Mako employs whiskbroom scanning to yield areal acquisition rates  $\sim 20 \text{ km}^2/\text{minute}$  at 2-m GSD. Depending on aircraft altitude, Mako images a 0.5-2 meter pixel at the ground. Its performance characteristics are summarized in Table 4.

Parameter	Specification
Instantaneous pixel field-of-view	0.55 mrad
Cross-track pixels	400 – 2750
Cross-track field-of-regard (relative to nadir)	$\pm 42^\circ$ (max.)
Spectral coverage	7.45 – 13.46 $\mu\text{m}$
Spectral resolution (128 channels)	47 nm
Noise-equivalent spectral radiance (10 $\mu\text{m}$ )	$0.7 \text{ }\mu\text{W cm}^{-2} \text{ sr}^{-1} \text{ }\mu\text{m}^{-1}$
Noise-equivalent temp. difference (300 K)	0.05 K

Table 4: Mako performance specifications.



In the event, aircraft availability restrictions precluded Mako's participation in the main COMEX field experiment. Instead, the sensor was flown over a subset of the COMEX areas of interest during the period between the two phases of COMEX (Table 5). The Chino collection was coordinated with AMOG Surveyor in situ measurements.

Date		Mako Target	AMOG
22. Jul	Tu	COP (T13)	
24. Jul	Th	Kern (T1)	
25. Jul	Fr	Chino (T11)	Chino (T11)

Table 5: Summary of COMEX-related data collected by Mako in July 2014. Reference to the target number (Tx) can be found in Annex 1.

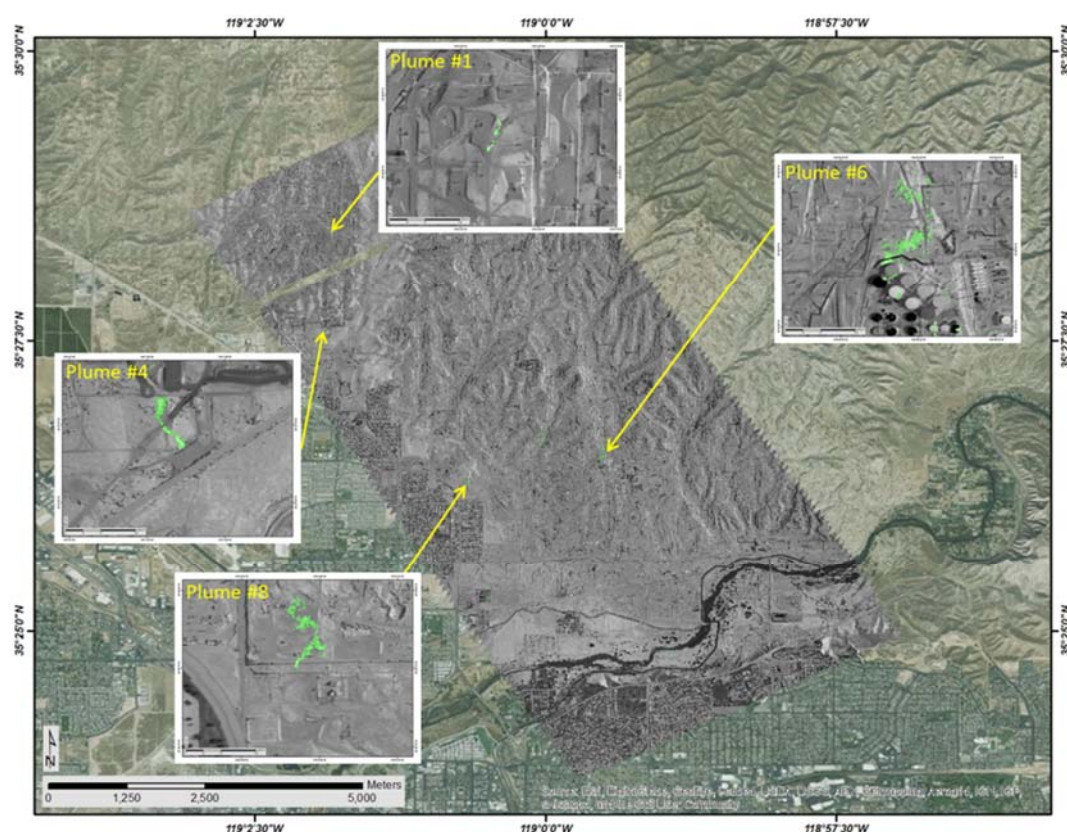


Figure 7: Mako thermal imagery of the Kern River Oil Field showing retrieved methane emissions.

Figure 7 provides a sample Mako data set, illustrating both the spatial resolution and areal coverage capability. This imagery is of the Kern River Oil Field and comprises a thermal radiance mosaic over the site overlaid onto a visible image of the scene. A total of 10 methane plumes were recovered from this data set, but are too small to be appreciated at the scale of the main image. Hence, insets are provided that show four of the most prominent methane plumes rendered green on the gray-scale thermal radiance field. Some, though not all, of these emission sources appear to correspond to those inferred from the COMEX experimental data. Quantification of these emissions is ongoing.

## 4.7. PICARRO GHG sensor (Alpha Jet)

Laura Iraci, NASA Ames Research Center

The Alpha Jet is owned by H211, LLC, a current collaborative partner with NASA. It is based at and operated from Moffett Field under a Space Act Agreement, which has already facilitated H211's support of over 175 science missions. The Alpha Jet is a tactical strike fighter developed by Dassault-Breguet and Dornier through a German-French NATO collaboration. Carrying a crew of two, it has a length 40 ft, wingspan of 30 ft, and height of 13 ft 9 inches, an empty weight of 7800 lbs, and a maximum take-off weight of 17,637 lbs. It has a ceiling of 40,000 ft, at a speed of 150-550 knots, and a range of ~1,200 miles with full fuel. The Alpha Jet stationed at NASA Ames–Moffett Field has a 2 hr flight duration.



Figure 8: Alpha Jet

H211 has provided significant upgrades to the aircraft to support scientific studies. Extensive wiring and cabling provisions have been installed to both wing pod locations, as well as the centerline pod, to allow for distribution of 120 and 26 volt AC and 28 volt DC to each wing pod, as well as additional 120 volt AC and 28 volt DC service to the centerline pod. Redundant heavy-duty Ethernet cables have been provided from the wing pods to the centerline pod and backseat control console. An operator interface panel has been installed in the rear cockpit to allow power on/off/failure interface to each scientific instrument. Additionally, the pilot has a payload master power switch that can remove all electrical power from the NASA payloads in the event an abnormal electrical condition is encountered.

Two wing-mounted pods have been modified by NASA-ARC to carry instrumentation, with three down-looking window ports available on each pod. Each wing pod has an approximate payload volume of 3.5 cubic feet and maximum payload weight of 300 lbs. The centerline pod has two payload areas of ~34x10x12 inches and 27x6.5x10 inches, carrying combined payloads up to 350 lbs total.

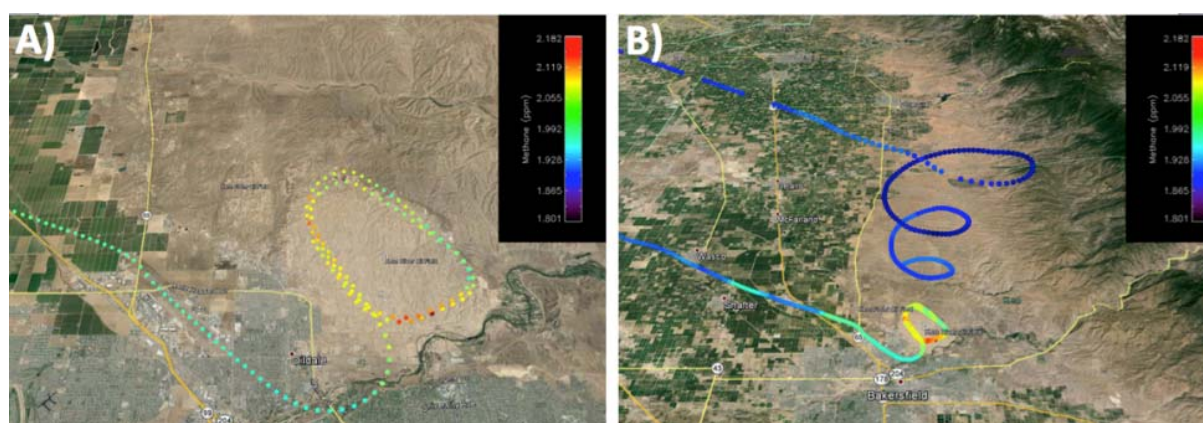


Figure 9: Methane concentrations from the Alpha Jet over Kern River oil field and environs on 10 June 2014. The Alpha Jet acquires in-situ data and no column information.

During COMEX a fast greenhouse gas CRS (Picarro) measured  $\text{CH}_4$ ,  $\text{CO}_2$ , and  $\text{H}_2\text{O}$  at 3 Hz with an accuracy of 0.2 ppm or better on  $\text{CO}_2$ , 2.2 ppb on  $\text{CH}_4$ , and 100 ppm on  $\text{H}_2\text{O}$ . An example is given in Figure 9.



#### 4.8. LOS GATOS ICOS Instruments (AMOG Surveyor)

Ira Leifer, Bubleology Research International

During COMEX, on-ground data were collected by the AMOG (AutoMOBILE greenhouse Gas) Surveyor, developed for mobile high-speed observations of greenhouse gases, winds, temperature and other trace gases (Leifer et al., 2014). The AMOG Surveyor is a Nissan Versa commuter car that has been modified for scientific trace gas surveys (see Figure 10). AMOG surveyor has been designed to facilitate effective adaptive surveys for real-time, trace gas plume characterization. The Surveyor includes subsystems for power management, sample gas handling, gas analysis, thermal management, ancillary measurements, data communication, and real-time software.



Figure 10: AMOG Surveyor images at the California State University Polytechnic Dairy waste pool showing roof and trunk packages.

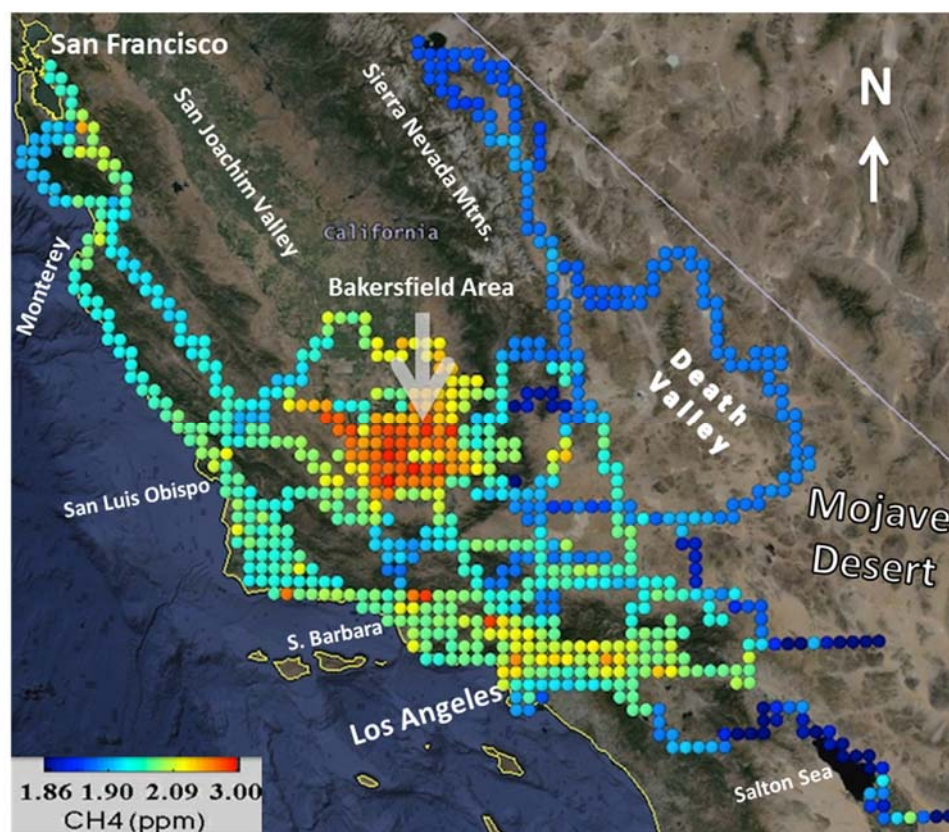



Figure 11: Summary of all AMOG data 2014-2015 (9-km spatially binned) in Southern and Central California. Arrow identifies Bakersfield, CA. Data key on figure.




	<p style="text-align: center;"><b>COMEX</b> <b>Final Report</b></p>	<p style="text-align: right;">Version: 2.0 Doc ID: IUP-COMEX-FR Date: 3. July 2016</p>
--	---	--

The AMOG Surveyor uses a high flow vacuum pump to draw samples down two sample lines from 5 and 3 m above ground into three ICOS / OF-CEAS instruments. The higher, ½" sample line connects to a machine that measures CO<sub>2</sub>, CH<sub>4</sub>, and H<sub>2</sub>O at up to 10 Hz, set at 5 Hz for these data (Fast Greenhouse Gas Analyzer – FGGA, Los Gatos Research, Inc., CA). Recent AMOG system improvements beyond Leifer et al. (2014) include two redundant high performance GPS receivers (19X HVS, Garmin) that use the GLONASS, GPS, Galileo, and QZSS satellites for 10 Hz positioning, a high speed thermocouple (50416-T, Cooper-Atkins, CT) for temperature anomaly mapping at 0.01°C, a high accuracy (±0.05 hPa linearity) pressure sensor (PTB-100B, Vaisala, Finland). The thermocouple and pressure sensors are mounted under a passive radiation shield (7710, Davis Instruments, CA) to minimize radiation and airflow effects.

Real-time data monitoring and visualization was found to be key to successful surveys, which needs to be collected in the wind frame of reference. Real-time data visualization and integration is in a mapping environment (Google Earth), including winds to aid adaptive survey route planning in the wind frame of reference. Adaptive surveying involves altering the survey route to adjust to active sources and the winds. Custom software provides real-time integration and visualizations of AMOG data in the Google Earth environment of up to five parameters, typically, CH<sub>4</sub>, CO<sub>2</sub>, NH<sub>3</sub>, wind data, and temperature are displayed, although humidity and CO<sub>2</sub> can be displayed optionally.

In support of COMEX, CH<sub>4</sub> data were collected covering a significant area, a subset of which is shown in Figure 11. These data are 1-minute-averaged to minimize the effect of local intense plume measurements. CH<sub>4</sub> anomalies for the Bakersfield area and eastern San Joachim valley are significantly larger even than values observed in the Los Angeles Basin. CH<sub>4</sub> is near background in the deserts and mountains while strongly enhanced in the South San Joachim Valley and Los Angeles Basin. CH<sub>4</sub> concentrations are 1-minute averages to reduce local hotspots.

	<p style="text-align: center;"><b>COMEX</b> <b>Final Report</b></p>	<p style="text-align: right;">Version: 2.0 Doc ID: IUP-COMEX-FR Date: 3. July 2016</p>
--	---	--

## 5. Summary of campaign as performed

In this section, an overview is given about the campaign as performed. The campaign was performed during two windows (May/June and August/September 2014) driven by the planned AVIRIS/ER-2 flights and AVIRIS-NG availability.

The targets were pre-selected based on literature values, inventories and pre-surveys of the AMOG Surveyor and of the MACLab (see CIP (RD-4)). This approach was performed for landfills which need to be monitored in the US according to regulatory. In contrast, for oil fields, reliable emission estimates could not easily be accessed. Ground-based in-situ sampling could not provide reliable estimates on fluxes required for modeling of expected total column increases, due to the large extend of the oil field, insufficient knowledge of atmospheric parameters and mixing as well as the inability to exactly localize the source position due to (mostly) restricted access to the fields. The initial pre-selection of oil fields was made based on production data obtained for the Division of Oil, Gas & Geothermal Resources (<http://www.conservation.ca.gov/DOG/Pages/Index.aspx>). In addition, it was originally planned to select the most promising targets with in-situ pre-survey before the actual flight day by airborne surveys (Alpha Jet) and ground based measurements (AMOG surveyor). Due to the limited availability and refueling restrictions of the Alpha Jet and the time required for relocation of AMOG, the strategy was changed during the campaign. Instead, extensive use of the recently implemented real-time retrieval capabilities, MAMAP was used for pre-survey and guidance. The measurement strategy was adopted accordingly and two promising targets were selected for each flight day. In case of absence of measurable signals from the first target, the second target was flown. Hence, an optimization of available flight time was achieved. Drawback of this strategy was the increased and more difficult coordination between the different aircraft and also with ATC (Air Traffic Control).

For glint data only one accessible (with respect to available flight time) target in the area was identified in the literature. The well-studied Coal Oil Point (COP) natural seep near Santa Barbara (first observed by the early Spanish settlers and English explorers, Hornafius et al., 1999) was previously estimated with different sonar methods to release locally between 15 ktCH<sub>4</sub>/yr (Clark et al., 2010) and 29.2 ktCH<sub>4</sub>/yr (Hornafius et al., 1999), to the atmosphere and, therefore, has emissions above the MAMAP detection limit, of similar magnitudes as the selected landfills.

Based on this approach, the targets list in Table 6 evolved from those presented in the CIP, which was further adapted based on quick look results during the campaign. For example, just on the second flight day (03.06.2014), an unexpectedly large methane plume was measured over the Poso Creek, Kern River and Kern Front Oil Fields (T1) by the MAMAP and Picarro instrument. Kern River as heavy oil field with high well density but low natural gas production was expected to have lower emissions than the adjacent Elk Hills field which was chosen as secondary target for that day. Hence, T1 became a high priority target and was overflown in total 7 times, to collect a very meaningful data set for COMEX which will also allow the characterization of the variability of CH<sub>4</sub> emissions from an oil field under production.

The flights over the COP field were disappointing (in terms of emissions), as no large signals were observed in the MAMAP and in-situ data (in the boundary layer) opposite to previous estimates (Clark et al., 2010, Hornafius et al., 1999). As the collected remote sensing glint data was of good quality, it was decided to downscale COP from high priority to lower priority, which results in the fact the COP was flown on two days.

Another example of adapting the target selection during the campaign were the landfills, where only for Olinda Alpha significant CH<sub>4</sub> was detected (see Figure 13), and priority was given then to target that landfill several times to collect a good data set over landfills.

	<b>COMEX</b> <b>Final Report</b>	Version: 2.0 Doc ID: IUP-COMEX-FR Date: 3. July 2016
---	-------------------------------------	--

Target number	Ref to CIP	Name	Type	Lat	Lon	CO <sub>2</sub>	CH <sub>4</sub>	inland	coast
T1	1	Kern Front and Kern River	Petroleum/Gas Production	35,45°	-118,98°	(x)	x	x	
T2	2	Elk Hills	Petroleum/Gas Production	35,28°	-119,44°	(x)	x	x	
T3	11	North Belridge and South Belridge	Petroleum/Gas Production	35,45°	-119,70°	(x)	x	x	
T4	12	Midway Sunset	Petroleum/Gas Production	35,15°	-119,51°	(x)	x	x	
T5	---	Buena Vista	Petroleum/Gas Production	35,19°	-119,45°	(x)	x	x	
T6	15	Olinda Alpha	Landfill	33,94°	-117,84°	x	(x)	x	
T7	13	Puente Hills	Landfill	34,02°	-118,02°	(x)	x	x	
T8	18	Scholl Canyon	Landfill	34,16°	-118,19°	x	(x)	x	
T9	---	BKK	Landfill	34,04°	-117,90°	x	(x)	x	
T10	9	Harris Ranch	Cattle Ranch / Feedlot	36,31°	-120,27°		x	x	
T11	---	Chino	Cattle Ranch / Feedlot	34,01°	-117,63°		x	x	
T12	7	Los Angeles Basin Survey	Megacity	33,92°	-118,14°	x	x	x	x
T13	8	Coal Oil Point	Natural oil and gas	34,39°	-119,87°		x		x
T14	3	La Brea Tar Pits	Natural oil and gas	34,07°	-118,36°		x		x
T15	---	Baldwin Hills	Petroleum/Gas Production	34,00°	-118,37°	(x)	x		x
T16	5	Carson	Refinery	33,81°	-118,24°	(x)	x		x
T17	6	Tesoro	Refinery	33,79°	-118,23	(x)	x		x

Table 6: COMEX targets flown during the campaign.

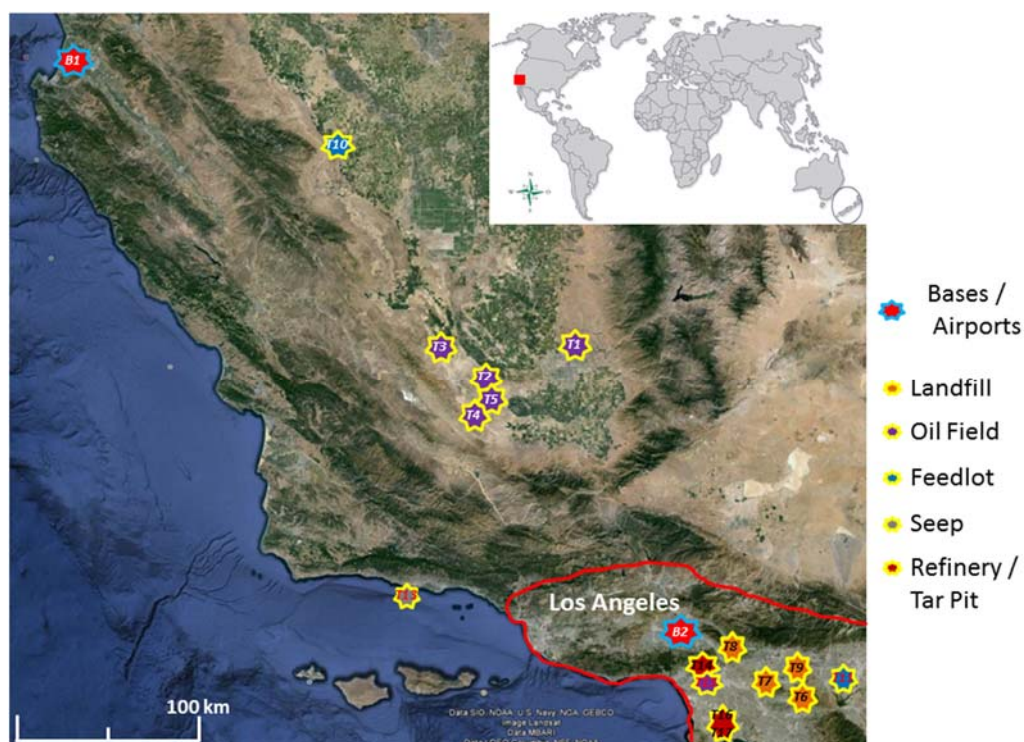


Figure 12: Overview map of Southern California. The two airports where the CIRPAS Twin Otter was based are labelled by a red/blue star. In the northern part, B1 marks the homebase of CIRPAS in Marina and in the southern part, B2 marks the airport in Burbank, Los Angeles. Reference to the single target numbers (Tx) can be found in Annex 1. The Los Angeles Basin is encircled in red.

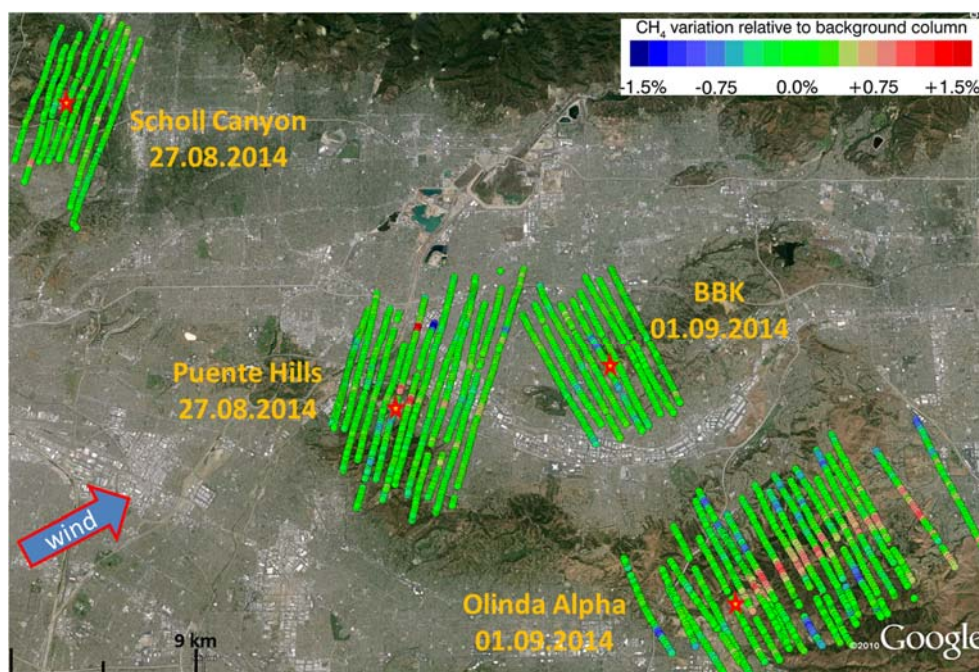


Figure 13: Quick look of landfills surveyed during COMEX. Only Olinda Alpha showed significant CH<sub>4</sub> emissions.

Figure 12 shows an overview map of Southern California and the locations of all flown targets. The flights in the May/June window were flown out of the CIRPAS home base in Marina and in the



August/September window out of the airport in Burbank, Los Angeles, except 1 flight (also compare to Table 7)

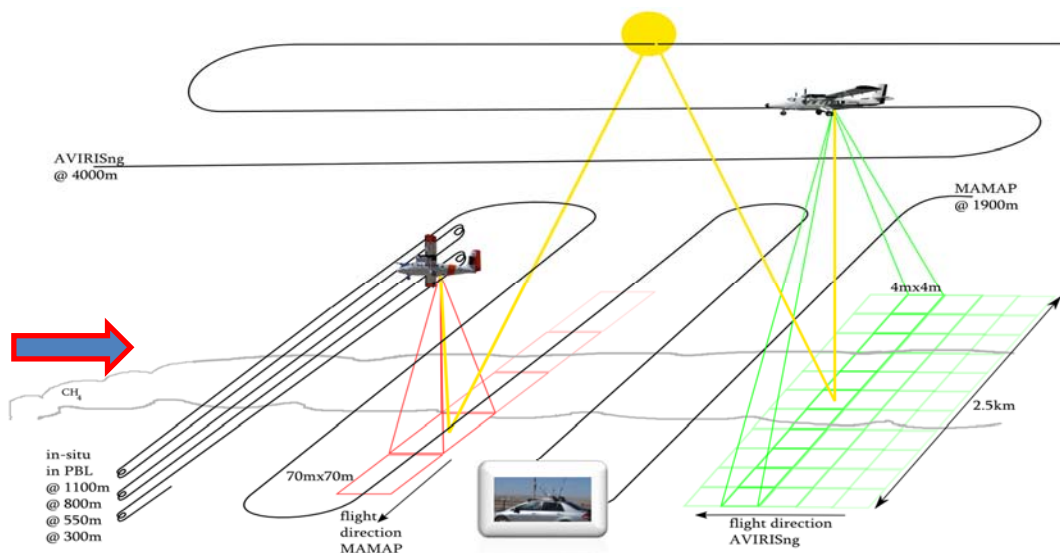


Figure 14: Idealised scheme of measurement and flight strategy during COMEX.

The overall flight planning, as well as the flight strategy (see Figure 14) was performed as documented in the Campaign Implementation Plan (RD-04).



	<b>COMEX</b> <b>Final Report</b>	Version: 2.0 Doc ID: IUP-COMEX-FR Date: 3. July 2016
--	-------------------------------------	--

Table 7 summarises the campaign activities as performed from MAMAP/CIRPAS perspective.

Date	Day of Week	Flight Activity	Comment / Co-flight by
04.5. to 29.5.2014		Testing of MAMAP after shipping and integration/certification CIRPAS Twin Otter	Start of COMEX part 1
30.5.2014	Fri	Engineering flight, T10	Failure of CIRPAS suite
03.6.2014	Tue	T1	AVIRIS-NG (T13)
04.6.2014	Wed	T13	AVIRIS-C ; glint-measurement with stabilization platform
09.6.2014	Mon	T1	
10.6.2014	Tue	Kern (T1)	AlphaJet only
12.6.2014	Thu	T7, T11	AVIRIS-C AVIRIS-NG
13.6.2014	Fri	T1	AVIRIS-NG, AMOG
16.6. to 20.6.2014		Disintegration of MAMAP. Preparation for storage.	End of COMEX part 1. Instrument was kept in storage in the CIRPAS hangar in Marina until COMEX-part 2.
-----	---	-----	-----
18.8. to 29.8.2014		Integration of MAMAP into CIRPAS Twin Otter	Start of COMEX part 2
20.8.2014	Wed	Very short engineering flight	Just over the airport
21.8.2014	Thu	T1	
23.8.2014	Sat	T2, T3, T4, T5	Transit from Marina to Burbank
25.8.2014	Mon	T13	Glint- measurements with stabilized platform
26.8.2014	Tue	T1	AVIRIS-C (one leg over Kern)
27.8.2014	Wed	T9, T10, T11	Difficulties with air space in the southern part of Puente Hills
28.8.2014	Thu	T9, T10, T12	
29.8.2014	Fri	T12, T16, T17	AMOG; T16 and T17 were part of the LA Basin survey
01.9.2014	Mon	T6, T9	AVIRIS-NG but were thrown out of the air space
02.9.2014	Tue	T1	AVIRIS-NG
03.9.2014	Wed	T6, T11	AVIRIS-NG, AMOG
04.9.2014	Thu	T1	AVIRIS-NG, AMOG
05.9.2014	Fri	Transit from Burbank to Marina	
08.9. to 10.9.2014		Disintegration of MAMAP and preparing for shipping back to Bremen	End of COMEX part 2

Table 7: Campaign schedule as executed. If not other stated otherwise, the targets shown in in the column 'activity' were flown by the CIRPAS Twin Otter (with following instruments: MAMAP, CIRPAS atmospheric measurement suite, Picarro GH sensor, Los Gatos isotope analyser). Details of the targets flown by MAMAP onboard the CIRPAS Twin Otter are listed in Table 10. Reference to the target number (Tx) can be found in Table 6.

Table 8 and Table 9 summarise the campaign activities/measured targets of all platforms (instruments) for the first part and second part of the campaign, respectively. Reference to the target numbers (Tx) can be found in Table 6.

	<b>COMEX</b> <b>Final Report</b>	Version: 2.0 Doc ID: IUP-COMEX-FR Date: 3. July 2016
--	-------------------------------------	--

Date	CIRPAS TO / MAMAP* <sup>1</sup>	ER-2 / AVIRIS-C	TOI / AVIRIS-NG	Alpha Jet / Picarro GHG sensor	AMOG / LGR ICOS instruments
30. Mai	Harris (T10)				
02. Jun					
03. Jun	Kern (T1)		COP (T13) (transit)		
04. Jun	COP (T13)	COP (T13), Kern (T1)			
07. Jun					Chino (T11), Puente (T7)
09. Jun	Kern (T1)				
10. Jun				Kern (T1)	
12. Jun	Puente (T7), Chino (T11)				
13. Jun	Kern (T1)	LA Basin (T12)	Kern (T1)		Kern (T1)

Table 8: Summary of collected data in May/June 2014 (First part of COMEX). \*<sup>1</sup> Besides MAMAP, also the CIRPAS atmospheric measurement suite, the Picarro GHG sensor and the LGR CO<sub>2</sub> isotope analyser were onboard the CIRPAS TO.

Date	CIRPAS TO / MAMAP* <sup>1</sup>	ER-2 / AVIRIS-C	TO Int. / AVIRIS-NG	Alpha Jet / Picarro GHG sensor	AMOG / LGR ICOS instruments
21. Aug	Kern (T1)				
23. Aug	Oil Fields (Transit) (T2,T3,T4,T5)				
25. Aug	COP (T13)				
26. Aug	Kern (T1)	Los Angeles, one Leg@Kern			
27. Aug.	T9,T10,T11, T14,T15				
28. Aug	T9,T10,T12				
29. Aug	T12,T16,T17	Santa Barbara Box		Mojave	Los Angeles
01. Sep	T6,T9				
02. Sep	Kern (T1)		Kern (T1)		
03. Sep	T6,T11		T6,T11		Chino (T11)
04. Sep	Kern (T1)		Kern (T1)		Kern( T1)

Table 9: Summary of collected data in Aug/Sep. 2014 (Second part of COMEX) . \*<sup>1</sup> Besides MAMAP, also the CIRPAS atmospheric measurement suite, the Picarro GHG sensor and the LGR CO<sub>2</sub> isotope analyser were onboard the CIRPAS TO.



In Table 10 and Table 11, the campaign activities of the MAMAP instrument on board the CIRPAS Twin Otter are further detailed and a first assessment about the quality of the data and its suitability for further analysis/flux inversion is given.

#	Target	30.5	3.6	4.6	9.6	12.6	13.6
T1	Kern Front and Kern River Oil Field		x		x		x
T2	Elk Hills Oil Field						
T3	North Belridge and South Belridge Oil Field						
T4	Midway Sunset Oil Field						
T5	Buena Vista Oil Field						
T6	Olinda Alpha Landfill						
T7	Puente Hills Landfill					x	
T8	Scholl Canyon Landfill						
T9	BKK Landfill						
T10	Harris Cattle Ranch / Feed Lot	x					
T11	Chino Cattle Rancho / Feed Lot					x	
T12	Los Angeles Basin Survey						
T13	Coal Oil Point Seep Field			x			
T14	La Brea Tar Pits						
T15	Baldwin Hills Oil Field						
T16	Carson Refinery						
T17	Tesoro Refinery						

no XCH <sub>4</sub> signal			T13			
no wind or too extreme change in wind direction	T10					
patchy XCH <sub>4</sub> pattern					T7,T11	
flight was within PBL					T7,T11	
just fly-by						

Table 10: Flights performed in May/June 2014 by MAMAP/CIRPAS and initial indication about plume signals detected and suitability for further data analysis. Days and targets which are marked in green are suitable for emission rate estimates and are proposed to be analysed further with high priority. Days and targets which are marked in red are not suitable for an emission rate estimate because of e.g., no XCH<sub>4</sub> signal, no wind, etc.. The overall quality of the MAMAP data is good.

#	Target	21.8	23.8	25.8	26.8	27.8	28.8	29.8	1.9	2.9	3.9	4.9
T1	Kern Front and Kern River Oil Field	x			x					x		x
T2	Elk Hills Oil Field		x									
T3	North Belridge and South Belridge Oil Field		x									
T4	Midway Sunset Oil Field		x									
T5	Buena Vista Oil Field		x									
T6	Olinda Alpha Landfill					x	x		x		x	
T7	Puente Hills Landfill					x	x					
T8	Scholl Canyon Landfill					x						
T9	BKK Landfill						x		x			
T10	Harris Cattle Ranch / Feed Lot											
T11	Chino Cattle Ranch / Feed Lot										x	
T12	Los Angeles Basin Survey							x				
T13	Coal Oil Point Seep Field			x								
T14	La Brea Tar Pits					x						
T15	Baldwin Hills Oil Field					x						
T16	Carson Refinery							x				
T17	Tesoro Refinery							x				

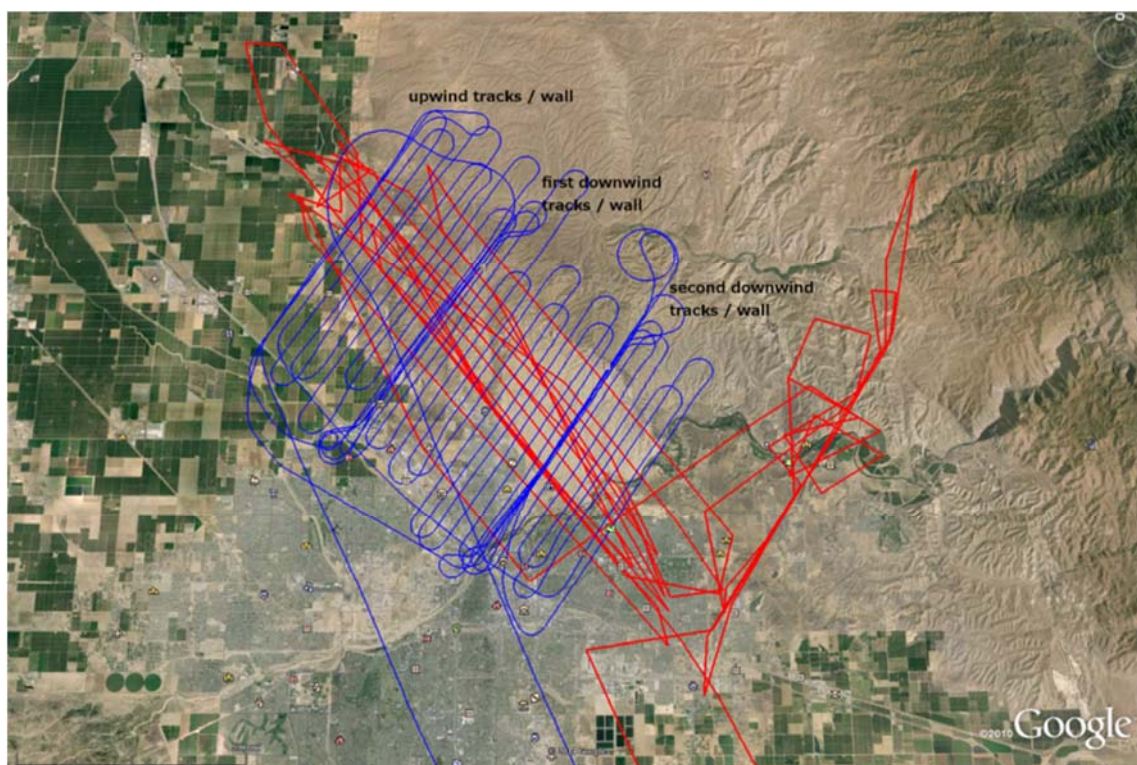
no XCH4 signal		T2,T3, T4,T5	T13		T1,T14, T15,T7			T9				
no wind or to extrem change in wind direction	T1						T12,T16, T17					
patchy XCH4 pattern					T7	T7				T11		
flight was within PBL												
just fly-by						T9						

Table 11: Flights performed in August/September 2014 by MAMAP/CIRPAS and initial indication about plume signals detected and suitability for further data analysis. Days and targets which are marked in green are suitable for emission rate estimates and are proposed to be analysed further with high priority. Days and targets which are marked in red are not suitable for an emission rate estimate because of e.g., no XCH<sub>4</sub> signal and/or no wind, etc. The overall quality of the MAMAP data is good.

## 6. Examples of Collected Data


In the following, to give an impression on the data quality based on quick look data analysis; initial results are presented for one selected campaign day. The selected day is the 04.09.2014 when a coordinated flight with the CIRPAS Twin Otter (MAMAP, NASA AMES in-situ Picarro, LGR isotopic ICOAS), the Twin Otter International (AVIRIS-NG) and AMOG Surveyor (LGR ICOS instruments) was performed in the afternoon (around 13:40 to 17:00 local time) over the Poso Creek, Kern Front and Kern River Oil Fields (T1) (see Figure 15).

In a first step, the CIRPAS Twin Otter gathered remote sensing data with MAMAP (also compare to Figure 16) at a flight altitude of around 2100 m whereas also the in-situ instruments took measurements. In a second step, in-situ data within the boundary layer were collected by flying three walls, one upwind and two downwind of the assumed source(s), perpendicular to the wind direction (north-west) (compare to Figure 15).



*Figure 15: Flight pattern of the CIRPAS Twin Otter (blue line) and the Twin Otter International with AVIRIS-NG (red line) over Poso Creek, Kern Front and Kern River Oil Fields on 04.9.2014. The Twin Otter International flight track is exported from NASA's Mission Tools Suite which provides it only with a low temporal resolution. The brighter areas in the middle of the picture are the Oil Fields. Wind direction is north-west. Topography map underneath is provided by Google Earth.*

During this flight, the weather was dominated by clear sky conditions and wind speeds of around 4.5 m/s from NW. A documentation of all campaign days can be found in Annex 2. Two examples with additional details can be found in chapter 6.1.

	<p style="text-align: center;"><b>COMEX</b></p> <p style="text-align: center;"><b>Final Report</b></p>	<p style="text-align: right;">Version: 2.0 Doc ID: IUP-COMEX-FR Date: 3. July 2016</p>
--	--	--

## 6.1. Quick look processing

After each flight, the team performed a quality check on the raw data, normally on the same day, to determine data quality sufficiency. A quick look data analysis up to concentration maps was performed for all targets typically also on the same day (for the de-briefing) to verify data quality and to decide if the flight could be declared as successful. Quick look CIRPAS/MAMAP/Picarro data from selected targets were distributed to the entire COMEX team within some days.

### Data saving and quick looks MAMAP instrument (onboard CIRPAS TO)

During measurements, MAMAP data were saved on different solid state disks of the instrument (separate for O<sub>2</sub>, CH<sub>4</sub>/CO<sub>2</sub>, and camera/gyro). Correct functioning of the instrument was ensured in-flight by the operator checking the recorded spectra. Additionally, a newly developed MAMAP real time retrieval performed the data processing already during flight and stored the XCO<sub>2</sub> or XCH<sub>4</sub> dry column ratio in a kml file. This kml file could be viewed in Google Earth and was refreshed every two seconds. The operator was then able to adapt the flight path based on the current measurements and signals / dry column ratios. This data was also presented during de-briefing.

Raw data were downloaded post flight and stored on at least one hard drive and three different USB-sticks (separate for O<sub>2</sub>, CH<sub>4</sub>/CO<sub>2</sub>, and camera/gyro) at different locations. Higher quality quick looks in form of quality filtered geo-referenced qualitative total column information as kmz-file using a generic radiative transfer model simulation were typically available within a few days at latest, depending on maintenance and calibration work to be conducted at the instrument and distributed to the COMEX team.

Figure 16 shows an example quick look of XCH<sub>4</sub> data from the Kern Front and Kern River Oil Field flight on 2014-09-04, where the source location is not well known (see also above) and Figure 17 shows an example quick look of XCH<sub>4</sub> data from the Olinda Alpha Landfill within the Los Angeles Basin where the source location can be constraint. All quick looks of the MAMAP data (Figure 16, Figure 17, Figure 22, Annex 2) are normalized by a 300-point moving average and smoothed by a 3-point moving average (as also provided in the data acquisition report of C-MAPEXp (RD-7)). For a qualitative analysis of the MAMAP data (plume: yes or no), the 300-point moving average is sufficient in order to remove the effect of a changing solar zenith angle during the measurement (when using one radiative transfer model).





# COMEX Final Report

Version: 2.0  
Doc ID: IUP-COMEX-FR  
Date: 3. July 2016

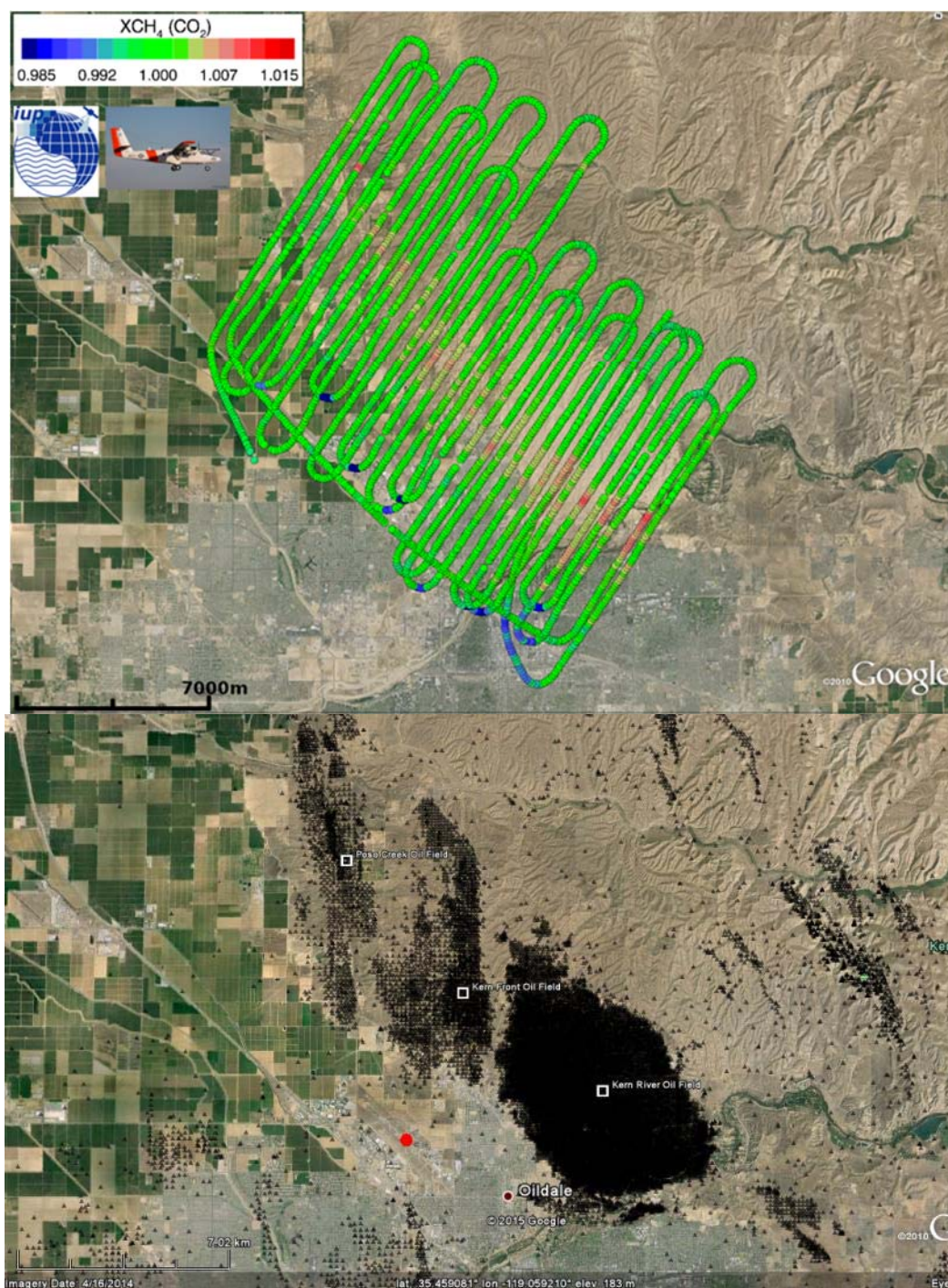


Figure 16: Top: MAMAP flight pattern and quick-look analysis of Poso Creek, Kern Front and Kern River Oil Field (rectangles) on 2014-09-04, between 13:40 and 15:50 local time. Flight altitude was around 2100m above sea level. Surface elevation is around 200m above sea level. The  $CH_4$  plume(s) are visible as an enhancement in the  $XCH_4$  dry column ratio. Bottom: The black triangles mark the positions of wells in the areas of the three Oil Fields. Wind direction was north-west and the wind speed was between 3.5 and 5.5m/s (wind speed is based on data of the Meadows Field Airport- KBFL (red dot) which is located at the western edge of the oil field and is in good agreement with the in-situ data taken by the CIRPAS aircraft (compare to Figure 21). Topography map underneath is provided by Google Earth. Quick look data is not filtered for inclination, therefore artefacts in the data during turns of the aircraft due to insufficient levelling could occur.



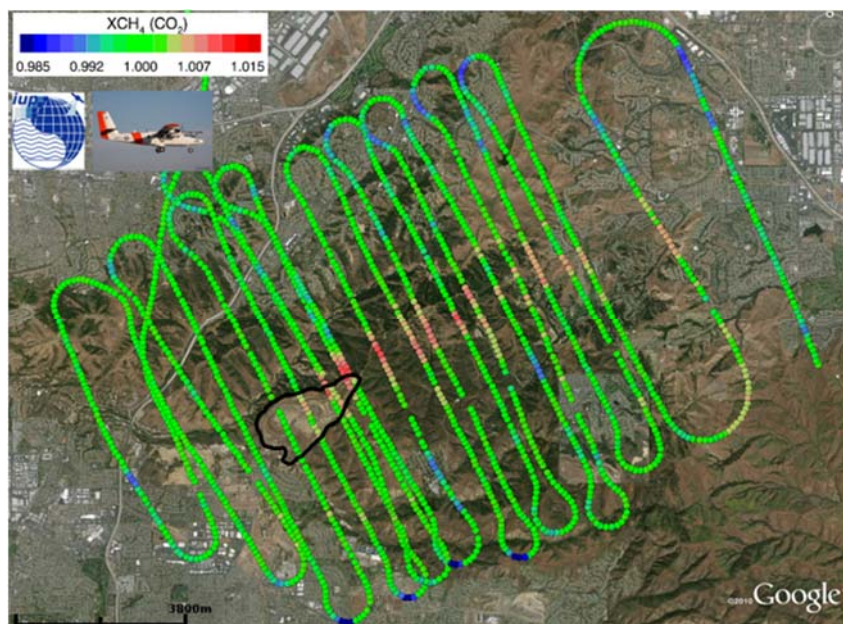


Figure 17: MAMAP flight pattern and quick-look analysis of the Olinda Alpha Landfill (enclosed by black line) on 2014-09-01, between 15:00 and 16:00 local time. Flight altitude was around 1800m above sea level. Surface elevation is around 300m above sea level. The CH<sub>4</sub> plume is visible as an enhancement in the XCH<sub>4</sub> dry column ratio. Wind direction was south-west and the wind speed was between 4.0 and 5.0m/s. Topography map underneath is provided by Google Earth. Quick look data is not filtered for inclination, therefore artefacts in the data during turns of the aircraft due to insufficient levelling could occur.

The results of the quick-look data screening are summarised in Table 10 and Table 11. Additionally, the quick-look data of the remaining flight days/targets for the MAMAP instrument are shown in Annex 2.

#### Quick looks Picarro GHG sensor (onboard CIRPAS TO)

All data are saved on a solid state disk during flight. After the flight, raw data are downloaded and stored on at least one hard drive and one USB-stick at different locations. Quick looks in form of geo-referenced (latitude, longitude, and flight altitude) kmz-files of the three main quantities dry gas mixing ratio of CH<sub>4</sub> and CO<sub>2</sub>, and H<sub>2</sub>O from selected targets are produced within 2 days.

As the in-situ Picarro instrument is operated by NASA AMES, but the quick looks and a first quality check is performed by the IUP Bremen, a more quantitative analysis of the data set in cooperation with NASA AMES is required. Two major points have been recognized so far:

- a) Possible overheating of the instrument which can lead to wrong XCH<sub>4</sub>, XCO<sub>2</sub>, and H<sub>2</sub>O values potentially occurring at one flight.
- b) Geo-location correction due to a time lag in the measurements (time which the air sample needs from the inlet in the aircraft to the Picarro instrument and actual measurement, respectively) leads to a shift of the single data points in flight direction.

A quick-look example for the Poso Creek, Kern Front and Kern River Oil Field flight on 2014-09-04 is given in Figure 18. On that day three walls were flown, one upwind and two downwind walls. Each wall consists of several measurement legs at different altitudes:

- Upwind wall: 1: 470m, 2: 770m
- 1. Downwind wall: 1: 500m, 2: 790m, 3: 1050m, 4: 1340m, 5: 1640m
- 2. Downwind wall: 1: 490m, 2: 760m, 3: 1020m, 4: 1300m, 5: 1630m

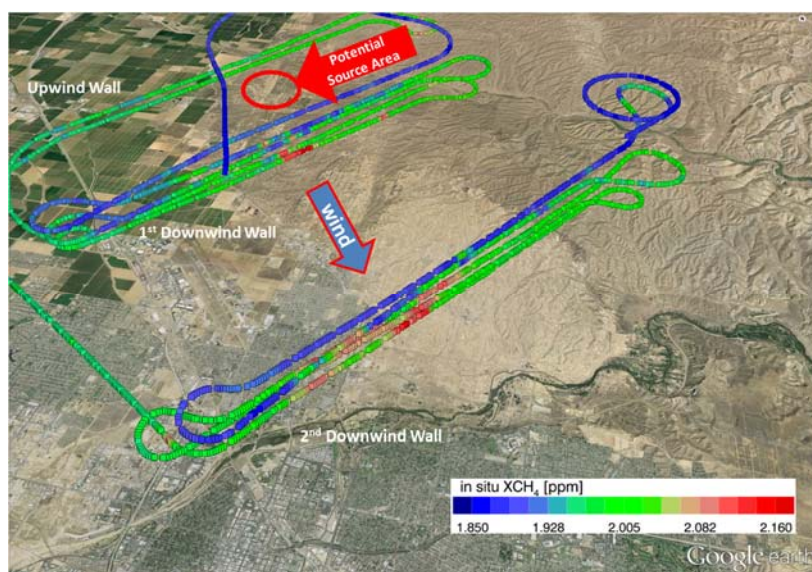


Figure 18: Subsequent airborne in-situ only measurements performed with the CIRPAS aircraft for validation of the collected remote sensing data. The color code depicts dry gas mixing ratios of  $\text{CH}_4$ . The in-situ data shows distinct methane enhancements (white color  $>2.10\text{ppm}$ ) over the oil field as measured during two vertical soundings at two downwind distances from the expected source areas. The upwind vertical sounding indicates no methane influx from outside the area. Measurement was performed on the 2014-09-04, between 15:50 and 17:00 local time. Topography map underneath is provided by Google Earth.

These measurements can also be depicted as vertical profiles as shown in Figure 19 and used to estimate a planetary boundary layer for the time of the measurement on the 2014-09-04. These profiles consist of measurements starting with the last leg of the remote sensing measurements at around 2100 m above sea level and ending with the lowest leg of the second in-situ wall at around 490 m. Hence, these measurements were directly recorded after the remote sensing measurement part and allow performing a rough estimate of the planetary boundary layer height to be proximately 1400 m.

#### Data handling and quality check CIRPAS atmospheric measurement suite (onboard CIRPAS TO)

The CIRPAS instrumentation was supervised by the CIRPAS scientists. The data was processed by CIRPAS scientists within a few days after a flight and distributed to the team.

As an example, Figure 20 depicts verticals profiles of the ambient dew point temperature and the particle concentration and Figure 21 shows vertical profiles of the relative humidity and wind speed for the Kern River and Kern Front Oil Field flight on the 2014-09-04. Based in these profiles, the planetary boundary layer height is estimated in agreement with the vertical profiles from the Picarro in-situ greenhouse gas analyzer (Figure 19) to be around 1400 m. Hence, it could be confirmed, that the aircraft altitude chosen for the remote sensing measurements was as required above the planetary boundary layer on that particular day.

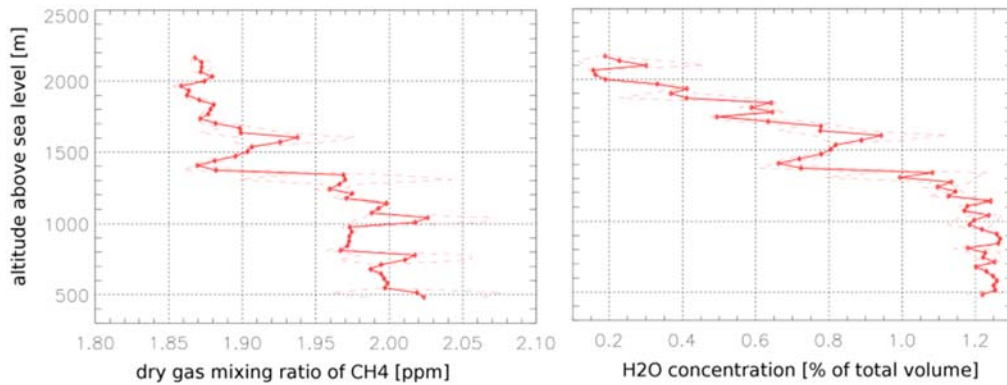


Figure 19: Shown are vertical profiles of the dry gas mixing ratio of  $\text{CH}_4$  (left) and the  $\text{H}_2\text{O}$  concentration recorded by NASA's Ames greenhouse gas analyser as a solid red line. The profiles consist of altitude binned (33m) measurements starting with the last leg of the remote sensing measurements at around 2100m above sea level and ending with the lowest leg of the second in-situ wall at around at around 490m. The dashed lines give the  $1-\sigma$  variability within each binned interval.

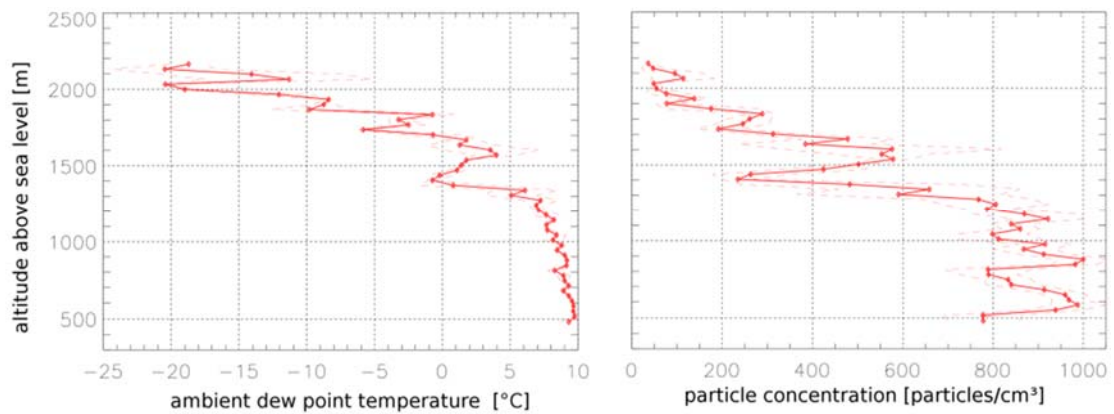


Figure 20: Similar to Figure 19 but for measurements taken by the CIRPAS instrumentation. Shown are vertical profiles of the ambient dew point temperature (left) and the particle concentration (right).

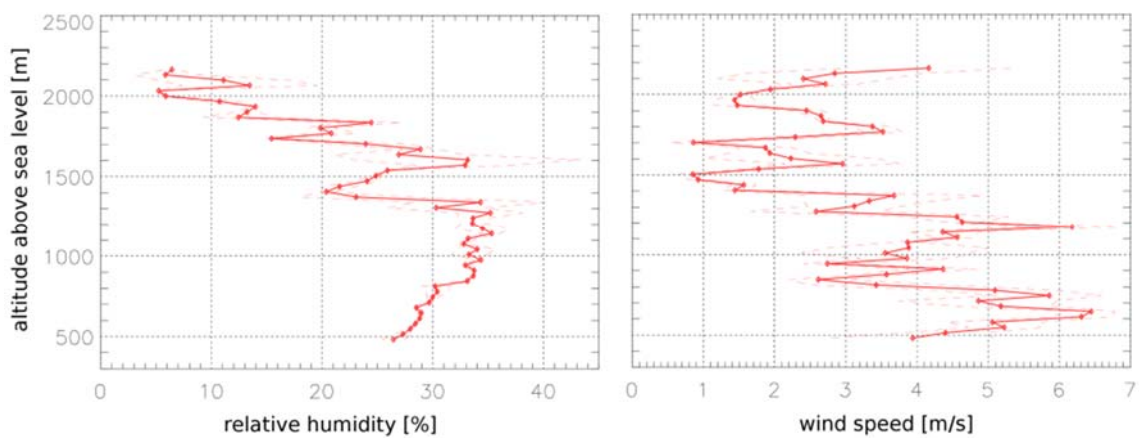


Figure 21: Similar to Figure 19 but for measurements taken by the CIRPAS instrumentation. Shown are vertical profiles of the relative humidity (left) and the wind speed (right).



### Data handling LGR CO<sub>2</sub> isotope analyzer (onboard CIRPAS TO)

The LGR instrument (engineering flights) was supervised by the IUP Bremen team. Data was stored on a USB-stick immediately after each flight and sent to the LGR scientists. No processed and geolocated data actually provided by LGR.

### Data handling AVIRIS-C (onboard ER-2) and AVIRIS-NG (onboard TOI)

The NASA instruments were supervised by the NASA scientists. Quick looks of selected flights were available within days after the flight. An example of the processed AVIRIS-NG data is shown in Figure 22, with MAMAP data overlayed. The AVIRIS-NG data allows pinpointing to the potential origin of the fugitive CH<sub>4</sub> emissions detected by MAMAP. AVIRIS-NG Processed data (as JPG and PNG) of 3 Kern flights is actually made available by JPL to IUP for data overlays with MAMAP processed data (for more details, see Section 9.4).

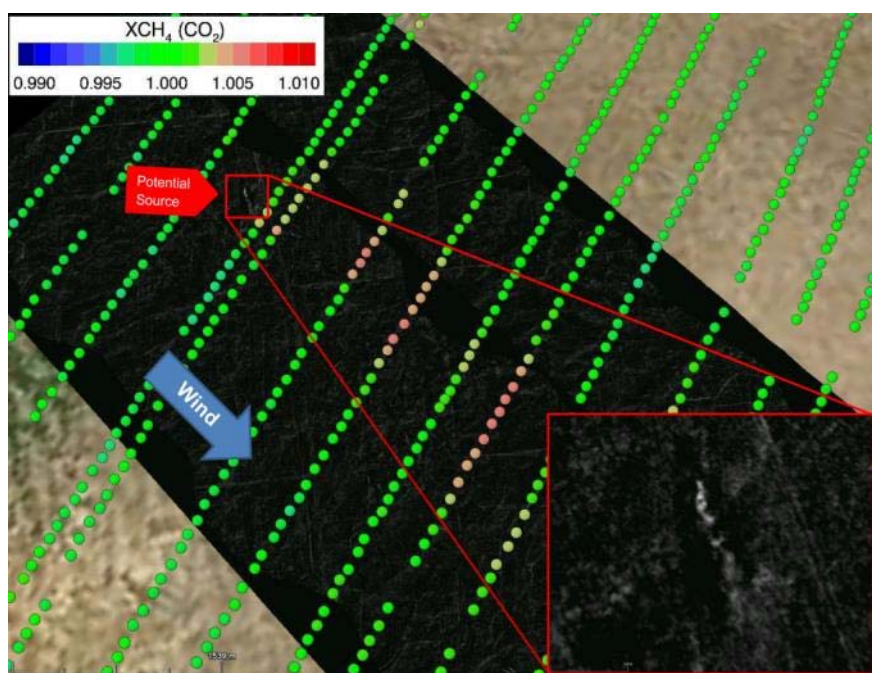



Figure 22: Overlay of MAMAP and AVIRIS-NG remote sensing data as collected during COMEX over the Poso Creek, Kern Front and Kern River Oil Fields (T1) on the 2014-09-04 showing the position of one prospective methane source, potentially responsible for substantial parts of the large scale plume as measured by MAMAP. Inset: AVIRIS-NG methane column map of a localized emission plume. Credits: University of Bremen; NASA's Jet Propulsion Laboratory, California Institute of Technology.

	<p style="text-align: center;"><b>COMEX</b> <b>Final Report</b></p>	<p style="text-align: right;">Version: 2.0 Doc ID: IUP-COMEX-FR Date: 3. July 2016</p>
---	---	--

## 7. Processing of campaign data

The campaign data set is divided into 3 independent parts (primarily analyzed by the IUP), the CIRPAS in-situ data set (meteorological parameters), the Picarro in-situ data set ( $\text{CH}_4$ ,  $\text{CO}_2$ , and  $\text{H}_2\text{O}$  mixing ratios), and the MAMAP remote sensing data set (total column information of  $\text{CH}_4$  and  $\text{CO}_2$ ). Beside that and additionally to the provided AVIRIS-NG flight lines by JPL, also part of the AVIRIS-NG data set is analyzed by the IUP with an adapted version of the MAMAP retrieval algorithm (for more details, see Chapter 7.1 and Chapter 11).

Usually a target survey with the CIRPAS aircraft was divided in two parts. First, MAMAP remote sensing measurements were taken flying above the boundary layer, with the Picarro and the CIRPAS in-situ instruments also collecting data. Next, the CIRPAS aircraft penetrated into the boundary layer to probe it with its in-situ instruments only for validation of the MAMAP remote sensing data. This flight pattern was chosen due to flight time considerations and also to avoid thermal stability disturbance of the remote sensing instrumentation due to the very high ambient temperatures inside the boundary layer at many of the targets.

In the following, the processing of the different data sets is explained.

### 7.1. The MAMAP remote sensing data

This section describes the processing of the MAMAP data. In the first part, the MAMAP retrieval algorithm is described in general and in the second part, the retrieval is applied to the COMEX MAMAP data set.

#### 7.1.1. The MAMAP retrieval algorithm in general

The data processing of the MAMAP campaign data has used the already developed and tested tools as described in RD-1, RD-2, RD-5 and RD-6 and the C-MAPEX Final Report (RD-8). For the processing of MAMAP data, a modified version of the Weighting Function Modified Differential Optical Absorption Spectroscopy (WFM-DOAS) algorithm has been used to obtain vertical column information of  $\text{CH}_4$ ,  $\text{CO}_2$  (and  $\text{O}_2$ ) (Level 1 data product).

It is based on a least squares fit of the logarithmic simulated radiance spectrum to the measurements after correction for dark signal and pixel-to-pixel gain. The fit parameters are:

- 1 atmospheric parameters of interest: partial or total columns of  $\text{CH}_4$ ,  $\text{CO}_2$  and  $\text{O}_2$ ,
- 2 additional trace gas atmospheric parameters for spectrally interfering gases (water vapor),
- 3 other atmospheric parameters (temperature),
- 4 a low order polynomial (usually of the second or third order) in the spectral domain to account for spectrally smooth varying parameters which are not explicitly modelled or less well known. These parameters include, for example, the MAMAP absolute radiometric calibration function, aerosol scattering and absorption parameters, and the surface spectral reflectance,
- 5 and shift and squeeze parameters from an iterative spectral calibration procedure.

The results of the algorithm are profile scaling factors for the respective trace gases. Model radiances and required weighting functions that refer to the sensitivity of model radiances to individual fit parameters are computed with the radiative transfer model SCIATRAN using the HITRAN 2008 spectroscopic data base.

For the interpretation of the MAMAP measurements with respect to sources and sinks of the greenhouse gases  $\text{CO}_2$  and  $\text{CH}_4$ , the column averaged dry air mole fractions (in ppm for  $\text{CO}_2$  or ppb for  $\text{CH}_4$ ) are the preferred quantity rather than the total columns (in molecules  $\text{cm}^{-2}$ ). This is because dry



air mole fractions are less affected by changes in surface topography, pressure and flight altitude compared to the absolute column.

Dry air mole fractions ( $XCH_4$ ,  $XCO_2$ ) from MAMAP column data are generally obtained by using a proxy method. Assuming light path errors at different wavelengths to cancel,  $XCH_4$  can be computed by using  $CO_2$  as a reference and vice versa.  $O_2$  can be used as reference as well but, due to the larger spectral distance, correlation between light paths can be slightly worse in comparison (Krings et al. 2011).

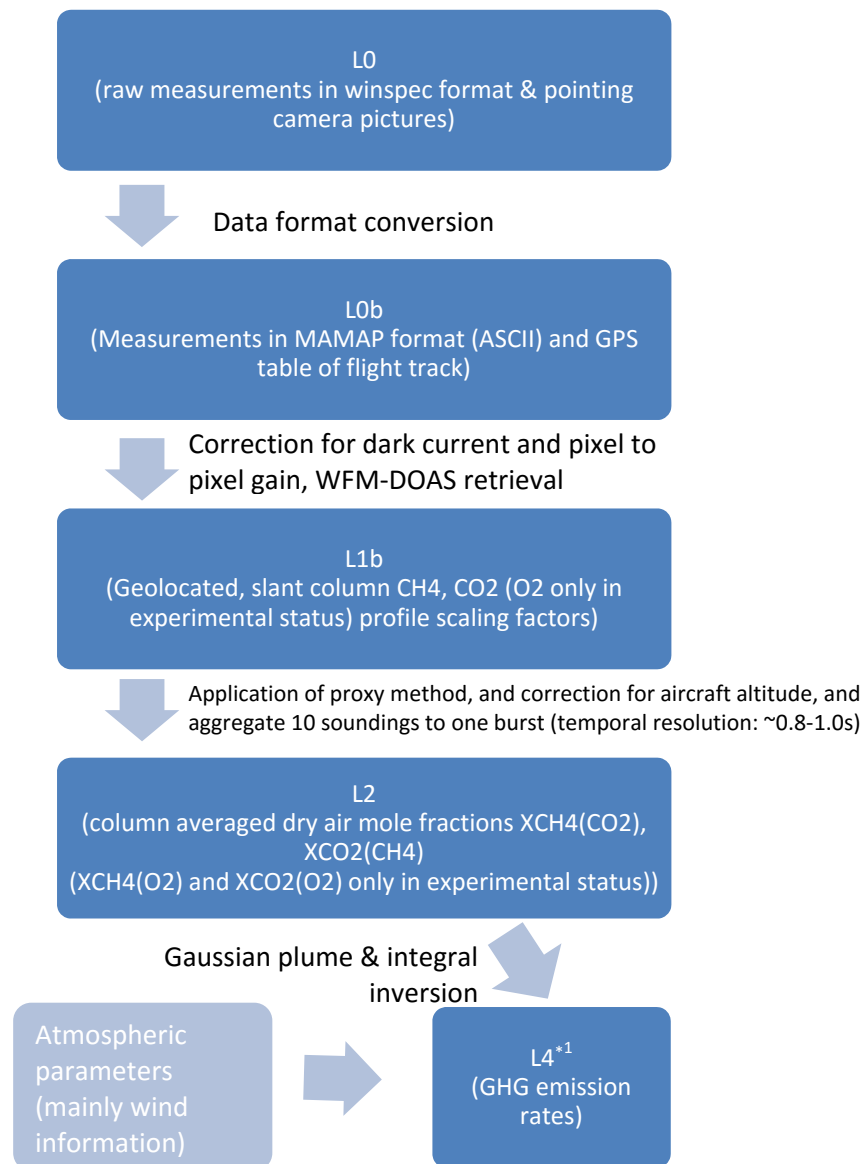



Figure 23: Data processing scheme for MAMAP data. (\*in accordance with the CarbonSat specifications)

The MAMAP WFM-DOAS retrieval does not resolve different altitude levels. However, the retrieval has different sensitivities for different altitudes. This behavior can be characterized by the so called column averaging kernels (AK). Below the aircraft, the averaging kernels are increased by a factor of about 2 (for low aircraft altitudes) compared to above the aircraft. This is due to the fact that light from the sun passes through the absorber below the aircraft twice - once before and once after surface reflection. The higher the aircraft flies, the less pronounced the effect becomes, since the height averaged AK are about unity (see RD-1, RD-2 and RD-5).

	<p style="text-align: center;"><b>COMEX</b> <b>Final Report</b></p>	<p style="text-align: right;">Version: 2.0 Doc ID: IUP-COMEX-FR Date: 3. July 2016</p>
--	---	--

For a typical MAMAP measurement, variations in trace gas concentrations can be expected mainly below the aircraft due to activity at the surface, for example, power plants emitting CO<sub>2</sub> or landfills releasing CH<sub>4</sub>. Since the retrieval is not height sensitive, the measurements will be weighted with the mean averaging kernel (ideally being close to unity). If the concentration changes occur equally at all altitude levels, this will deliver the correct result. If concentration changes occur below the aircraft only, this has to be accounted for in the final Level 2 product, for instance, by a conversion factor. Otherwise, the column averaged mole fraction variations from the retrieval appear about a factor of 2 larger, as they actually are (see RD-1, RD-2, RD-5).

### 7.1.2. The MAMAP retrieval algorithm for the COMEX data set

The COMEX campaign (flights over the SJV area, greater LA and Santa Barbara) focused mainly on CH<sub>4</sub> emitting targets with large uncertainties of the reported CH<sub>4</sub> emissions. It has been assumed for all targets, that co-emitted CO<sub>2</sub> could be neglected in the retrieval due to the (with respect to mass) 500 times higher sensitivity of MAMAP to CH<sub>4</sub> in comparison to CO<sub>2</sub>. Therefore, the column averaged dry air mole fraction of CH<sub>4</sub> has been retrieved using CO<sub>2</sub> as a proxy: XCH<sub>4</sub>(CO<sub>2</sub>). To what extent this assumption is valid, is discussed in Sections 9.2.3 and 9.3.3. The validity of this assumption as well as the impact of co-emitted CO<sub>2</sub> on estimated fluxes will be analyzed by co-located airborne Picarro in-situ measurements for targets, for which fluxes are estimated.

To account for different atmospheric conditions and viewing geometries, a separate reference radiative transfer has been simulated by the radiative transfer model SCIATRAN for each target (see Table 1). Important input parameters are:


- a) **Mean solar zenith angle (SZA):** Calculated from the local time of the measurements.
- b) **Mean flight altitude:** Calculated from the Global Positioning System (GPS) coordinates of measurements.
- c) **Mean surface elevation:** Based on the SRTM digital elevation model (Shuttle Radar Topography Mission (SRTM) version 2.1, [http://dds.cr.usgs.gov/srtm/version2\\_1/](http://dds.cr.usgs.gov/srtm/version2_1/)) having a spatial resolution of one arc second in the U.S.A. (around 30 m at the equator).
- d) **Aerosol scenario:** A standard OPAC urban aerosol scenario has been used as in RD-2. This can be further refined in further studies using the CIRPAS in-situ aerosol measurements. It is expected, that small deviations of the aerosol scenario from the (for the RMT) assumed are captured for the measurements by the slope of the low order polynomial used in the retrieval.
- e) **Surface spectral reflectance / albedo:** For each target the surface type has been roughly estimated based on the IGBP Land Ecosystem Classification map (<http://modis-atmos.gsfc.nasa.gov/ECOSYSTEM/browse.html>). Subsequently, for each surface type, an albedo has been selected from the values derived in Sun-Mack et al. (2004), which are based on measurements in the 1.6 μm channel of the Moderate Resolution Imaging Spectrometer (MODIS) on-board the Terra satellites, and the Visible Infrared Scanner (VIRS) on-board the Tropical Rainfall Measuring Mission (TRMM) spacecraft. It is expected, that small deviations of the surface spectral reflectance from the values assumed for the RTM are captured by the low order polynomial of the retrieval.
- f) **Background profiles of CH<sub>4</sub> and CO<sub>2</sub>:** The U.S. standard atmosphere (U.S. Committee on Extension to the Standard Atmosphere, 1976) has been used, which has been scaled based on in-situ measurements of CH<sub>4</sub> and CO<sub>2</sub> collected with the Picarro instrument aboard of CIRPAS. In order to scale the U.S. standard atmosphere to current conditions, the CO<sub>2</sub> and CH<sub>4</sub> in-situ measurements were utilized in then following way: First the atmosphere was divided into the boundary layer and the free troposphere based on the CIRPAS atmospheric measurements suite (mainly UFCPC, ambient dew point, potential temperature). For each section, free

troposphere and boundary layer, the median for CH<sub>4</sub> and CO<sub>2</sub> was calculated from the in-situ measurements. Subsequently, these values were used to scale the U.S. standard atmosphere profiles of CO<sub>2</sub> and CH<sub>4</sub>.

	sza		aa		surelv*		aerosol	albedo	XCO <sub>2</sub>	XCH <sub>4</sub>	CV
	mean	std	mean	std	mean	std	type	[-]	[ppm]	[ppb]	
	[°]	[°]	[m]	[m]	[m]	[m]	[-]	[-]			
20140530											
HR	28,1	2,2	1737	13,1	155	57,4	urban	0,40	399,0	1820,7	0,57
20140603											
KOF	25,7	2,8	1431	10,8	206	63,3	urban	0,31	400,0	1779,6	0,55
20140604											
COP*	14,5	2,7	1404	4,9	0	6,9	urban	glint	399,3	1807,8	0,54
20140609											
KOF	30,5	6,1	1811	13,6	215	85,0	urban	0,31	401,1	1827,8	0,57
20140612											
PHL	13,3	1,2	1111	4,4	150	4,4	urban	0,31	401,9	1792,4	0,52
CF	12,8	1,9	1109	5,6	220	69,0	urban	0,31	401,9	1792,4	0,52
20140613											
KOF	17,1	4,4	1721	6,8	197	73,9	urban	0,31	398,5	1807,7	0,55
20140821											
KOF	26,6	3,5	2395	14,0	213	63,3	urban	0,31	394,3	1775,7	0,60
20140823											
MS,EH,B,BV	26,9	2,7	2100	67,7	249	164,1	urban	0,40	393,3	1787,4	0,58
20140825											
COP*	28,4	5,0	2068	13,2	0	4,7	urban	glint	389,3	1793,2	0,59
20140826											
KOF	38,2	4,8	2086	61,6	211	61,6	urban	0,31	390,5	1797,4	0,60
20140827											
LB_BH	32,9	1,0	1785	2,3	81	68,0	urban	0,22	396,6	1747,6	0,58
SCL	28,6	1,3	1773	15,6	304	114,0	urban	0,31	396,6	1747,6	0,57
PHL	24,2	0,4	1228	10,4	148	70,3	urban	0,31	396,6	1747,6	0,54
OAL	33,4	2,1	1971	55,6	245	97,0	urban	0,31	396,6	1747,6	0,58
20140828											
OAL	35,4	2,2	1627	10,7	246	92,4	urban	0,31	396,0	1750,6	0,57
PHL	48,2	1,3	1467	11,4	166	84,8	urban	0,31	396,0	1751,9	0,59
20140829											
LA	29,4	2,9	2112	19,7	32	47,5	urban	0,22	392,7	1764,8	0,60
20140901											
BKKL	35,9	1,3	1771	14,8	162	50,7	urban	0,31	391,4	1801,6	0,58
OAL*	44,6	3,8	1794	15,9	283	75,6	urban	0,31	391,4	1801,6	0,59
20140902											
KOF	39,8	7,1	2111	18,8	221	64,6	urban	0,31	392,0	1826,1	0,60
20140903											
OAL	29,8	1,5	1945	12,5	279	77,2	urban	0,31	392,7	1797,4	0,57
CF	50,7	6,7	1778	13,5	209	12,5	urban	0,31	395,8	1787,3	0,61
20140904											
KOF*	38,3	5,7	2117	14,0	201	58,8	urban	0,31	392,2	1810,5	0,60

Table 12: Summary of the parameters used in the radiative transfer model for each target (sza: solar zenith angle, aa: flight altitude, surelv: surface elevation, CV: conversion factor). HR: Harris Ranch (T10), KOF: Kern Front and River Oil Field (T1), COP: Coal Oil Point (T13), PHL: Puente Hills Landfill (T7), CF: Chino Feedlot (T11), MS: Midway Sunset Oil Field (T4), EH: Elk Hills Oil Field (T2), B: North and South Belridge Oil Field (T3), BV: Buena Vista Oil Field (T5), LB: La Brea Tar Pits (T14), BH: Baldwin Hills Oil Field (T15), SCL: Scholl Canyon Landfill (T8), OAL: Olinda Alpha Landfill (T6), LA: Los Angeles Basin Survey (T12), BKKL: BKK Landfill (T9). All altitudes are given in meters above mean sea level (mamsl). \*for these targets a look-up table (LUT) approach is used. \*310 mamsl and 210 mamsl have been used for all OAL and KOF flights, respectively. Reference to the target number (Tx) can be found in Annex 1.

For the four targets Coil Oil Point on 2014-06-04 and 2014-08-25, Olinda Alpha Landfill (OAL) on 2014-09-01, and Poso Creek, Kern River and Kern Front Oil Fields (KOF) on 2014-09-04, a more accurate approach was implemented. The radiative transfer models used for these targets were interpolated using a two dimensional look-up table (LUT) based on solar zenith angle and surface elevation (see Section 9.2.1 and 9.3.1). For the Coal Oil Point (COP) offshore measurements SCIATRAN was operated

	<p style="text-align: center;"><b>COMEX</b> <b>Final Report</b></p>	<p style="text-align: right;">Version: 2.0 Doc ID: IUP-COMEX-FR Date: 3. July 2016</p>
--	---	--

in a dedicated glint mode to account for solar spectral reflectance / sun glint on the sea surface (see also Section 10).

Areal plots of the normalized column averaged dry air mole fractions derived from the MAMAP remote sensing surveys of all COMEX flights can be found in Annex 2.

## 7.2. The CIRPAS in-situ data set

The CIRPAS aircraft meteorological suite delivers various kinds of meteorological parameters. They are used to characterize the atmosphere, especially the boundary layer, and are also used as input parameters for estimates of  $\text{CH}_4$  (and  $\text{CO}_2$ ) emissions, based on data obtained by the MAMAP and Picarro instruments installed in addition for COMEX aboard the aircraft.

### Boundary layer

The lowest layer of the atmosphere, which pollutants, such as  $\text{CO}_2$  or  $\text{CH}_4$ , are emitted to, is called mixing layer or boundary layer. Normally, the boundary layer is separated from the layer above, the free troposphere, by a boundary which prohibits vertical movement of air parcels and, thus, exchange of air masses. The boundary layer is usually well-mixed due to solar heating at the surface and convection. Therefore, pollutants like aerosols but also water vapor is relatively constant with altitude and decreases in the free troposphere. Furthermore, the profiles of potential temperature and dew point temperature are generally constant with altitude, but increase and decrease in the free troposphere, respectively.

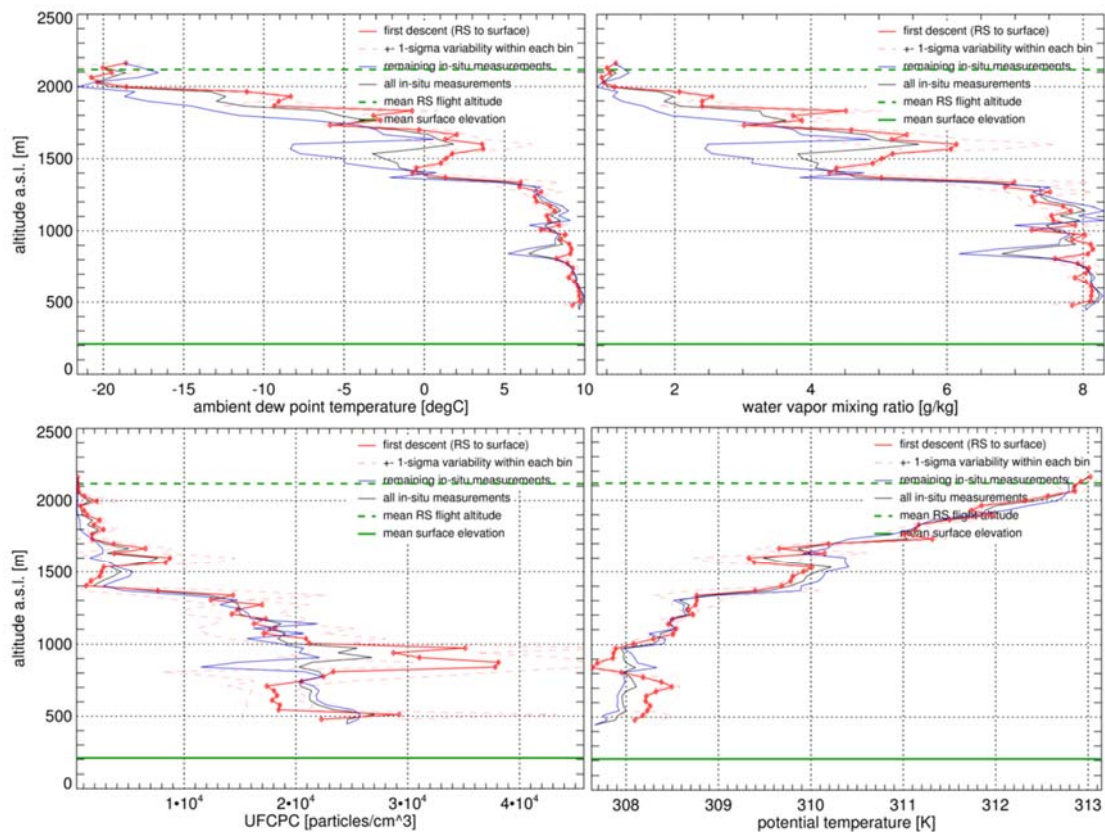



Figure 24: Shown are vertical profiles of ambient dew point temperature (upper left), water vapour mixing ratio (upper right), aerosol concentration from the Ultra Fine Condensation Particle counter (UFPCPC) (lower left), and potential temperature (lower right) recorded by the CIRPAS instrumentation during the Kern Front and Kern River Oil Field survey on 2014-09-04. All altitudes are given in meters above mean sea level (mamsl) (equal to a.s.l [m]). The profiles consist of altitude binned (33 m) measurements. Red depicts the first descent of the aircraft from remote sensing (RS) altitude at around 2117 mamsl to the lowest (in-situ) flight altitude at around 500 mamsl (it comprise CIRPAS measurements at remote sensing altitude and the subsequent in-situ wall, which was flown directly after the remote sensing data collection). Blue depicts the profile derived from the remaining in-situ measurements and black depicts all in-situ measurements.



	<p style="text-align: center;"><b>COMEX</b> <b>Final Report</b></p>	<p style="text-align: right;">Version: 2.0 Doc ID: IUP-COMEX-FR Date: 3. July 2016</p>
--	---	--

The boundary layer height has been estimated for each target individually based on the parameters aerosol concentration from the CIRPAS - Ultra Fine Condensation Particle Counter (UFCPC), ambient dew point temperature, potential temperature, water vapor mixing ration, and ambient temperature. Figure 24 shows an example for the Kern Front and Kern River Oil Fields survey on 2014-09-04. The upper limit of the boundary layer has been estimated to be around 1700 meters above mean sea level (mamsl) with an possible intermediate layer at around 1300 mamsl, and , thus, was well below the altitude of around 2117 mamsl, where remote sensing measurements with MAMAP were taken (remote sensing altitude).

Proximate boundary layer heights (derived in a similar way) for all targets are given in Annex 2.

### **Wind information**

Wind information for all CIRPAS flights was obtained by the CIRPA 5-hole turbulence probe. This information is needed for calculating the emission rate. Further details are given in Section 9, where fluxes of two targets are estimated. Whenever available, wind information from ground stations was also incorporated in the calculations.

For the two targets Olinda Alpha Landfill (OAL) on 2014-09-01 and Poso Creek, Kern River and Kern Front Oil Fields (KOF) on 2014-09-04, 3D wind fields can also be found in Annex 2. They give a more comprehensive picture of the wind situation at time of the overflight for these two targets.

### 7.3. The Picarro in-situ data set

The Picarro in-situ data set has been used estimating the emission rates of two targets (further details in Section 9) and to scale background atmospheric profiles for the radiative transfer model SCIATRAN used for the MAMAP retrieval (compare to Section 7.1.2).

For the Picarro in-situ instrument, a time lag  $t_{lag}$  between the actual concentration measurement and the position, where the air sample was taken, has been calculated. This time lag is induced by the time, an air sample needs to move from the inlet to the instrument through the sampling lines. A total instrument time lag (for the whole Picarro dataset) of around 16 seconds has been determined empirically based on flights where plume structures are observed. As an example, Figure 25 depicts the difference between a corrected and a not corrected data set for  $CO_2$  measurements and Figure 26 for the according  $CH_4$  measurements, respectively.

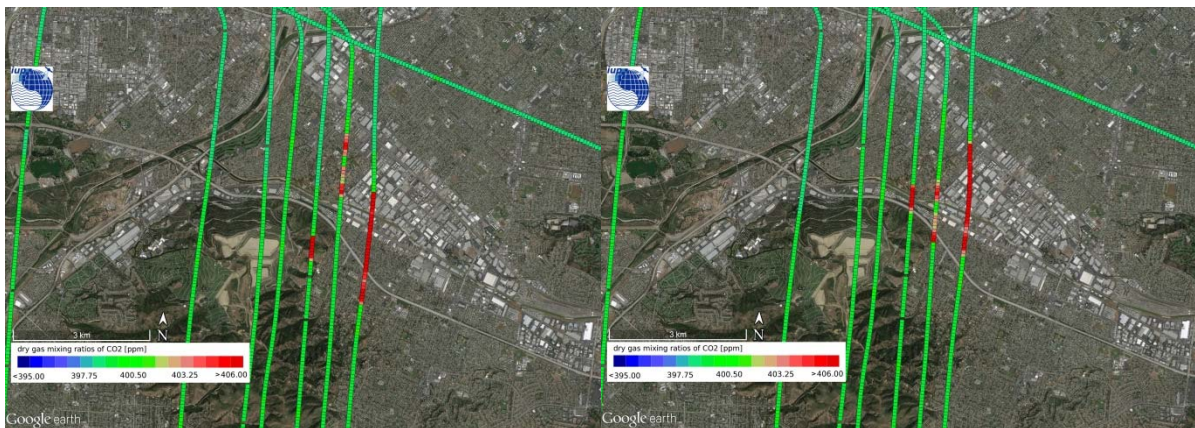


Figure 25: Picarro in-situ measurements of  $CO_2$  at remote sensing altitude over the Puente Hills Landfill on 2014-06-12. Left: Original data set. Right: By 16 s corrected data set.

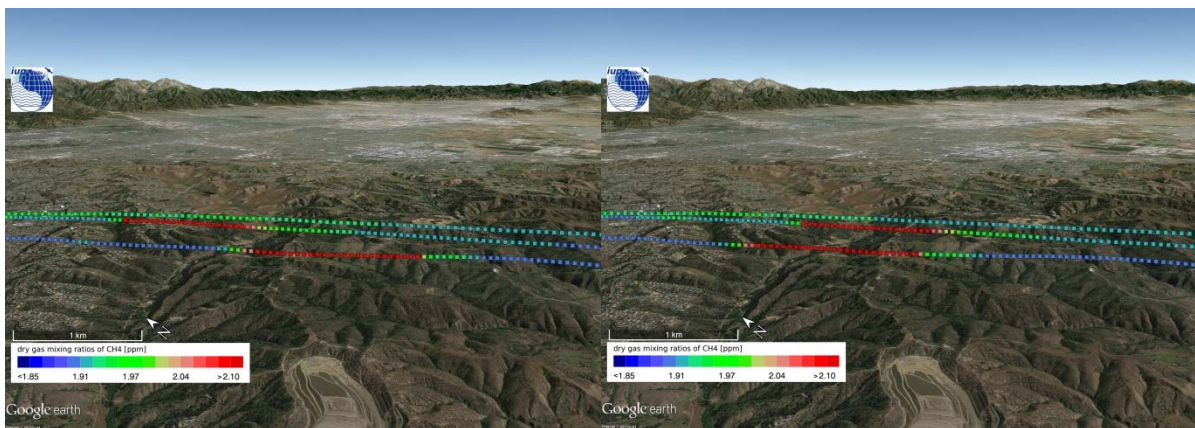


Figure 26: Picarro in-situ measurements of  $CH_4$  of one in-situ wall acquired at the Olinda Alpha Landfill at 2014-09-01. Left: Original data set. Right: Corrected data set with 16 s.

The dry gas mixing ratios plots of  $CH_4$  and  $CO_2$  of Picarro in-situ collected data for all flights can be found in Annex 2.

## 8. Data formats and data archive

### 8.1. Data Format MAMAP

For MAMAP obtained data products the following notation has been denoted:

- L0 data - raw measurements in winspec format and pointing camera pictures
- L0b data - measurements in MAMAP format (ASCII) + gps-table data of flight path. The MAMAP data is organized in a file which is structured by headers followed by the detector read outs pixel by pixel. The Level 0b data also contains dark current spectra and white light calibration spectra, both to be applied.
- L1b data - processed geo-located column data of CH<sub>4</sub> and CO<sub>2</sub> with an adapted SCIATRAN reference scenario for each target area, ASCII format.
- L2 data - geolocated XCH<sub>4</sub>(CO<sub>2</sub>) or XCO<sub>2</sub>(CH<sub>4</sub>) for one SCIATRAN reference scenario per target area/flight day, ASCII format. Each data file contains a header including the date of the measurement, description of the target, the background XCH<sub>4</sub> (or XCO<sub>2</sub>) value and a description of the data format. The data will be organized in columns and will at least cover data as specified in Table 13, but may include other auxiliary data.
- L3 data - Flux data for selected targets, ASCII format.

```
#####
# SPEC: 000001
# VERSION: 1.4.0 PROCESSED-ON: 2011-06-05
# FILENAME: open_98ms_10x1_zenith_ch4_1.SPE
# DATE: 04.06.2011 TIME: 08:16:59.4 WINSPECTIME: 08:17:52 SYSTIME: 08:18:16.6
# LAT: N 053:30:12 LON: E 008:34:16 ALT: +00003
# P: +000.000 R: +000.000 Y: +000.000
# CHN: 1024 ROWS: 0001 RO: 00010 EXP: 00.09800 ACCUMS: 0001 SHUT: 1 SAT: 0 NADIR: 0
#####
00807 00717 00966 00816 00875 00844 00838 00831 00872 00866 00963 00847 00847 00843 00912 00796 00878 00784 008
@@@
00802 00697 00962 00818 00870 00842 00829 00831 00878 00881 00973 00845 00838 00844 00902 00785 00854 00794 008
@@@
00811 00708 00954 00794 00866 00844 00841 00840 00886 00864 00966 00844 00838 00857 00901 00792 00856 00795 008
@@@
00815 00703 00954 00808 00864 00842 00819 00841 00869 00868 00973 00840 00838 00859 00901 00797 00851 00798 008
@@@
00814 00710 00956 00810 00877 00840 00833 00821 00886 00877 00963 00860 00831 00849 00896 00794 00861 00798 008
@@@
00814 00687 00961 00809 00874 00844 00827 00827 00870 00872 00950 00853 00838 00847 00895 00778 00859 00797 008
@@@
00808 00708 00962 00804 00877 00842 00830 00833 00871 00875 00969 00839 00844 00850 00908 00800 00852 00807 008
@@@
00804 00693 00960 00801 00868 00846 00835 00835 00880 00870 00965 00839 00829 00838 00902 00787 00852 00802 008
@@@
00794 00712 00959 00806 00873 00832 00841 00830 00877 00865 00979 00852 00828 00851 00909 00793 00875 00797 008
@@@
00803 00702 00938 00805 00881 00838 00844 00835 00877 00870 00975 00850 00831 00851 00905 00802 00862 00801 008
@@@
#####
# SPEC: 000002
# VERSION: 1.4.0 PROCESSED-ON: 2011-06-05
# FILENAME: open_98ms_10x1_zenith_ch4_2.SPE
# DATE: 04.06.2011 TIME: 08:17:01.6 WINSPECTIME: 08:18:17 SYSTIME: 08:18:18.7
# LAT: N 053:30:12 LON: E 008:34:16 ALT: +00003
# P: +000.000 R: +000.000 Y: +000.000
# CHN: 1024 ROWS: 0001 RO: 00010 EXP: 00.09800 ACCUMS: 0001 SHUT: 1 SAT: 0 NADIR: 0
#####
00793 00705 00948 00810 00868 00836 00850 00834 00869 00864 00963 00848 00837 00845 00906 00802 00881 00801 008
```

Figure 27: File format for MAMAP L0b spectra. The aircraft attitude (roll (R), pitch (P) and yaw (Y)) is not yet implemented in the file. CHN refers to the number of pixels in a row. ROWS is 1 for a line detector. RO refers to the number of readouts in a burst (before a new header occurs), EXP the exposure time for single measurements in seconds, ACCUMS the number of stacked spectra. SHUT: 1 indicates an open shutter, whereas a value of 0 denotes a dark current measurement. NADIR is a flag for the referred port. Note that the external telescope is coupled in via the zenith sky port and the flag is hence set to 0 for this configuration.

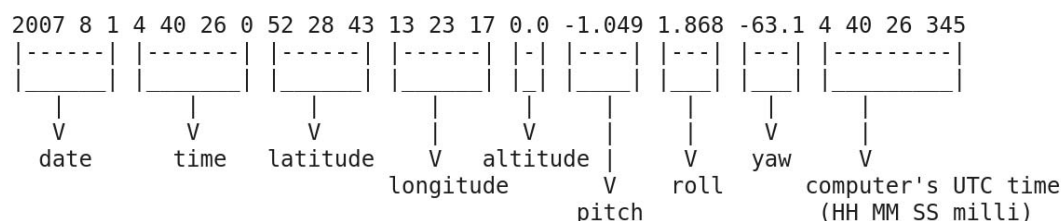


Figure 28: File format for MAMAP L0b GPS files. Latitude and longitude are given in degrees, minutes and seconds, the aircraft attitude information in degrees. The aircraft altitude is given in m.

Column	Parameter name	Parameter unit	Description
1	Longitude	degree	Ground pixel center longitude
2	Latitude	degree	Ground pixel center latitude
3	XCH4(CO2) or XCO2(CH4)	-	Scaling factor for background XCH4 or XCO2
4	Precision	-	Measurement precision (1 $\sigma$ ) for scaling factors for XCH4(CO2) or XCO2(CH4)
5	Aircraft Altitude	m	Aircraft altitude (amsl) during measurement
6	Hour	hr	UTC time
7	Minute	min	UTC time
8	Second	s	UTC time
[...]	[...]	[...]	[...]

Table 13: Raw data format of processed MAMAP L2 data (provided with the final report). Additionally, the file may contain other auxiliary data.

## 8.2. Data Format In-situ

### Picarro GHG sensor (onboard CIRPAS TO)

The NASA AMES fast greenhouse gas analyzer data is arranged in tab-delimited ASCII-Files containing columns for the major quantities dry air mole fraction of CH<sub>4</sub> and CO<sub>2</sub>, (and H<sub>2</sub>O) but also general parameters like date, time and position, and engineering parameters for cavity temperature or cavity pressure. The values are given in approximately 2Hz intervals and can be directly imported in Excel.


**CIRPAS meteorology airborne suite (onboard CIRPAS TO)**

The standard format of the CIRPAS instrumentation data are comma-delimited ASCII-Files. They contain important engineering and meteorological parameters like time, latitude, longitude, altitude, pitch, roll, heading, ambient temperature, ambient dew point temperature, wind speed, wind direction, aerosols, etc. The data was originally measured at 10 Hz but 1 Hz averages are also available and can be directly imported in Excel or MATLAB.

### 8.3. Description of Data Archive

Data will be organized in a COMEX folder with subfolders for MAMAP, NASA AMES Picarro and CIRPAS data. Data will additionally be separated by subfolders for each day. The data archive includes a Word-file with a more detailed description of the different formats and types of available data.



	<p style="text-align: center;"><b>COMEX</b> <b>Final Report</b></p>	<p style="text-align: right;">Version: 2.0 Doc ID: IUP-COMEX-FR Date: 3. July 2016</p>
--	---	--

## 9. Examples on emissions estimated from COMEX campaign data

To demonstrate that the data quality is sufficient to derive flux estimates, the two surveys (out of around 8 successful flights suitable for a flux estimate) of the campaign (Olinda Alpha Landfill on 2014-09-01 and the Kern River and Kern Front Oil Field on 2014-09-04) have been selected. A distinct plume signature/structure was visible in the quick-looks of both remote sensing and in-situ data set of both targets.

The following sections describe the methods which are used to calculate the emission rate (or flux) of a target for the two examples Olinda Alpha Landfill and the Kern River and Front Oil Field and also discuss the main error sources.

### 9.1. Approach

This section gives a description of how two separate fluxes have been derived based on the MAMAP remote sensing data and the Picarro in-situ data.

#### 9.1.1. The MAMAP remote sensing data

In contrast to the retrieved column averaged dry air mole fractions of CH<sub>4</sub> of the other MAMAP surveys using one RTM simulation with fixed solar zenith angle (SZA) and surface elevation (as described in Section 7.1.2), a look up table (LUT) approach has been applied for these two targets [RD-5; RD-8]. The LUT accounts for a varying surface elevation in the target area and a changing solar zenith angle during the flight.

The flux estimates are based on a mass balance approach similar to those described in RD-2 and RD-5 and used in RD-8. In contrast to the C-MAPEX data set (RD-8), where source positions and extents were well-known in most cases, the Gaussian plume inversion modeling has not been applied to the COMEX data set. The emission rate estimates derived from the Gaussian plume inversion modeling typically considerably depend on source location, their extent as well as the number of sources. For the targets flown during COMEX, only a limited knowledge of the source location(s) and extents as well as the number of active sources inside the selected target areas is available.

The mass balance approach used is depicted in Figure 29. The wind direction can be directly determined from the MAMAP measurements, based on the enhancement in the XCH<sub>4</sub>(CO<sub>2</sub>) at the different flight lines downwind the proximate source areas. A similar method has been applied in RD-2 and RD-5. Assuming the plume propagation follows a Gaussian distribution (at sufficient distance from the source(s)), a center line parallel to the prevailing wind direction could be constructed, intersecting each flight line at the positions, where the proximately highest XCH<sub>4</sub>(CO<sub>2</sub>) enhancements are measured.



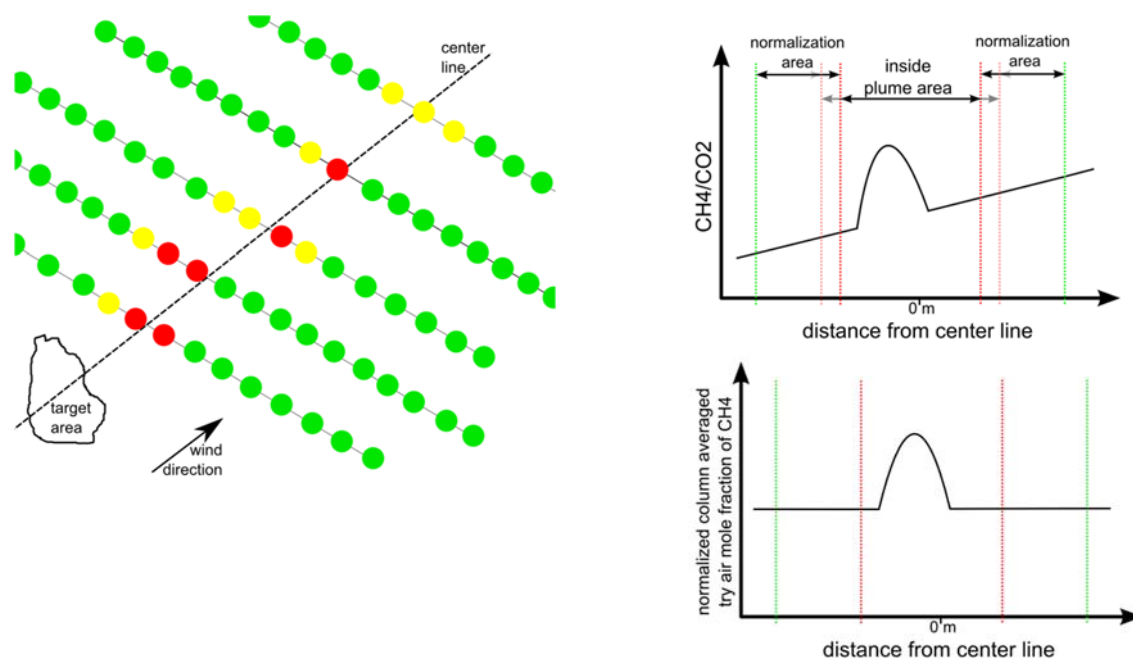


Figure 29: MAMAP mass balance approach. Left: Schematic of MAMAP remote sensing measurements downwind of the target area. Upper right:  $\text{CH}_4/\text{CO}_2$  ratio along a flight line whereas as the x-axis depicts the distance from the center line. Lower right: Normalized flight track by the measurements in the normalization area.

In the next step, each flight line is normalized by the flanks/edges of the respective track, in order to get the column averaged dry air mole fraction of  $\text{CH}_4$  or column enhancements of  $\text{CH}_4$  relative to the background. This approach is necessary to correct for possible gradients in the background concentrations of  $\text{CH}_4$  and/or  $\text{CO}_2$  in along track or in downwind direction. Such gradients could be expected in areas like oil fields or mega cities like Los Angeles. The column enhancements derived this way, are then used in a mass balance approach to estimate the emission strength of the target (RD-2 and RD-5).

### 9.1.2. The Picarro in-situ data

Besides the MAMAP remote sensing data, also Picarro in-situ data (collected during the same flights) is used to independently estimate emission rates for the two selected targets, i.e. Olinda Alpha Landfill on 2014-09-01 and the Poso Creek and the Kern Front and Kern River Oil Fields on 2014-09-04.

For this purpose, also a mass balance approach has been applied (similar to the C-MAPExp campaign (RD-8)).

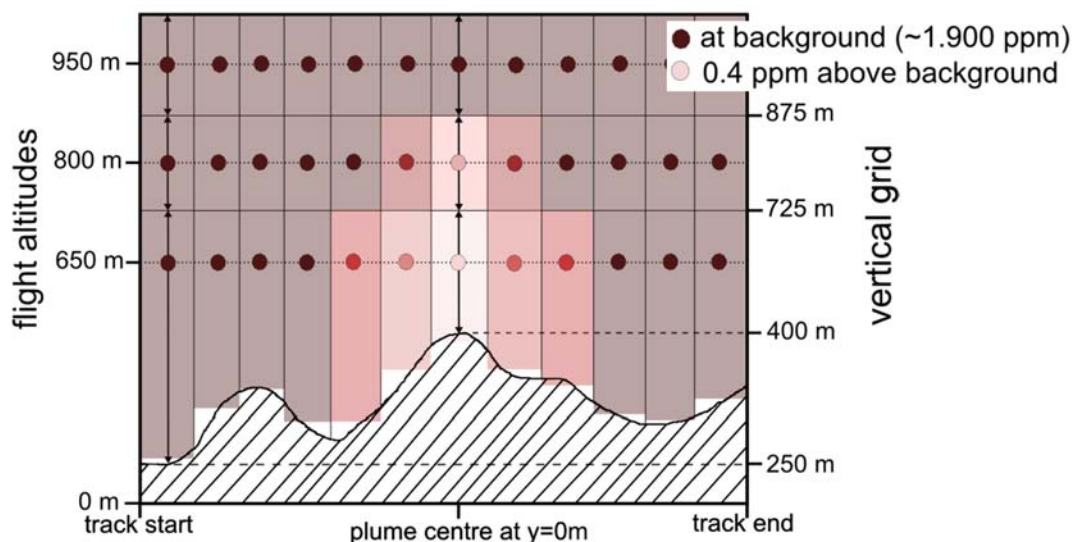



Figure 30: Schematic of one in-situ wall with the single in-situ measurements (circles) taken within the boundary layer at different altitudes and an exemplary surface elevation. All altitudes are given in meters above mean sea level (mamsl).

The schematic of the applied mass balance approach is shown in Figure 30. Depicted is one in-situ wall (flight altitude in meters above mean sea level (mamsl) over the distance from the plume center). The plume center (used only for visualization purposes) is defined by an empirically derived center line in the same way as for the MAMAP remote sensing data. For the emission rate estimate, the orientation of the wind direction at the positions of the measurements is calculated individually (compare to Equation 1 below) from the according in-situ wind measurements. Due to the time difference between the remote sensing measurements and the in-situ measurements (performed within the boundary layer), the center lines do not need to be identical due to a possible shift in wind direction. The colored circles correspond to the in-situ measurements, which were sampled, in this case, at three different altitudes (650 mamsl, 800 mamsl, 950 mamsl). These measurements exhibit a clear  $\text{CH}_4$  plume/enhancement of around 0.400 ppm (light red) above the background of around 1.900 ppm (dark red). The background concentrations are individually calculated for each track/flight altitude (in a similar way as done for the MAMAP remote sensing measurements) by defining an inside plume area and an outside plume (normalization) area, or more appropriate, a background area (compare to Figure 29), to account for a possible vertical concentration gradient within the boundary layer. Furthermore, it is assumed that each measurement is valid for a rectangular grid box, whereas the horizontal and vertical dimensions are determined by the distance to the next measurements. An exception is the lowest flight track. Its vertical extent to the surface is defined by the surface elevation given by SRTM digital elevation model. Furthermore, in a first order approximation, it is assumed that the measurements of the lowest flight track are valid down to the surface reflecting well-mixed conditions.

	<b>COMEX</b> <b>Final Report</b>	Version: 2.0 Doc ID: IUP-COMEX-FR Date: 3. July 2016
---	-------------------------------------	--

The measured mixing ratios of CH<sub>4</sub> and CO<sub>2</sub> by the Picarro instruments and the measured meteorological parameters by the Cirpas instrumentation are used to calculate the emission rate by a mass balance approach for each grid box *i* of thickness  $\Delta z_i$  [m] and width  $\Delta y_i$  [m]:

$$F_{IS} = \sum_i MFaB_i * \frac{p_i}{T_i * k} * CF * \Delta z_i * \Delta y_i * u_i * \cos(\alpha_i), \quad \text{Equation 1}$$

where MFaB<sub>*i*</sub> is mole fraction above background [ppm], *p<sub>i</sub>* is the pressure [Pa], *T<sub>i</sub>* is the temperature [K], *k* is the Boltzmann constant [J/K], CF is a conversion factor for molec/s to g/s, *u<sub>i</sub>* is the wind speed [m/s],  $\alpha$  is the angle between the wind direction and the normal of the length segment  $\Delta y_i$  in grid box *i* [°], and *F<sub>IS</sub>* is the total flux through one in-situ wall.

## 9.2. Example 1: Landfill Olinda Alpha

A landfill produces CH<sub>4</sub> through the decomposition of biodegradable waste, which is then partly oxidized to CO<sub>2</sub>. Both gases contribute to the released landfill gas (LFG), whereas the relative contribution and the total amount depends on technical/structural aspects like thickness and type of landfill cover, or efficiency of a gas recovery system, meteorological aspects like surface pressure variation, and environmental conditions within the landfill like amount of waste, type of waste, age of waste, temperature and moisture content (Lohila et al., 2007; Amini et al., 2013 and references within).

The Olinda Alpha Landfill is located in the middle of the Los Angeles Basin (around 33.94°N and 117.84°W) and is surrounded by a hilly environment from west to south-east and by an urban area from south-east to west. Previous airborne in-situ assessments (performed in 2010) have estimated the emission to 12.5 ± 2.9 ktCH<sub>4</sub>/yr at the time of overflights based on 5 single tracks on five different days (Peischl et al., 2013) and the Climate Action Plan of the city of La Habra (Atkins, 2014) specify an inventory value of 13.8 ktCH<sub>4</sub>/yr for the year 2010 based on emission factor, whereas the projected emission increases to 15.0 ktCH<sub>4</sub>/yr in the year 2020.

The Olinda Alpha Landfill was surveyed on 2014-09-01 and consists of MAMAP remote sensing measurements, taken while flying above the boundary layer (around 850 mamsl) at around 1794 mamsl and three in-situ walls within the boundary layer, one upwind and two downwind walls.

The following sections describe the results of the emission rate estimates based on the MAMAP remote sensing data and the Picarro in-situ data separately. Furthermore, the Picarro in-situ data is used to investigate whether the co-emitted CO<sub>2</sub> from the landfill has an impact on the MAMAP assumption of a constant CO<sub>2</sub> background, used for the XCH<sub>4</sub>(CO<sub>2</sub>) proxy approach to derive the column averaged dry air mole fractions of CH<sub>4</sub>.

### 9.2.1. The MAMAP remote sensing data

The MAMAP remote sensing survey over the Olinda Alpha Landfill on 2014-09-01 took place in the afternoon between 15:00 and 16:00 local time. The mean solar zenith angle during the overflight is calculated to be around 44.6° with a minimum of around 38.0° at the beginning and a maximum of around 52.0° at the end of the measurement period. The corresponding surface elevation derived by the SRTM digital elevation model varies from around 100 mamsl to around 500 mamsl with a mean value of around 310 mamsl downwind of the landfill.

The mean, maximum, and minimum values of solar zenith angle and surface elevation are used in the LUT approach for the radiative transfer model calculations (by SCIATRAN) beside the other already derived parameters like flight altitude (1796 mamsl), aerosol scenario (urban type), surface spectral

reflectance (0.31) and background concentrations of  $\text{XCH}_4$  (1801.8 ppb) and  $\text{XCO}_2$  (391.4 ppm, see also Section 7.1.2 for comparison). The  $\text{XCO}_2$  background concentration is also in reasonable agreement with the prediction of the SECM model (Reuter et al., 2012) of 393.1 ppm.

A mean wind speed of 4.7 m/s has been calculated as weighted mean on basis of the relative  $\text{CH}_4$  distribution of the lowest legs, inside the plume area (compare to Picarro in-situ data in Section 9.2.2), of the second downwind wall, which was acquired directly after the remote sensing pattern. The wind direction has been determined empirically based on the  $\text{CH}_4$  plume detected by the MAMAP remote sensing measurements to around  $241^\circ$ , which is in proximate agreement to the Cirpas in-situ measurements (around  $252^\circ$  for the second downwind wall).

Figure 31 shows the normalized column averaged dry air mole fractions of  $\text{CH}_4$  for that day. The measurements have been smoothed by a 3-point moving average, normalized by a 300-point moving average (similar to RD-8), and filtered by an inclination angle of  $< \pm 4^\circ$  of the downwelling optical path with respect to the nadir direction. The normalization is only for visualization purposes and has no influence on the estimated emission rate, as each flight line is normalized individually by its flanks/edges for the estimate of emissions (see Section 9.1.1 for more details).

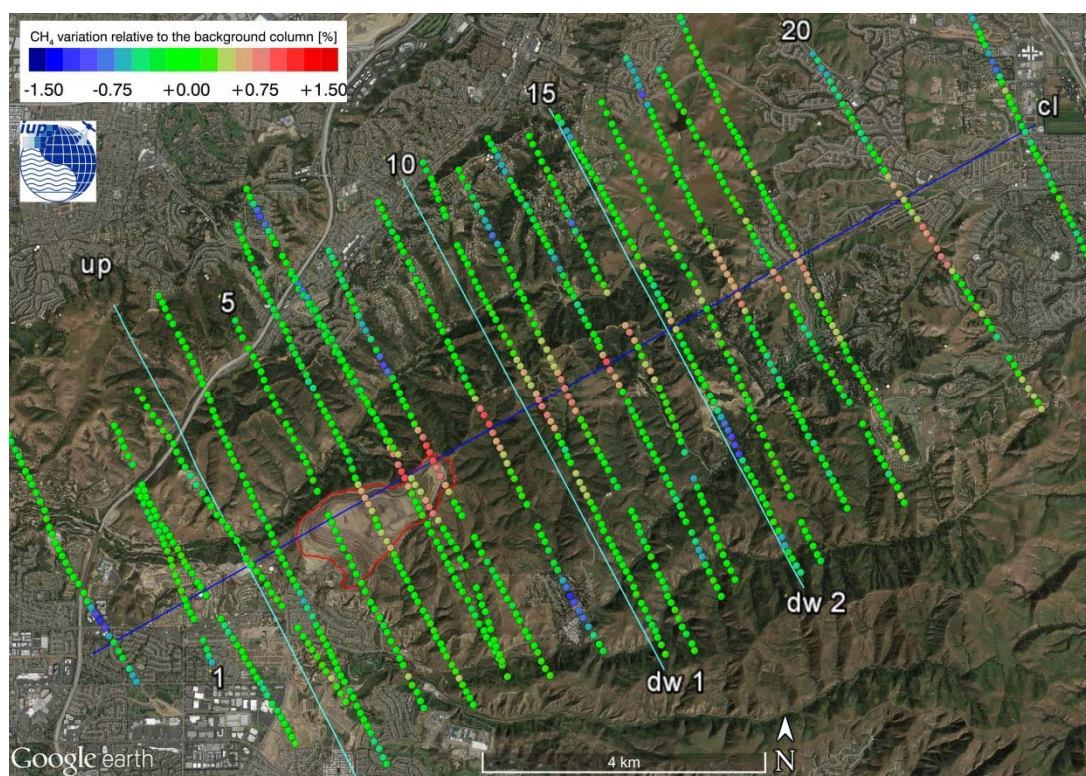


Figure 31: MAMAP flight pattern and LUT analysis of the Olinda Alpha Landfill (enclosed by solid red line) on 2014-09-01, between 15:00 and 16:00 local time. Flight altitude was around 1796 mamsl. Surface elevation is around 310 mamsl. The  $\text{CH}_4$  plume is visible as an enhancement in the normalized column averaged dry air mole fractions of  $\text{CH}_4$ . Wind direction was south-west and the wind speed was around 4.7 m/s. Topography map underneath is provided by Google Earth. The data is filtered by an inclination angle of  $\pm 4^\circ$ . Additionally, the center line (cl) (solid blue line), as discussed in Section 7.1.1, and the three in-situ walls upwind wall (up), first downwind wall (dw 1) and second downwind wall (dw 2) (solid cyan lines) are shown. Numerals give the track numbering.

Figure 32 summarizes the results of the integral inversion method for the downwind tracks. For the final emission rate estimate, track 9 (first track which is downwind of the landfill) to 21 have been used. The data has additionally been smoothed by 3-point moving average. The emission rate for the Olinda Alpha Landfill survey on 2014-09-01 has been estimated to around 15.1 kt $\text{CH}_4$ /yr.





# COMEX Final Report

Version: 2.0  
Doc ID: IUP-COMEX-FR  
Date: 3. July 2016

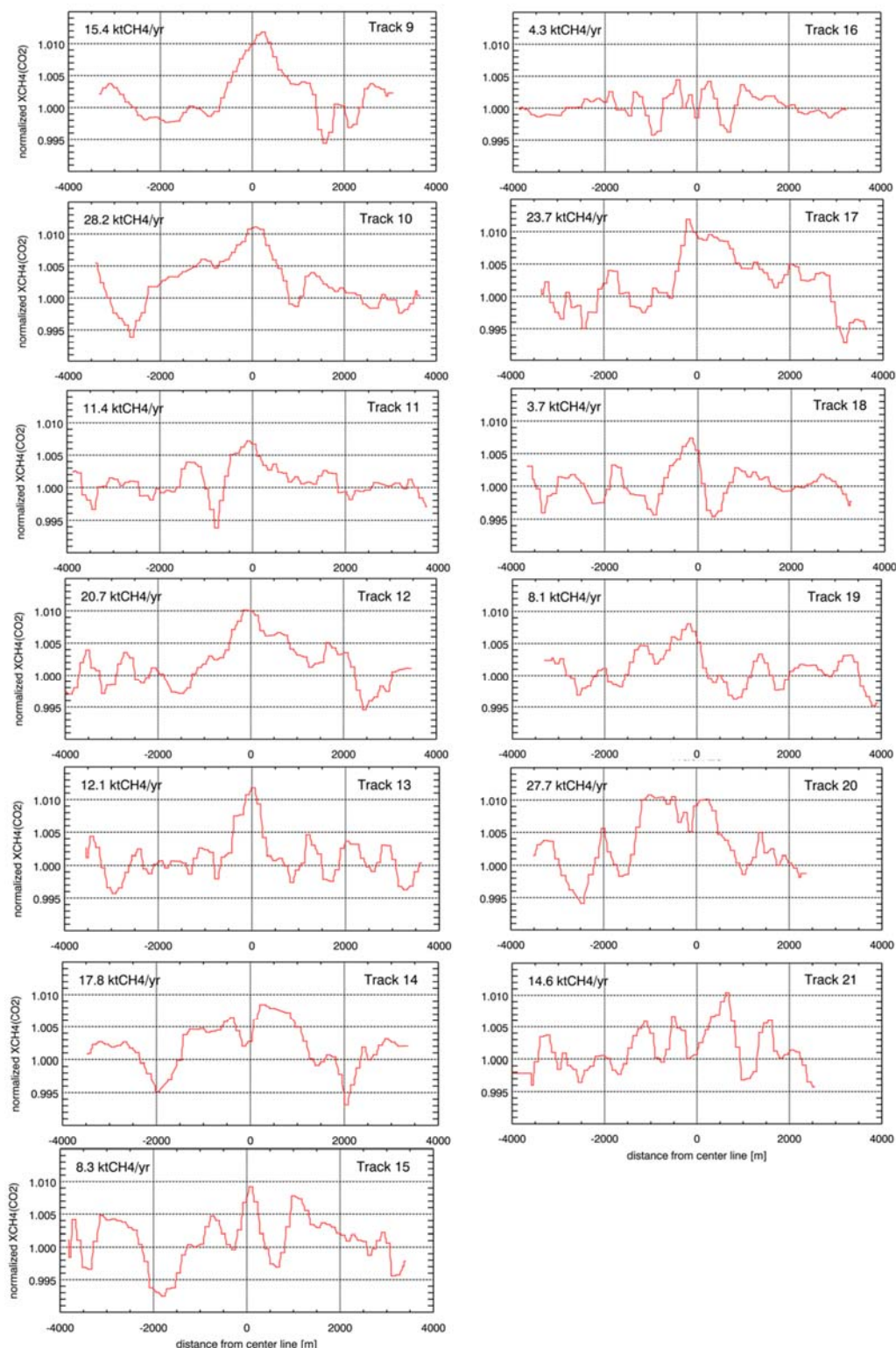



Figure 32: Cross sections of the normalized column averaged dry air mole fraction of  $\text{CH}_4$  of the MAMAP remote sensing measurements at the Olinda Alpha Landfill on 2014-09-01. The plume limits are  $\pm 2000$  m and the normalization limits are 1500 m to 4000 m on each side of the centre line (compare to Section 9.1.1). The emission rate estimates from the individual tracks are shown in the upper left corners.



	<p style="text-align: center;"><b>COMEX</b> <b>Final Report</b></p>	<p style="text-align: right;">Version: 2.0 Doc ID: IUP-COMEX-FR Date: 3. July 2016</p>
--	---	--

### **Uncertainty of the remote sensing emission rate estimate**

This section briefly describes the initial analysis of the uncertainty of the derived emissions.

Changing the plume limits to  $\pm 1500$  m (minimum),  $\pm 3000$  m and  $\pm 4000$  m (whole track) changes the emission rate estimate by maximal  $0.2 \text{ ktCH}_4/\text{yr}$  (1%).

In this case, the influence of the wind direction on the emission rate is relatively small because the flight tracks are nearly perpendicular to the wind direction. For example, an uncertainty of around  $10^\circ$  ( $15^\circ$ ) would lead to a change in the flux of around  $\pm 1.5\%$  ( $\pm 3.2\%$ ). Varying the wind speed (one of the major error sources (RD-2, RD-5, RD-8)) by  $\pm 0.5$  to  $0.8 \text{ m/s}$  (accuracy of the wind probe, reported by CIRPAS) induces an error of around  $\pm 11\%$  to  $\pm 17\%$  to the emission rate estimate.

The track-to-track variability is  $8.2 \text{ ktCH}_4/\text{yr}$  (54%). This translates to a standard uncertainty in the mean value of the flux of  $\pm 2.3 \text{ ktCH}_4/\text{yr}$  (15%).

Assuming the wind speed and the track-to-track variability are uncorrelated, the combined standard uncertainty of the flux is around  $\pm 3.5 \text{ ktCH}_4/\text{yr}$  (23%). As the wind speed is linearly related to the column enhancements, which are measured by MAMAP, and thus, to the estimated emission rate calculated for each track, the two quantities might be correlated to some degree and the error of the flux is larger. Taking this into account, the combined standard error of the flux increases to  $\pm 4.8 \text{ ktCH}_4/\text{yr}$  (32%) in case of a perfect correlation.

Furthermore, the emission rate estimate based on the normalized column averaged dry air mole fraction of  $\text{CH}_4$  using  $\text{CO}_2$  as proxy, can be biased by co-emitted  $\text{CO}_2$  (further details are found in Section 9.2.3).

The  $\text{CH}_4$  emission rate estimate of  $15.1 \text{ ktCH}_4/\text{yr}$  based on the MAMAP remote sensing measurements is in good agreement with the inventory value from 2010 of  $13.8 \text{ ktCH}_4/\text{yr}$  (Atkins, 2014) and agrees well within the uncertainty with the finding from Peischl et al. (2013) of  $12.5 \pm 2.9 \text{ ktCH}_4/\text{yr}$ .

### 9.2.2. The Picarro in-situ data

Immediately, after the MAMAP remote sensing measurements over the boundary layer, in-situ surveys with the CIRPAS aircraft inside the boundary layer (intersecting and sampling the landfill plume with the aircraft in-situ instrumentation) were performed between 16:00 to 17:15 local time, starting with the second downwind wall (compare Figure 33).

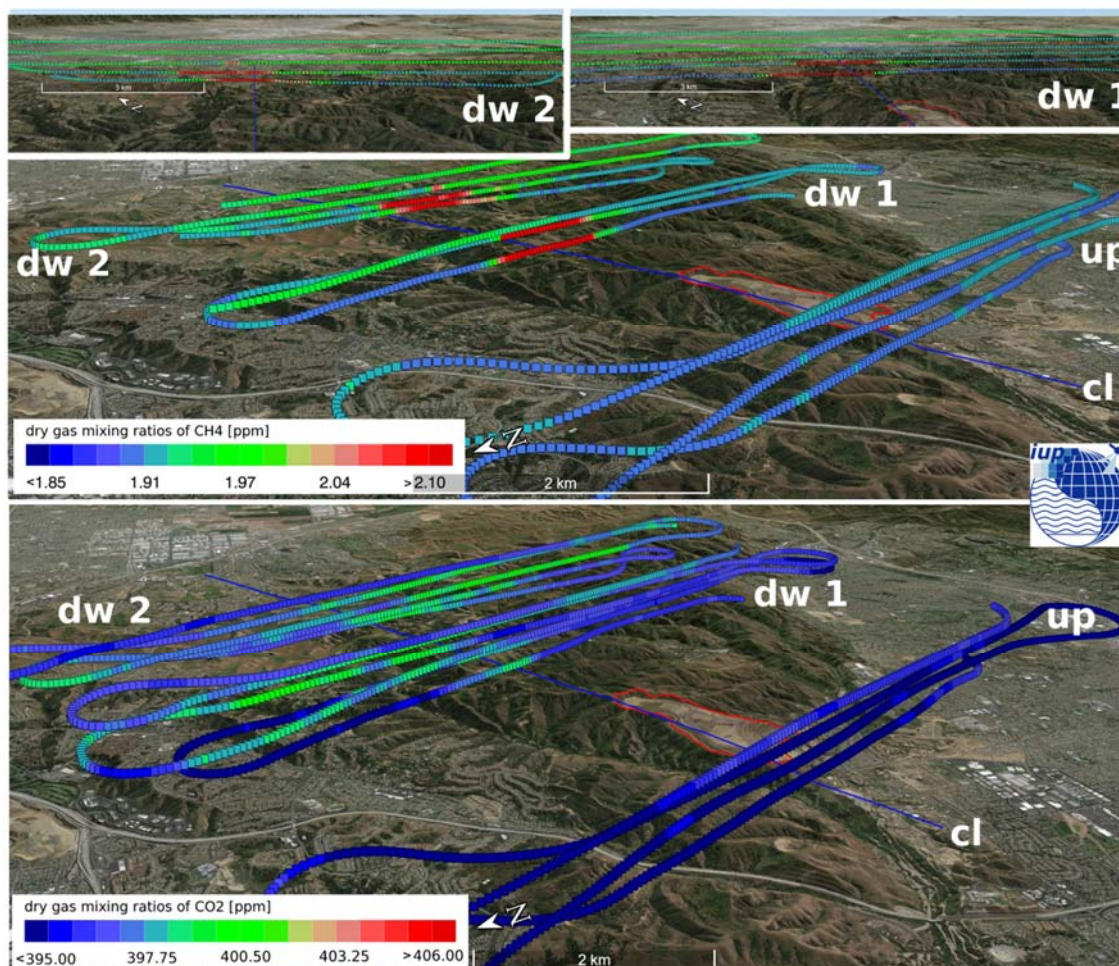


Figure 33: Subsequent airborne in-situ only measurements performed with the CIRPAS aircraft for validation of the collected remote sensing data. The Olinda Alpha Landfill is encircled by the solid red line. Shown are dry gas mixing ratios of  $\text{CH}_4$  (top and middle) and  $\text{CO}_2$  (bottom) of the Picarro instrument. The in-situ data shows distinct methane enhancements (red color  $>2.10$  ppm) west of the Olinda Alpha Landfill during two vertical soundings at two downwind distances from the landfill. Measurement was performed on 2014-09-01, between 16:00 to 17:15 local time. For clarity, only the three lowest legs for the first (dw 1) and the 4 lowest legs for second downwind wall (dw 2) are shown for the  $\text{CH}_4$  measurements (middle). The complete walls of  $\text{CH}_4$  are depicted at the top left (second downwind wall) and top right (first downwind wall). Additionally, also the center line (blue, solid line), as discussed in Section 7.1.1, is shown. Topography map underneath is provided by Google Earth.

Each wall consists of several measurement legs at different altitudes in meters above mean sea level (mamsl):

- Upwind wall: 1: 640, 2: 910, 3: 1170, 4: 1280
- 1. Downwind wall: 1: 640, 2: 772, 3: 899, 4: 1021, 5: 1155, 6: 1220
- 2. Downwind wall: 1: 641, 2: 806, 3: 965, 4: 1119, 5: 1294

As the main focus of the in-situ landfill emission measurement is CH<sub>4</sub> and validation of the according remote sensing data, the CO<sub>2</sub> concentrations and the resulting CO<sub>2</sub> fluxes are analyzed in a less quantitative and qualitative manner (in comparison to CH<sub>4</sub>) to mainly assess the uncertainty of the XCH<sub>4</sub>(CO<sub>2</sub>) proxy approach applied for analysis of the remote sensing data (a more comprehensive analysis of the CO<sub>2</sub> in-situ data could be done in an additional study).

When analyzing the three in-situ walls, distinct CH<sub>4</sub> enhancements can be observed for the two downwind walls at the two lowest flight altitudes originating from the landfill. In contrast, a relatively homogeneous distribution of CH<sub>4</sub> at all flight altitudes can be observed for the upwind wall.

These CH<sub>4</sub> enhancements peak at around 400 ppb above the background (compare to Figure 34). Furthermore, the maximum altitude of the CH<sub>4</sub> landfill plume is constrained by the highest in-situ leg where no CH<sub>4</sub> enhancement can be observed. For the first downwind wall no CH<sub>4</sub> anomalies are detected at the third leg and for the second downwind wall, no CH<sub>4</sub> anomalies are observed at the forth leg, whereas already the third leg shows negligible CH<sub>4</sub> enhancements.

As expected, the measured CO<sub>2</sub> mixing ratios show pronounced enhancements at the location of the CH<sub>4</sub> plume (Figure 34). However, in addition to the pronounced CO<sub>2</sub> enhancements, distinct CO<sub>2</sub> peaks with unclear origin could be observed in some legs. Figure 34 clearly shows CO<sub>2</sub> peaks only in the second lowest legs of both walls (first wall: at +2700 m; second wall: at +2400 m and -1500 m) which are co-located with a very tiny CH<sub>4</sub> enhancement compared to the main plume.

For calculation of the emission rate, only the two lowest legs of the first and second downwind wall are used. Furthermore, the plume area is restricted to an area of +/- 3000 m around the center line, whereas measurements in distance between 3000 m and 5000 m on each side are used to determine the background.

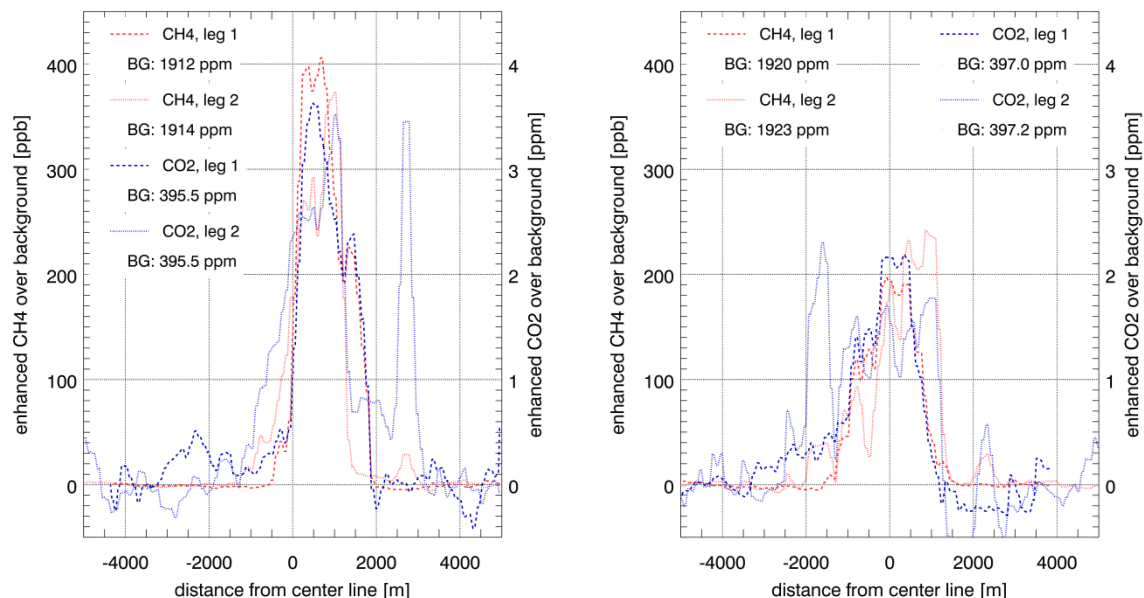



Figure 34: Left: Shown are the lowest (1, dashed line) and the second lowest (2, dotted line) tracks of the first (left) and second (right) in-situ wall for CH<sub>4</sub> (red) and CO<sub>2</sub> (blue). Negative distances point to the south and positive distances point to the north of the landfill.

The emission rates for the first and second downwind wall are 17.2 ktCH<sub>4</sub>/yr and 15.0 ktCH<sub>4</sub>/yr for CH<sub>4</sub>, and 529.9 ktCO<sub>2</sub>/yr and 462.6 ktCO<sub>2</sub>/yr, for CO<sub>2</sub> respectively.

	<b>COMEX</b> <b>Final Report</b>	Version: 2.0 Doc ID: IUP-COMEX-FR Date: 3. July 2016
---	-------------------------------------	--

### Uncertainties of in-situ emission rate estimates

This section briefly describes the initial analysis of the uncertainty of the derived emissions.

The major CH<sub>4</sub> enhancements are confined within around 2000 m and around 3000 m for the first and second downwind wall, respectively (compare to Figure 34 and Figure 35). Varying the limits for the background calculation by 1000 m or extending the plume limits to the whole track (5000 m) change the CH<sub>4</sub> flux by less than 2%. This is in accordance with the very smooth CH<sub>4</sub> background concentration on each side of the plume as observed in Figure 34.

The two largest uncertainties originate from the extent of the plume to the surface and from the wind speed error. The upper part of the plume is well confined by the flight legs, but for the lower part, surface measurements are not available. To estimate the lower part of the plume down to the surface, it has not been assumed a well-mixed situation as in the previous section, but 1) a linear decrease of the concentration till the surface having a surface value of 50% of the lowest leg and 2) a linear increase of the concentration till the surface having a surface value of 150% of the lowest leg.

The resulting emission rates are

- 1) first downwind wall: 14.3 ktCH<sub>4</sub>/yr (-17%) and 446.3 ktCO<sub>2</sub>/yr (-16%),  
second downwind wall: 13.1 ktCH<sub>4</sub>/yr (-13%) and 402.3 ktCO<sub>2</sub>/yr (-13%), and
- 2) first downwind wall: 19.9 ktCH<sub>4</sub>/yr (+16%) and 610.3 ktCO<sub>2</sub>/yr (+15%),  
second downwind wall: 16.8 ktCH<sub>4</sub>/yr (+12%) and 520.5 ktCO<sub>2</sub>/yr (+13%).

The accuracy of the 5-hole turbulence probe is around 0.5 to 0.8 m/s (reported by CIRPAS). This error linearly propagates to the calculated fluxes. To roughly estimate its influence onto the fluxes of the two downwind walls, a mean wind speed has been calculated for each wall (dw1: 4.1 m/s and dw2: 4.7 m/s). Thus, an error of 0.8 m/s leads to a flux uncertainty of +- 3.4 ktCH<sub>4</sub>/yr (20%, dw1) and +- 2.6 ktCH<sub>4</sub>/yr (17%, dw2).

Assuming the not well-known surface concentration and the wind speed are uncorrelated, the combined standard uncertainty of the flux is around +- 4.5 ktCH<sub>4</sub>/yr (26%) and +- 3.2 ktCH<sub>4</sub>/yr (21%) for the first and second downwind wall, respectively. As discussed in Section 9.2.1 for the MAMAP remote sensing data, also for the Picarro in-situ data, the wind speed and the concentration measurements, which are used for the extrapolation to the surface, might be correlated to some degree. For the extreme case (errors are perfectly correlated), the combined standard uncertainty of the flux increases to +- 6.4 ktCH<sub>4</sub>/yr (37%, dw1) and +- 4.5 ktCH<sub>4</sub>/yr (30%, dw2).

Comparing the estimated CH<sub>4</sub> emission rates based on the Picarro in-situ measurements to the inventory value from 2010 of 13.8 ktCH<sub>4</sub>/yr (Atkins, 2014) shows a good agreement within the uncertainty range. The MAMAP remote sensing based emission rate of 15.1 ktCH<sub>4</sub>/yr from the previous Section is also within the uncertainty of the in-situ estimate. Both, the in-situ and the remote sensing based flux estimate also agree well within the uncertainty with the finding from Peischl et al. (2013) of 12.5 +-2.9 ktCH<sub>4</sub>/yr (23%).



### 9.2.3. Investigation of co-emitted CO<sub>2</sub> induced error on the MAMAP retrieval XCH<sub>4</sub>(CO<sub>2</sub>) proxy approach for the Olinda Alpha Landfill

The CH<sub>4</sub> and CO<sub>2</sub> Picarro in-situ data is used to also investigate the CH<sub>4</sub>(CO<sub>2</sub>) proxy assumption used in the MAMAP retrieval to derive XCH<sub>4</sub>. This is of particular interest for landfill emissions because they also emit CO<sub>2</sub>, which could be co-located to CH<sub>4</sub>. A co-located CO<sub>2</sub> plume would lead to a concentration dependent negative bias in the retrieved normalized column averaged dry air mole fractions of CH<sub>4</sub>, i.e. the retrieved XCH<sub>4</sub>(CO<sub>2</sub>) columns would appear lower. Gerilowski et al. (2015) (RD-6) for example, have estimated a bias of -0.02% in the retrieved XCH<sub>4</sub>(CO<sub>2</sub>) in case of a 10 ktCH<sub>4</sub>/yr emission source if 100 ktCO<sub>2</sub>/yr is co-emitted.

As done in the final report of the C-MAPEX campaign (RD-8), the Picarro in-situ measurements have been used to calculate total columns for comparison with the columns retrieved from the MAMAP remote sensing data. To estimate the influence of the co-emitted CO<sub>2</sub> on the proxy method, the in-situ columns are treated in a similar manner as it has been done for the MAMAP remote sensing data. Figure 35 depicts these normalized ratios of integrated in-situ columns (IISC) of CH<sub>4</sub> and CO<sub>2</sub> at the position of the first (left) and second (right) downwind wall. The CO<sub>2</sub> peaks on each side of main plume in the second lowest flight legs (as seen in Figure 34) are not visible in the IISC anymore because the layer is too thin to have a significant influence on the overall column.

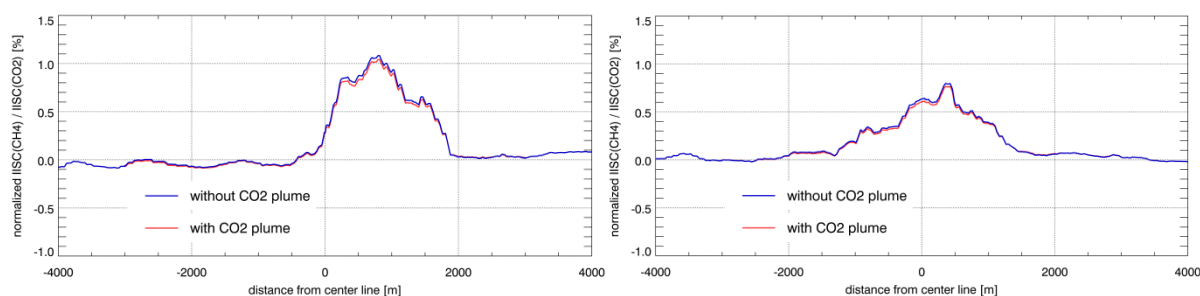


Figure 35: Left: First downwind wall. Right: Second downwind wall. Negative distances point to the south and positive distances point to the north of the landfill. The two colors depict two different approaches for calculating integrated in-situ columns (IISC). Red: In-situ measurements are not modified. Blue: The CO<sub>2</sub> measurements of the two lowest legs of each wall, which have also been used for calculating the flux, have been replaced by the mean value of CO<sub>2</sub> measurements outside the plume area to simulate how a column would look like if there was no co-emitted CO<sub>2</sub> present.

Based on the in-situ data, the maximum column enhancement of CH<sub>4</sub> relative to the background is slightly above 1.0% and slightly below 0.8% for the first and second in-situ wall, respectively. These enhancements are in the same order of magnitude (around 1%) as seen by the MAMAP remote sensing instrument (compare to Figure 36 and Figure 37). These two sets of measurements were recorded 60 to 90 minutes apart to the nearest remote sensing tracks. Additionally, for the IISC of each in-situ wall, several legs at different altitudes have been used, which were also not taken simultaneously. The remaining column above the remote sensing altitude, which was not surveyed, has been complemented by the scaled U.S. standard atmosphere. Therefore, it is not expected that the two types of columns agree exactly.



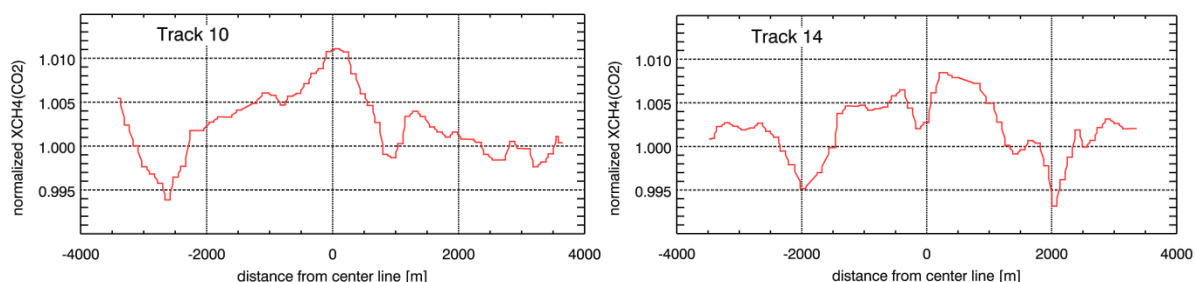


Figure 36: Normalized column averaged dry air mole fraction of  $\text{CH}_4$  of the first MAMAP leg in upwind direction of the respective in-situ wall. Left: First track upwind of the first downwind wall. Right: First track upwind of the second downwind wall.

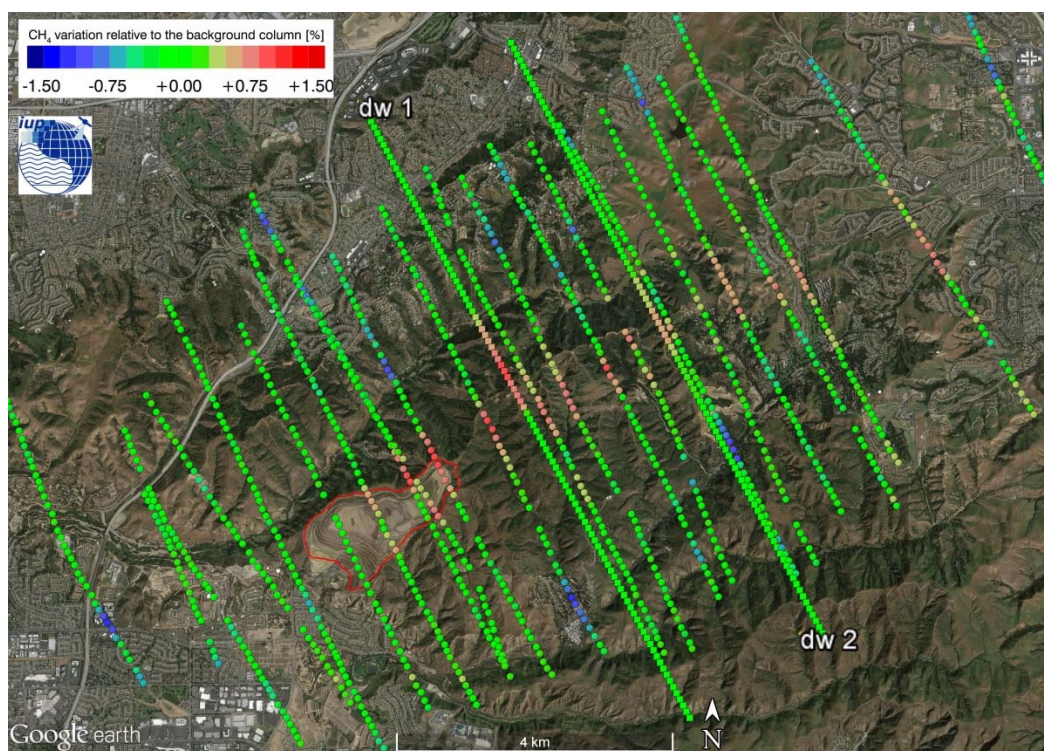


Figure 37: Shown are the normalized column averaged dry air mole fractions of  $\text{CH}_4$  (circles; similar to Figure 31) and the normalized ratios of the integrated in-situ columns of  $\text{CH}_4$  and  $\text{CO}_2$  for the first (dw1) and second (dw2) downwind wall (squares).

Concerning a possible offset of the normalized column averaged dry air mole fractions by the co-emitted  $\text{CO}_2$  and, thus, the validity of the proxy assumption for the MAMAP retrieval, Figure 35 indicates an offset of maximal -0.04%. This is in good agreement with Gerilowski et al. (2015) (RD-6). First investigations using these normalized IISC columns for estimating a flux, indicate a difference in the emission rate between a plume ‘without  $\text{CO}_2$ ’ and ‘with  $\text{CO}_2$ ’ of around 6%. Assuming, this is also valid for the MAMAP remote sensing measurements, which took place around one hour earlier, the effect of the co-emitted  $\text{CO}_2$  may lead to an underestimation of the emission rate estimate based on the MAMAP measurements of the Olinda Alpha Landfill on 2014-09-01 in the same order of magnitude.

### 9.3. Example 2: Poso Creek, Kern River and Kern Front Oil Fields

The Kern River Oil Field, located near Bakersfield, California, was discovered in 1899. The field is about 6 miles long and 4 miles wide [10 km by 6.4 km], and produces heavy oil from the Miocene- to Pleistocene-aged Kern River formation (Curtis et al., 2002).

In the direct vicinity of this field, two other adjacent fields (i.e. Kern Front and Poso Creek) are located. In 2012, these three fields produced 32.2 millions of barrels of heavy crude and 12430 Mcf (= 267 tones) of associated gas (Laird et al., 2013).

Oil production in all three fields is supported by enhanced oil recovery (mainly by steam injection/cyclic steaming).

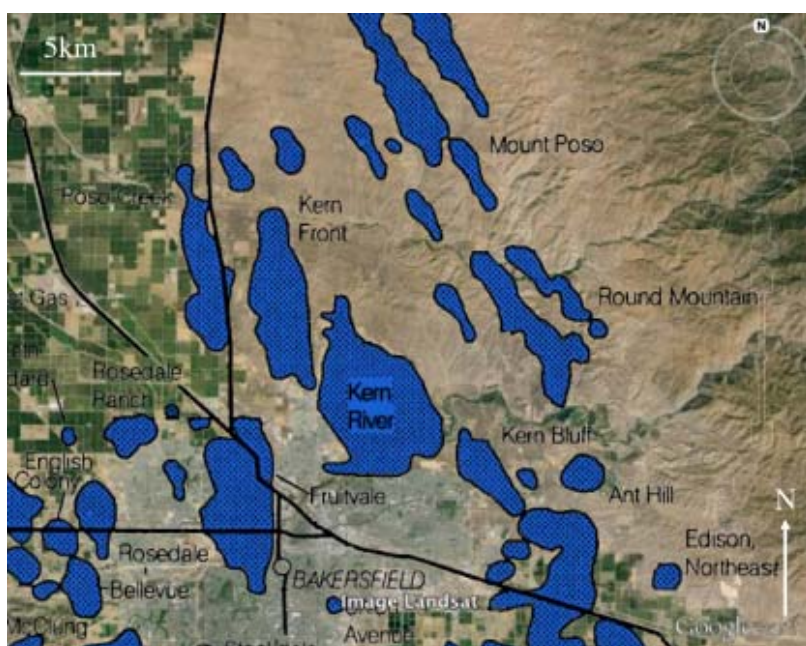


Figure 38: Kern River, Kern Front and Poso Creek Oil Fields near Bakersfield (from Thompson et al. (2015)).

The Kern River, Kern Front and Poso Creek Oil Fields survey on 2014-09-04 consists of MAMAP remote sensing measurements, acquired above the boundary layer (boundary layer height around 1700 mamsl) at around 2117 mamsl and three in-situ walls within the boundary layer (i.e. one upwind and two downwind walls over the fields). The wall positions for the in-situ pattern were chosen (and adopted during the flight by the MAMAP real-time retrieval) in a way to best validate the CH<sub>4</sub> anomalies observed by the remote sensing data over the fields on the particular day. For the MAMAP remote sensing measurements, an interlace pattern had been chosen. Thus, the oil field was screened two times from north to south with a time difference of around one hour.

The following sections describe the results of the emission rate estimates based on the MAMAP remote sensing data and the Picarro in-situ data separately. Furthermore, the Picarro in-situ data has been used to investigate the MAMAP assumption of a constant CO<sub>2</sub> background used in the CO<sub>2</sub> proxy method to derive the column averaged dry air mole fractions of CH<sub>4</sub> (i.e. XCH<sub>4</sub>(CO<sub>2</sub>)).

### 9.3.1. The MAMAP remote sensing data

The MAMAP remote sensing survey over the Kern River, Kern Front and Poso Creek Oil Fields on 2014-09-02 took place in the afternoon between 13:40 and 15:50 local time. The mean solar zenith angle during the overflight is calculated to be around  $38.3^\circ$  with a minimum of around  $29.0^\circ$  at the beginning and a maximum of around  $50.0^\circ$  at the end of the measurement period. The corresponding surface elevation derived by the SRTM digital elevation model has a minimum of around 110 mamsl, a maximum at around 370 mamsl, and a mean value of around 210 mamsl.

The mean, maximum, and minimum values of solar zenith angle and surface elevation are used in the LUT approach for the radiative transfer model SCIATRAN besides the already derived parameters (also compare to Section 7.1.2) flight altitude (2117 mamsl), aerosol scenario (urban), surface spectral reflectance (0.31) and background concentrations of  $\text{XCH}_4$  (1810.5 ppb) and  $\text{XCO}_2$  (392.2 ppm). The  $\text{XCO}_2$  background concentration is also in good agreement with the prediction of the SECM model (Reuter et al., 2012) of 393.0 ppm.

A mean wind speed of 4.1 m/s has been calculated as weighted mean for the second downwind wall, (which was flown directly after the remote sensing pattern) on basis of the relative  $\text{CH}_4$  distribution of the lowest legs, where the primary part of the plume is located (compare to Picarro in-situ data in Section 9.3.2). This weighted mean value is in good agreement with the mean wind speed of 4.0 m/s, calculated from the lowest leg of the same wall. In addition to the CIRPAS data also hourly METAR information is available for the Meadows airport (KBFL) (see Figure 39) located at central-south-west of the measurement area (see Figure 40).

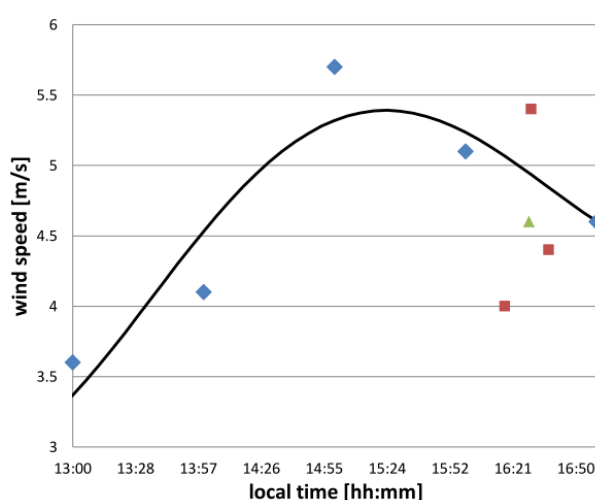


Figure 39: Hourly METAR data (10 minute averages) as reported by the Meadows Airport (blue squares) in comparison to the mean wind speed as calculated from each lowest leg (~4 to 6 min of average) of the three in-situ walls (brown squares) as acquired by the turbulence probe of the CIRPAS aircraft. For comparison, also the mean wind speed from all three legs is shown (green triangle). For interpolation, the KBFL wind measurements were fitted by a 4th order polynomial. Ground based data is in good agreement to the ground based measurements and within the reported accuracy of the CIRPAS turbulence probe of  $\sim 0.5$  to  $0.8$  m/s.

The wind direction has been determined empirically based on the  $\text{CH}_4$  plume observed in the MAMAP measurements to around  $332^\circ$  for the northern part of the field and to around  $307^\circ$  for the southern part of the field. The CIRPAS in-situ measurements indicate a wind direction of around  $337^\circ$  and  $320^\circ$  at the position of the first and second downwind wall, respectively. The difference in wind direction between the northern and southern part of the field were most likely induced by topography effect due to the mountain ridge on the eastern side of the field.



Figure 40 shows the normalized column averaged dry air mole fractions of  $\text{CH}_4$  for that day. The measurements have been smoothed by a 3-point moving average, normalized by a 300-point moving average (similar to RD-8), and filtered by an inclination angle of  $< +4^\circ$  of the downwelling optical path with respect to the nadir direction. The moving average normalization is only for visualization purposes and has no influence on the estimated emission rate, as each flight line is normalized individually by its flanks/edges for the estimate of emissions (see Section 9.1.1 for more details)

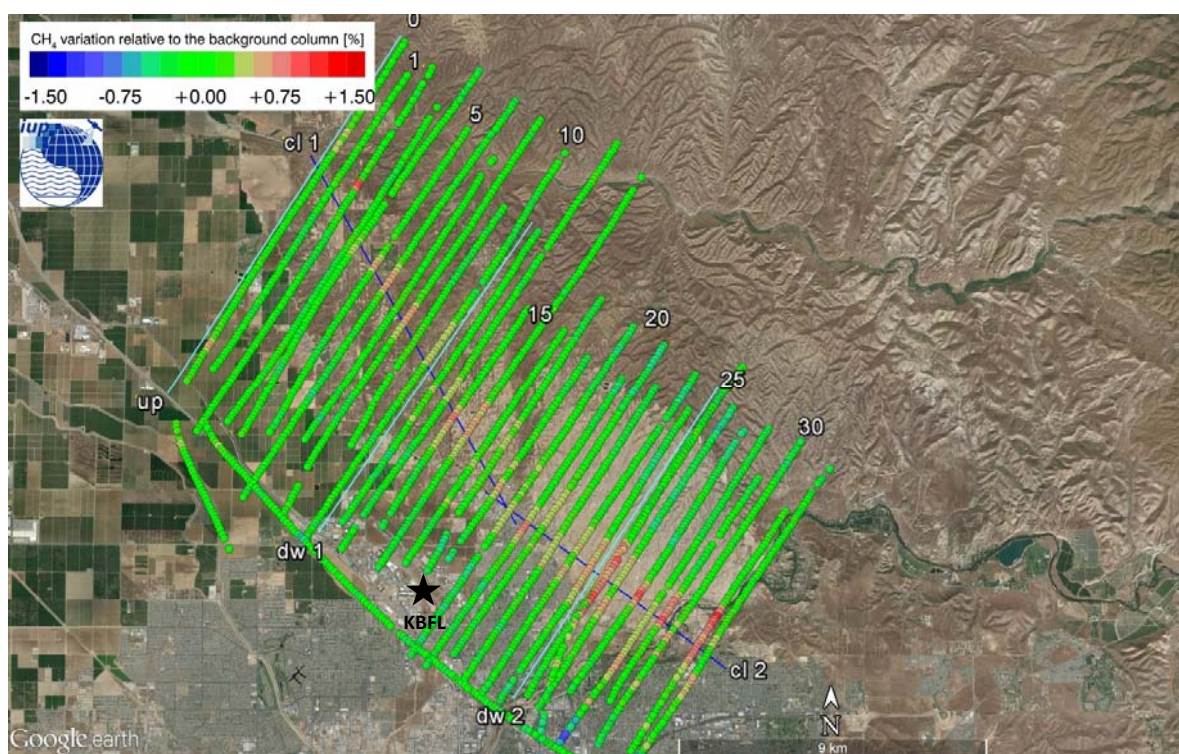


Figure 40: MAMAP flight pattern and LUT analysis of the Kern River, Kern Front and Poso Creek Oil Fields on 2014-09-04, between 13:40 and 15:50 local time. Flight altitude was around 2117 mamsl. Surface elevation is around 210 mamsl. The  $\text{CH}_4$  plume is visible as an enhancement in the normalized column averaged dry air mole fractions of  $\text{CH}_4$ . Wind direction was north-west and slightly shifting over the field due topography. Topography map underneath is provided by Google Earth. The data is filtered by an inclination angle of  $< +4^\circ$ . Additionally, also the two center lines (as discussed in Section 7.1.1), are shown reflecting as first approximation the topography induced wind shift over the field. Also shown are the three in-situ walls; upwind wall (up), first downwind wall (dw 1) and second downwind wall (dw 2) (solid cyan lines), as well as the position of the Meadows airport (KBFL). Numerals give the track numbering.

Figure 41, Figure 42 and Figure 43 summarize the results of the integral inversion method for the downwind tracks. Hourly time resolved wind information from the Meadows airport has been used to correct for temporal wind variations for the calculated fluxes. As can be seen in the overview, the emissions and, thus, the plume starts developing around track 4 to 6, increases till around track 16 and, then, stays relatively constant at  $\sim 25$  to  $35 \text{ ktCH}_4/\text{yr}$ .



# COMEX Final Report

Version: 2.0  
Doc ID: IUP-COMEX-FR  
Date: 3. July 2016

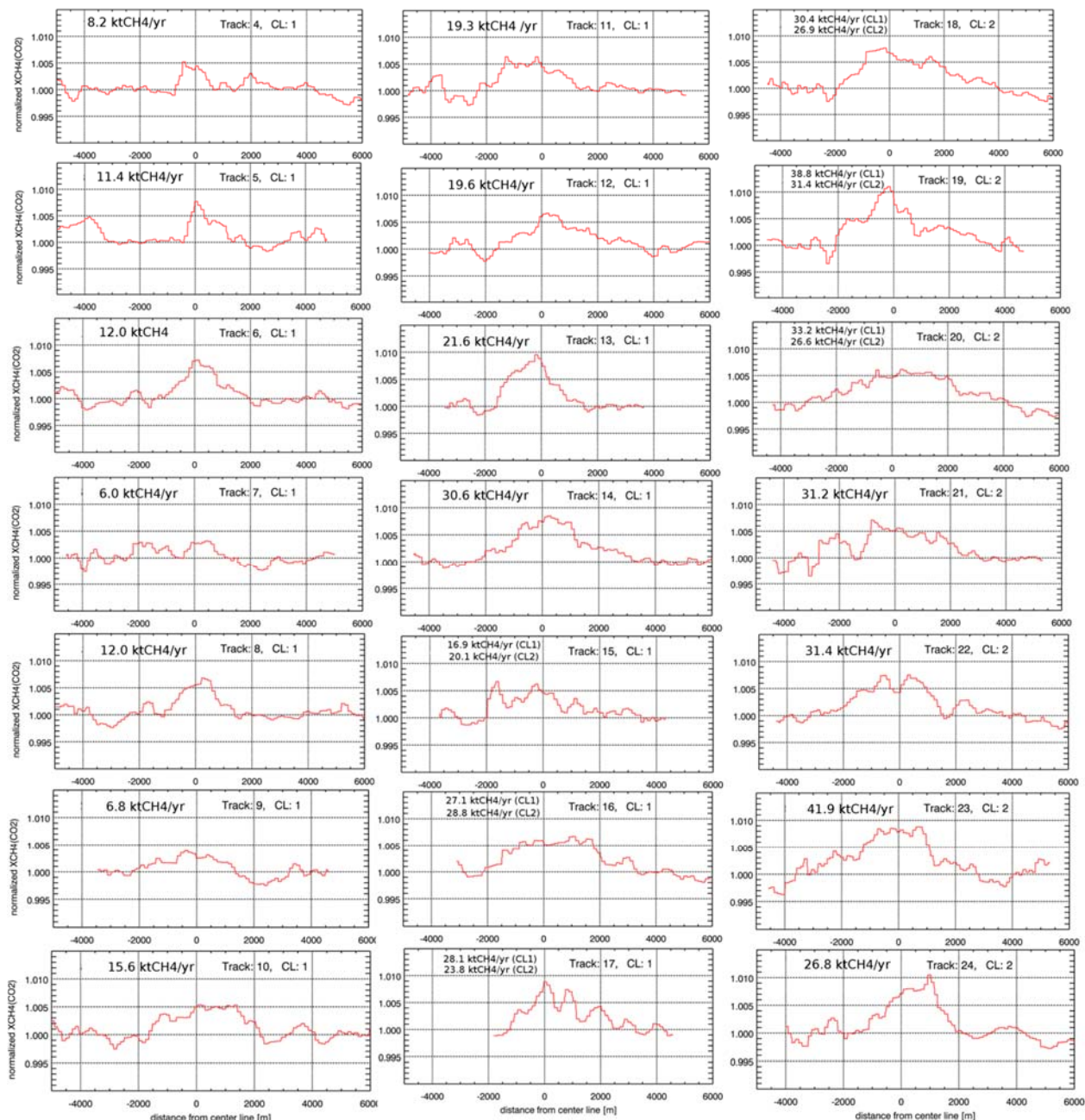


Figure 41: Cross sections of tracks 4 to 24 (to be continued in Figure 42) of the normalized column averaged dry air mole fraction of  $\text{CH}_4$  of the MAMAP remote sensing measurements at the Kern Front and Kern River Oil Field on 2014-09-01. The plume limits are  $\pm 3000$  m and the normalization limits are  $-5000$  m to  $-2000$  m and  $+3000$  m to  $+5000$  m (compare to Section 9.1.1). The limits for track 5 and track 17 are slightly narrower due to an obvious offset of the plume, which is caused by the increased  $\text{XCH}_4(\text{CO}_2)$  at around  $\pm 4000$  m, and a very short track, respectively. Each cross section contains labels for the estimated flux and the corresponding center line 1 (northern part) or 2 (southern part). At the transition zone of the wind turn (track 15 to 20), fluxes are given for both center lines. Negative distances point to the south-west and positive distances point to the north-east of the oil field. Wind information from KBFL was used to account for temporal wind variations.



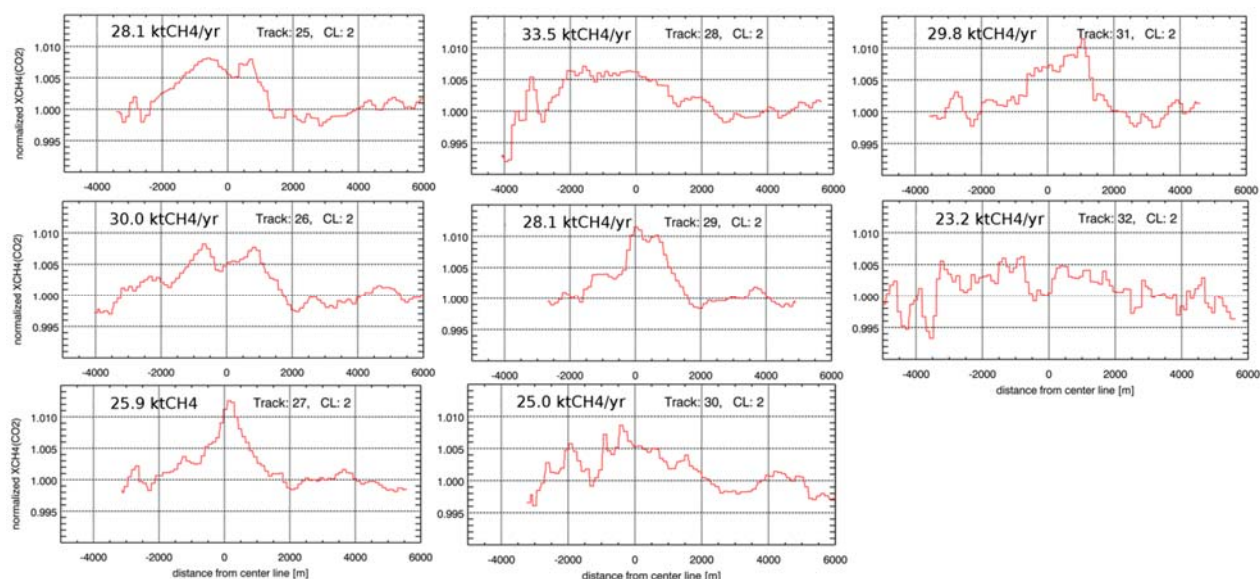


Figure 42: Continuation of Figure 41, showing track 25 to 32.

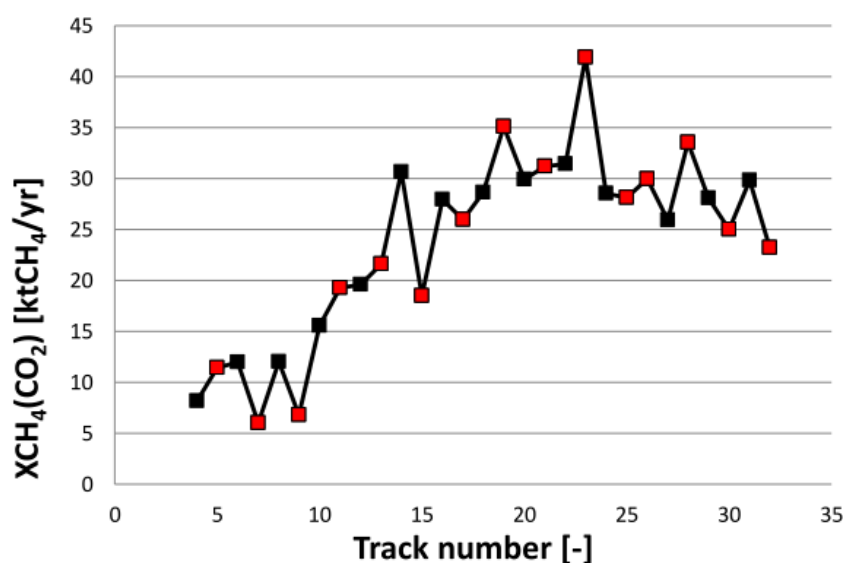



Figure 43: Estimated emission rates of CH<sub>4</sub> of the Poso Creek, Kern Front and Kern River Oil Fields on 2014-09-04. Fluxes at the transition zone where the wind turned are based on the mean value of the emission rate estimates of both center lines (compare to Figure 41). Temporal wind information from KBFL is used to account for wind variations. To account for temporal variability of the emission an interlaced flight pattern was flown over the measurement area. Black squares denote the flight pattern starting at 13:40 local time. Red squares denote the flight pattern starting at 14:45 local time. Emission estimates from both flight patterns are in good agreement reflecting steady emissions from the field during the measurement period of MAMAP remote sensing instrument of about 2 h.

	<p style="text-align: center;"><b>COMEX</b> <b>Final Report</b></p>	<p style="text-align: right;">Version: 2.0 Doc ID: IUP-COMEX-FR Date: 3. July 2016</p>
--	---	--

### **Uncertainty of the remote sensing emission rate estimate**

This section briefly describes the initial analysis of the uncertainty of the derived emissions.

Changing the plume limits to cover the whole track, changes the total emission rate of the field (track 14 to 32) by around -2 ktCH<sub>4</sub>/yr (-9%).

An uncertainty in the wind direction of around 10° (15°), translates to an uncertainty of the total flux of around +-1.5% (+-3.2%).

The variability of the wind speed based on the CIRPAS reported measurement accuracy of +-0.5 to 0.8 m/s, which is in good agreement to the ground based measurements, resulting in a flux uncertainty of +-13% to +-20 %.

The impact from co-emitted CO<sub>2</sub> is estimated to ~ -8 % on the total emission, see Section 9.3.3.

### 9.3.2. The Picarro in-situ data

Immediately, after the MAMAP remote sensing measurements over the boundary layer, in-situ surveys with the CIRPAS aircraft inside the boundary layer (intersecting and sampling the by remote sensing observed plume with the aircraft in-situ instrumentation) were performed between 15:50 to 17:00 local time, starting with the second downwind wall (compare to Figure 44).

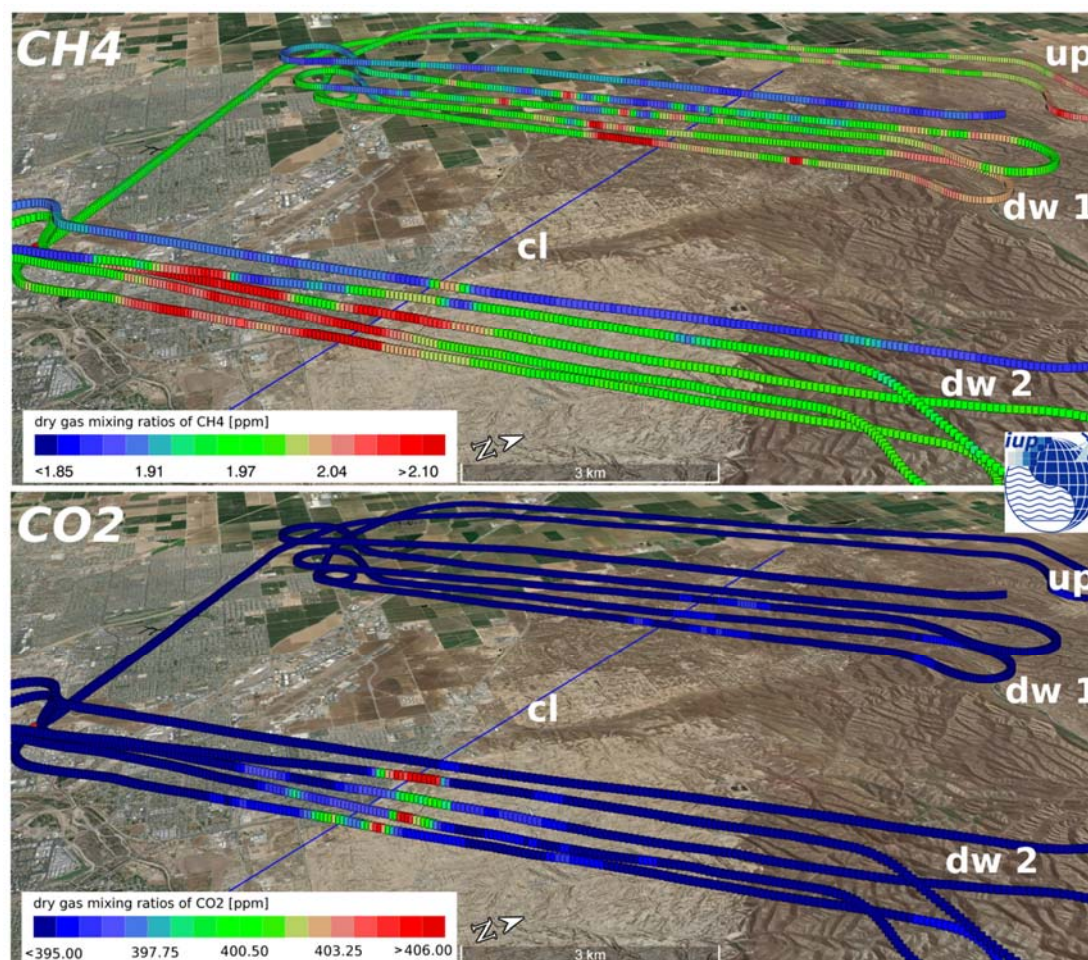



Figure 44: Subsequent airborne in-situ only measurements performed with the CIRPAS aircraft for validation of the collected remote sensing data. Shown are dry gas mixing ratios of  $\text{CH}_4$  (top) and  $\text{CO}_2$  (bottom) of the Picarro instrument. The in-situ data shows distinct methane enhancements (red color  $>2.10$  ppm) over the Kern River oil field at the position of the second downwind wall (dw 2) and weaker enhancements south of the Poso Creek oil field at the position of the first downwind wall (dw 1); similar for  $\text{CO}_2$ . Measurement was performed on 2014-09-04, between 15:50 to 17:00 local time. Additionally, also the center line (blue solid line) is shown. As discussed in Section 7.1.1, this center line is only for visualization purposes and has no influence on the Picarro in-situ flux estimates. Topography map underneath is provided by Google Earth.

	<b>COMEX</b> <b>Final Report</b>	Version: 2.0 Doc ID: IUP-COMEX-FR Date: 3. July 2016
--	-------------------------------------	--

Each wall consists of several measurements legs at different altitudes in meters above mean sea level (mamsl):

- Upwind wall: 1: 490, 2: 770
- 1. Downwind wall: 1: 486, 2: 771, 3: 1044, 4: 1327, 5: 1629
- 2. Downwind wall: 1: 493, 2: 767, 3: 1033, 4: 1336, 5: 1639

As the main focus of the in-situ Oil Field measurement is CH<sub>4</sub> and validation of the according remote sensing data, the CO<sub>2</sub> concentrations and the resulting CO<sub>2</sub> fluxes are analyzed in a less quantitative and qualitative manner (in comparison to CH<sub>4</sub>) to mainly assess the uncertainty of the XCH<sub>4</sub>(CO<sub>2</sub>) proxy approach applied for analysis of the remote sensing data (a more comprehensive analysis of the CO<sub>2</sub> in-situ data could be done in an additional study).

When examining the three in-situ walls of the Picarro CH<sub>4</sub> measurements, some outstanding features are observed. CH<sub>4</sub> is relatively homogeneous distributed in the middle of the upwind wall, whereas on the north-eastern side (to the right, Figure 44), slight enhancements are visible. The first downwind wall exhibits distinct enhancements at the lower flight altitudes, but also an overall increase on the north-eastern side. Going further in downwind direction, the CH<sub>4</sub> enhancements become stronger and broader, peaking at around 220 ppb above background values. Furthermore, the maximal altitude of the CH<sub>4</sub> plume is constraint by the highest leg where no CH<sub>4</sub> enhancement could be seen, or separated from the background. For the first downwind wall, no significant CH<sub>4</sub> enhancement can be observed in the fourth leg and for the second downwind wall, no CH<sub>4</sub> enhancements are seen at remote sensing altitude at around 2117 mamsl (not shown in Figure 44), whereas the CH<sub>4</sub> peak in the fifth leg is already very small.

A similar pattern is observed for CO<sub>2</sub>, having weak signals in the first downwind wall, which become more pronounced in the second downwind wall.

For the calculation of the emission rate, the three lowest legs of the first and the five lowest legs of the second downwind wall have been used. The plume area has been restricted to -3500 m to +3500 m and -3500 m to +4500 m for the first and second downwind wall, respectively. For determining the background, measurements between distances of 3500 m to 5000 m, on each side of the center line, have been used for the first downwind wall, and between -4500 m to -3500 m and +4500 m to +7000 m have been used for the second downwind wall. The asymmetric limits are due to the longer flight legs on the eastern side of the plume compared to the western side of the second downwind wall.





# COMEX Final Report

Version: 2.0  
Doc ID: IUP-COMEX-FR  
Date: 3. July 2016

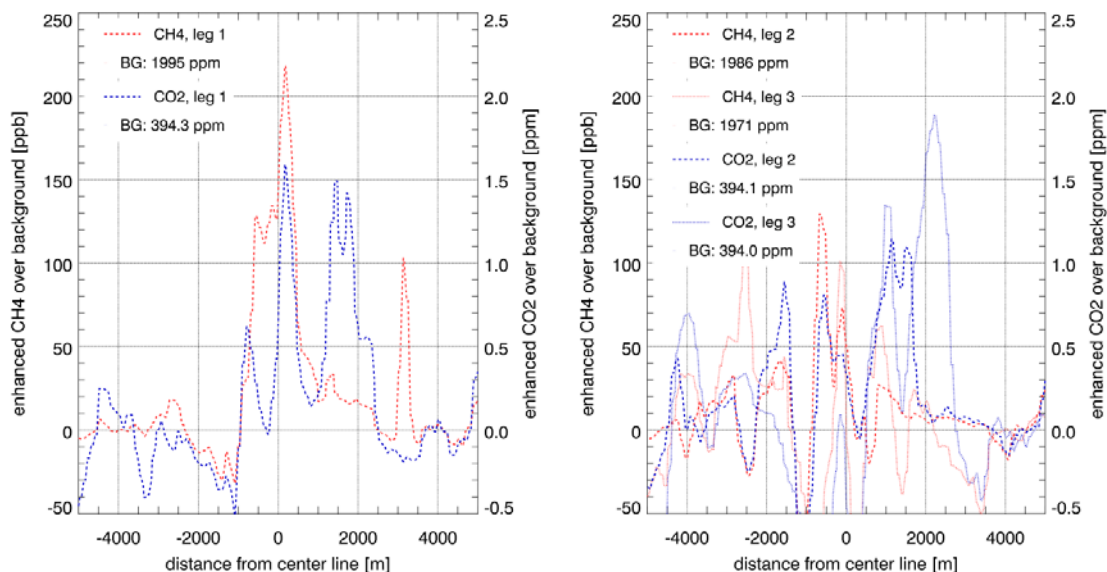


Figure 45: Shown are the three lowest legs of  $\text{CH}_4$  (red) and  $\text{CO}_2$  (blue) of the first downwind wall. Left: The lowest leg. Right: The second (dashed line) and third (dotted line) lowest leg. Negative distances point to the south-west and positive distances point to the north-east of the oil field.

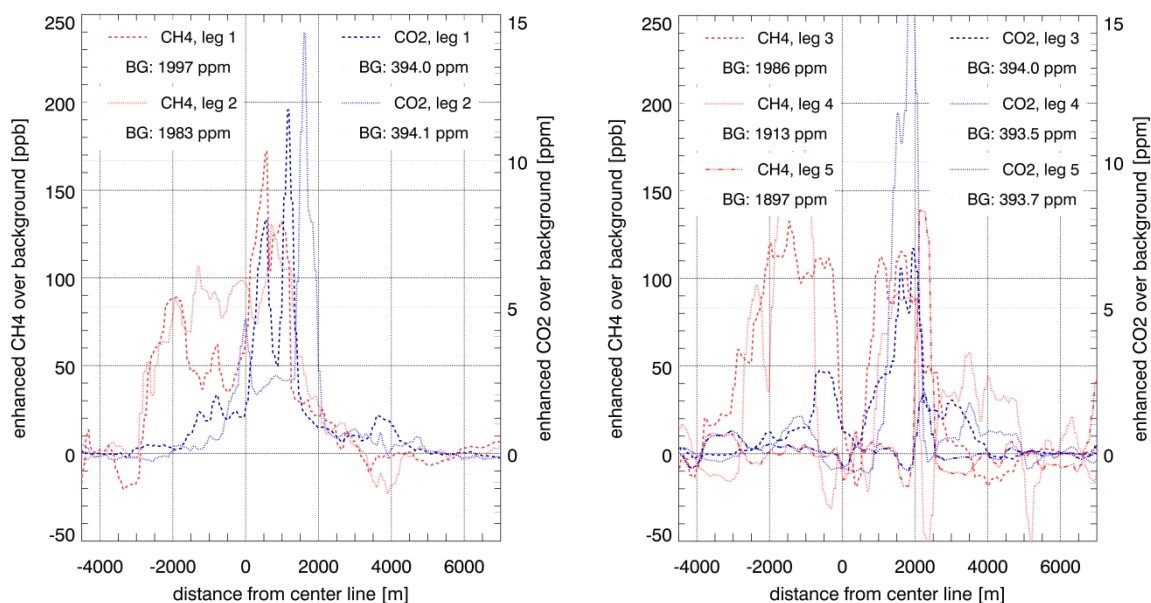



Figure 46: Shown are the five lowest legs of  $\text{CH}_4$  (red) and  $\text{CO}_2$  (blue) of the second downwind wall. Left: The lowest (dashed line) and second lowest (dotted line) leg. Right: The third (dashed line), fourth (dotted line) and fifth (dashed-dotted line) lowest leg. Negative distances point to the south-west and positive distances point to the north-east of the oil field.

The estimated emission rates for the first and second downwind wall are for  $\text{CH}_4$  9.6  $\text{ktCH}_4/\text{yr}$  and 30.9  $\text{ktCH}_4/\text{yr}$ , and for  $\text{CO}_2$  290.1  $\text{ktCO}_2/\text{yr}$  and 2815.8  $\text{ktCO}_2/\text{yr}$ , respectively.



	<b>COMEX</b> <b>Final Report</b>	Version: 2.0 Doc ID: IUP-COMEX-FR Date: 3. July 2016
---	-------------------------------------	--

### Uncertainties of in-situ emission rate estimates

This section briefly describes the initial analysis of the uncertainty of the derived emissions.

The main CH<sub>4</sub> plume of the first downwind wall is well confined within 2000 m around the center line (compare to Figure 45, left and Figure 47, left). The small peak at about +3000 m contributes only with around 0.5 ktCH<sub>4</sub>/yr to the overall plume. Extending, for example, the plume limits to +5000 m (whole track) increases the emission rate by only +2%. Varying the limits for the background calculation by 1000 m, modifies the flux by maximal +-16%, whereas most of the variability originates from the upper tracks, where no clear plume structure is visible and, thus, complicates the calculation of a background (compare to Figure 45, right).

Applying similar sensitivity tests to the second downwind wall, give an increase of less than 2% for increasing the plume limits to cover the whole track (-4500 m to +7000 m) or varying the limits for the background calculation, for example, between +3500 m and +5500 m on the positive distance side.

As for the Olinda Alpha Landfill in-situ emission rate estimates, a large uncertainty originates from the plume propagation to the surface. To estimate the lower part of the plume down to the surface, it has not been assumed a well-mixed situation, but 1) a linear decrease of the concentration till the surface having a surface value of 50% of the lowest leg and 2) a linear increase of the concentration till the surface having a surface value of 150% of the lowest leg.

The resulting emission rates are

- 1) first downwind wall: 8.4 ktCH<sub>4</sub>/yr (-13%) and 265.9 ktCO<sub>2</sub>/yr (-8%),  
second downwind wall: 29.0 ktCH<sub>4</sub>/yr (-6%) and 2613.2 ktCO<sub>2</sub>/yr (-7%), and
- 2) first downwind wall: 10.8 ktCH<sub>4</sub>/yr (+13%) and 313.5 ktCO<sub>2</sub>/yr (+8%),  
second downwind wall: 32.7 ktCH<sub>4</sub>/yr (+6%) and 3010.6 ktCO<sub>2</sub>/yr (+7%).

The error originating from the accuracy of the turbulence probe has been estimated to +-19% (dw1, mean wind speed of 4.2 m/s) and +-20% (dw2, mean wind speed of 4.1 m/s) (also compare to Section 9.2.2).

As discussed in Section 9.2.2, the wind speed and the concentration measurements might be correlated to some degree. The combined standard uncertainties of flux the of the first and second downwind wall, respectively, are +-28% (including the sensitivity of the flux to varying limits for the background calculation) and +-21% in case of no correlation, and +-35% and +-26% in case of correlation.

The CH<sub>4</sub> emission rate estimate of around 9.6 ktCH<sub>4</sub>/yr for the first downwind wall and 30.9 ktCH<sub>4</sub>/yr for the second downwind based on the Picarro in-situ measurements show a clear increase in CH<sub>4</sub> (and also in CO<sub>2</sub>) when moving in downwind direction of the plume. A similar behavior is also observed in the MAMAP remote sensing data.

### 9.3.3. Investigation and justification of the MAMAP $\text{XCH}_4(\text{CO}_2)$ proxy retrieval assumption over the Kern Oil Fields

The  $\text{CH}_4$  and  $\text{CO}_2$  Picarro in-situ data is used to also investigate the  $\text{CH}_4(\text{CO}_2)$  proxy assumption used in the MAMAP retrieval to derive  $\text{XCH}_4$ . Compared to the Olinda Alpha Landfill investigation, where the main focus was the impact of  $\text{CO}_2$  “contamination” on the MAMAP  $\text{XCH}_4(\text{CO}_2)$  proxy retrieval, for the Kern Oil Fields, also possible  $\text{CO}_2$  gradients (inside the boundary layer) introduced by transport or topography are analyzed.

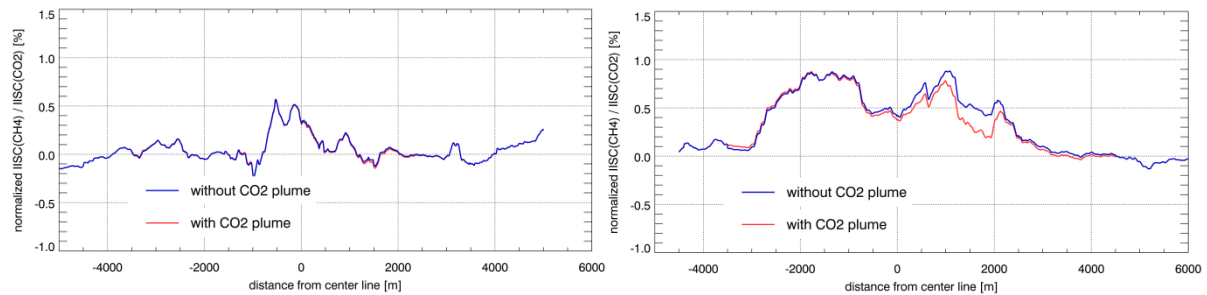


Figure 47: Left: First downwind wall. Right: Second downwind wall. Negative distances point to the south-west and positive distances point to the north-east of the oil field. The two colors depict two different approaches for calculating integrated in-situ columns (IISC). Red: In-situ measurements are not modified. Blue: The  $\text{CO}_2$  measurements of the four lowest legs of each wall, which have also been used for calculating the flux, have been replaced by the mean value of  $\text{CO}_2$  measurements outside the plume area to simulate how a column would look like if there was no co-emitted  $\text{CO}_2$  present.

Based on the in-situ data, the maximum column enhancement of  $\text{CH}_4$  relative to the background is slightly below 0.6% and at around 0.8% for the first and second in-situ wall, respectively. These enhancements are in the same order of magnitude (around 0.5% and 0.8%, respectively) as seen by the MAMAP remote sensing instrument (compare to Figure 48 and Figure 49). These two sets of measurements were recorded 60 to 150 minutes apart. Additionally, for the IISC of each in-situ wall, several legs at different altitudes have been used, which were also not taken simultaneously. The remaining column above the remote sensing altitudes, which was not surveyed, has been complemented by the scaled U.S. standard atmosphere. Therefore, it is not expected that the two types of columns agree exactly.

The IISC also reflects the spatial distribution and/or emission strength of the sources over the fields. The plume (and according emission) is weaker and narrower in the northern part (downwind of Poso Creek) at the location of the first downwind wall. At the proximate center of the Kern River Oil Field (i.e. location of the second downwind wall) additional sources (located between the first and second downwind wall) contribute to the overall plume, as confirmed by the MAMAP remote sensing and Picarro in-situ data set.

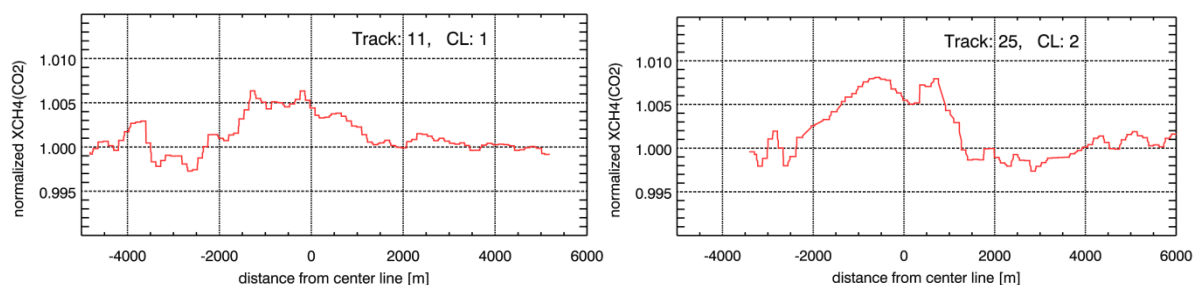


Figure 48: Normalized column averaged dry air mole fraction of  $\text{CH}_4$  of the two MAMAP legs which are closest in time to first (MAMAP track 11) and second downwind (MAMAP track 25), respectively.

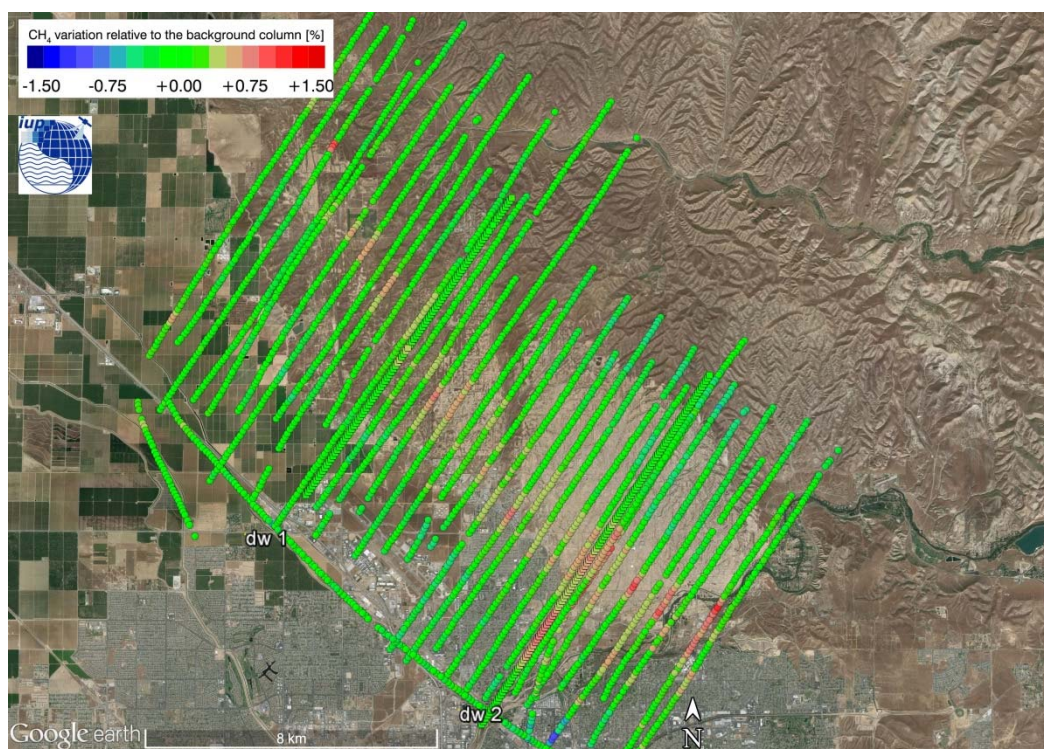


Figure 49: Shown are the normalized column averaged dry air mole fractions of  $\text{CH}_4$  (circles; similar to Figure 40) and the normalized ratios of the integrated in-situ columns of  $\text{CH}_4$  and  $\text{CO}_2$  for the first (dw1) and second downwind (dw2) wall (squares).

Concerning the possible offset of the normalized column averaged dry air mole fractions of  $\text{CH}_4$  by  $\text{CO}_2$  anomalies and, thus, the validity of the  $\text{CO}_2$  proxy approach actually used for the  $\text{XCH}_4(\text{CO}_2)$  MAMAP retrieval, an offset of -0.24% could be estimated on the right side of the plume for the second downwind wall (Figure 47). The  $\text{CO}_2$  impact on the in-situ estimated (normalized)  $\text{XCH}_4$  of the first downwind wall is below -0.03%. First investigations using these normalized IISC columns for flux inversions, indicate a  $\text{CO}_2$  induced difference in the emission rate for the second downwind wall of around -8%. Assuming, this is also valid for the MAMAP remote sensing measurements, which took place around one hour earlier, the effect of co-emitted  $\text{CO}_2$  in the area may lead to an underestimation of the total emission rate estimate for that day based on the MAMAP measurements for the Kern River, Kern Front and Poso Creek Oil Fields in the same order of magnitude.

In contrast to the Olinda Alpha Landfill (Figure 35) where the  $\text{CO}_2$  plume is in good alignment with the  $\text{CH}_4$  plume, for the oil fields, the  $\text{CO}_2$  plume is most pronounced on the eastern side of the  $\text{CH}_4$  plume of the second collected downwind wall.

The apparent slight decrease in  $\text{XCH}_4(\text{CO}_2)$  observed in the MAMAP data (and according potential gradient of  $\text{CO}_2$ ) in the south-eastern part of the oil field cannot be confirmed by the Picarro in-situ observations. Therefore the origin of this slight gradient observed on this day is unclear.



#### 9.4. Comparison of MAMAP XCH<sub>4</sub> data with AVIRS-NG methane anomaly maps acquired over Kern River, Kern Front and Poso Creek Oil Fields

On 2014-09-04, contemporaneous measurements to MAMAP over the Kern River, Kern Front and the Poso Creek Oil Fields were performed with the AVIRIS-NG Visible & Shortwave Infrared (VSWIR) imaging spectrometer, operated by the NASA - Jet Propulsion Laboratory (JPL), California Institute of Technology (CALTECH). The AVIRIS-NG imaging spectrometer measures (in contrast to the MAMAP non imaging spectrometer) 598 across track spectra simultaneously at 100 Hz temporal resolution (Thompson et al., 2015) but at lower spectral resolution and spectral sampling in comparison to MAMAP (e.g. ~ 5 nm spectral resolution at a spectral sampling of 1 pixel for AVIRIS-NG in comparison to ~ 0.9 nm spectral resolution at a spectral sampling of ~ 8-9 pixel/FWHM for MAMAP). The AVIRIS-NG data was analyzed for its ability for CH<sub>4</sub> anomaly detection by different methods (e.g. band ratio approach, columnwise matched filter approach; see Thompson et al., 2015). For analysis of CH<sub>4</sub> by the columnwise matched filter the spectral window between 2100 and 2450 nm was used for the AVIRIS-NG dataset (Thompson et al., 2015). MAMAP uses in contrast for the retrieval of XCH<sub>4</sub> by WFM-DOAS the spectral window between ~ 1590 and 1690 nm (for the CO<sub>2</sub> proxy approach). Methane anomaly maps derive from the AVIRIS-NG data by the columnwise matched filter approach are compared and superimposed to total column XCH<sub>4</sub>(CO<sub>2</sub>) distributions derived from the MAMAP remote sensing data. Flux distribution derived from the MAMAP remote sensing data is compared to source distributions derived from the AVIRIS-NG methane anomaly maps. For comparison also in-situ derived fluxes are shown in Figure 51.

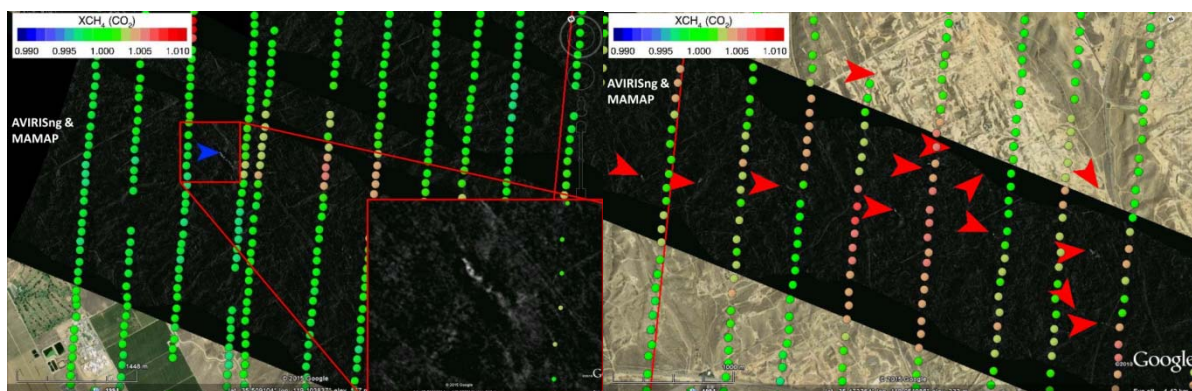


Figure 50: Left: MAMAP XCH<sub>4</sub>(CO<sub>2</sub>) data acquired on 2014-09-04 over Poso Creek in comparison to contemporaneous acquired AVIRIS-NG data. Inset shows a large source detected by the AVIRIS-NG columnwise matched filter likely responsible for the large scale plume observed by MAMAP over the Poso Creek area. Right: Overlay of MAMAP data with AVIRIS-NG data acquired over the Kern Front (and Kern River) area. Red arrows denote CH<sub>4</sub> sources detected by AVIRIS-NG, contributing additionally to the large scale plume observed by MAMAP. AVIRIS-NG data was provided by David Thompson, NASA - Jet Propulsion Laboratory (JPL), California Institute of Technology (CALTECH).



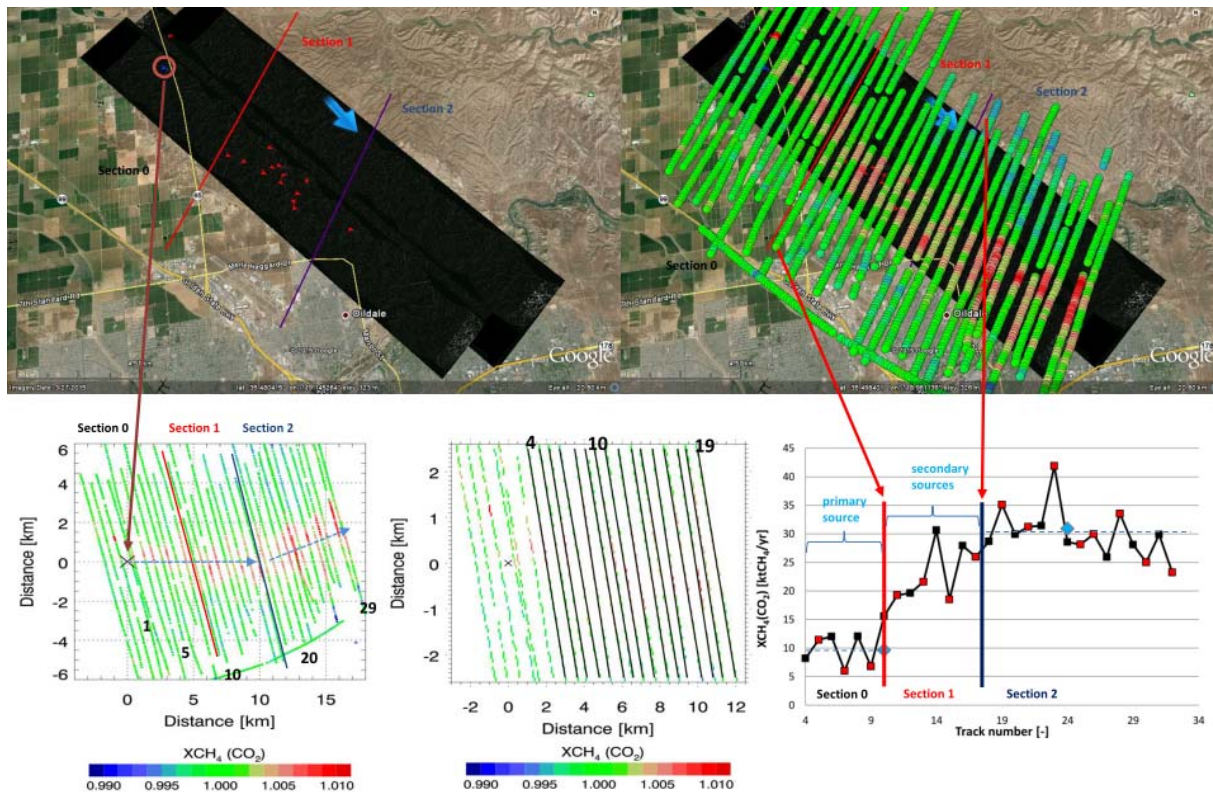


Figure 51: Upper Left: Source distribution as observed by AVIRIS-NG over the Poso-Creek, Kern-Front and Kern-River Oil Fields. The measurement area was divided in three sections representing different distribution of sources as observed by AVIRIS-NG. Section 0 contains mainly the primary source likely responsible for the first part of the MAMAP observed plume. Upper Right: Overlay of the AVIRIS-NG data with MAMAP data. Lower Left: MAMAP data rotated in wind direction (wind direction taken from the first part of the measurements, see also Section 9.3.1). Lower Central: Number of MAMAP tracks used for the inversion (only tracks of the first part, before change in wind direction are displayed, see also Section 9.3.1). Lower Right: Flux rates as obtained from MAMAP data for each track. Blue and black rectangles indicate interlaced MAMAP measurements, measured with approximately 1h difference. For comparison, also fluxes derived from the two in-situ walls at the according positions were shown. Total flux from the three oil fields has been estimated to  $\sim 30$  ktCH<sub>4</sub>/yr for the time of the overflight. Flux from the Poso Creek Oil Field, likely induced primarily by the large source shown in Figure 50 (left), has been estimated to be  $\sim 10$  ktCH<sub>4</sub>/yr by both, remote sensing and in-situ measurements.

In Figure 51, an excellent spatial agreement between MAMAP derived fluxes and AVIRIS-NG derived source distribution could be observed. In section 0, Figure 51 (Poso Creek Area), emissions with a flux magnitude of  $\sim 10$  ktCH<sub>4</sub>/yr (for the time of the overflight) could be derived by MAMAP data. This flux is caused most likely mainly by the well, where a large plume could be identified (on small spatial scales) also in the AVIRIS-NG dataset (see Figure 50, left). In section 1, Figure 51, an increase of the derived flux could be identified by the MAMAP dataset in accordance to the AVIRIS-NG observed increase in source distribution. In section 2, Figure 51, the MAMAP derived flux seems to reach again a steady total level of  $\sim 30$  ktCH<sub>4</sub>/yr (for the time of the overflight) in accordance to the observed decrease of sources in the according AVIRIS-NG data set. The, by remote sensing obtained fluxes for Poso Creek, the Kern Front and Kern River field areas are in excellent lateral agreement with the in-situ observed fluxes (see Figure 51, lower right). The fluxes derived from the in-situ data at the end of section 0, Figure 51 (first downwind wall), originating from the Poso Creek area, are estimated to CH<sub>4</sub> 9.6 ktCH<sub>4</sub>/yr (see Section 9.3.2) vs. the proximate 10 ktCH<sub>4</sub>/yr estimated for this section from the

MAMAP data. The in-situ flux of 30.9 ktCH<sub>4</sub>/yr estimated in the center of section 2, Figure 51, is also in good agreement with the (total) flux of ~30 ktCH<sub>4</sub>/yr as estimated from the MAMAP remote sensing data for this section (see Figure 51, lower right).

In Figure 52, also an overlay of the observed plume with well information as obtained by the Division of Oil, Gas, and Geothermal Resources (DOGGR), California is shown. As can be seen from the plot, there is no strong correlation between the well density and the areas, where larger enhancements in XCH<sub>4</sub>(CO<sub>2</sub>) are observed. These measurements demonstrate the ability of (combined) remotely obtained CH<sub>4</sub> column information (obtained on different spatial and spectral scales), to not only assess total field emissions, but to also attribute emissions to their origin. Furthermore, the ability of future space based sensors with imaging capabilities like CarbonSAT, to detect and image localized (anthropogenic) emissions (see Section 11) and thereby to better disentangle emissions from different origin could be analysed by such datasets.

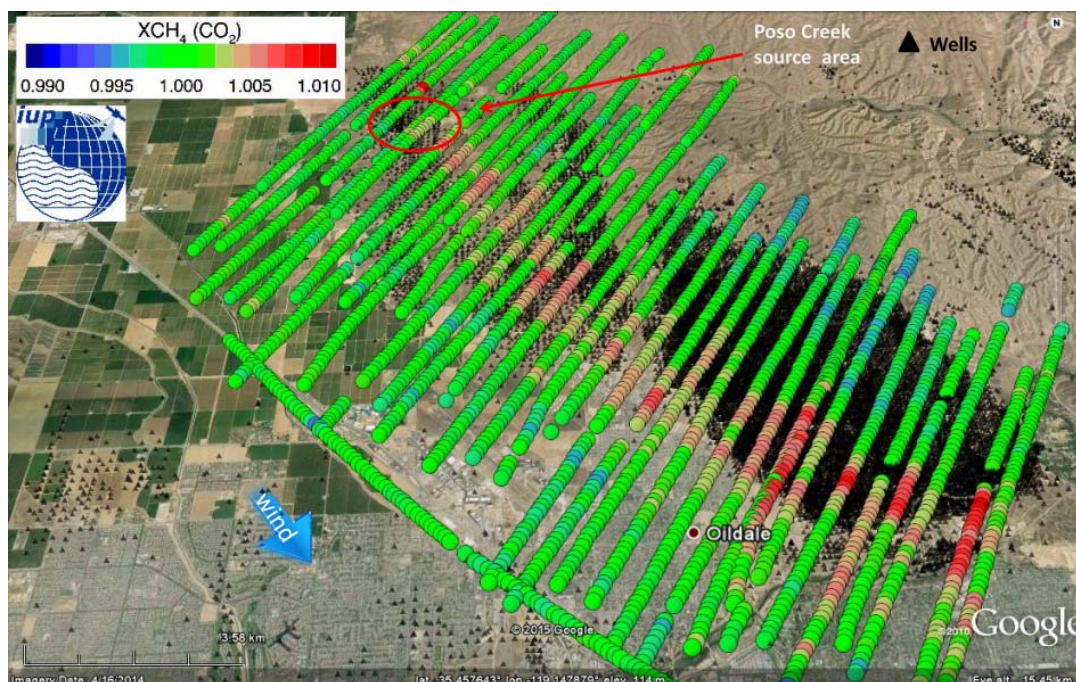


Figure 52: Overlay of XCH<sub>4</sub>(CO<sub>2</sub>) data as derived from MAMAP measurements with distribution of wells in the Poso Creek, Kern Front and Kern River area. The overlay demonstrates that observed emissions over the three fields are not strongly correlated with well density in the area. Position of large source in the Poso Creek area (Figure 51, left) is marked by red circle. Well distribution data is obtained from the Division of Oil, Gas, and Geothermal Resources (DOGGR), CA, (<http://www.conervation.ca.gov/dog>).



## 10. Analysis of Glint data over the Santa Barbara Seeps

Surveys at the Coal Oil Point close to Santa Barbara were performed on two days – 2014-06-04 and 2014-08-25. The marine seeps located here were expected to emit about 26 ktCH<sub>4</sub>/yr, estimated using data from 1994-1996 (Hornafius et al., 1999). According to Bradley et al. (2010) emissions were decreasing until 1997 and then increased again at least until 2008 (end of analyzed time series).

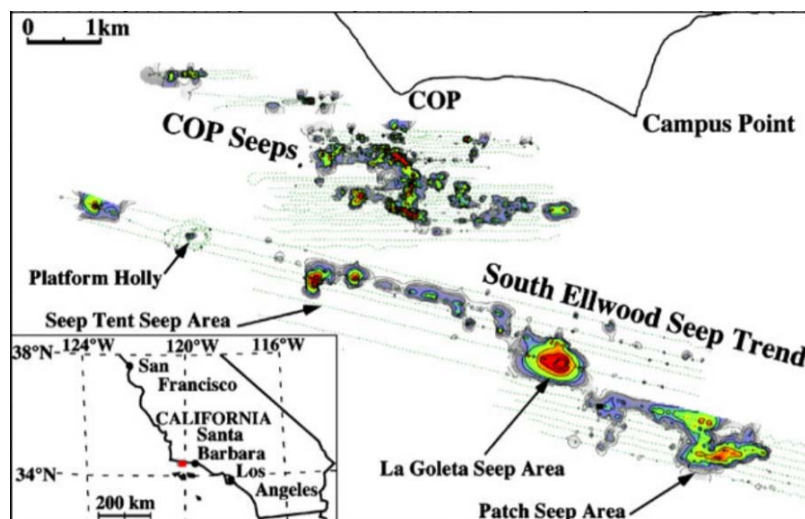


Figure 53: Seep area with the most prominent seeps, derived from sonar return measurements, including La Goleta and Trilogy (Leifer et al., 2010).

The time series from Bradley et al. (2010) recorded at West Campus Station (WCS) north of the seep area recently was extended to include the COMEX campaign (Ira Leifer, 2015, personal communication). The methodology for the analysis was as follows. After removing non-physical data entries for wind speed, wind direction, and total hydrocarbons (THC), primarily during daily calibrations entries, THC data were smoothed by a 3-point (3-minute or 3-hour) running average, while wind data were smoothed on a 5-point (5-minute or 5 hour) running average basis. The longer smoothing time represents data before 2008, which was hourly and the shorter, more recent data recorded at 1-minute intervals.

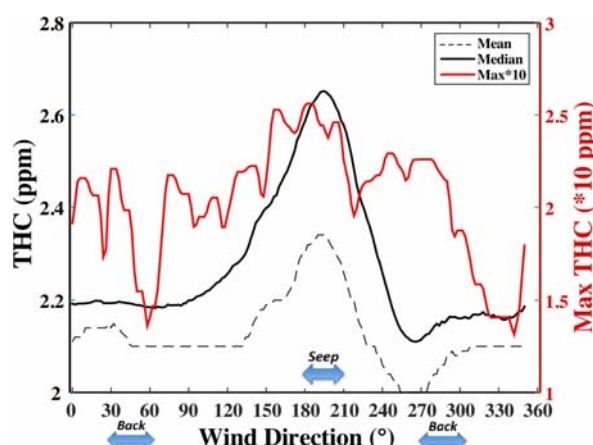



Figure 54: Average,  $C_{ave}$ , median,  $C_{med}$ , and maximum,  $C_{max}$ , THC concentration versus wind direction,  $\phi$ , at WCS for 10° bins every 2°. Arrows show directions used to differentiate seep field emissions from background emissions for anomaly analysis (Ira Leifer, 2015, personal communication).

To de-convolve the trend in the seep emissions from the larger regional trends, specific wind directions were chosen as representative of seep and background values based on the angular distribution of

	<p style="text-align: center;"><b>COMEX</b> <b>Final Report</b></p>	<p style="text-align: right;">Version: 2.0 Doc ID: IUP-COMEX-FR Date: 3. July 2016</p>
--	---	--

emissions (see Figure 54). The strongest emissions clearly arise from the seep field, direction, with most emissions spanning from  $130^\circ$  to  $270^\circ$ , although persistent offshore seepage occurs at directions as far as  $90^\circ$  from WCS. The depression in the average concentration with respect to wind direction,  $C_{ave}(\phi)$ , at  $\approx 270^\circ$  results from stronger prevailing winds that dilute seep emissions more than other directions.

The maximum of the angular distribution,  $C_{max}(\phi)$ , is significantly larger, by more than a factor of 10, and exhibits far less overall angular dependency, although it also exhibits far more structure. Note, the overlapping binning scheme imposes averaging of  $\approx 10^\circ$ , preventing interpretation of smaller angular scale structures. Of course, anomaly is not emissions, as dilution due to dispersion and wind occurs during transport. However, as Bradley et al (2010) showed, winds have been seasonally stable over the decades, and the locations of the seeps are fixed by geology – changes in emission location are largely fixed. Thus relative changes in WCS observations are approximately linear with relative changes in emissions.

More recent (and temporally better resolved) data since 2008 show that the anomaly from the seep field direction was at a maximum around 2009, and has been decreasing since, by about a factor of three (I. Leifer, personal communication). Methane concentrations from the direction of the seep field appear to have stabilized, this however arises in part from the increasing regional trend (Santa Barbara Channel, and also California  $\text{CH}_4$  “ambient” are well above the latitudinal mean). Thus, the anomaly from the seep field has continued decreasing approximately linearly since 2010. Between 2009 and 2010, there is a significant decrease. The anomaly is about a factor of two lower in the summer than in the winter.

#### **10.1.1. Coal Oil Point 2014-06-04**

The MAMAP measurements on 2014-06-04 over the Coal Oil Point area were performed at about 11:35 to 13:45 local time. Aircraft altitude for the remote sensing measurements was 1400 mamsl and the MAMAP instrument was mounted with a preselected viewing angle of  $11.6^\circ$  to capture the solar glint/glitter spot on the sea surface. The viewing angle was manually set before reaching the target area.

This measurement geometry was taken into account for determination of the geolocations for the measurements. The background concentrations were about 1807.8 ppb for  $\text{XCH}_4$  and about 399.2 ppm for  $\text{XCO}_2$  derived from PICARRO in-situ measurements. For  $\text{XCO}_2$  the value is in excellent agreement with the SECM model (Reuter et al., 2012) which predicts a background of 398.5 ppm.

To account for the special geometry and reflectance behavior for the sun glint, the SCIATRAN radiative transfer model was operated in sun glint mode, applying the glint parameterization of Cox and Munk (1954) for the complete data set. To reduce observations that missed the sun glint spot, measurements were only accepted for further processing in case the detector filling was at least 20% of the full well capacity. Additionally measurements were filtered out when the viewing angle deviated more than  $2^\circ$  from the prescribed value, e.g. when the aircraft is turning.

The data that pass the filter are of good quality and the corresponding retrieved  $\text{XCH}_4(\text{CO}_2)$  data are shown in Figure 55 (left). With wind from about  $250^\circ$  as derived from the CIRPAS wind probe, there is no clear plume structure of  $\text{CH}_4$  visible downwind of the seep area, which is indicated in the plot by the two black crosses. The crosses represent the prominent Trilogy (northwest) and the La Goleta (southeast) seeps, which belong to the largest seeps in the Coal Oil Point area.

The data also exhibits several land sea transitions that allow further analysis in the future. For the present initial analysis that focused on potential emissions of the marine seep area, land and sea



spectra were both treated with the same glint RTM and therefore land measurements have to be interpreted with care.

Also shown are the solar zenith angles for each measurement time and location (Figure 55, right), indicating that the SZA varied from about 11° to 22° during the survey, but that the preset inclination angle of about 12° was well suited for most measurements to guarantee appropriate signal strengths.

To support the assumption that the CH<sub>4</sub> from the seeps should have been observed by MAMAP – for the case when the source strength was as expected - simulations were performed applying a Gaussian plume model and emission rates of 26 ktCH<sub>4</sub>/yr as reported by Hornafius et al. (1999), split equally between the approximate locations of the currently two prominent seeps, Trilogy and La Goleta. At the Trilogy seep area also AVIRIS picked up CH<sub>4</sub> column enhancements of a few percent in 2008 (Thorpe et al., 2014). To account for the existence of various other seeps, the source diameter was set to 300 m. Of course this can only be a rough estimation of the actual distribution of emissions in the seep area. Wind speed and direction were inferred from the CIRPAS turbulence probe data to about 5 m/s for the area of interest blowing from about 250°. To compare measurements and simulation, the data was gridded to 100 m x 100 m and the simulation was then performed for locations where actual MAMAP observations were recorded. The results are shown in Figure 56. They show that a clear signal could be expected (centre) and that it should have been visible also in the presence of noise (right). Thereby the precision was about 0.27% evaluated as standard deviation from the data and similar to MAMAP glint observations in the North Sea from 2011 (RD-6). The conclusion from the MAMAP data is therefore that the emission rate for the time of the overflight was significantly lower than 26 ktCH<sub>4</sub>/yr.

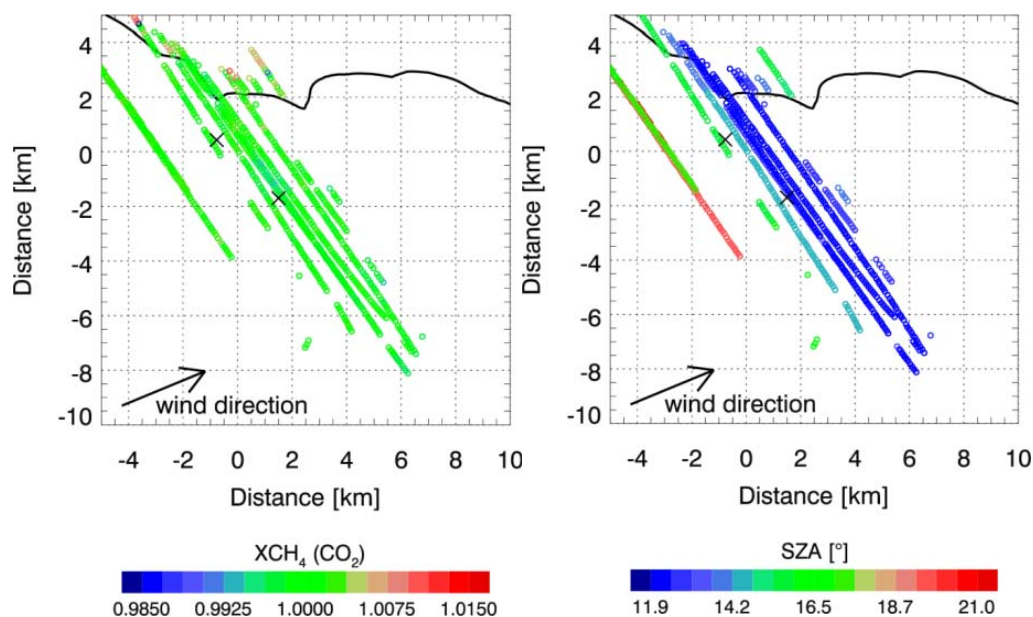


Figure 55: The left plot shows the unsmoothed XCH<sub>4</sub> data normalized by a regional mean. The corresponding solar zenith angle (SZA) for each data point is shown on the right.

When inspecting the in-situ measurements (see Figure 57 and Figure 58) maximum enhancements in the signal of about 6% (or 120 ppb) in the lower boundary layer are observed. This is in agreement with the lower range of the on-shore in-situ data (I. Leifer, personal communication) which was recorded closer to the surface but on the other hand further away from the sources. Assuming that this enhancement is representative for about the lowest 210 m this would yield a total column enhancement of only about 0.15% which is below MAMAP's noise level and hence challenging to be detected on the investigated scales. This value is also well below what was predicted for MAMAP by

simulations using emission rates from Hornafius et al. (1999) (see Figure 56) and from results obtained from AVIRIS data from 2008 (Thorpe et al., 2014). These findings are in agreement with the MAMAP observations and further strengthen the conclusions that the seep methane emissions at the time of the overflight were significantly lower than initially expected.

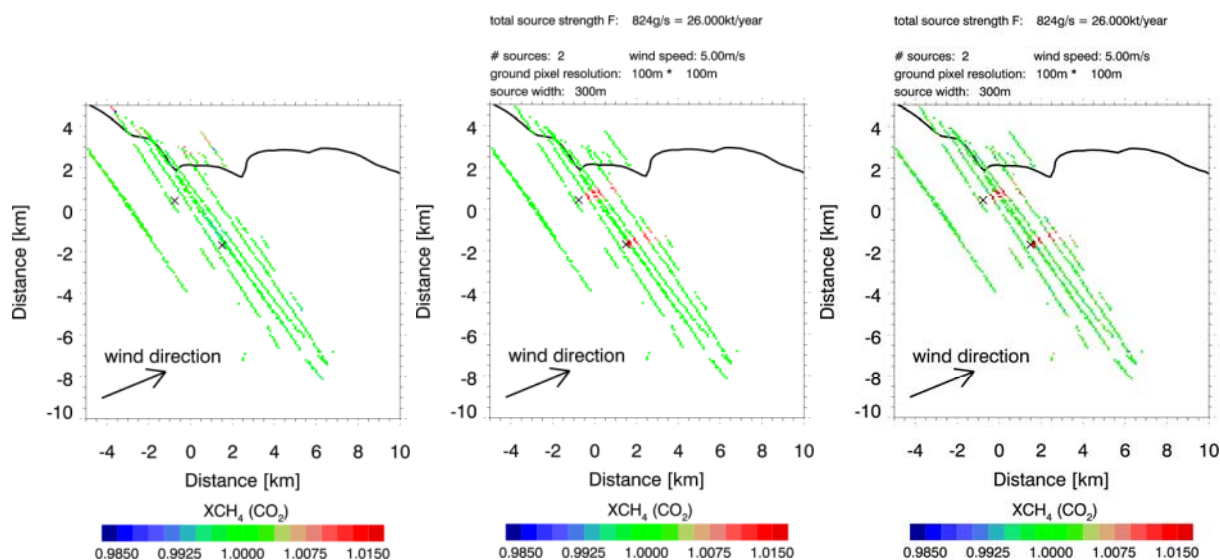


Figure 56: Measurement data gridded (left) and simulations without noise (centre) and with random noise (right) for two equal sources of a total source strength of 26 ktCH<sub>4</sub>/yr.

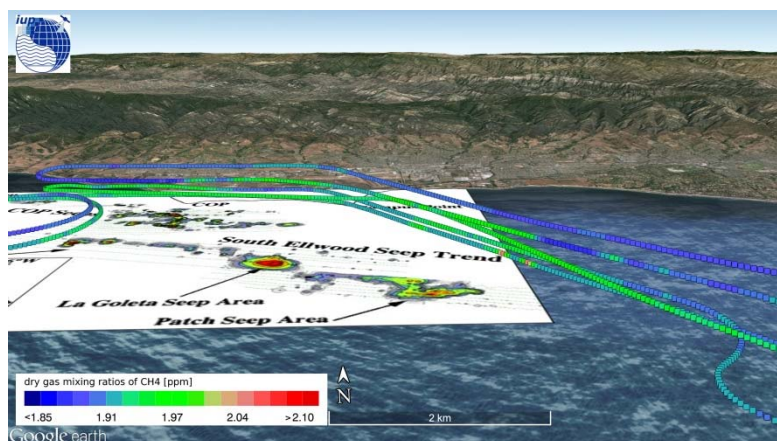


Figure 57: Google Earth image of the in-situ measurements from 2014-06-04. The source area is expected to be located between the land and the colour bar. The underlying seep map has been taken from Leifer et al. (2010).

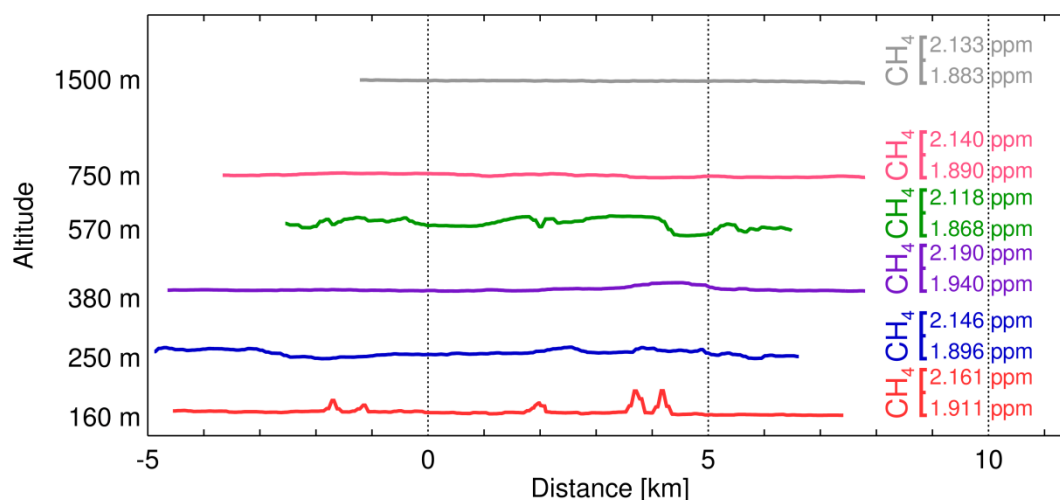


Figure 58: Cross section of the in-situ tracks shown for the five dedicated in-situ altitudes and for the closest located remote sensing track at far higher altitude from 2014-06-04. The scale on the x-axis denotes the distance to where the aircraft turns from a more north-south direction to an east-west direction. Positive distances refer to measurement locations further south-east from the turning point and negative distances to locations further west from the turning point. The y-axis shows the approximate altitude of the flight lines and is not to scale, while the variations in CH<sub>4</sub> are according to the scales on the right.

#### 10.1.2. Coal Oil Point 2014-08-25

The MAMAP measurements on 2014-08-25 over the Coal Oil Point area were performed at about 12:30 to 15:15 local time. Aircraft altitude for the remote sensing measurements was about 2060 mamsl and the MAMAP instrument was mounted with a preselected viewing angle of 25.0° to capture the solar glint/glitter spot on the sea. The viewing angle was manually pre-set before reaching the target area and (manually) modified at one point during the flight to 28.5°.

This measurement geometry was taken into account for determination of the geolocations for the measurements. The background concentrations were about 1793.0 ppb for XCH<sub>4</sub> and about 389.3 ppm for XCO<sub>2</sub> derived from PICARRO in-situ measurements. For XCO<sub>2</sub> the value is in reasonable agreement with the SECM model (Reuter et al., 2012) which predicts a background of 393.2 ppm.

When inspecting the measurements for this flight, it becomes clear that the detector was mostly below 10 % of the full well capacity (see Figure 59, left) in the second part of the flight. The main reason is most likely, that the glint spot was not perfectly hit for the measurements performed in the second part, leading to a low signal and also low signal to noise ratio. In Figure 59 (center) the change in solar zenith angle during the survey is shown spanning a range from about 23° to 39° whereas the preselected viewing angle was manually set to 25.0° (and later to 28.5°). This shows that for surveys that take longer than an hour it is important to fly around solar noon as on 2014-06-04 or continuously track the sun glint spot on the ocean. The latter however, was not possible with the current (experimental) MAMAP instrument glint configuration allowing predominantly a manual pre-set of the viewing angle geometry before reaching the target area and the possibility to automatically track only the Yaw direction during the flight. Furthermore, due to an underestimation of the time required to finalize the entire dense flight pattern, there are only few flight lines downwind of the seep area, which are most relevant for the detection of potential emissions.

To allow for an at least qualitative inspection of the low signal data, the measurements were additionally smoothed by applying a normalization of a 100-point moving average which is generally not applied when quantitatively analyzing MAMAP data, e.g. for derivation of emission rates.

Furthermore a basic signal filter was applied (5% of the full well capacity) and the inclination filter ( $\pm 2^\circ$  as before). The resulting, qualitative  $\text{XCH}_4(\text{CO}_2)$  map is shown in Figure 59 (right).

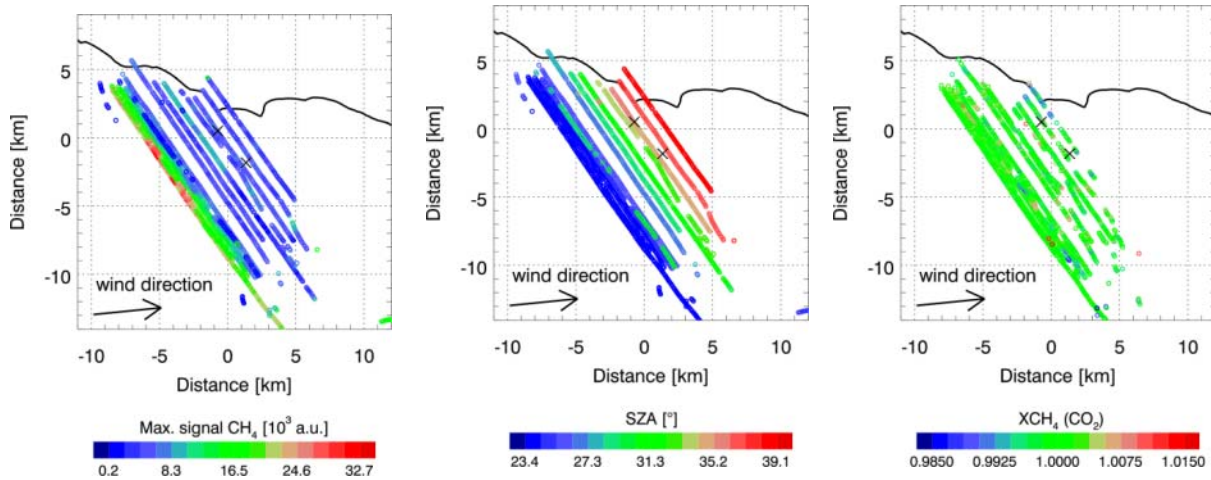


Figure 59: Maximum signal strength (left) and solar zenith angle (SZA) (centre) for measurement flight over Coal Oil point on 2014-08-25. To the right also a qualitative retrieval result is shown including an additional signal filter and the geolocation correction.

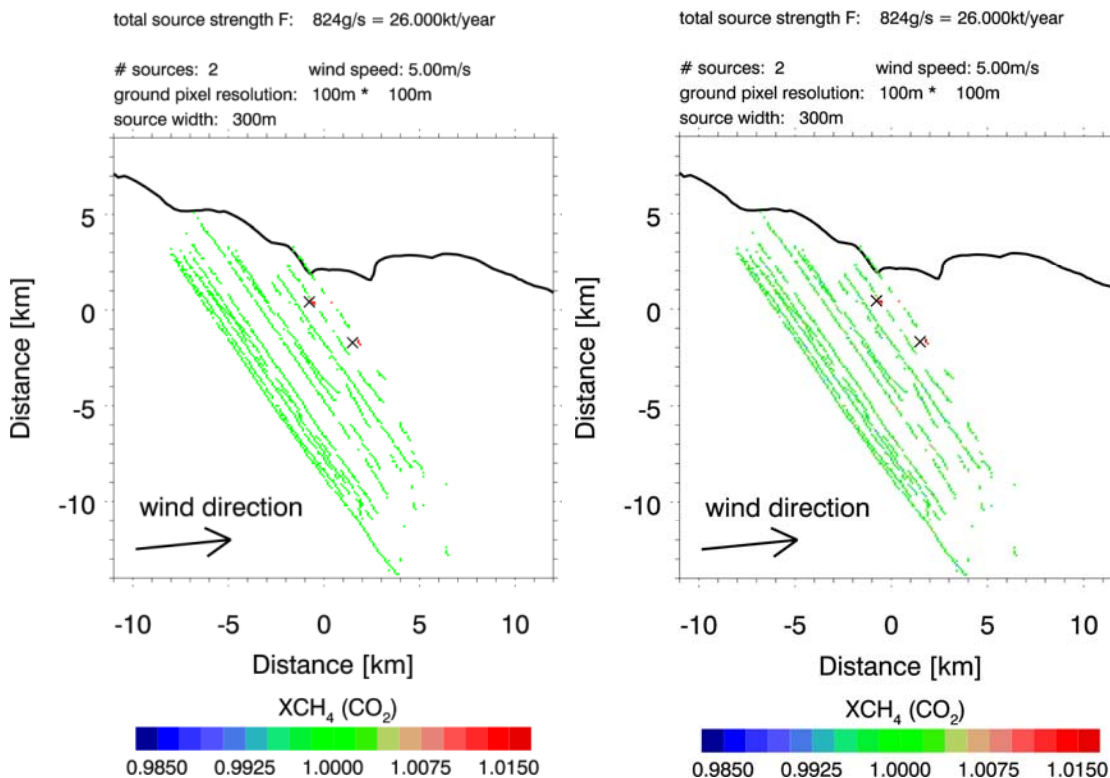


Figure 60: Simulations for 2014-08-25 using a Gaussian dispersion model without noise (left) and including a random noise component (right). It is evident that there are too few flight tracks downwind of the sources to pick up the signal.

The lack of additionally required flight lines downwind of the sources is also visible in the simulation performed for the measurement day (Figure 60). The two downwind flight lines would not have been



sufficient to clearly identify methane plumes originating at the two seep locations. To avoid insufficient coverage of the target area, an interlaced flight pattern was introduced during several of the remaining onshore flights also allowing to better capture source and atmospheric variations.

Even though only very few high quality glint measurements were resulting from this flight, the recorded data can be used to analyze to what extent low signal MAMAP data over water can still be used to derive relevant greenhouse gas information. This however requires additional efforts to apply dedicated radiative transfer simulations and potential adjustments to the retrieval algorithm.

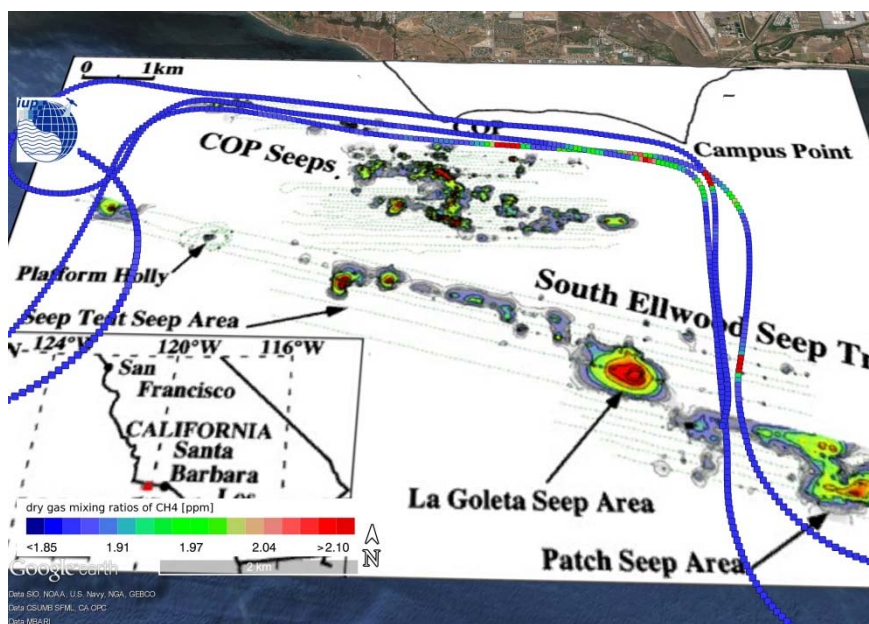


Figure 61: Google Earth image of the in-situ measurements from 2014-08-25. The source area is expected to be located between the land and the colour bar. Underlying seep map taken from Leifer et al. (2010).

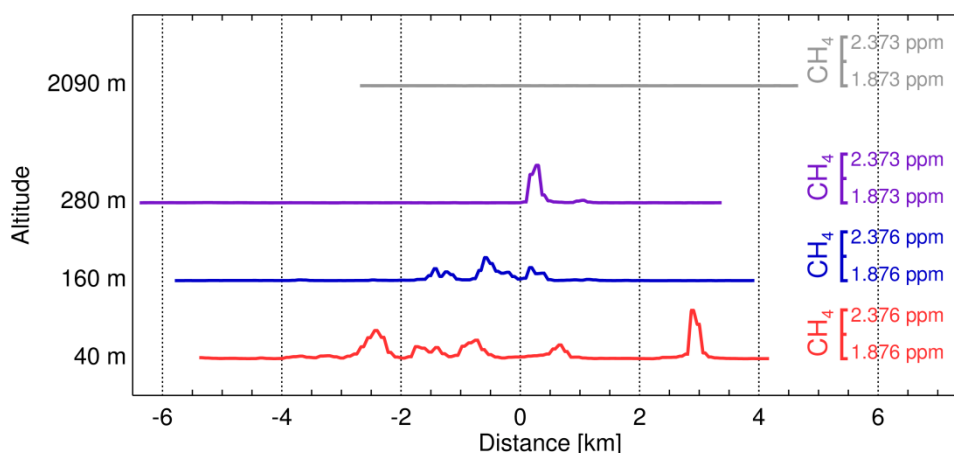



Figure 62: Cross section of the in-situ tracks shown for the three dedicated in-situ altitudes and for the closest located remote sensing track at far higher altitude from 2014-08-25. The scale on the x-axis denotes the distance to where the aircraft turns from a more north-south direction to an east-west direction. Positive distances refer to measurement locations further south from the turning point and negative distances to locations further west from the turning point. The y-axis shows only the approximate altitude of the flight lines and is not to scale, while the variations in  $\text{CH}_4$  are according to the scales on the right.

	<p style="text-align: center;"><b>COMEX</b> <b>Final Report</b></p>	<p style="text-align: right;">Version: 2.0 Doc ID: IUP-COMEX-FR Date: 3. July 2016</p>
--	---	--

The in-situ measurements for this day show strong, localized increases in CH<sub>4</sub> downwind of Trilogy and La Goleta seep (see Figure 61 and Figure 62) with a maximum of about 480 ppb above background (25%) close to the sea surface downwind of La Goleta seep. The order of magnitude is in good agreement with the in-situ measurements (I. Leifer, personal communications). The highest in-situ flight line still shows significant enhancements in CH<sub>4</sub> downwind of the Trilogy seep area and the remote sensing flight track is too high to give a reasonable vertical constraint. Therefore a column estimate will have a high uncertainty. Assuming the enhancement of the third flight line to be representative up to the boundary layer height of 500 m, the total column increase might be in the range of about 0.8% as an upper estimate. This is still below the enhancements expected from simulations, which predict enhancements of 2% and more close to the source. However, since the distance to the supposed source location is not perfectly known this can give only an indication.

## 11. Spatial and spectral tradeoffs and extrapolation to satellite scales

To address two of the main COMEX objectives, namely to:

- Investigate spatial/spectral resolution trade-offs for CH<sub>4</sub> anomaly detection and flux inversion by comparison of MAMAP-derived emission estimates with AVIRIS/AVIRIS-NG derived data.
- Characterize the effect of Surface Spectral Reflectance (SSR) heterogeneity on trace gas retrievals of CO<sub>2</sub> and CH<sub>4</sub> for medium and low-resolution spectrometry.

and to extrapolate the results to satellite scales, retrieved CH<sub>4</sub> from AVIRIS-NG and MAMAP data measured contemporaneously over two different targets with different emission properties have been superimposed for a qualitative comparison. Some of the measurements (containing the largest observed CH<sub>4</sub> anomaly signals) were furthermore interpolated and/or re-gridded to mimic the spatial resolution of current or future satellite sensors. For the comparison, the WFM-DOAS retrieval used for MAMAP was adapted and applied to the AVIRIS-NG measured dataset. The spectral window used for the CH<sub>4</sub> retrieval with the AVIRIS-NG dataset was between 2300 and 2380 nm. The sensitivity of the WFM-DOAS retrieval regarding detection of CH<sub>4</sub> anomalies was similar to that achieved by Thompson et al., 2015 using the column-wise matched filter approach (see for comparison, inset Figure 22 and inset Figure 63, right.)

### 11.1.1. Sensitivity comparison between medium and low spectral resolution data

The first sensitivity comparison between low (i.e. 5.5 nm) and medium (i.e. 0.9 nm) resolution spectroscopy was performed with the contemporaneously collected MAMAP and AVIRIS-NG dataset measured with both instruments on 2014-09-04 over the Kern River, Kern Front and Poso Creek Oil Fields. The MAMAP dataset (Figure 63, left) was collected between 20:40-22:50 UTC (13:40 to 15:50 local time). The AVIRIS-NG dataset was collected between 20:15-22:23 UTC (13:15 to 15:23 local time).

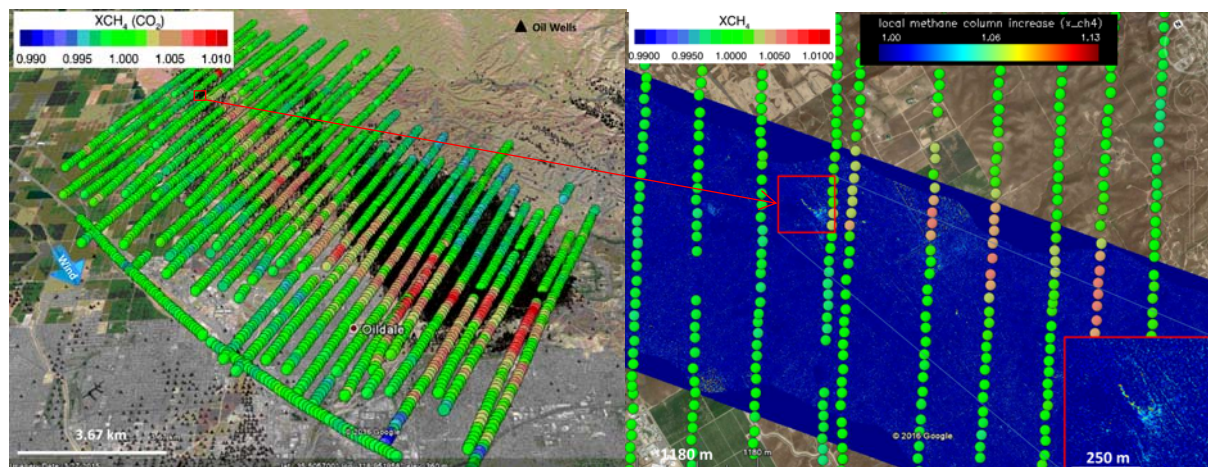


Figure 63: Left: WFM-DOAS retrieved XCH<sub>4</sub> derived from MAMAP measurements collected over the Kern Oil Fields on 2014-09-04, between 20:40-22:50 UTC. A large scale plume extending over several kilometres was detected with MAMAP's large SNR and medium spectral resolution of ~ 0.9 nm. Right: Overlay of AVIRIS-NG WFM-DOAS retrieved data collected at 20:45 UTC and WFM-DOAS retrieved MAMAP XCH<sub>4</sub> data. The MAMAP tracks collected downwind the primary source area were measured at 21:55, 20:51, 22:00, 20:55, 22:03, 21:00 and 22:07 UTC from left to right respectively.

From the overlay of Figure 63 (right) it is obvious, that enhancements in the total column in the range of ~ 0.5 - 1% XCH<sub>4</sub> column increase could be detected with sufficient SNR and a medium spectral resolution of 0.9 nm. Such enhancements were detected in a distance of more than 1 km in downwind direction from the primary source area and could be traced over several kilometres regardless of the



coarse spatial resolution of  $\sim 70\text{m} \times 70\text{m}$  of MAMAP for that flight. The low spectral resolution of  $\sim 5.5\text{ nm}$  in the SWIR of AVIRIS-NG allows plume detection in the same source area only over a distance of less than 500 m. Furthermore, much larger interferences between the surface spectral reflectance and the  $\text{CH}_4$  retrieved data could be observed for  $\sim 5.5\text{ nm}$  low spectral resolution spectrometry in comparison to the medium resolution spectrometry (see Figure 63). In contrast, due to the fine spatial resolution and imaging capabilities of AVIRIS-NG of  $\sim 2.1\text{m} \times 2.1\text{m}$ , direct attribution of the source is possible with low spectral resolution imaging spectrometry. It needs furthermore to be noted, that AVIRIS-NG was never designed for exclusive measurements of  $\text{CH}_4$ . An instrument, specifically designed to identify small sources as observed for the Kern Oil Field and able to detected enhancements in the total column of below  $\sim 1\%$  for (large scale) flux inversion will therefore benefit from a higher spectral resolution (i.e.  $\sim 1\text{ nm}$  or below) and high SNR (similar to that of MAMAP) as well as imaging capabilities with a spatial resolution of some meters similar to that of AVIRIS-NG.

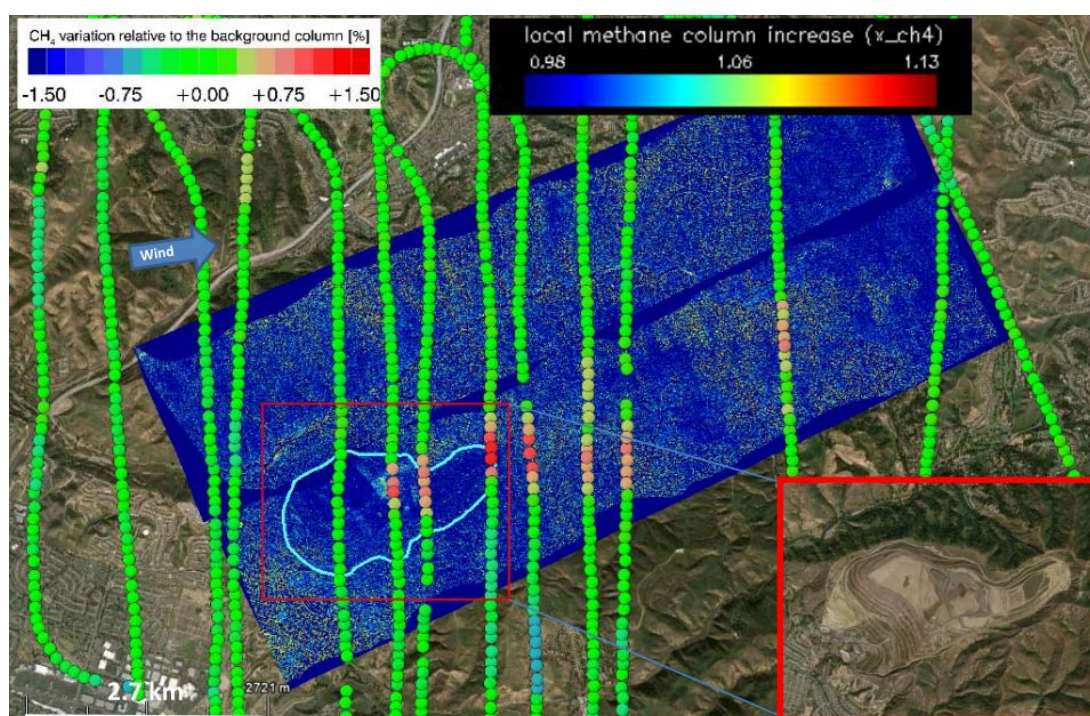


Figure 64: MAMAP and AVIRIS-NG measurements performed contemporaneously on 2014-09-03. The MAMAP data was collected between 20:30-21:15 UTC. AVIRIS-NG overflights shown in the plot were measured at 20:59 UTC and 21:10 UTC, respectively.

The second comparison between low spectral resolution imaging spectroscopy and medium spectral resolution spectroscopy was performed for contemporaneous measurements obtained with MAMAP and AVIRIS-NG over the Olinda Alpha landfill on 2014-09-03. The Olinda Alpha landfill represents a large areal source with an extent of  $\sim 2.5\text{km} \times 1.3\text{km}$  and an estimated emission rate in the range of around  $15\text{--}17\text{ ktCH}_4/\text{yr}$  (see Section 9.2). Furthermore the flux distribution over the landfill area was not known (a-priori) before the measurements. Figure 64 shows results from both datasets. A clear plume originating from the landfill could be detected with the medium spectral resolution MAMAP instrument. With the low spectral resolution AVIRIS-NG instrument, no clear plume signatures could be observed. Furthermore, the observed interference between the surface spectral reflectance and the low spectral resolution AVIRIS-NG data was much higher with respect to the medium spectral resolution MAMAP data. From the comparison it could be concluded, that for detection of emissions from areal sources like the Olinda Alpha landfill, spectral resolution in the range of  $1\text{ nm}$  (or below) is of benefit.



### 11.1.2. Extrapolation of AVIRIS-NG data to HypsIRI and EnMAP satellite scales

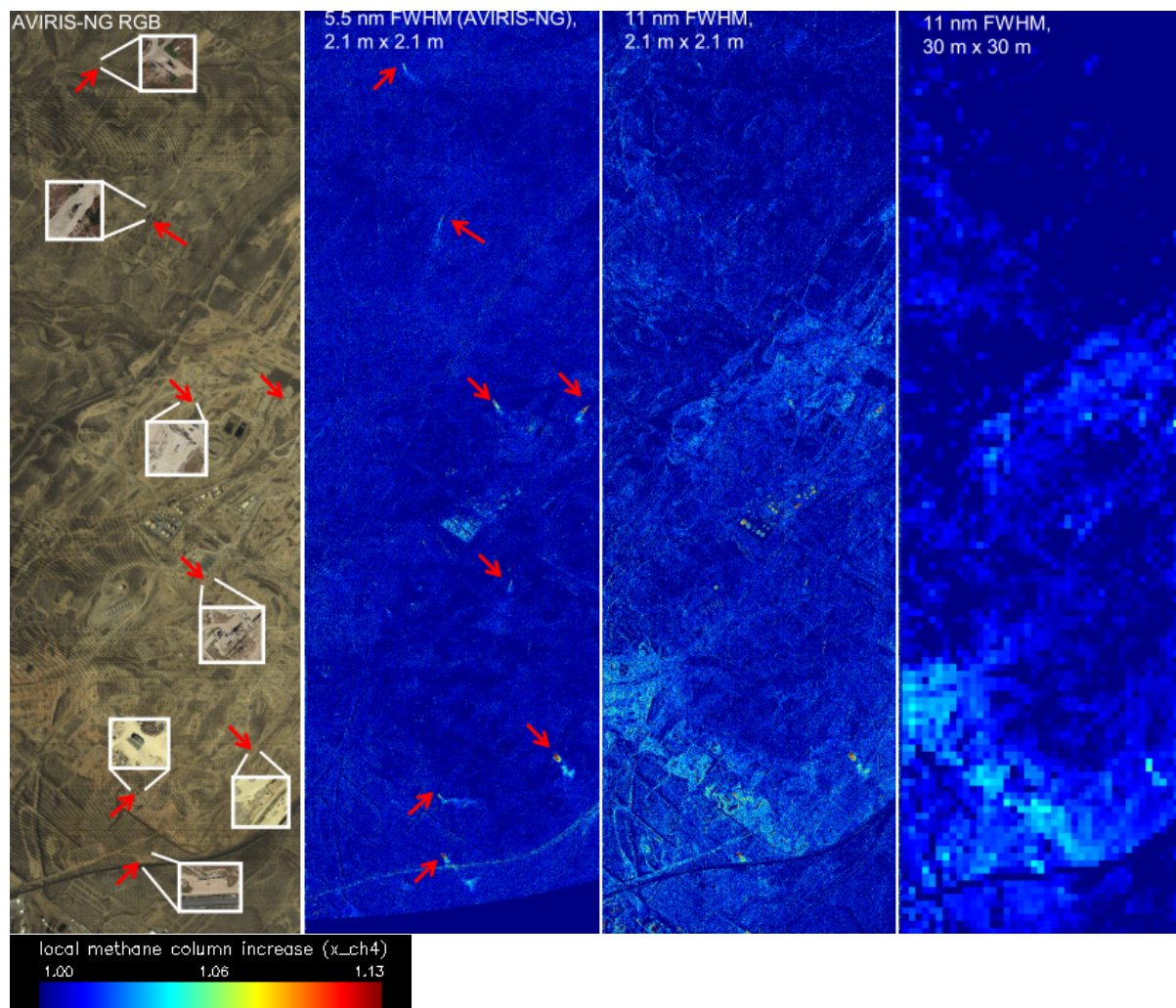


Figure 65: Spatial and spectral extrapolation of AVIRIS-NG data to satellite scales. Left: Sources and source positions for typical magnitudes as identified by WFM-DOAS retrieved 5.5 nm spectral and 2.1 m x 2.1 m spatial resolution AVIRIS-NG data, collected on 2014-09-04 at 21:16 UTC over the Kern Oil Fields (central left). Central right: WFM-DOAS retrieval of the same dataset but for spectrally binned data corresponding to measurements as would have been taken with an instrument having 2.1 m x 2.1 m spatial and 11 nm spectral resolution. Right: WFM-DOAS retrieval applied to the same dataset but spectrally and spatially binned to 11 nm and 30 m x 30 m, representing measurements as would have been taken by a satellite sensor with a pixel size of 30 m x 30 m and a spectral resolution of 11 nm. For the observed source strengths, unambiguous identification of the sources is only possible with the high spatial and spectral resolution imaging measurements as taken by AVIRIS-NG (central-left).

To extrapolate AVIRIS-NG collected data to satellite scales, several simulations have been performed. For the simulations two AVIRIS-NG flight lines have been selected. The first flight line contains several sources with typical single source signatures as observed over the Kern Oil Fields (see Figure 65). The second flight line contains one of the largest single source signatures, observed during the 2014-09-04 flight (Figure 66).

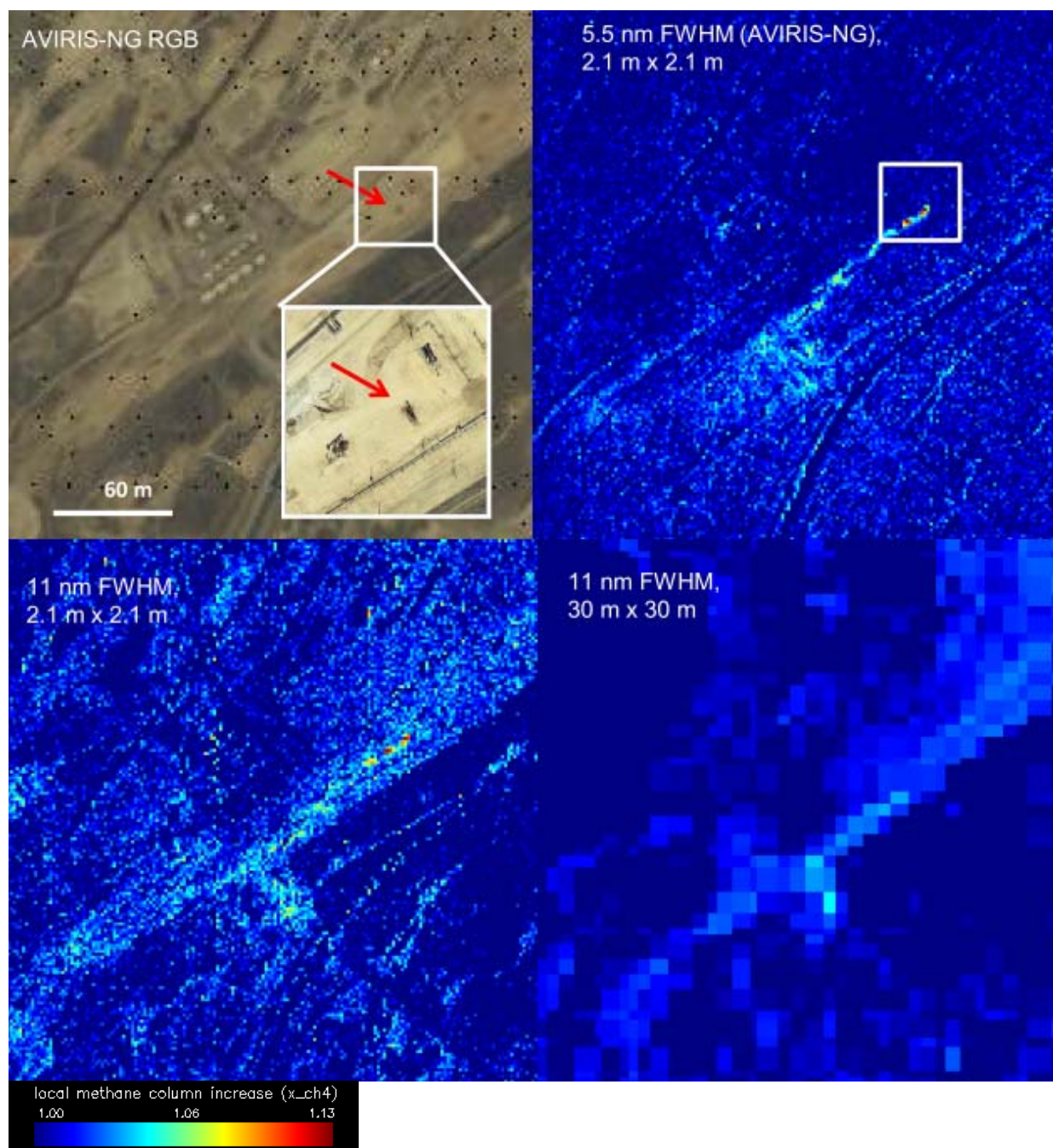



Figure 66: Same as for Figure 65, but for the largest source as observed with AVIRIS-NG during COMEX. Data collected on 2014-09-04 at 20:45 UTC over the Poso Creek Oil Field. Unambiguous identification of this source was only possible with 5.5 nm spectral and high spatial resolution provided by AVIRIS-NG. With an instrument with lower spectral resolution of  $\sim 11$  nm like AVIRIS-C, an unambiguous detection of the source is challenging. According to this simulation, such sources could not be detected with a satellite sensor with  $\sim 30$  m x 30 m spatial and  $\sim 11$  nm spectral resolution.

For the first simulation, the AVIRIS-NG radiance data was spectrally binned to mimic an instrument with lower spectral resolution of  $\sim 11$  nm and the full AVIRIS-NG spatial resolution (i.e.  $\sim 2.1$  m x 2.1 m for the 2914-09-04 flight lines). In the second step, the AVIRIS-NG data was spectrally and spatially binned to  $\sim 11$  nm and 30 m x 30 m to mimic a space based instrument (i.e. like envisaged for HypsIRI or EnMAP). The WFM-DOAS retrieval was applied to both datasets (from Figure 65 and Figure 66) after binning. The results show, that unambiguous identification of single sources with source magnitudes

	<p style="text-align: center;"><b>COMEX</b> <b>Final Report</b></p>	<p style="text-align: right;">Version: 2.0 Doc ID: IUP-COMEX-FR Date: 3. July 2016</p>
--	---	--

like the observed is difficult with high spatial (i.e.  $\sim 2\text{m} \times 2\text{m}$ ) and lower spectral resolution of  $\sim 11\text{ nm}$  and challenging with lower spectral and spatial resolution (i.e.  $\sim 11\text{ nm}$ ,  $30\text{ m} \times 30\text{ m}$ ) like it would be expected for a hyperspectral satellite sensor not especially designed for atmospheric trace gas measurements. To unambiguously detect methane sources with a  $\sim 11\text{nm}$  spectral and  $\sim 30\text{m} \times 30\text{m}$  spatial resolution hyperspectral instruments from space, larger source emissions than the observed would be required.



### 11.1.3. Extrapolation of MAMAP data to CarbonSat, Sentinel 5p and GOSAT satellite scales

To assess how the observed signal from the Kern Oil Fields would look like if recorded from satellites with dedicated designs for atmospheric trace gas measurements but lower spatial resolution, such as CarbonSat, Sentinel-5 Precursor or GOSAT, in comparison to hyperspectral satellite sensors, MAMAP data has been interpolated and then regridded to the corresponding satellite horizontal resolutions. The original MAMAP  $\text{XCH}_4(\text{CO}_2)$  and the interpolated dataset are shown in Figure 67 left and right, respectively. For the experiment, MAMAP measurements from 2014-08-26 with a strong  $\text{CH}_4$  signature over the Kern Oil Fields have been selected.

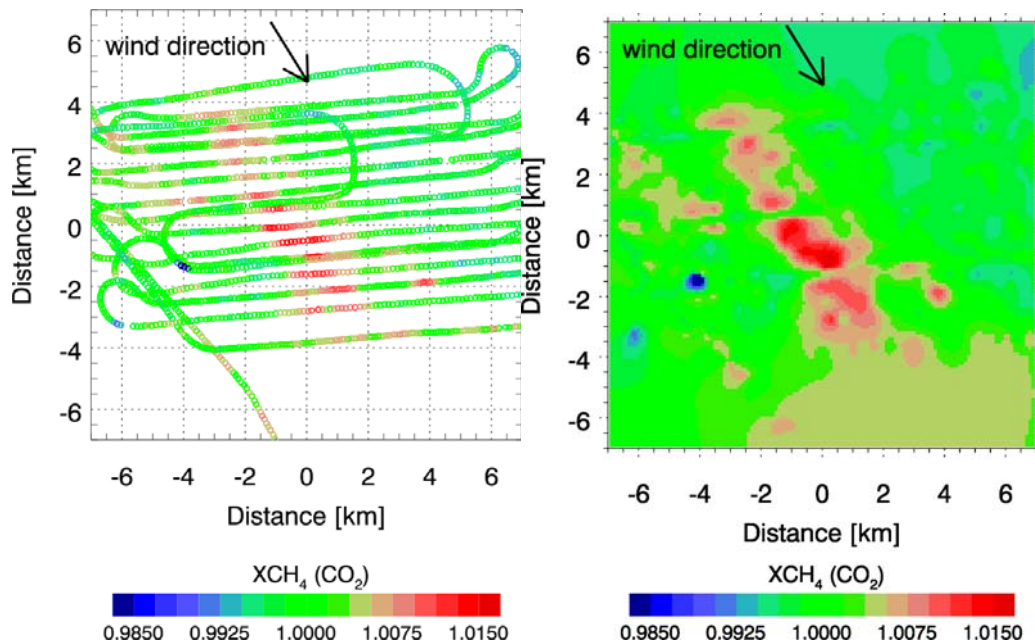


Figure 67:  $\text{XCH}_4(\text{CO}_2)$  retrieved from MAMAP data over Kern Oil Field on 2014-08-26 (left) and interpolated using a Kriging approach (right).

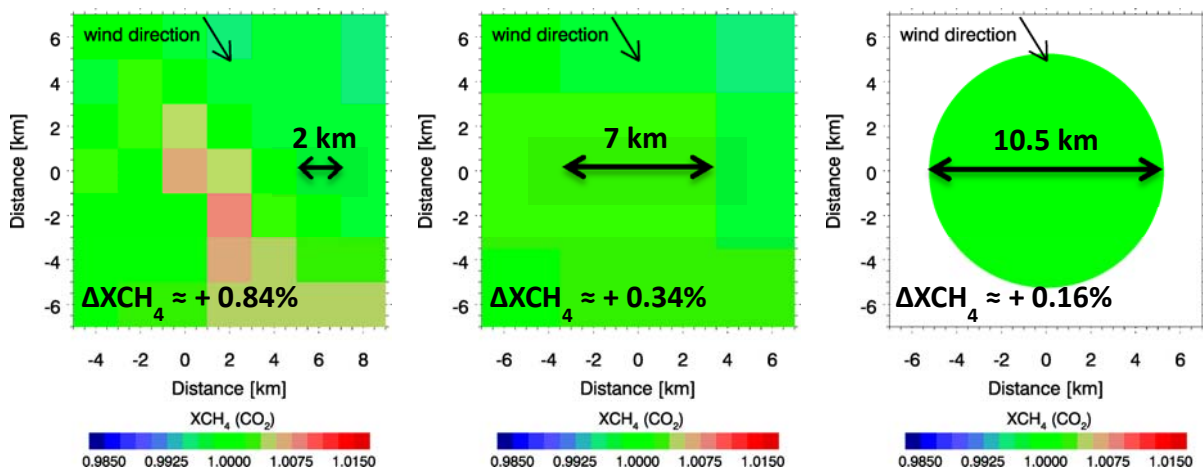


Figure 68: MAMAP retrieved  $\text{XCH}_4(\text{CO}_2)$  regridded to CarbonSat resolution (left), Sentinel-5 Precursor resolution (centre) and GOSAT resolution (right).

Subsequently the data was regridded to the horizontal resolution of different existing and proposed satellite systems. Figure 68 (left) shows the methane enhancement over the oil field as it would have been observed using CarbonSat with an approximate horizontal resolution of 2 km. It shows that the maximum  $\text{XCH}_4$  enhancement inside the plume area is about 0.84% relative to background. To detect



by a single satellite overpass a source producing such an increase, typically a 3-sigma single measurement precision in the range of the increase would be required. This source would therefore potentially be also detectable via CarbonSat satellite measurements assuming a 1-sigma  $\text{XCH}_4$  single measurement precision of about 0.3 % or better could be achieved by the instrument. Sentinel-5 Precursor will have a larger footprint with a size of  $\sim 7 \times 7 \text{ km}^2$  resulting in a maximum enhancement of about 0.34% relative to the background  $\text{XCH}_4$ , while the nominal precision requirement is 0.6% (Veefkind et al., 2012). The plume is furthermore only located in one pixel, making the detection of the plume more challenging. For GOSAT with its horizontal resolution of 10.5 km in diameter the maximum enhancement in  $\text{XCH}_4$  is only 0.16% with no adjacent measurements due to the sampling pattern that includes gaps between measurements. The precision is on the order of 0.8%-1.0% (Buchwitz et al., 2015), i.e. is a factor 5-6 larger than the derived enhancement inside the GOSAT pixel. For GOSAT, the signal will likely be lost in the noise. Figure 69 shows for comparison a similar dataset but acquired during the C-MAPEX campaign on 2012-08-18 over the coal fired power plant Weisweiler with an estimated emission rate of  $\sim 15 \text{ MtCO}_2/\text{yr}$  for the time of the overflight. For improved detection and quantification of sources with magnitudes as the observed by future atmospheric trace gas satellite systems, it will be of advantage to further reduce pixel sizes below  $2 \text{ km} \times 2 \text{ km}$  while keeping the single measurements  $\text{XCO}_2$  and  $\text{XCH}_4$  precision of the instruments at 0.3 % or below.

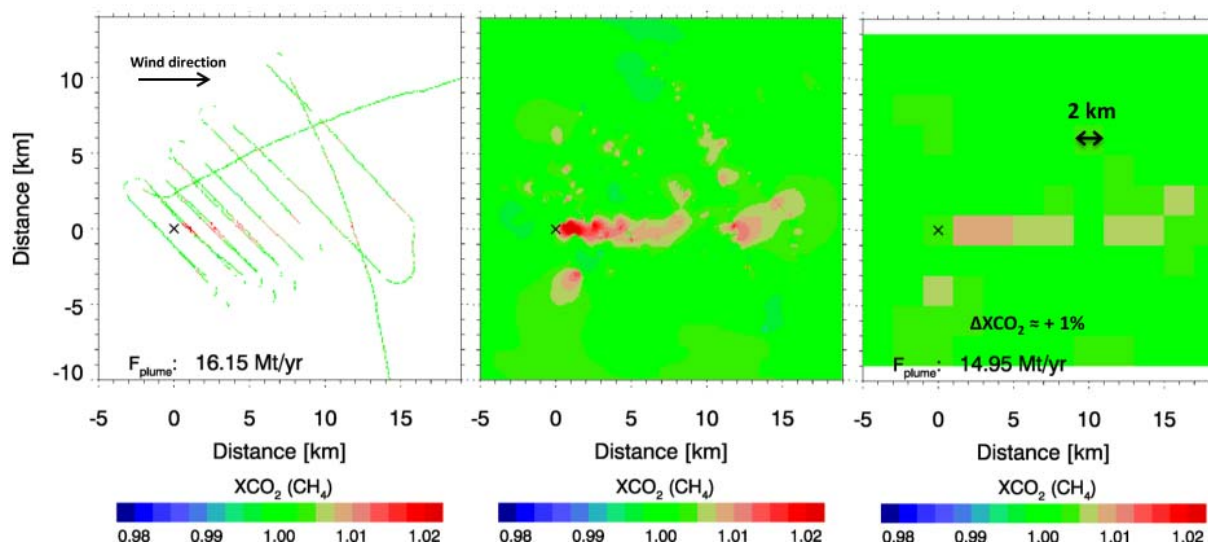



Figure 69: Similar to Figure 70 and Figure 71 but for  $\text{XCO}_2(\text{CH}_4)$  for the coal fired power plant Weisweiler with an emission rate of  $\sim 15 \text{ MtCO}_2/\text{yr}$  for the time of the overflight. Data acquired on 2012-08-18.

	<p style="text-align: center;"><b>COMEX</b> <b>Final Report</b></p>	<p style="text-align: right;">Version: 2.0 Doc ID: IUP-COMEX-FR Date: 3. July 2016</p>
---	---	--

## 12. Recommendations and Lessons Learned

### 12.1. Future analysis of the campaign data set

The current project focused as planned on the data collection, processing and initial interpretation to demonstrate that the data quality is fit for purpose. Nevertheless the data set will allow a lot more investigations, a few are listed below:

1. As it was shown that co-emitted CO<sub>2</sub> or CO<sub>2</sub> emitted within the CH<sub>4</sub> source area is not a dominating error source for the CH<sub>4</sub> proxy approach (normalization via CO<sub>2</sub>), the estimated errors are still significant. As MAMAP also provides co-located O<sub>2</sub>- A-band measurements, it would be relevant to extend the 1-band retrieval to a 2-band retrieval and test advantages (less interference with CO<sub>2</sub> for XCH<sub>4</sub>-proxy) and potential disadvantages (higher sensitivity to aerosol and surface albedo). The collected data set is very well suited for that, as it provides also reference data of independent CO<sub>2</sub> and CH<sub>4</sub> (from in-situ) on aerosol (in-situ) and surface spectral reflectance (AVIRIS-NG).
2. The glint spectra are of sufficient quality to allow for detailed investigations on the physical understanding of glint radiative transfer schemes in the NIR and SWIR.
3. The data collected during the campaign will allow to study in detail the spatial (MAMAP and AVIRIS-NG) and temporal variability (MAMAP time series) of CH<sub>4</sub> from oil field emissions.
4. The MAMAP and AVIRIS-NG data collected over land will allow investigations of the impact of spectral surface albedo variations on CO<sub>2</sub> and CH<sub>4</sub>, down to the point in how far high spatial resolution spectral surface albedo information might be used to mitigate sporadic systematic errors in XCO<sub>2</sub> and XCH<sub>4</sub>.


### 12.2. Lessons learned from campaign preparation and execution

The lessons learned during the COMEX multi aircraft campaign can be summarized as follows:

**Campaign Coordination:** In the early stage of the campaign, a skilled flight coordinator is required acting as interface between the scientists and the pilots of the different aircraft. A “pre campaign” aircraft coordination meeting with participation of pilots and scientist is required some weeks before the campaign.

**Flight planning and flight pattern:** For COMEX, real-time retrieval capabilities were implemented for the MAMAP remote sensing instrument and in the later stage as well as for AVIRIS-NG (see also Thompson et al. 2015). The real-time retrieval of MAMAP enabled to interactively optimize the flight patterns flown by the CIRPAS aircraft and also to search for unassessed and unknown sources. Furthermore, this new capability allows placing in-situ measurements for validation proposes at exactly the positions, where plume structures are observed. The success of COMEX, especially over complex target areas comprising many potential sources like the Oil-Fields around Bakersfield, could be largely attributed to this new capability of MAMAP and AVIRIS-NG. Direct inter communication between the MAMAP and AVIRIS-NG equipped aircraft via radio and exchange of real-time derived information between both instruments, also largely improves the quality of the collected data sets.

To better assess source strengths and temporal source variability with MAMAP, an interlaced flight pattern was introduced in the second half of the campaign (see section 9.4). Such a pattern is


	<p style="text-align: center;"><b>COMEX</b> <b>Final Report</b></p>	<p style="text-align: right;">Version: 2.0 Doc ID: IUP-COMEX-FR Date: 3. July 2016</p>
--	---	--

recommended also for future campaigns (if compatible with the available flight time). This interlaced flight pattern also guarantees that the measurement area is covered at least once completely, in case of lack of available flight time to entirely finalize the (dynamic) pattern. In case fluxes for the measurement area need to be derived, it is recommended to install wind measurement stations delivering better temporal wind information, than for instance the 1h resolved information delivered by Meadows for Kern. If possible, installation of a portable wind LIDAR is also recommended.

**Campaign objectives:** To fulfill the campaign objectives, a dedicated analysis and simulations for target selection is required. In case of CarbonSat, targets with the ability to produce atmospheric gradients on the scales probed by the satellite need to be selected. Regarding CO<sub>2</sub> and CH<sub>4</sub> emissions in Europe, this task was accomplished for C-MAPEX by analysis of facility level emissions as reported by the European Pollutant Release and Transfer Register (E-PRTR). However for CH<sub>4</sub> reported information was mostly not available for many of the investigated targets during COMEX. Therefore selection of CH<sub>4</sub> targets during COMEX was performed based on extensive literature research. Due to the sparse information regarding US CH<sub>4</sub> emissions on local and facility level scales in the 2013-2014 planning period of COMEX especially for the Oil and Gas sector, pre-flight planning for the campaign was challenging. Therefore to maximize the COMEX prospect of success, a flexible flight planning was necessary, incorporating primary and secondary targets for each day and taking the real-time retrieval capabilities of the instruments into account. This approach enables to maximize the flight time over the most prospective targets (with unknown a-priori emissions) by prescreening.

**Campaign Organization:** For a multi aircraft campaign like COMEX, a comprehensive organization and planning is required and recommended in the early stage of the project, including external consultancy from pilots, familiar with the Air Traffic Control (ATC) regulations and other restrictions in the envisaged target areas. For multi aircraft campaigns in the US incorporating a NASA aircraft, equipment or staff, also consultancy by the according NASA Airworthiness and Flight Safety Review Boards (AFSRBs) responsible for the campaign safety (if any) is required in the early stage of the project. Also early consultancy from the aircraft operators regarding instrument certifications and potentially necessary instrument modifications is required in the very early stage/proposal of the project. Furthermore it is recommended to reduce the number of aircraft, required to fly contemporaneously on the same day in the same target area to a minimum. If contemporaneous multi aircraft operation is required in the US with NASA involvement, a clear altitude separation between the different aircraft is typically requested by the according NASA AFSRB for the preflight planning. For instance, clearance to operate two with in-situ sensors equipped aircraft sharing the same altitude range and air space in the same target area was not issued by the NASA-Ames AFSRB for COMEX. Also no clearance was issued for remote sensing instrumentation equipped aircraft to share the same altitude, i.e. a vertical separation of aircraft of minimum 1500 ft was required by the NASA Ames AFSRB during COMEX. In case multi altitude operation for one aircraft is required, this altitude separation requirement implies a high level of complexity for pre (and in-flight) planning if more than two aircraft are involved. Also inter aircraft communication is an issue, especially when operation needs to be performed sometimes in non-controlled airspace like during COMEX over several areas in the US. When operation needs to be performed in controlled airspace, close coordination between pilots and ATC is required. In case, operation at airport - Controlled Traffic Regions (airport-CTRs) is desired, it needs to be taken into account that the number of aircraft cleared to operate and perform grid-work in the area could be limited, sometimes even to one. Similar restrictions are valid also for airport-CTRs in Europe.

To simplify flight planning and reduce communication complexity, a deployment of all involved aircraft at the same airport is recommended for future campaigns.

	<p style="text-align: center;"><b>COMEX</b> <b>Final Report</b></p>	<p style="text-align: right;">Version: 2.0 Doc ID: IUP-COMEX-FR Date: 3. July 2016</p>
--	---	--

### 13. Summary

Within the COMEX campaign, two different airborne remote sensing (RS) techniques (MAMAP non imaging medium spectral resolution soundings of XCO<sub>2</sub> and XCH<sub>4</sub> similar to CarbonSat and AVIRIS-NG low spectral resolution imaging spectroscopy similar to HypsIRI) were successfully combined with airborne in-situ measurements of atmospheric CO<sub>2</sub> and CH<sub>4</sub> concentration as well as wind speed and direction within the atmospheric boundary layer in summer 2014.

In May/June 2014, in total 6 successful flight days were executed. They include the test of the MAMAP glint mode, detection of the CH<sub>4</sub> from cattle (Harris Ranch), the successful detection mapping of unexpected strong plumes over the Poso Creek, Kern Front and Kern River Oil Fields, an AVIRIS (on ER2) under flight by CIRPAS at the Coal Oil Point, as well as coordinated data acquisitions with AVIRIS-NG and coverage of several other targets (Chino feedlot complex, Puente Hills Landfill etc.).

In August/September 2014 in total 10 successful flight days were executed, including the characterization of the CH<sub>4</sub> emissions variability of the Poso Creek, Kern Front and Kern River Oil fields as well as a systematic characterization of CH<sub>4</sub> plumes from landfills with MAMAP, AVIRIS-NG, AJAX (Alpha Jet), and ground based in-situ measurements. The collected data covers in addition local CH<sub>4</sub> enhancements in the Los Angeles metropolitan area and the Coal Oil Point offshore natural CH<sub>4</sub> seep area near Santa Barbara. During all science flights, there were no problems with the CIRPAS aircraft or the CIRPAS core science instrumentation (i.e. IUP-UB MAMAP, ARC Picarro, CIRPAS 5-hole turbulence probe) affecting the data quality of the according science products. During one flight some MAMAP shutter problems occurred in the second part of the flight not affecting the quality of the MAMAP science products. One flight over the greater LA area was aborted due to too low wind conditions. During several flights, unexpected large scale CH<sub>4</sub> plumes were observed over the Poso Creek, Kern River and Kern Front Oil Fields. CH<sub>4</sub> plumes were observed over the Olinda Alpha and Puente Hills Landfills. Three CIRPAS flights were successful co-flown with AVIRIS - NG (two over the Poso Creek, Kern Front and Kern River Oil Fields and one over the Olinda Alpha Landfill & the Chino feedlot complex). One CIRPAS flight was flown during an ER-2 overpass over the Poso Creek, Kern Front and Kern River Oil Fields.


Initial screening of the remote sensing and in-situ data revealed a good quality of all acquired datasets. Preliminary data analysis of the remote sensing data was performed with the WFM-DOAS retrieval algorithm (MAMAP) and a column-wise matched filter approach (AVIRIS-NG).

Glint mode observation MAMAP data – together with airborne in-situ - from the Coal Oil Point natural seeps area offshore Santa Barbara were successfully analysed. An assessment of newly available in-situ data from the West Campus station (see chapter 10) revealed that at the time of the campaign the emissions were much lower than expected during the initial planning for the campaign. Together with simulations this explains why no significant CH<sub>4</sub> enhancement in the remote sensing data was observed. Small enhancements observed in the airborne collected in-situ data indicate that total column enhancements were below the detection limit of MAMAP during those flights and significantly smaller then reported in the literature for earlier years.

Preliminary flux estimates using the data collected during the campaign for Poso Creek, Kern Front & Kern River Oil Field on the 2014.09.04 were performed. Preliminary fluxes were also estimated for data collected over the Olinda Alpha landfill on the 2014.09.01.

For the Olinda Alpha landfill, the CH<sub>4</sub> emission rate estimate of 13.1 ktCH<sub>4</sub>/yr to 19.9 ktCH<sub>4</sub>/yr based on Picarro in-situ measurements and the emission rate of 15.1 ktCH<sub>4</sub>/yr based on MAMAP remote sensing measurements are in good agreement with the inventory value from 2010 of 13.8 ktCH<sub>4</sub>/yr (Atkins, 2014). Both, the in-situ and the remote sensing based flux estimate also agree well within the uncertainty with the finding from Peischl et al. (2013) of 12.5 ± 2.9 ktCH<sub>4</sub>/yr.



	<p style="text-align: center;"><b>COMEX</b> <b>Final Report</b></p>	<p style="text-align: right;">Version: 2.0 Doc ID: IUP-COMEX-FR Date: 3. July 2016</p>
---	---	--

For uncertainty analysis, different contributing error sources were assessed. For the Olinda Alpha Landfill, it was demonstrated that co-emitted CO<sub>2</sub> introduces biases well below 8% for the used remote sensing XCH<sub>4</sub>(CO<sub>2</sub>) proxy approach (which was applied to the MAMAP retrieved data) and therefore is not a dominating error source.

The Poso Creek, Kern Front & Kern River Oil Fields are multi-point source areas and interpretation in terms of not a-priori known source positions and associated emission rates is more complex. From the MAMAP XCH<sub>4</sub> inferred flux a substantial increase of emissions across the area was observed. The flux was estimated to 10 kTCH<sub>4</sub>/yr in the north easterly part and around 30 kT CH<sub>4</sub>/yr in the south west part of the measurement area over the fields. Both in-situ and remote sensing inferred fluxes supported that finding. The in-situ data furthermore clearly showed some CO<sub>2</sub> enhancements in the area which were obviously not co-located with the observed CH<sub>4</sub> enhancements. With the in-situ data it could be demonstrated that systematic errors introduced by the use of the remote sensing XCH<sub>4</sub>(CO<sub>2</sub>) proxy approach are well below 10% of the by remote sensing estimated CH<sub>4</sub> emissions.


**These findings are of high relevance for a CarbonSat like satellite, as they demonstrate that the XCH<sub>4</sub>(CO<sub>2</sub>) proxy approach can be used for flux estimates of CH<sub>4</sub> sources in several cases, even if weaker not co-emitting (Oil Fields) and co-emitting (landfills) CO<sub>2</sub> emitters are present in the measurement area of interest. However, for application of this approach, a case by case analysis is always required.**

The contemporaneously collected AVIRIS-NG data over the Kern Oil Fields (on 2014.09.04) supported the hypothesis, that the north east part of the area is dominated likely by only one strong source and several point sources in the proximate center of the probed area significantly contributing to the increase in emissions from 10 kTCH<sub>4</sub>/yr to approximately 30 kT CH<sub>4</sub>/yr estimated as the total emission of the three Kern Oil Fields for that day. The combination of hyperspectral imaging (AVIRIS-NG) and medium spectral resolution non-imaging (MAMAP) spectroscopic techniques allows both, the identification of dominating point source emitters and the quantification of the total filed emissions as well.

To extrapolate COMEX results to satellite scales, two different spatial and spectral trade-offs have been performed.

To extrapolate COMEX results to a hyperspectral-imaging instrument of the HypsIRI type, higher spectral and spatial resolution AVIRIS-NG data has been spatially and spectrally binned to mimic the expected pixel size and spectral resolution of this type of sensors. After binning, the data was analysed for CH<sub>4</sub> anomalies with the WFM-DOAS retrieval algorithm. The results suggest that unambiguous detection for typical single source magnitudes as observed over the Kern River Oil Fields would be difficult from space with instruments having a spectral resolution of proximately 10 nm and pixel sizes of proximately 30m x 30m. For unambiguous single source detection from space with this type of sensors, larger source magnitudes than the typically observed or improved spectral resolution of the Instruments would be required.


To extrapolate COMEX results to atmospheric satellite instrument scales like for CarbonSat, Sentinel 5P and GOSAT, higher spatial resolution MAMAP retrieved XCH<sub>4</sub> data was used. The retrieved MAMAP XCH<sub>4</sub> data collected over the Kern River Oil Fields was interpolated to a full high resolution map and this map was then regridded to the spatial resolution of the different satellite sensors. The maximum XCH<sub>4</sub> anomaly amplitudes produced by the fields for the different satellite ground pixel sizes were 0.84 % XCH<sub>4</sub> for CarbonSat, 0.34 % XCH<sub>4</sub> for S5P, and 0.16 % XCH<sub>4</sub> for GOSAT. For comparison, a similar approach but for CO<sub>2</sub> was applied to a similar dataset acquired during the C-MAPEX campaign in 2012 over a coal fired power plant with an estimated emission rate of ~ 15 MtCO<sub>2</sub>/yr for the time of the overflight. The estimated maximum XCO<sub>2</sub> anomaly for a CarbonSat like instrument with a ground pixel size of 2km x 2km was in the range of 1%.

	<p style="text-align: center;"><b>COMEX</b> <b>Final Report</b></p>	<p style="text-align: right;">Version: 2.0 Doc ID: IUP-COMEX-FR Date: 3. July 2016</p>
---	---	--

Assuming that for an unambiguous detection of the emissions by one satellite overpass a 3-sigma single measurement precision (per ground pixel) in the range of the increase would be required, emissions from these oil fields (and the power plant) could be potentially detected only by a CarbonSat like instrument (with ground pixel sizes in the range of 2km x 2km or smaller) in case a single measurement precision (per ground pixel) of about 0.3 % could be maintained by the instrument. For improved single overpass detection and quantification of sources (with magnitudes as above) by future atmospheric trace gas satellite systems, it will be of advantage to further reduce pixel sizes below 2km x 2km while keeping the XCH<sub>4</sub> and XCO<sub>2</sub> single measurements precision of the instruments at levels of ~ 0.3 % or below.

The campaign data demonstrated that a sensor using solar backscatter absorption spectroscopy and delivering 0.3% single measurement precision with sufficient spatial resolution will allow the determination of the concentration distributions of CH<sub>4</sub> with sufficient quality so that flux estimates not only of point sources (like landfills) but also of unknown localised area sources (like oil fields) can be performed quantitatively.

**Together with the verification of the emissions derived from MAMAP remote sensing data by in-situ data and the interpolation and regridding of the remote sensing CH<sub>4</sub> anomaly data to the CarbonSat spatial resolution, for the first time a quantitative experimental link between in-situ and remote sensing of localized CH<sub>4</sub> emissions up to the satellite scale was established. That complements the similar approach and results for CO<sub>2</sub> from CarbonSat from the C-MAPexp campaign (RD-8).**

	<p style="text-align: center;"><b>COMEX</b> <b>Final Report</b></p>	<p style="text-align: right;">Version: 2.0 Doc ID: IUP-COMEX-FR Date: 3. July 2016</p>
--	---	--

## 14. References

Amini, H. R.; Reinhart, D. R. & Niskanen, A., Comparison of first-order-decay modeled and actual field measured municipal solid waste landfill methane data, *Waste Management*, 33, 2720 – 2728, 2013.

Atkins, Climate Action Plan of the City of La Habra,  
[www.lahabracity.com/DocumentCenter/Home/View/192](http://www.lahabracity.com/DocumentCenter/Home/View/192), 2014.

Bovensmann, H., Buchwitz, M., Burrows, J. P., Reuter, M., Krings, T., Gerilowski, K., Schneising, O., Heymann, J., Tretner, A., and Erzinger, J.: A remote sensing technique for global monitoring of power plant CO<sub>2</sub> emissions from space and related applications, *Atmos. Meas. Tech.*, 3, 781-811, 2010.

Bradley, E., Leifer, I., Roberts, D., Long-term monitoring of a marine geologic hydrocarbon source by a coastal air pollution station in Southern California, *Atmospheric Environment*, Volume 44, Issue 38, Pages 4973-4981, ISSN 1352-2310, <http://dx.doi.org/10.1016/j.atmosenv.2010.08.010>, 2010.

Buchwitz, M., Reuter, M., Bovensmann, H., Pillai, D., Heymann, J., Schneising, O., Rozanov, V., Krings, T., Burrows, J. P., Boesch, H., Gerbig, C., Meijer, Y., and Löscher, A.: Carbon Monitoring Satellite (CarbonSat): assessment of atmospheric CO<sub>2</sub> and CH<sub>4</sub> retrieval errors by error parameterization, *Atmospheric Measurement Techniques*, 6, 3477–3500, doi:10.5194/amt-6-3477-2013, <http://www.atmos-meas-tech.net/6/3477/2013/>, 2013.

Buchwitz, M., Dils, B., Boesch, H., Crevoisier, C., Detmers, R., Frankenberg, C., Hasekamp, O., Hewson, W., Laeng, A., Noel, S., Notholt, J., Parker, R., Reuter, M., Schneising, O., ESA Climate Change Initiative (CCI) Product Validation and Intercomparison Report (PVIR) for the Essential Climate Variable (ECV) Greenhouse Gases (GHG) for data set Climate Research Data Package No. 2 (CRDP#2), 2015.

Butz, A., Galli, A., Hasekamp, O., Landgraf, J., Tol, P., Aben, I., TROPOMI aboard Sentinel-5 Precursor: Prospective performance of CH<sub>4</sub> retrievals for aerosol and cirrus loaded atmospheres, *Remote Sensing of Environment*, Volume 120, Pages 267-276, ISSN 0034-4257, <http://dx.doi.org/10.1016/j.rse.2011.05.030>, 2012.

CARB, California Air Resource Board, Greenhouse Gas Inventory – Archive  
<http://www.arb.ca.gov/cc/inventory/pubs/pubs.htm>

Clark, J. F., Washburn, L., and Schwager Emery, K.: Variability of gas composition and flux intensity in natural marine hydrocarbon seeps, *Geo-Marine Letters*, 30, 379–388, doi:10.1007/s00367-009-0167-1, <http://dx.doi.org/10.1007/s00367-009-0167-1>, 2009.


Cox, Charles, Munk, Walter, Measurement of the Roughness of the Sea Surface from Photographs of the Sun's Glitter, *J. Opt. Soc. Am.* 44, 838-850, 1954.

Curtis, C. et al., Heavy-Oil Reservoirs,  
[https://www.slb.com/~media/Files/resources/oilfield\\_review/ors02/aut02/p30\\_51.pdf](https://www.slb.com/~media/Files/resources/oilfield_review/ors02/aut02/p30_51.pdf), 2002

EPA, Environmental Protection Agency, U.S. Greenhouse Gas Inventory Report,  
<https://www3.epa.gov/climatechange/ghgemissions/usinventoryreport.html>

Gerilowski, K., A. Tretner, T. Krings, M. Buchwitz, P. P. Bertagnolio, F. Belemmezov, J. Erzinger, J. P. Burrows, and H. Bovensmann, MAMAP – a new spectrometer system for column-averaged methane and carbon dioxide observations from aircraft: instrument description and performance analysis, *Atmos. Meas. Tech.*, 4, 215-243, 2011.

Gerilowski, K., Krings, T., Hartmann, J., Buchwitz, M., Sachs, T., Erzinger, J., Burrows, J.P.; Bovensmann, H.; Methane Remote Sensing Constraints on direct Sea-Air Flux from the 22/4b North Sea Massive Blowout Bubble Plume, *Journal of Marine and Petroleum Geology*, Volume 68, Part B, December 2015, Pages 824–835, 2015, doi:10.1016/j.marpetgeo.2015.07.011

	<b>COMEX</b> <b>Final Report</b>	Version: 2.0 Doc ID: IUP-COMEX-FR Date: 3. July 2016
--	-------------------------------------	--

Green, R. O., Eastwood, M. L., Sarture, C. M., Chrien, T. G., Aronsson, M., Chippendale, B. J., Faust, J. A., Pavri, B. E., Chovit, C. J., Solis, M. S., Olah, M. R., and Williams, O.: Imaging spectroscopy and the Airborne Visible Infrared Imaging Spectrometer (AVIRIS), *Remote Sens. Environ.*, 65, 227–248, 1998.

Hall, J.L., R.H. Boucher, D.J. Gutierrez, S.J. Hansel, B.P. Kasper, E.R. Keim, N.M. Moreno, M.L. Polak, M.G. Sivjee, D.M. Tratt, and D.W. Warren, “First flights of a new airborne thermal infrared imaging spectrometer with high area coverage,” *Proceedings of SPIE*, 8012, 801203, doi:10.1117/12.884865 , 2011.

Hornafius, J. S., D. Quigley, and B. P. Luyendyk, The world's most spectacular marine hydrocarbon seeps (Coal Oil Point, Santa Barbara Channel, California): Quantification of emissions, *J. Geophys. Res.*, 104(C9), 20703–20711, doi:[10.1029/1999JC900148](https://doi.org/10.1029/1999JC900148), 1999.

Krings, T., Gerilowski, K., Buchwitz, M., Reuter, M., Tretner, A., Erzinger, J., Heinze, D., Pflüger, U., Burrows, J. P., and Bovensmann, H.: MAMAP – a new spectrometer system for column-averaged methane and carbon dioxide observations from aircraft: retrieval algorithm and first inversions for point source emission rates, *Atmos. Meas. Tech.*, 4, 1735–1758, doi:10.5194/amt-4-1735-2011, 2011.

Krings, T., K. Gerilowski, M. Buchwitz, J. Hartmann, T. Sachs, J. Erzinger, J. P. Burrows, H. Bovensmann, Quantification of methane emission rates from coal mine ventilation shafts using airborne remote sensing data, *Atmos. Meas. Tech.*, 6, 151–166, 2013.

Laird, J. et al., 2012 Preliminary Report of California Oil and Gas Production Statistics, Department of Conservation (Division of Oil, Gas, and Geothermal Resources), [ftp://ftp.consrv.ca.gov/pub/oil/annual\\_reports/2012/PR03\\_PreAnnual\\_2012.pdf](http://ftp.consrv.ca.gov/pub/oil/annual_reports/2012/PR03_PreAnnual_2012.pdf), 2013.

Leifer, I.; Kamerling, M.; Luyendyk, B. & Wilson, D., Geologic control of natural marine hydrocarbon seep emissions, Coal Oil Point seep field, California, *Geo-Marine Letters, Springer-Verlag*, 30, 331–338., 2010.

Leifer, I., D. M. Tratt, V. J. Realmuto, K. Gerilowski, and J. P. Burrows, Remote sensing atmospheric trace gases with infrared imaging spectroscopy, *Eos Trans. AGU*, 93(50), 525, doi:10.1029/2012EO500006, 2012.

Leifer I, Culling D, Schneising O, et al. (2013) Transcontinental methane measurements: Part 2. Mobile surface investigation of fossil fuel industrial fugitive emissions *Atmos. Environ.*, Volume 74, 432–441, 2013.

Leifer, I., Melton, C., Manish, G. & Leen, B. Mobile monitoring of methane leakage. *Gases and Instrumentation*, July/August 2014, 20–24, 2014.


Lohila, A.; Tuomas Laurila; Juha-Pekka Tuovinen; Mika Aurela; Juha Hatakka; Tea Thum; Mari Pihlatie; Janne Rinne & Vesala, T. Micrometeorological Measurements of Methane and Carbon Dioxide Fluxes at a Municipal Landfill, *Environmental Science & Technology*, 41, 2717–2722, 2007.

Peischl, J., et al. (2013), Quantifying sources of methane using light alkanes in the Los Angeles basin, California, *J. Geophys. Res. Atmos.*, 118, 4974–4990, doi:10.1002/jgrd.50413.

Reuter, M., Buchwitz, M., Schneising, O., Hase, F., Heymann, J., Guerlet, S., Cogan, A. J., Bovensmann, H., and Burrows, J. P.: A simple empirical model estimating atmospheric CO<sub>2</sub> background concentrations, *Atmos. Meas. Tech.*, 5, 1349–1357, doi:10.5194/amt-5-1349-2012, 2012.

Roberts, D. A., Bradley, E. S., Cheung, R., Leifer, I., Dennison, P. E., and Margolis, J. S.: Mapping methane emissions from a marine geological seep source using imaging spectrometry, *Remote Sens. Environ.*, 114, 592–606, 2010.



	<p style="text-align: center;"><b>COMEX</b> <b>Final Report</b></p>	<p style="text-align: right;">Version: 2.0 Doc ID: IUP-COMEX-FR Date: 3. July 2016</p>
---	---	--

Sun-Mack, S.; Chen, Y.; Arduini, R. & Minnis, P., Clear-sky narrowband albedo variations from VIRS and MODIS data, *13th Conference on Satellite Meteorology and Oceanography*, 2004.


Tratt, D. M., Buckland, K. N., Hall, J. L., Johnson, P. D., Keim, E. R., Leifer, I., Westberg, K., and Young, S. J.: Airborne visualization and quantification of discrete methane sources in the environment, *Remote Sens. Environ.*, 154, 74–88, 2014.

Thorpe, A. K., Frankenberg, C., and Roberts, D. A.: Retrieval techniques for airborne imaging of methane concentrations using high spatial and moderate spectral resolution: application to AVIRIS, *Atmos. Meas. Tech.*, 7, 491-506, doi:10.5194/amt-7-491-2014, 2014.

Thompson, D. R., Leifer, I., Bovensmann, H., Eastwood, M., Fladland, M., Frankenberg, C., Gerilowski, K., Green, R. O., Krautwurst, S., Krings, T., Luna, B., and Thorpe, A. K.: Real-time remote detection and measurement for airborne imaging spectroscopy: a case study with methane, *Atmos. Meas. Tech.*, 8, 4383-4397, doi:10.5194/amt-8-4383-2015, 2015.

Veefkind, J.P. , I. Aben, K. McMullan, H. Förster, J. de Vries, G. Otter, J. Claas, H.J. Eskes, J.F. de Haan, Q. Kleipool, M. van Weele, O. Hasekamp, R. Hoogeveen, J. Landgraf, R. Snel, P. Tol, P. Ingmann, R. Voors, B. Kruizinga, R. Vink, H. Visser, P.F. Levelt, TROPOMI on the ESA Sentinel-5 Precursor: A GMES mission for global observations of the atmospheric composition for climate, air quality and ozone layer applications, *Remote Sensing of Environment*, Volume 120, Pages 70-83, ISSN 0034-4257, <http://dx.doi.org/10.1016/j.rse.2011.09.027>, 2012.

Warren, D.W., R.H. Boucher, D.J. Gutierrez, E.R. Keim, and M.G. Sivjee, “MAKO: A high-performance, airborne imaging spectrometer for the long-wave infrared,” *Proceedings of SPIE*, 7812, 78120N, doi:10.1117/12.861374, 2010.

	<p style="text-align: center;"><b>COMEX</b> <b>Final Report</b></p>	<p style="text-align: right;">Version: 2.0 Doc ID: IUP-COMEX-FR Date: 3. July 2016</p>
--	---	--

## Annex 1: Overview of targets

The targets were pre-selected based on literature values, inventories and pre-surveys of the AMOG Surveyor and of the MACLab (see also Table 15 from the CIP (RD-4)). This approach could be performed for landfills which need to be monitored in the US according to regulatory. In contrast, for oil fields, reliable emission estimates could not easily be accessed. Ground- based in-situ sampling could not provide reliable estimates on fluxes required for modeling of expected total column increases, due to the large oil field extend, insufficient knowledge of atmospheric parameters and mixing as well as the inability to exactly localize the source position due to (mostly) restricted access to the fields. First pre-selection of oil fields was made based on production data obtained for the Division of Oil, Gas & Geothermal Resources (<http://www.conservation.ca.gov/DOG/Pages/Index.aspx>). In addition, it was planned to select the most promising targets with in-situ pre-survey before the actual flight day by airborne surveys (Alpha Jet) and ground based measurements (AMOG surveyor). Due to the limited availability and refueling restrictions of the Alpha Jet and the time required for relocation of AMOG, this strategy was discarded and changed during the campaign. Instead extensive use of the recently implemented real-time retrieval capabilities of MAMAP was implemented for pre-survey.


The measurement strategy was adopted accordingly and two promising targets were selected for each flight. In case of absence of measurable signals from the first target, the second target was flown. Hence, an optimization of available flight time was achieved. Drawback of this strategy was the increased and more difficult coordination between the different aircraft and also with ATC (Air Traffic Control).

For glint measurements only one accessible (with respect to available flight time) target in the area could be identified in the prescreened literature. The well-studied Coal Oil Point (COP) natural seep field near Santa Barbara (first observed by the early Spanish settlers and English explorers, Hornafius et al., 1999) was previously estimated with different sonar methods to release locally between 15 ktCH<sub>4</sub>/yr (Clark et al., 2010) and 29.2 ktCH<sub>4</sub>/yr (Hornafius et al., 1999), to the atmosphere and, therefore, has emissions of similar magnitudes as the selected landfills.

Based on this approach, a target list (Table 14) has been compiled which was modified (based on MAMAP measurement results) dynamically during the COMEX campaign.


For example, just on the second flight day (2014-06-03), an unexpectedly large methane plume was measured over the Poso Creek, Kern River and Kern Front Oil Fields (T1) by the MAMAP and Picarro instrument. Kern River as heavy oil field with high well density but low natural gas production was expected to have lower emissions than the adjacent Elk Hills field which was chosen as secondary target for that day. Hence, T1 became a high priority target and was overflowed in total 7 times.

Over the COP filed, no large signals were observed in the MAMAP (and in-situ data) opposite to previous estimates (Clark et al., 2010, Hornafius et al., 1999). Even the collected remote sensing glint data being of good quality it was decided to downscale COP from high priority to low.

	<b>COMEX</b> <b>Final Report</b>	Version: 2.0 Doc ID: IUP-COMEX-FR Date: 3. July 2016
--	-------------------------------------	--

Target number	Ref to CIP	Name	Type	Lat	Lon	CO <sub>2</sub>	CH <sub>4</sub>	inland	coast
T1	1	Kern Front and Kern River	Petroleum/Gas Production	35,45°	-118,98°	(x)	x	x	
T2	2	Elk Hills	Petroleum/Gas Production	35,28°	-119,44°	(x)	x	x	
T3	11	North Belridge and South Belridge	Petroleum/Gas Production	35,45°	-119,70°	(x)	x	x	
T4	12	Midway Sunset	Petroleum/Gas Production	35,15°	-119,51°	(x)	x	x	
T5	---	Buena Vista	Petroleum/Gas Production	35,19°	-119,45°	(x)	x	x	
T6	15	Olinda Alpha	Landfill	33,94°	-117,84°	x	(x)	x	
T7	13	Puente Hills	Landfill	34,02°	-118,02°	(x)	x	x	
T8	18	Scholl Canyon	Landfill	34,16°	-118,19°	x	(x)	x	
T9	---	BKK	Landfill	34,04°	-117,90°	x	(x)	x	
T10	9	Harris Ranch	Cattle Ranch / Feedlot	36,31°	-120,27°		x	x	
T11	---	Chino	Cattle Ranch / Feedlot	34,01°	-117,63°		x	x	
T12	7	Los Angeles Basin Survey	Megacity	33,92°	-118,14°	x	x	x	x
T13	8	Coal Oil Point	Natural oil and gas	34,39°	-119,87°		x		x
T14	3	La Brea Tar Pits	Natural oil and gas	34,07°	-118,36°		x		x
T15	---	Baldwin Hills	Petroleum/Gas Production	34,00°	-118,37°	(x)	x		x
T16	5	Carson	Refinery	33,81°	-118,24°	(x)	x		x
T17	6	Tesoro	Refinery	33,79°	-118,23	(x)	x		x


Table 14: COMEX targets flown during the campaign.

	<b>COMEX</b> <b>Final Report</b>	Version: 2.0 Doc ID: IUP-COMEX-FR Date: 3. July 2016
--	-------------------------------------	--

Target number (old)	Name	Type	Lat	Lon	CO <sub>2</sub>	CH <sub>4</sub>	inland	coast	Emission/ Column increase	seasonal variation
1	Kern River	Petroleum/Gas Production	35,45°	-118,98°	(x)	X	x			small
2	Elk Hills	Petroleum/Gas Production	35,28°	-119,44°	(x)	X	x			small
3	La Brea	Natural oil and gas	34,07°	-118,36°		X		x		small
4	El Segundo	Refinery	33,91°	-118,41°	(x)	X		x		small
5	Carson	Refinery	33,81°	-118,24°	(x)	X		x		small
6	Tesoro	Refinery	33,79°	-118,23°	(x)	X		x		small
7	Los Angeles	Megacity	33,92°	-118,14°	X	X	x	x		small
8	Coal Oil Pt	Natural oil and gas	34,39°	-119,88°		X		x	2-3 % XCH <sub>4</sub> in a plume of ~ 1.5 km x ~ 0.5 km, wind of 2.4 m/s Thorpe et al.	Due to fog*
9	Harris Ranch	Feedlot	36,31°	-120,27°		X	x			small
10	Lost Hills	Petroleum/Gas Production	35,61°	-119,72°	(x)	X	x			small
11	Belridge South	Petroleum/Gas Production	35,45°	-119,70°	(x)	X	x			small
12	Midway Sunset	Petroleum Production	35,15°	-119,51°	(x)	X	x			small
13	Puente Hills	Landfill	34,02°	-118,02°	(x)	X	x		30-38 kT CH <sub>4</sub> /year, CARB (2008) 38.8 kTCH <sub>4</sub> /Yr, (from Peischl et al.), 17.3 kTCH <sub>4</sub> /Yr EPA (2012). Landfill closed in 2013 but emissions expected to continue within some years.	small
<b>Backup Targets</b>										
14	Moss Landing	Power Plant (near Marina for Test Flight)	36,80°	-121,78°	X			x	2 MT CO <sub>2</sub> / Yr (CARMA)	small
15	Olinda Alpha	Landfill	33.939°	-117.836°	X	(x)	x		9.5-24.3 kTCH <sub>4</sub> /year, CARB(2008) 11.8 kTCH <sub>4</sub> /Yr (from Peischl et al.), 15.7 kT EPA 2012	small
16	Sunshine Canyon	Landfill	34.3262°	-118.5084°	X	(x)	x		8.86 kT CH <sub>4</sub> /year EPA 2012	small
17	Tajiguas	Landfill (could be flown together with COP), sunglint	34.4825°	-120.128°	X	(x)	x		2.8 kT CH <sub>4</sub> /year EPA 2012	small
18	Scholl Canyon	Landfill (near Burbank airport)	34.155°	-118.1928°	X	(x)	x		Closed	small

Table 15: COMEX targets as proposed in RD-4.



	<p style="text-align: center;"><b>COMEX</b> <b>Final Report</b></p>	<p style="text-align: right;">Version: 2.0 Doc ID: IUP-COMEX-FR Date: 3. July 2016</p>
--	---	--

## **Annex 2: COMEX Flight Documentation (day-by-day)**

This Section shows Google Earth overlays of the MAMAP remote sensing and Picarro in-situ] data set of all targets using an adapted radiative transfer model (compare to Section 7.1.2) ordered by flight day. Additionally, the main characteristics of the meteorology (cloudiness, wind conditions, proximate boundary layer height), special incidents on the flight dates, time and aircraft altitude of the MAMAP remote sensing survey, spectrometer temperature and integration time of the MAMAP instrument, altitude range of the flown in-situ legs, and participation of other instruments platforms during the specific day.

All MAMAP remote sensing surveys are normalized by a 300-point moving average and smoothed by a 3-point moving average (similar as it was done for C-MAPEX (RD-7)). Furthermore, the data has only been filtered by an inclination angle of  $< \pm 4^\circ$  of the downwelling optical path with respect to the nadir direction to remove curves. Altitudes are given in meters above mean sea level (mamsl).

## Flight Day 2014-05-30

**Target:** Harris Cattle Ranch / Feed Lot (T10)

**Weather conditions:** clear sky

**Other instruments/platforms:** no

**Miscellaneous:**

- Engineering flight
- Failure of Cirpas suite

Start MAMA	End MAMAP	Wind dir.	Wind speed	Approx. BLH	RS alt.	IS in BL	Spec. T	Int. time
10:50	11:30	(S)E	Calm (1 m/s)	1350	1737	yes	32°C	100 ms

Table 16: Listed are the start and end local time of the MAMAP remote sensing survey, the wind direction (dir.), the wind speed, the approximate boundary layer height (BLH), the remote sensing (RX) altitude (alt.), whether in-situ (IS) measurements were acquired within the boundary layer (BL), the spectrometer (spec.) temperature (T) and the integration (int.) time of the MAMAP instruments. All altitudes are given in m above mean sea level (mamsl).

**Flight altitude of the in-situ legs:** between 320 and 950 mamsl

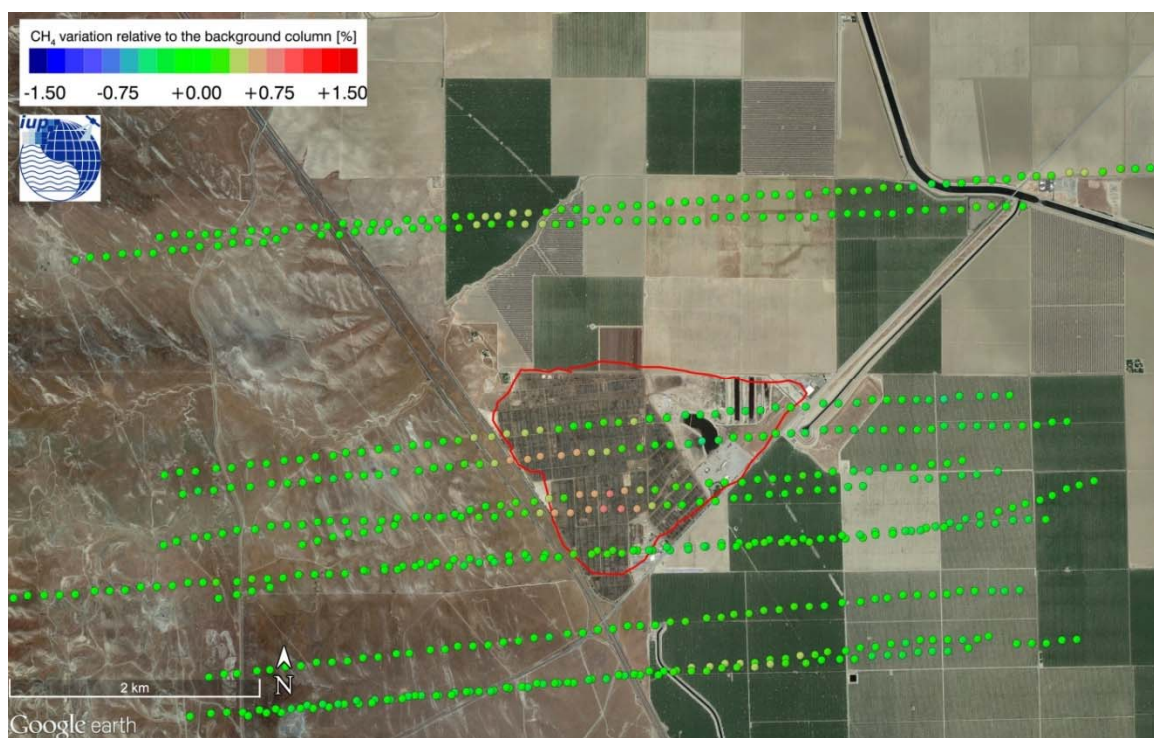


Figure 72: Normalized column averaged dry air mole fraction of  $\text{CH}_4$  of the MAMAP remote sensing sounding of Harris Ranch (encircled by the red solid line) on 2014-05-30.

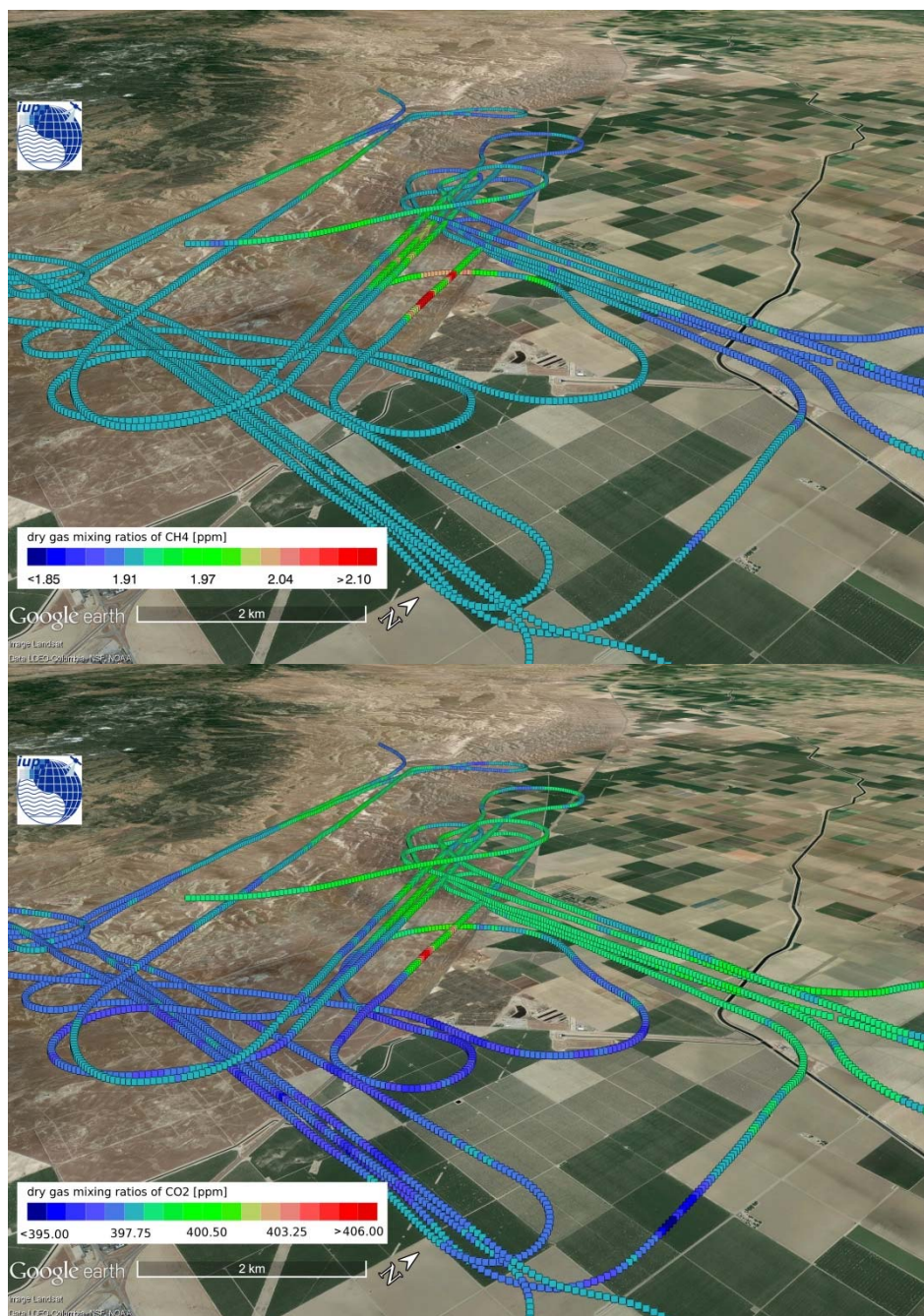


Figure 73: Picarro in-situ measurements of  $\text{CH}_4$  (top) and  $\text{CO}_2$  (bottom) below remote sensing altitude of Harris Ranch on 2014-05-30.



## Flight Day 2014-06-03

**Target:** Kern River and Kern Front Oil Field (T1)

**Weather conditions:** clear sky

**Other instruments/platforms:** AVIRISng

**Miscellaneous:**

Start	End	Wind	Wind	Approx.	RS	IS in	Spec.	Int.
MAMA	MAMAP	dir.	speed	BLH	alt.	BL	T	time
14:10	15:20	NW	3.5 to 4.5 m/s	1350	1421	yes	32°C	100 ms

Table 17: Listed are the start and end local time of the MAMAP remote sensing survey, the wind direction (dir.), the wind speed, the approximate boundary layer height (BLH), the remote sensing (RX) altitude (alt.), whether in-situ (IS) measurements were acquired within the boundary layer (BL), the spectrometer (spec.) temperature (T) and the integration (int.) time of the MAMAP instruments. All altitudes are given in m above mean sea level (mamsl).

**Flight altitude of the in-situ legs:** between 580 and 970 mamsl

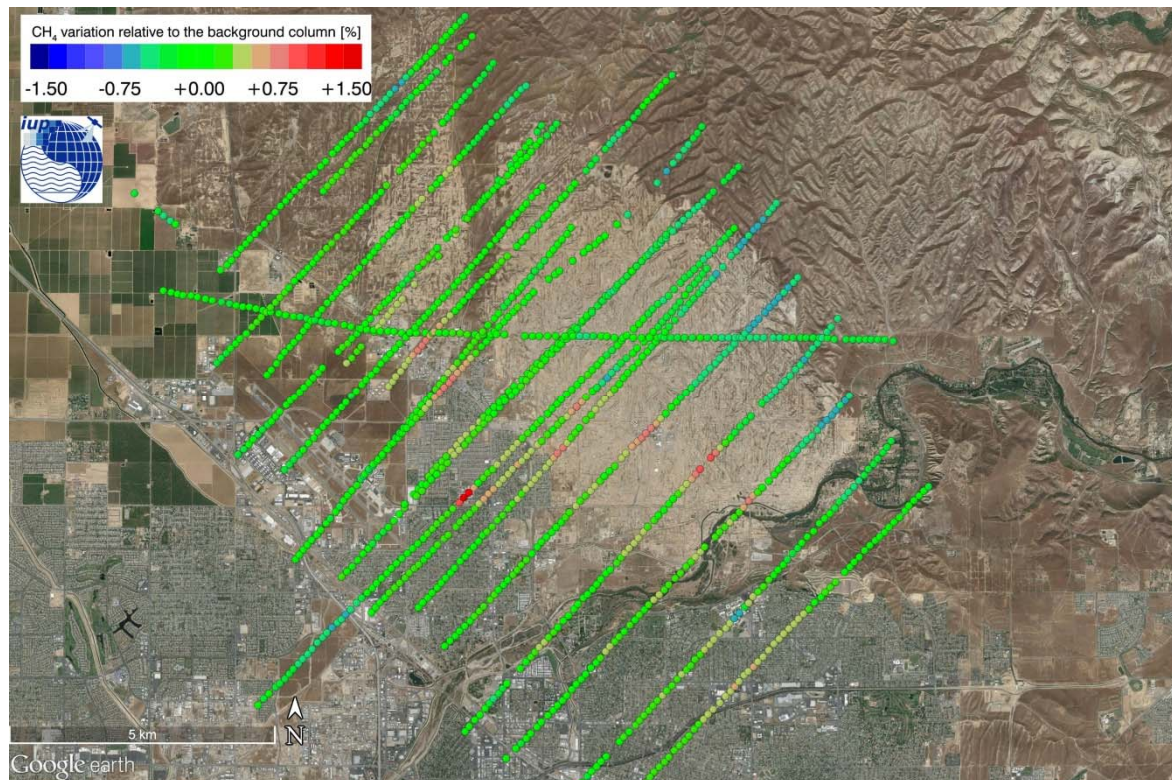


Figure 74: Normalized column averaged dry air mole fraction of  $\text{CH}_4$  of the MAMAP remote sensing sounding of the Kern River and Kern Front Oil Field on 2014-06-03.





**COMEX**  
**Final Report**

Version: 2.0  
Doc ID: IUP-COMEX-FR  
Date: 3. July 2016

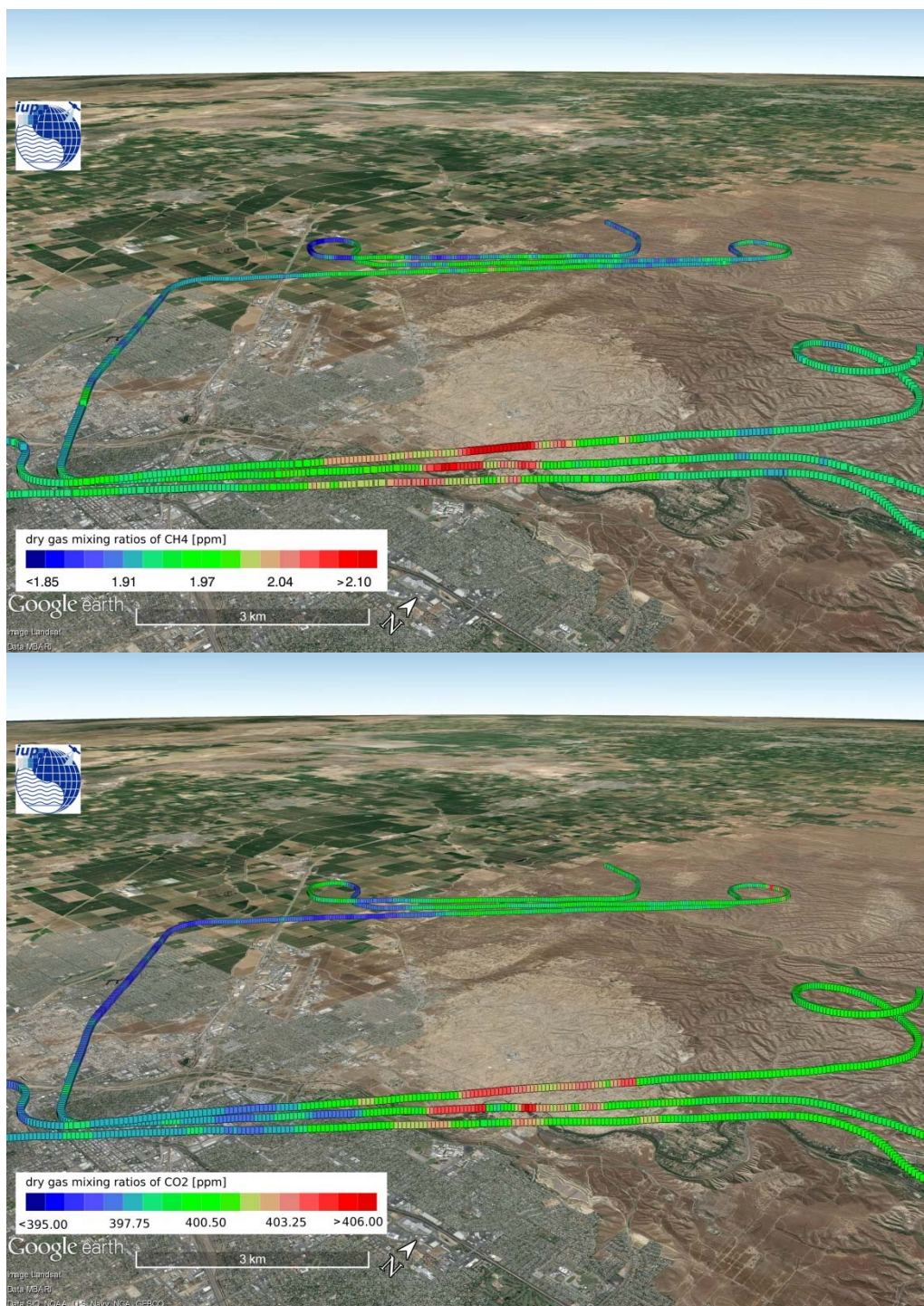


Figure 75: Picarro in-situ measurements of CH<sub>4</sub> (top) and CO<sub>2</sub> (bottom) below remote sensing altitude of the Kern River and Kern Front Oil Field on 2014-06-03.

## Flight Day 2014-06-04

**Target:** Coil Oil Point Seep Field (T13)

**Weather conditions:** clear sky

**Other instruments/platforms:** AVIRISc

**Miscellaneous:**

- For details see Section 10

Start MAMA	End MAMAP	Wind dir.	Wind speed	Approx. BLH	RS alt.	IS in BL	Spec. T	Int. time
11:35	13:45	SW	3 to 4 m/s	150	1404	yes	32°C	100 ms

*Table 18: Listed are the start and end local time of the MAMAP remote sensing survey, the wind direction (dir.), the wind speed, the approximate boundary layer height (BLH), the remote sensing (RX) altitude (alt.), whether in-situ (IS) measurements were acquired within the boundary layer (BL), the spectrometer (spec.) temperature (T) and the integration (int.) time of the MAMAP instruments. All altitudes are given in m above mean sea level (mamsl).*



## Flight Day 2014-06-09

**Target:** Kern River and Kern Front Oil Field (T1)

**Weather conditions:** clear sky

**Other instruments/platforms:** no

**Miscellaneous:**

- Possible overheating of NASA AMES Picarro instruments

Start	End	Wind	Wind	Approx.	RS	IS in	Spec.	Int.
MAMA	MAMAP	dir.	speed	BLH	alt.	BL	T	time
11:35	13:35	NW	4 to 5.7 m/s	850	1811	yes	32°C	100 ms

Table 19: Listed are the start and end local time of the MAMAP remote sensing survey, the wind direction (dir.), the wind speed, the approximate boundary layer height (BLH), the remote sensing (RX) altitude (alt.), whether in-situ (IS) measurements were acquired within the boundary layer (BL), the spectrometer (spec.) temperature (T) and the integration (int.) time of the MAMAP instruments. All altitudes are given in m above mean sea level (mamsl).

**Flight altitude of the in-situ legs:** between 560 and 1190 mamsl

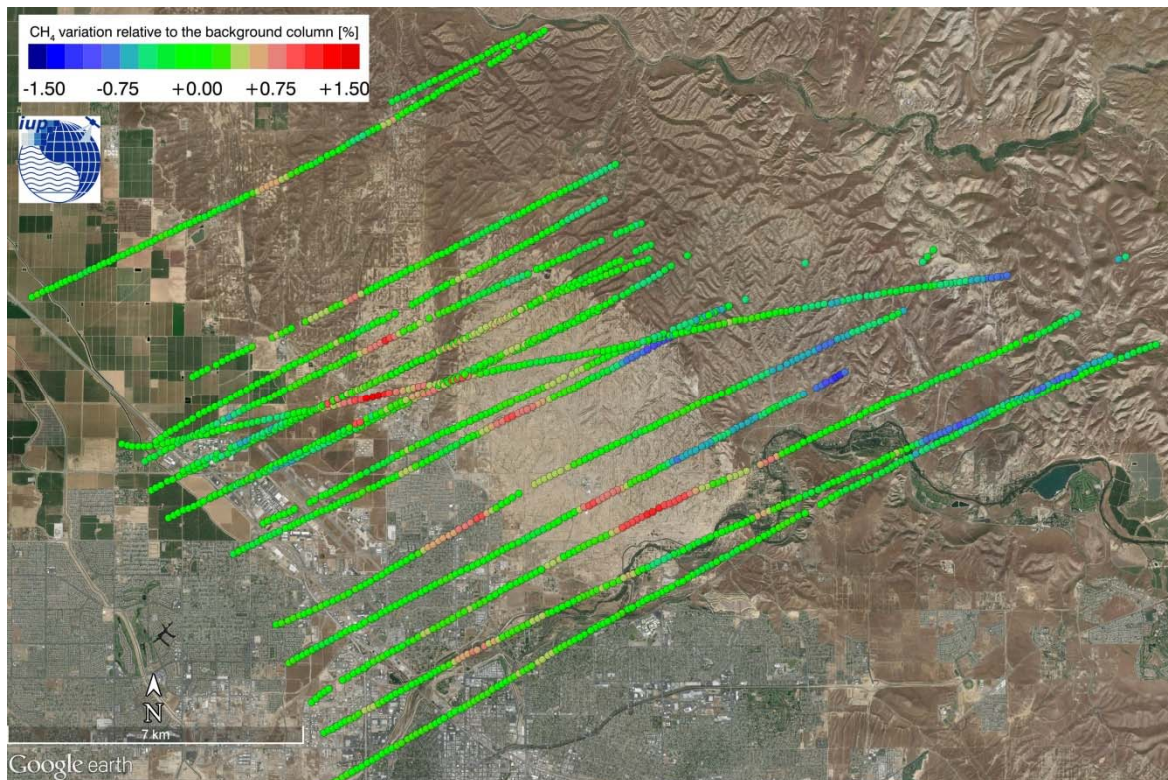


Figure 76: Normalized column averaged dry air mole fraction of  $\text{CH}_4$  of the MAMAP remote sensing sounding of the Kern River and Kern Front Oil Field on 2014-06-09.



**COMEX**  
**Final Report**

Version: 2.0  
Doc ID: IUP-COMEX-FR  
Date: 3. July 2016

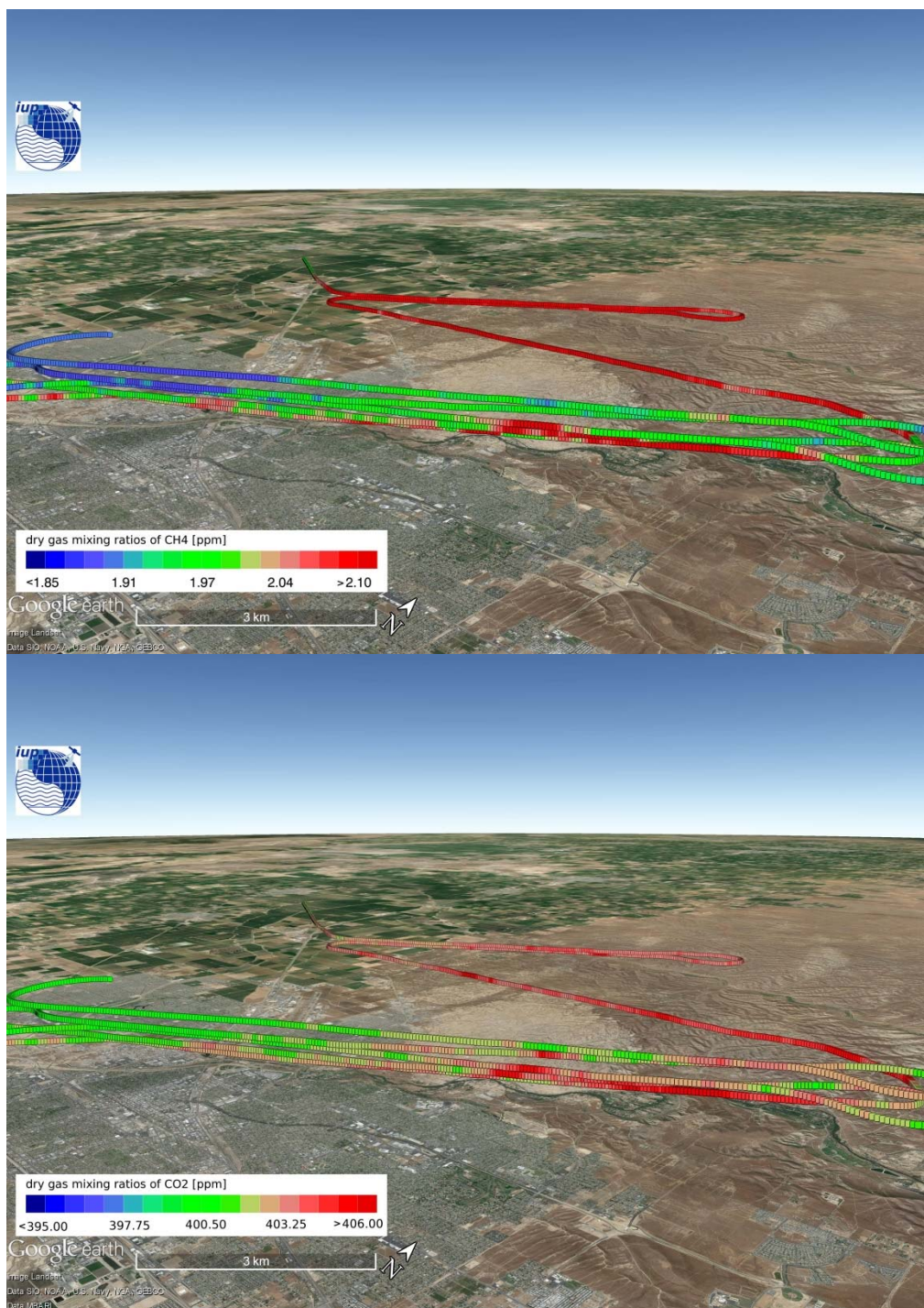


Figure 77: Picarro in-situ measurements of CH<sub>4</sub> (top) and CO<sub>2</sub> (bottom) below remote sensing altitude of the Kern River and Kern Oil Field on 2014-06-09.



## Flight Day 2014-06-12

**Target:** Puente Hills Landfill (T7)

**Weather conditions:** clear sky

**Other instruments/platforms:** AVIRISng

**Miscellaneous:**

Start	End	Wind	Wind	Approx.	RS	IS in	Spec.	Int.
MAMA	MAMAP	dir.	speed	BLH	alt.	BL	T	time
12:00	12:35	SW	1 to 2.5 m/s	900	1111	no	32°C	100 ms

Table 20: Listed are the start and end local time of the MAMAP remote sensing survey, the wind direction (dir.), the wind speed, the approximate boundary layer height (BLH), the remote sensing (RX) altitude (alt.), whether in-situ (IS) measurements were acquired within the boundary layer (BL), the spectrometer (spec.) temperature (T) and the integration (int.) time of the MAMAP instruments. All altitudes are given in m above mean sea level (mamsl).

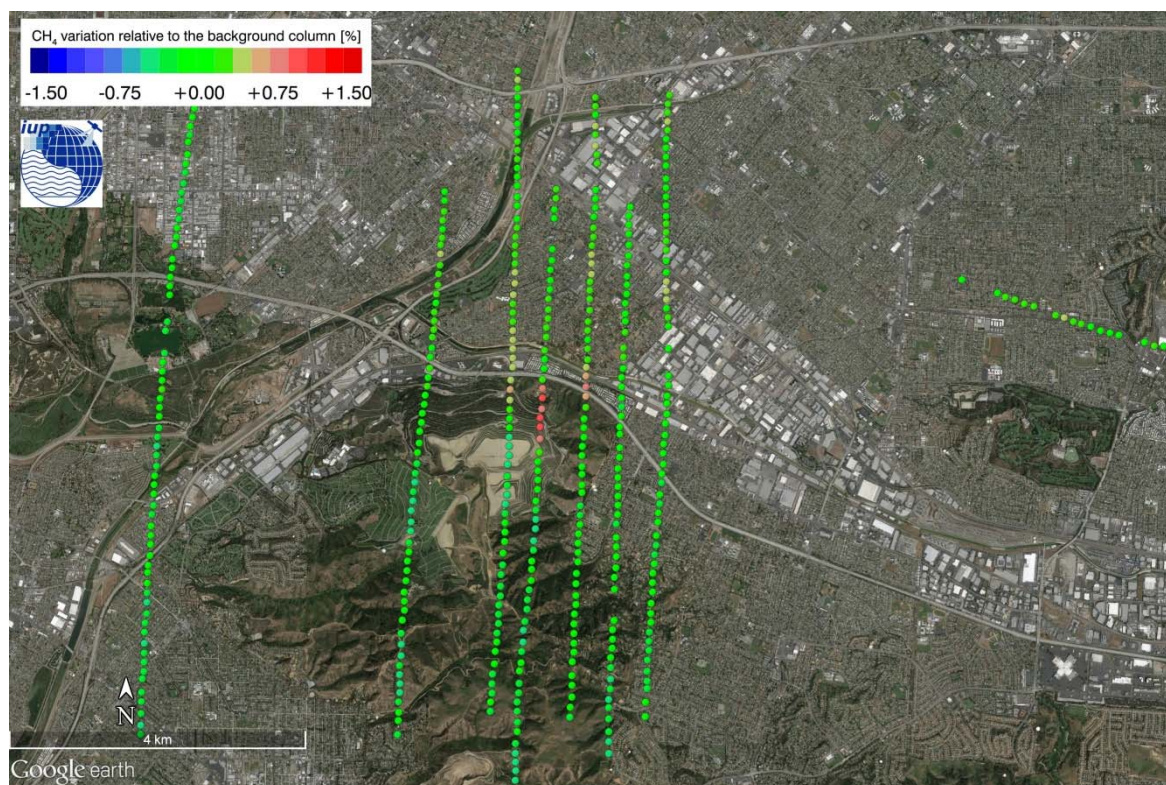


Figure 78: Normalized column averaged dry air mole fraction of  $\text{CH}_4$  of the MAMAP remote sensing sounding of the Puente Hills Landfill on 2014-06-12.

## Flight Day 2014-06-12

**Target:** Chino Cattle Ranch / Feed Lot (T11)

**Weather conditions:** clear sky

**Other instruments/platforms:** AVIRISng

**Miscellaneous:**

Start	End	Wind	Wind	Approx.	RS	IS in	Spec.	Int.
MAMA	MAMAP	dir.	speed	BLH	alt.	BL	T	time
12:40	13:50	NW	1.5 to 8 m/s	900	1109	yes	32°C	100 ms

Table 21: Listed are the start and end local time of the MAMAP remote sensing survey, the wind direction (dir.), the wind speed, the approximate boundary layer height (BLH), the remote sensing (RX) altitude (alt.), whether in-situ (IS) measurements were acquired within the boundary layer (BL), the spectrometer (spec.) temperature (T) and the integration (int.) time of the MAMAP instruments. All altitudes are given in m above mean sea level (mamsl).

**Flight altitude of the in-situ legs:** between 500 and 810 mamsl

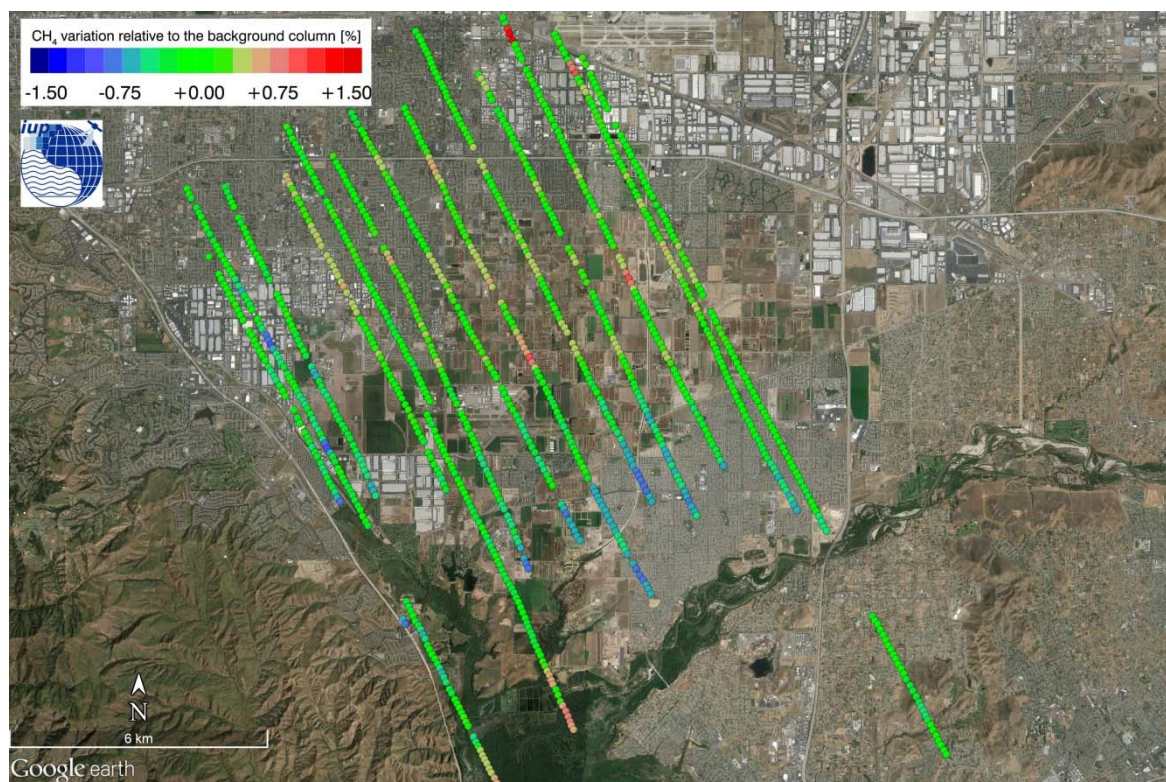


Figure 79: Normalized column averaged dry air mole fraction of  $\text{CH}_4$  of the MAMAP remote sensing sounding of the Chino Cattle Ranch / Feed Lot on 2014-06-12.



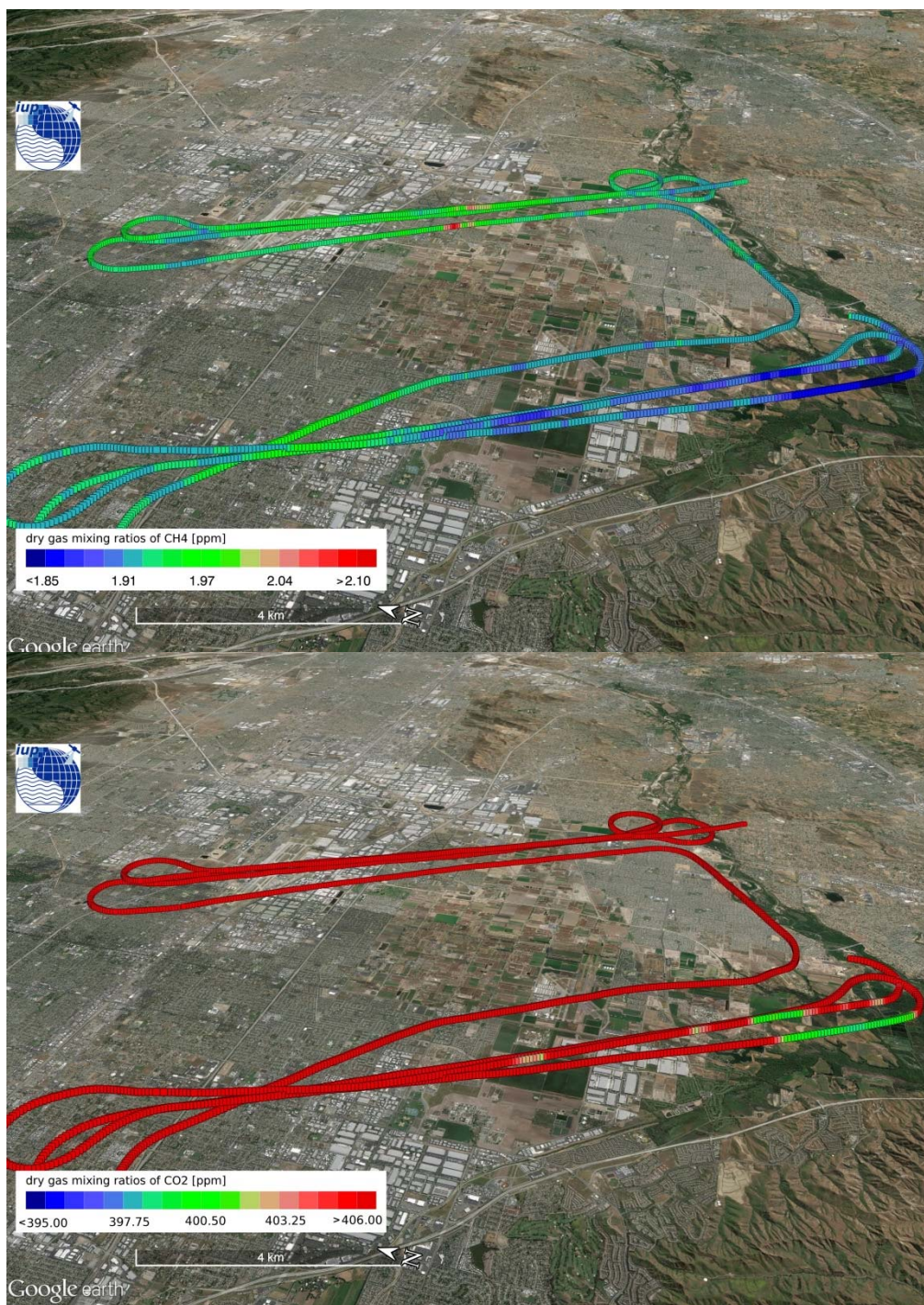


Figure 80: Picarro in-situ measurements of CH<sub>4</sub> (top) and CO<sub>2</sub> (bottom) below remote sensing altitude of the Chino Cattle Ranch / Feed Lot on 2014-06-12.



## Flight Day 2014-06-13

**Target:** Kern River and Kern Front Oil Field (T1)

**Weather conditions:** clear sky

**Other instruments/platforms:** AVIRISng, AMOG

**Miscellaneous:**

Start	End	Wind	Wind	Approx.	RS	IS in	Spec.	Int.
MAMA	MAMAP	dir.	speed	BLH	alt.	BL	T	time
11:10	13:20	NW	3.5 to 4.5 m/s	1400	1721	yes	32°C	100 ms

Table 22: Listed are the start and end local time of the MAMAP remote sensing survey, the wind direction (dir.), the wind speed, the approximate boundary layer height (BLH), the remote sensing (RX) altitude (alt.), whether in-situ (IS) measurements were acquired within the boundary layer (BL), the spectrometer (spec.) temperature (T) and the integration (int.) time of the MAMAP instruments. All altitudes are given in m above mean sea level (mamsl).

**Flight altitude of the in-situ legs:** between 470 and 940 mamsl

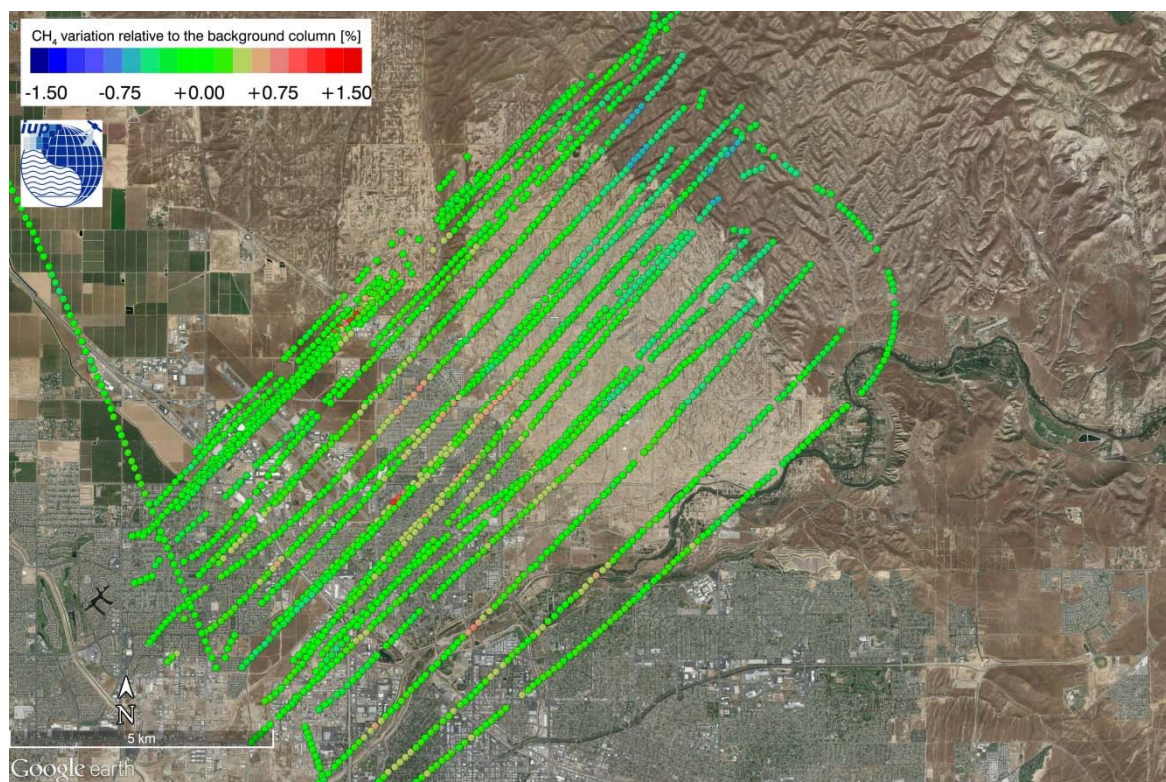


Figure 81: Normalized column averaged dry air mole fraction of  $\text{CH}_4$  of the MAMAP remote sensing sounding of the Kern River and Kern Front Oil Field on 2014-06-13.





# COMEX Final Report

Version: 2.0  
Doc ID: IUP-COMEX-FR  
Date: 3. July 2016

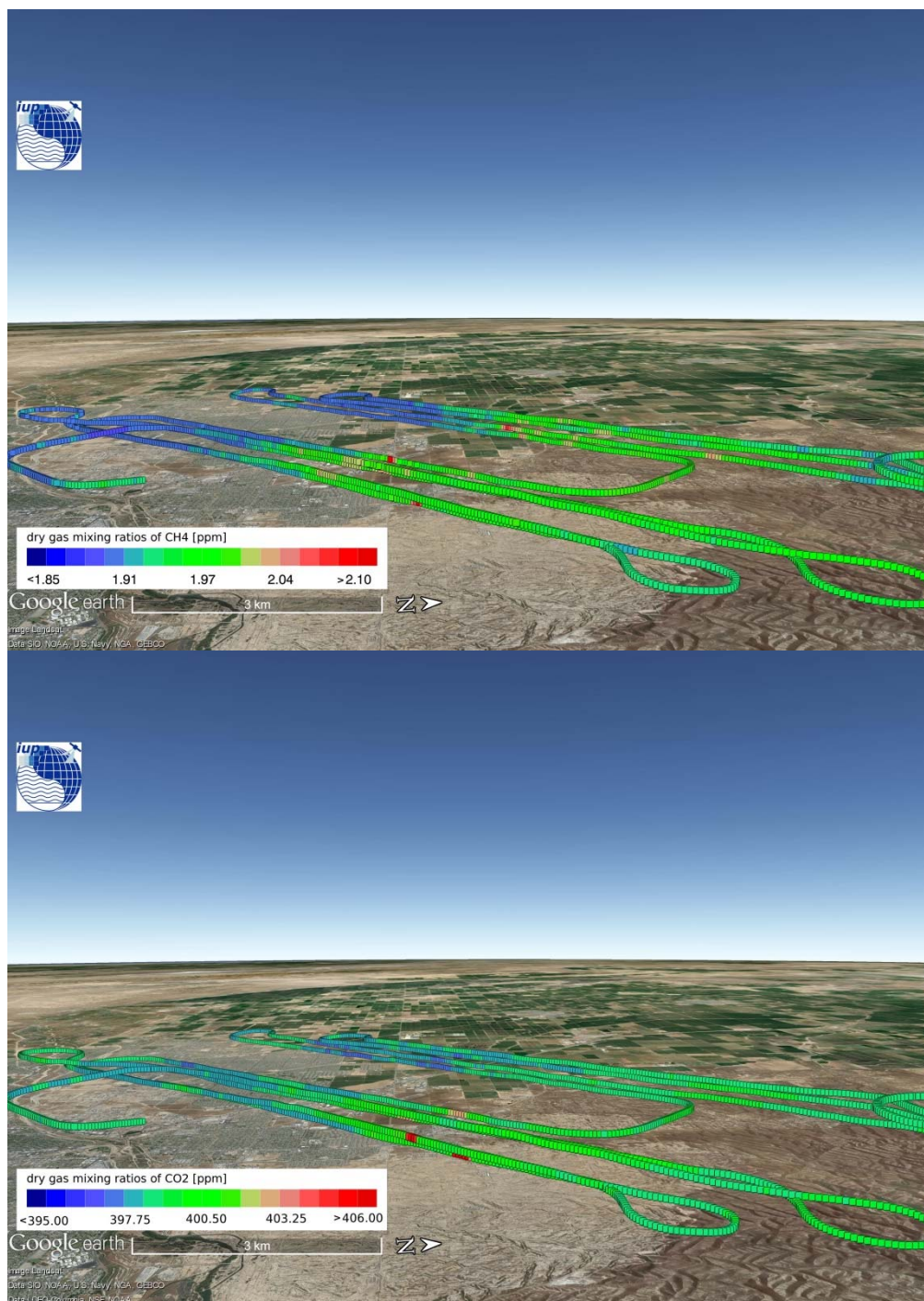


Figure 82: Picarro in-situ measurements of CH<sub>4</sub> (top) and CO<sub>2</sub> (bottom) below remote sensing altitude the Kern River and Kern Front Oil Field on 2014-06-13.

## Flight Day 2014-08-21

**Target:** Kern River and Kern Front Oil Field (T1)

**Weather conditions:** clear sky

**Other instruments/platforms:** no

**Miscellaneous:**

- Engineering flight
- Unsteady wind conditions

Start	End	Wind	Wind	Approx.	RS	IS in	Spec.	Int.
MAMA	MAMAP	dir.	speed	BLH	alt.	BL	T	time
11:05	13:10	-	2 to 3 m/s	1150	2395	yes	32°C	100 ms

Table 23: Listed are the start and end local time of the MAMAP remote sensing survey, the wind direction (dir.), the wind speed, the approximate boundary layer height (BLH), the remote sensing (RX) altitude (alt.), whether in-situ (IS) measurements were acquired within the boundary layer (BL), the spectrometer (spec.) temperature (T) and the integration (int.) time of the MAMAP instruments. All altitudes are given in m above mean sea level (mamsl).

**Flight altitude of the in-situ legs:** between 480 and 1000 mamsl

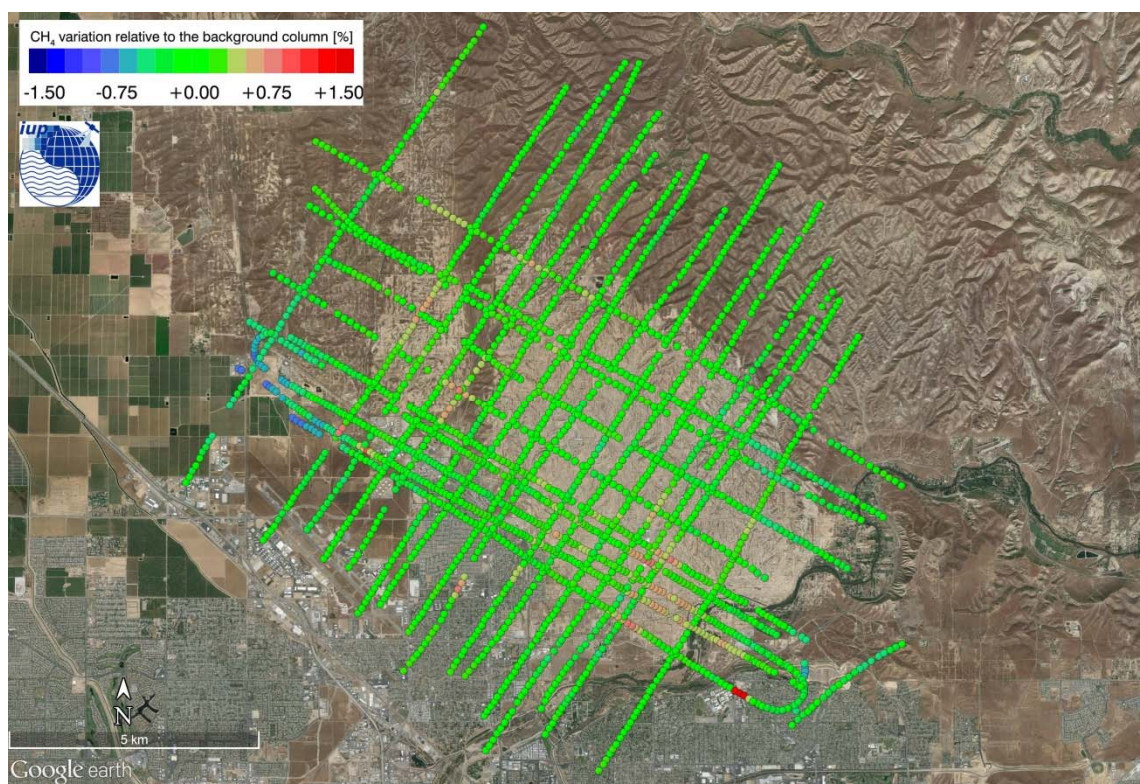


Figure 83: Normalized column averaged dry air mole fraction of  $\text{CH}_4$  of the MAMAP remote sensing sounding of the Kern River and Kern Front Oil Field on 2014-08-21.





**COMEX**  
**Final Report**

Version: 2.0  
Doc ID: IUP-COMEX-FR  
Date: 3. July 2016

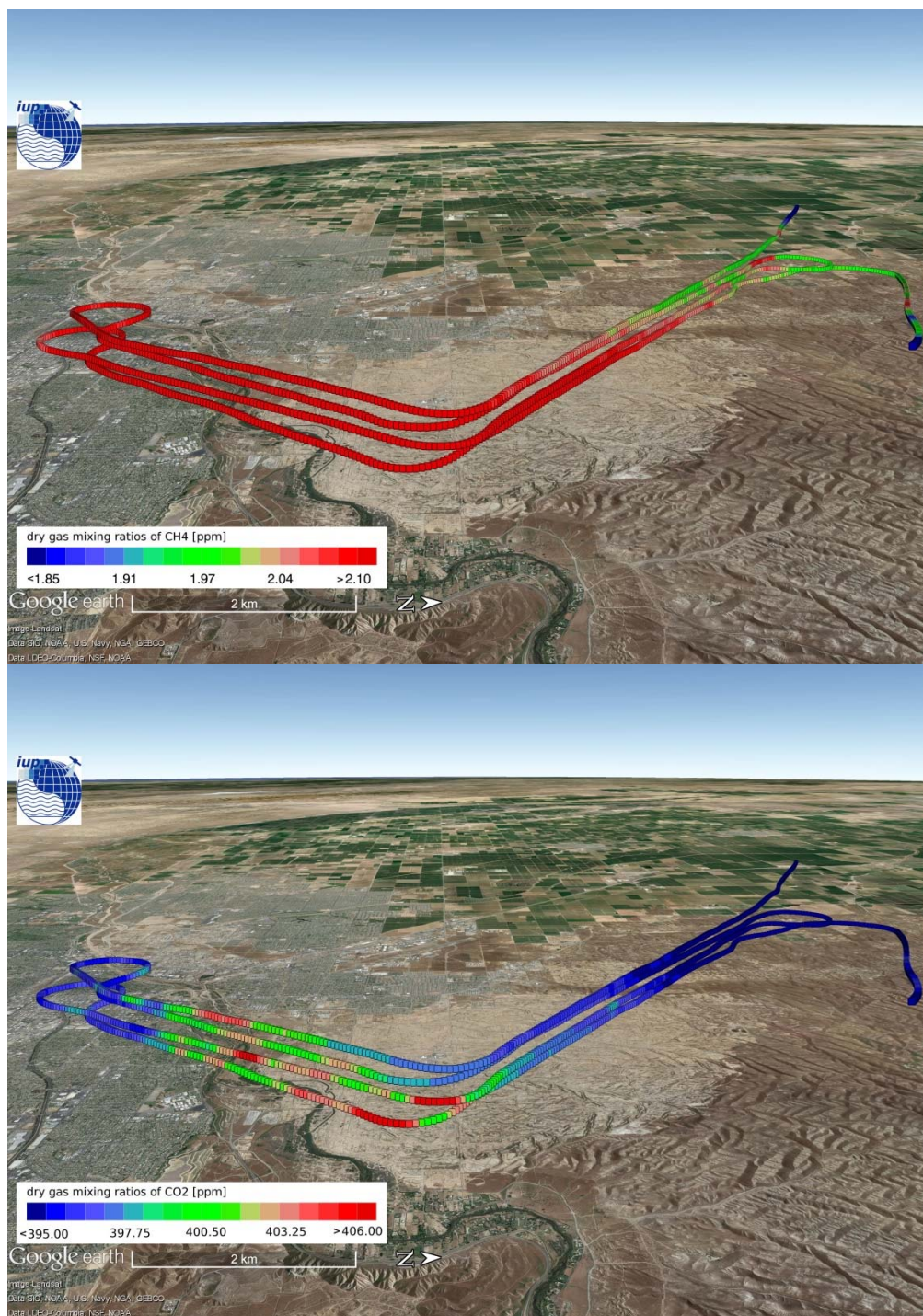


Figure 84: Picarro in-situ measurements of CH<sub>4</sub> (top) and CO<sub>2</sub> (bottom) below remote sensing altitude the Kern River and Kern Front Oil Field on 2014-08-21.

## Flight Day 2014-08-23

**Target:** Midway Sunset Oil Field (T4); Elk Hills Oil Field (T2); North Belridge and South Belridge Oil Field (T3); Buena Vista Oil Field (T5) [Transit flight from Marina to Burbank]

**Weather conditions:** clear sky

**Other instruments/platforms:** no

**Miscellaneous:**

- Unsteady wind conditions
- Integration time had to be adjusted (from 100 ms to 80 ms) in the middle of the flight due to detector saturation (smaller solar zenith angle than in the first part of COMEX and bright surface) → data gaps in the middle of the flight (compare to Figure 85)

Start MAMA	End MAMAP	Wind dir.	Wind speed	Approx. BLH	RS alt.	IS in BL	Spec. T	Int. time
11:35	14:40	-	calm	1150	2100	no	32°C	100/80 ms

Table 24: Listed are the start and end local time of the MAMAP remote sensing survey, the wind direction (dir.), the wind speed, the approximate boundary layer height (BLH), the remote sensing (RX) altitude (alt.), whether in-situ (IS) measurements were acquired within the boundary layer (BL), the spectrometer (spec.) temperature (T) and the integration (int.) time of the MAMAP instruments. All altitudes are given in m above mean sea level (mamsl).

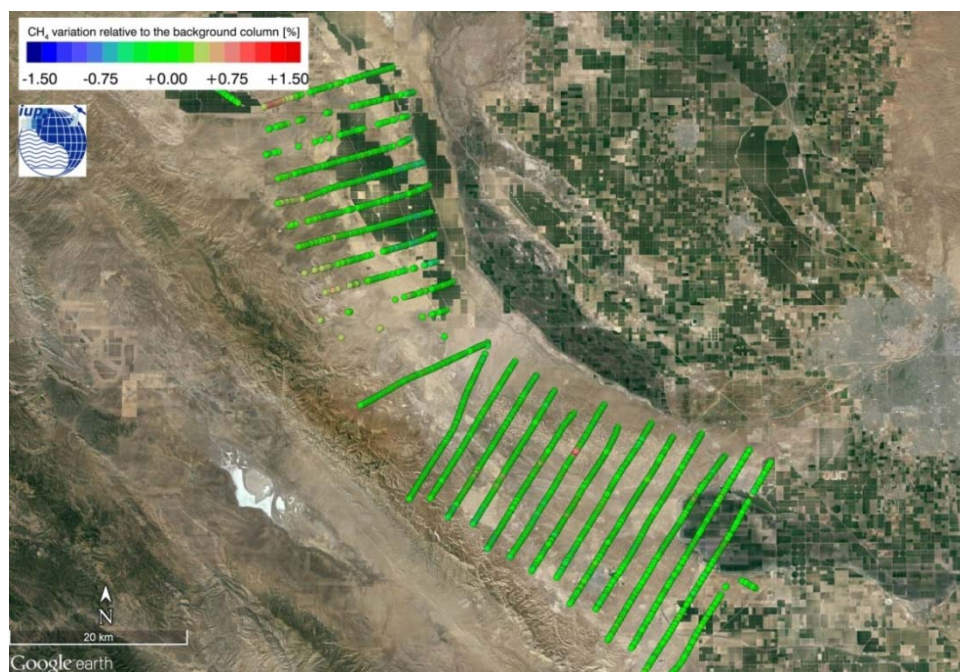


Figure 85: Normalized column averaged dry air mole fraction of  $\text{CH}_4$  of the MAMAP remote sensing sounding of the Midway Sunset Oil Field; Elk Hills Oil Field; North Belridge and South Belridge Oil Field; Buena Vista Oil Field on 2014-08-23.



## Flight Day 2014-08-25

**Target:** Coal Oil Point Seep Field (T13)

**Weather conditions:** clear sky with some high clouds at the end of the flight towards the south of the seep field

**Other instruments/platforms:** no

**Miscellaneous:**

- For details see Section 10

Start	End	Wind	Wind	Approx.	RS	IS in	Spec.	Int.
MAMA	MAMAP	dir.	speed	BLH	alt.	BL	T	time
12:30	15:15	SW	4 to 5 m/s	500	2068	yes	32°C	80 ms

*Table 25: Listed are the start and end local time of the MAMAP remote sensing survey, the wind direction (dir.), the wind speed, the approximate boundary layer height (BLH), the remote sensing (RX) altitude (alt.), whether in-situ (IS) measurements were acquired within the boundary layer (BL), the spectrometer (spec.) temperature (T) and the integration (int.) time of the MAMAP instruments. All altitudes are given in m above mean sea level (mamsl).*

## Flight Day 2014-08-26

**Target:** Kern River and Kern Front Oil Field (T1)

**Weather conditions:** clear sky

**Other instruments/platforms:** AVIRISc

**Miscellaneous:**

Start	End	Wind	Wind	Approx.	RS	IS in	Spec.	Int.
MAMA	MAMAP	dir.	speed	BLH	alt.	BL	T	time
14:15	15:50	NW	3 to 6 m/s	1600	2088	yes	32°C	80 ms

Table 26: Listed are the start and end local time of the MAMAP remote sensing survey, the wind direction (dir.), the wind speed, the approximate boundary layer height (BLH), the remote sensing (RX) altitude (alt.), whether in-situ (IS) measurements were acquired within the boundary layer (BL), the spectrometer (spec.) temperature (T) and the integration (int.) time of the MAMAP instruments. All altitudes are given in m above mean sea level (mamsl).

**Flight altitude of the in-situ legs:** between 420 and 1380 mamsl

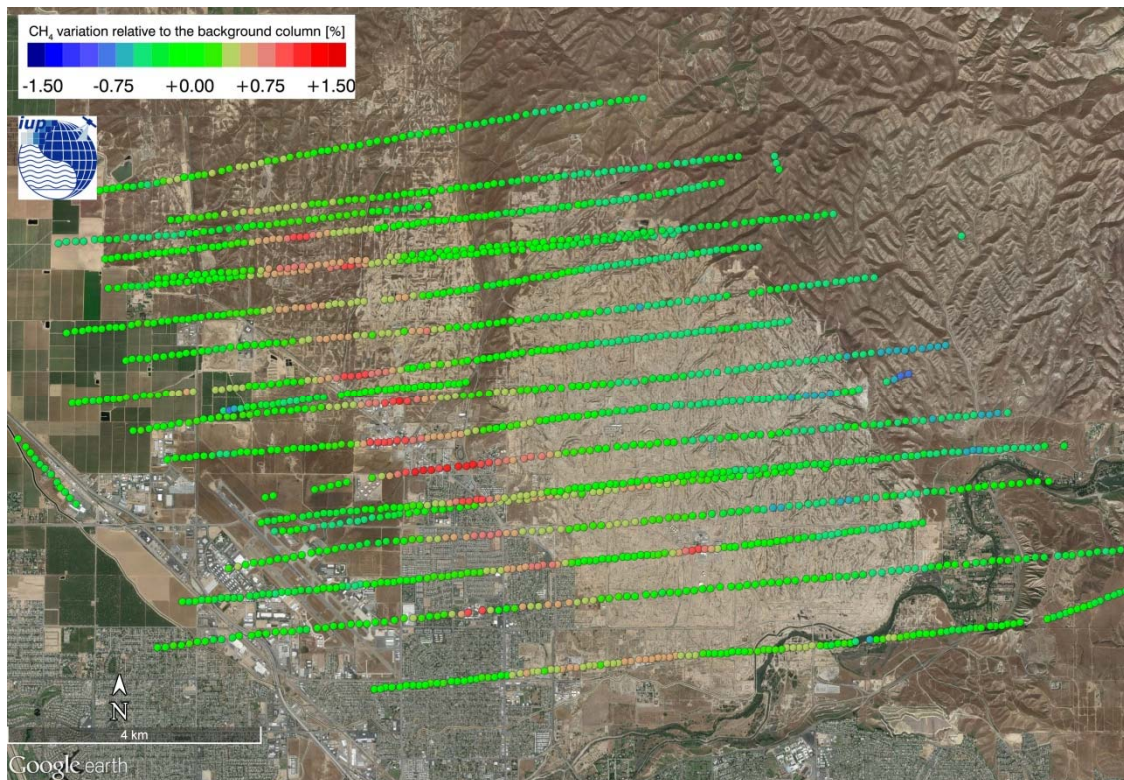


Figure 86: Normalized column averaged dry air mole fraction of  $\text{CH}_4$  of the MAMAP remote sensing sounding of the Kern River and Kern Front Oil Field on 2014-08-26.





COMEX  
Final Report

Version: 2.0  
Doc ID: IUP-COMEX-FR  
Date: 3. July 2016

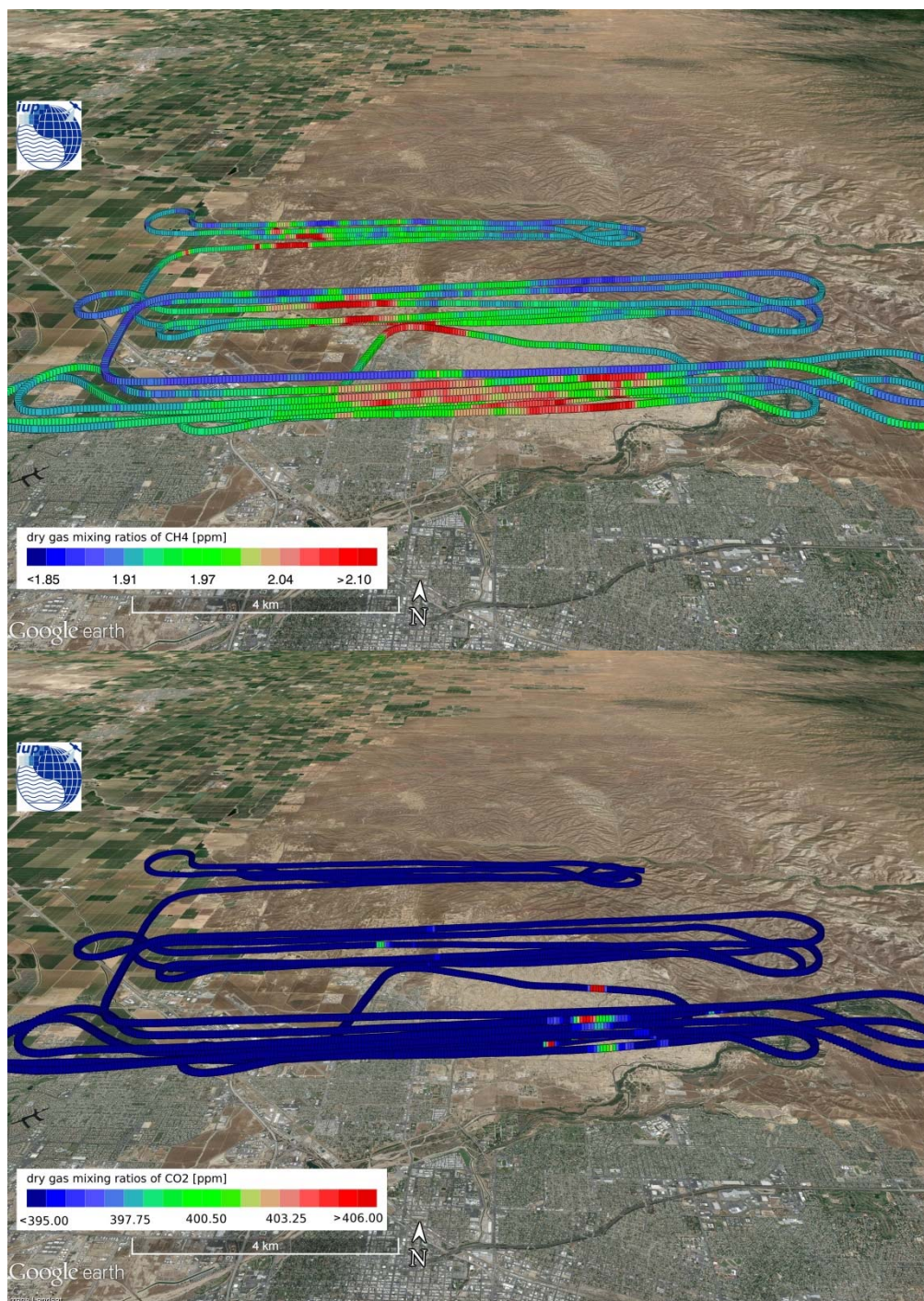


Figure 87: Picarro in-situ measurements of CH<sub>4</sub> (top) and CO<sub>2</sub> (bottom) below remote sensing altitude the Kern River and Kern Front Oil Field on 2014-08-26.



## Flight Day 2014-08-27

**Target:** La Brea Tar Pits (T14) and Baldwin Hills Oil Field (T15)

**Weather conditions:** clear sky

**Other instruments/platforms:** no

**Miscellaneous:**

Start	End	Wind	Wind	Approx.	RS	IS in	Spec.	Int.
MAMA	MAMAP	dir.	speed	BLH	alt.	BL	T	time
11:05	11:25	SW	Calm (~1.5 m/s)	1050	1785	no	32°C	80 ms

Table 27: Listed are the start and end local time of the MAMAP remote sensing survey, the wind direction (dir.), the wind speed, the approximate boundary layer height (BLH), the remote sensing (RX) altitude (alt.), whether in-situ (IS) measurements were acquired within the boundary layer (BL), the spectrometer (spec.) temperature (T) and the integration (int.) time of the MAMAP instruments. All altitudes are given in m above mean sea level (mamsl).

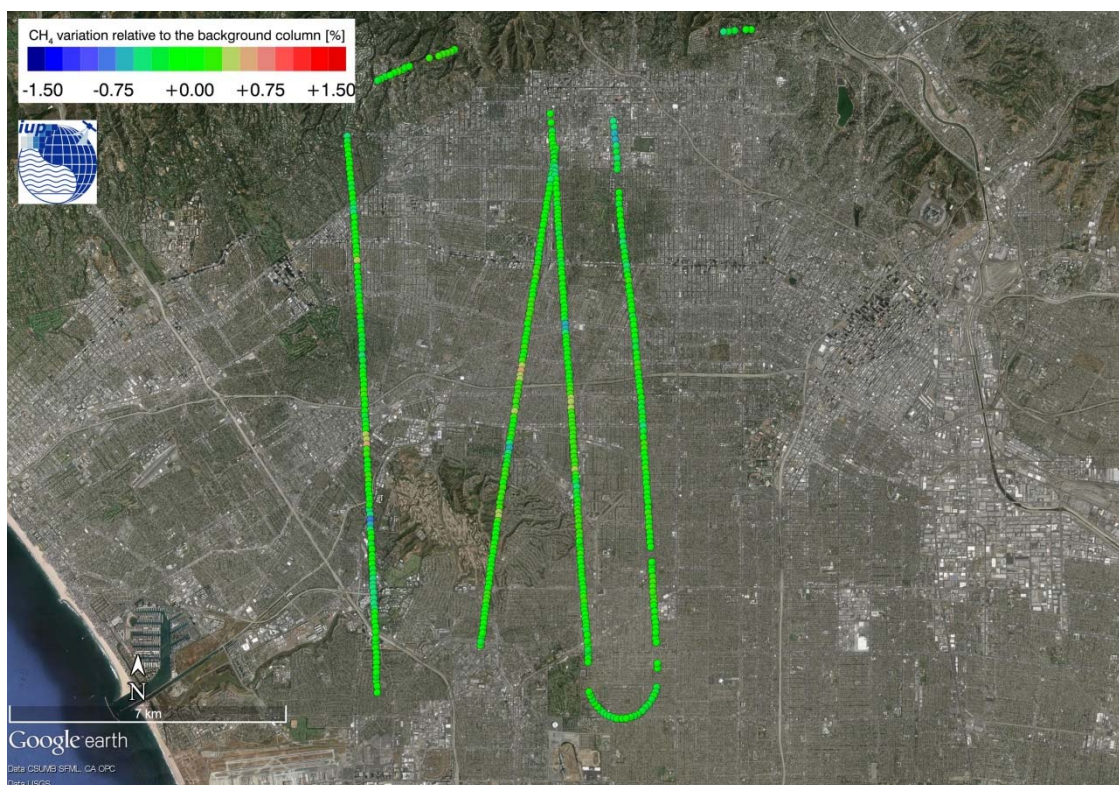


Figure 88: Normalized column averaged dry air mole fraction of  $\text{CH}_4$  of the MAMAP remote sensing sounding of the La Brea Tar Pits and the Baldwin Hills Oil Field on 2014-08-27.



## Flight Day 2014-08-27

**Target:** Scholl Canyon (T8)

**Weather conditions:** clear sky

**Other instruments/platforms:** no

**Miscellaneous:**

-

Start	End	Wind	Wind	Approx.	RS	IS in	Spec.	Int.
MAMA	MAMAP	dir.	speed	BLH	alt.	BL	T	time
11:25	12:05	SW	2 m/s	1050	1773	no	32°C	80 ms

Table 28: Listed are the start and end local time of the MAMAP remote sensing survey, the wind direction (dir.), the wind speed, the approximate boundary layer height (BLH), the remote sensing (RX) altitude (alt.), whether in-situ (IS) measurements were acquired within the boundary layer (BL), the spectrometer (spec.) temperature (T) and the integration (int.) time of the MAMAP instruments. All altitudes are given in m above mean sea level (mamsl).

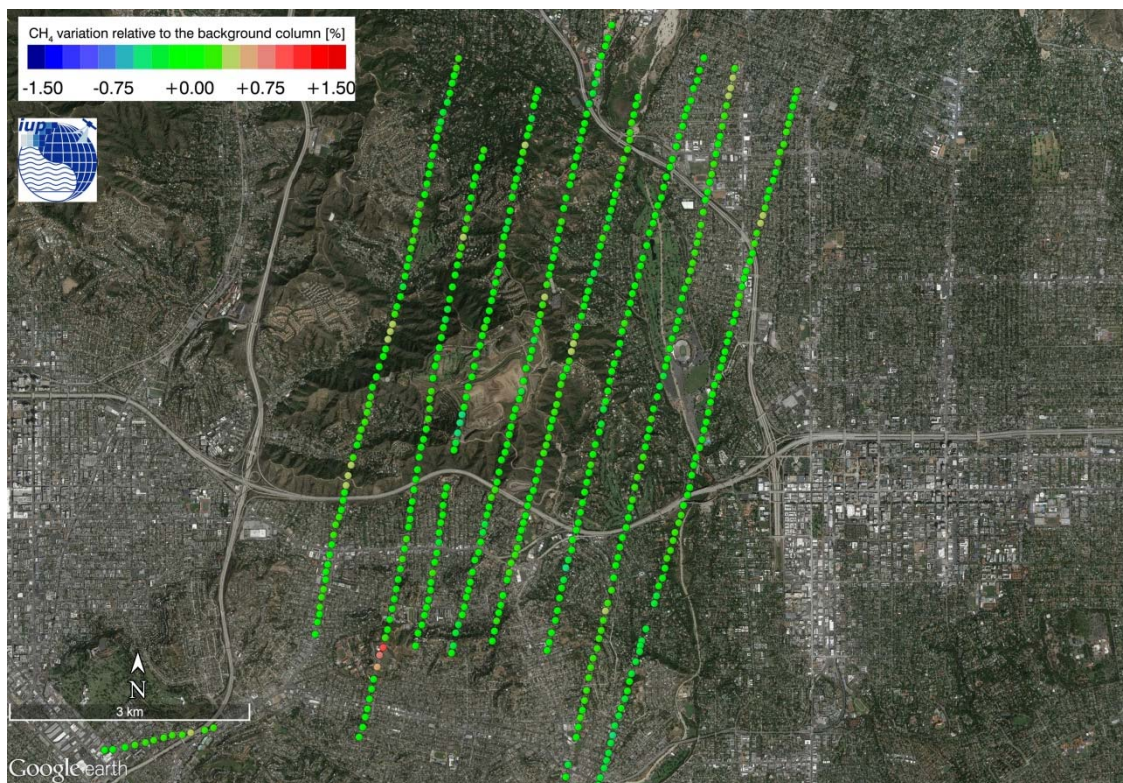


Figure 89: Normalized column averaged dry air mole fraction of  $\text{CH}_4$  of the MAMAP remote sensing sounding of the Scholl Canyon Landfill on 2014-08-27.

## Flight Day 2014-08-27

**Target:** Puente Hills Landfill (T7)

**Weather conditions:** clear sky

**Other instruments/platforms:** no

**Miscellaneous:**

-

Start MAMA	End MAMAP	Wind dir.	Wind speed	Approx. BLH	RS alt.	IS in BL	Spec. T	Int. time
12:15	13:20	SW	2 to 3 m/s	1150	1228	yes	32°C	80 ms

Table 29: Listed are the start and end local time of the MAMAP remote sensing survey, the wind direction (dir.), the wind speed, the approximate boundary layer height (BLH), the remote sensing (RX) altitude (alt.), whether in-situ (IS) measurements were acquired within the boundary layer (BL), the spectrometer (spec.) temperature (T) and the integration (int.) time of the MAMAP instruments. All altitudes are given in m above mean sea level (mamsl).

**Flight altitude of the in-situ legs:** between 460 and 1140 mamsl

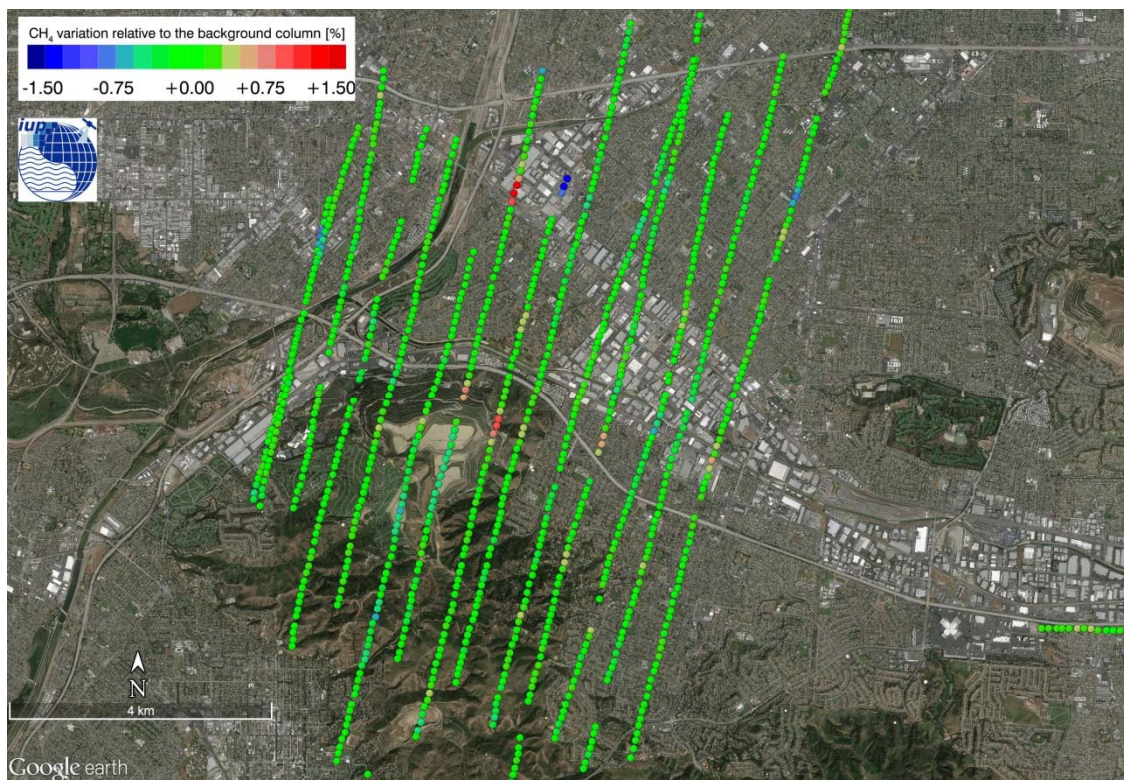


Figure 90: Normalized column averaged dry air mole fraction of  $\text{CH}_4$  of the MAMAP remote sensing sounding of the Puente Hills Landfill on 2014-08-27.





**COMEX**  
**Final Report**

Version: 2.0  
Doc ID: IUP-COMEX-FR  
Date: 3. July 2016

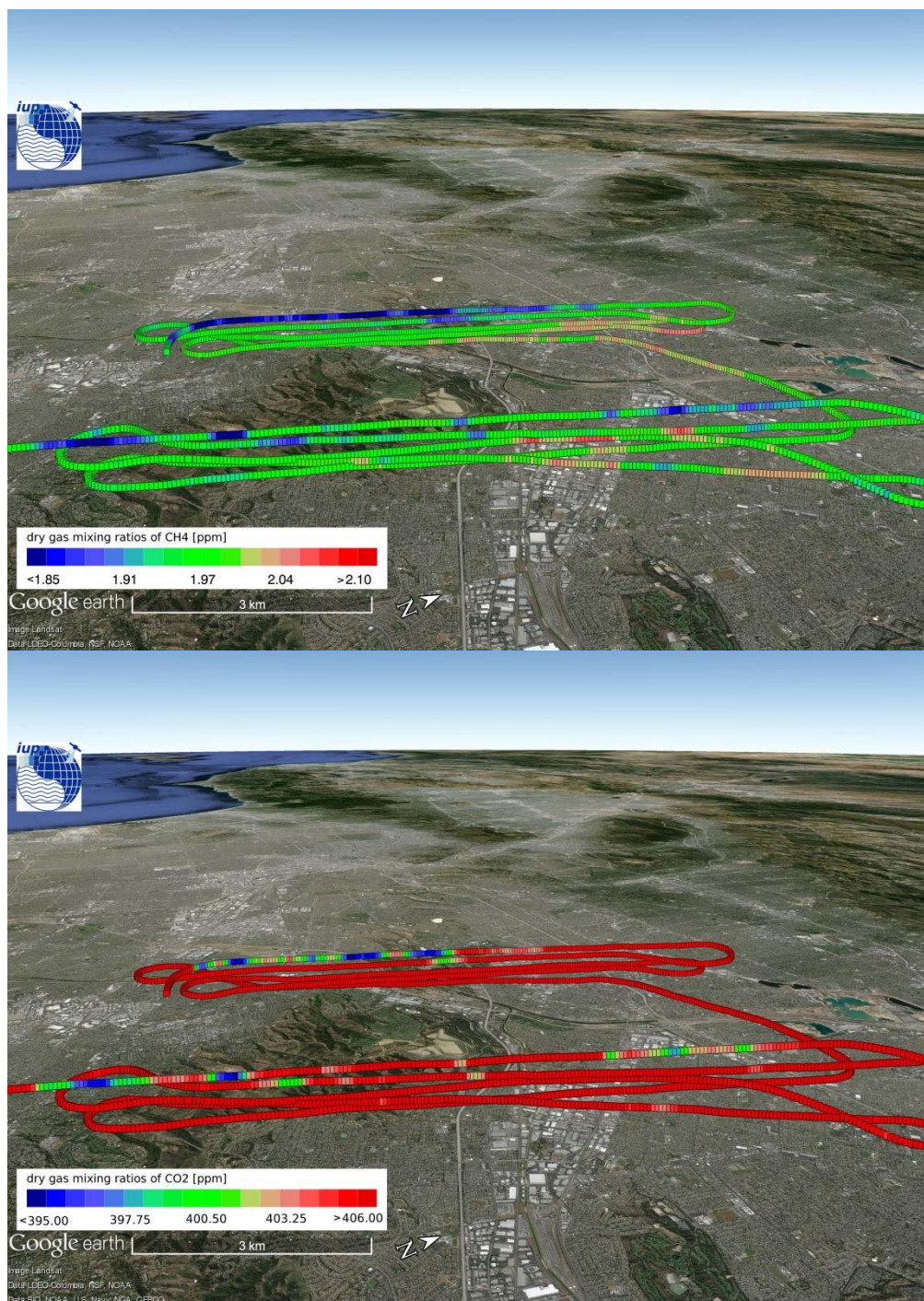


Figure 91: Picarro in-situ measurements of CH<sub>4</sub> (top) and CO<sub>2</sub> (bottom) below remote sensing altitude the Puente Hills Landfill on 2014-08-27.



## Flight Day 2014-08-27

**Target:** Olinda Alpha Landfill (T6)

**Weather conditions:** clear sky

**Other instruments/platforms:** no

**Miscellaneous:**

-

Start	End	Wind	Wind	Approx.	RS	IS in	Spec.	Int.
MAMA	MAMAP	dir.	speed	BLH	alt.	BL	T	time
14:10	14:55	SW	~5 m/s	1150	1971	yes	32°C	80 ms

*Table 30: Listed are the start and end local time of the MAMAP remote sensing survey, the wind direction (dir.), the wind speed, the approximate boundary layer height (BLH), the remote sensing (RX) altitude (alt.), whether in-situ (IS) measurements were acquired within the boundary layer (BL), the spectrometer (spec.) temperature (T) and the integration (int.) time of the MAMAP instruments. All altitudes are given in m above mean sea level (mamsl).*

**Flight altitude of the in-situ legs:** between 580 and 1140 mamsl

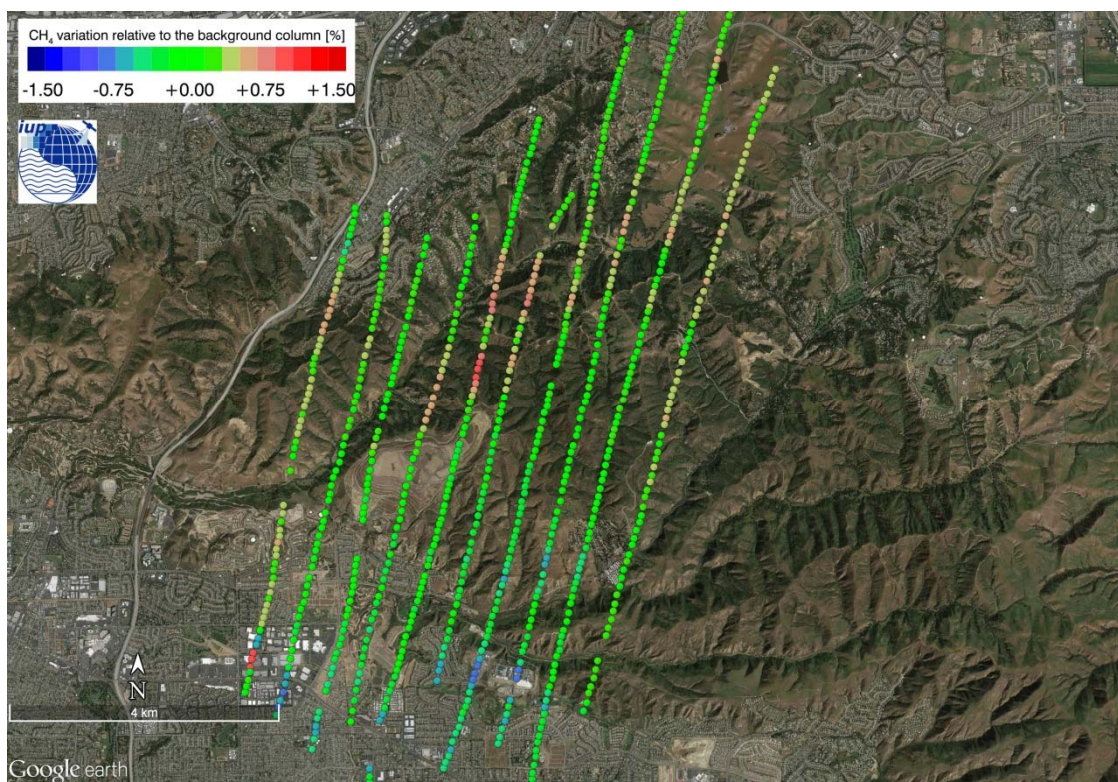


*Figure 92: Normalized column averaged dry air mole fraction of CH<sub>4</sub> of the MAMAP remote sensing sounding of the Olinda Alpha Landfill on 2014-08-27.*



COMEX  
Final Report

Version: 2.0  
Doc ID: IUP-COMEX-FR  
Date: 3. July 2016

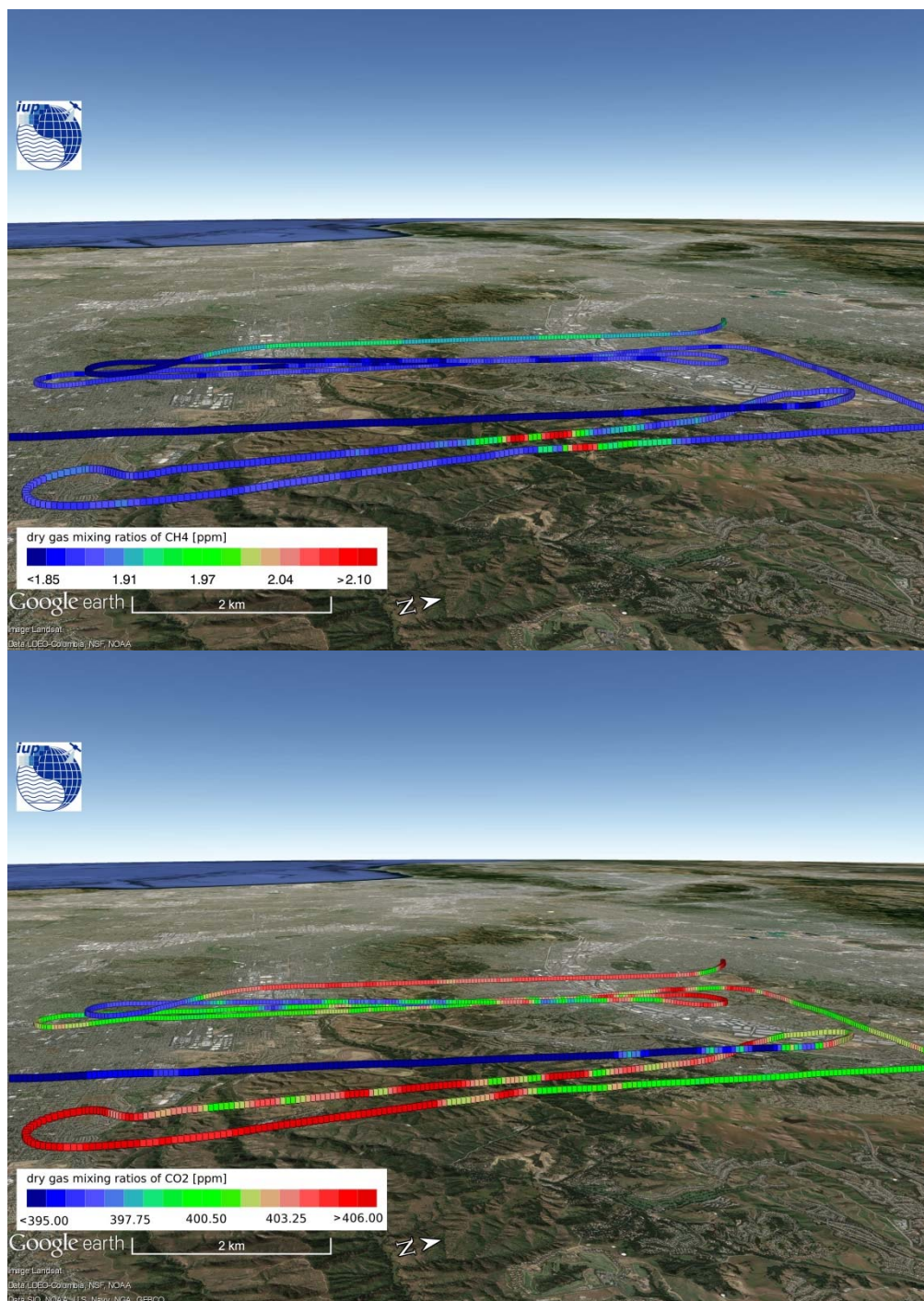


Figure 93: Picarro in-situ measurements of  $\text{CH}_4$  (top) and  $\text{CO}_2$  (bottom) below remote sensing altitude the Olinda Alpha Landfill on 2014-08-27.



## Flight Day 2014-08-28

**Target:** Olinda Alpha Landfill (T6)

**Weather conditions:** clear sky

**Other instruments/platforms:** no

**Miscellaneous:**

-

Start	End	Wind	Wind	Approx.	RS	IS in	Spec.	Int.
MAMA	MAMAP	dir.	speed	BLH	alt.	BL	T	time
14:20	15:05	WSW	5 to 6.5 m/s	1050	1627	yes	34°C	80 ms

Table 31: Listed are the start and end local time of the MAMAP remote sensing survey, the wind direction (dir.), the wind speed, the approximate boundary layer height (BLH), the remote sensing (RX) altitude (alt.), whether in-situ (IS) measurements were acquired within the boundary layer (BL), the spectrometer (spec.) temperature (T) and the integration (int.) time of the MAMAP instruments. All altitudes are given in m above mean sea level (mamsl).

**Flight altitude of the in-situ legs:** between 580 and 1140 mamsl

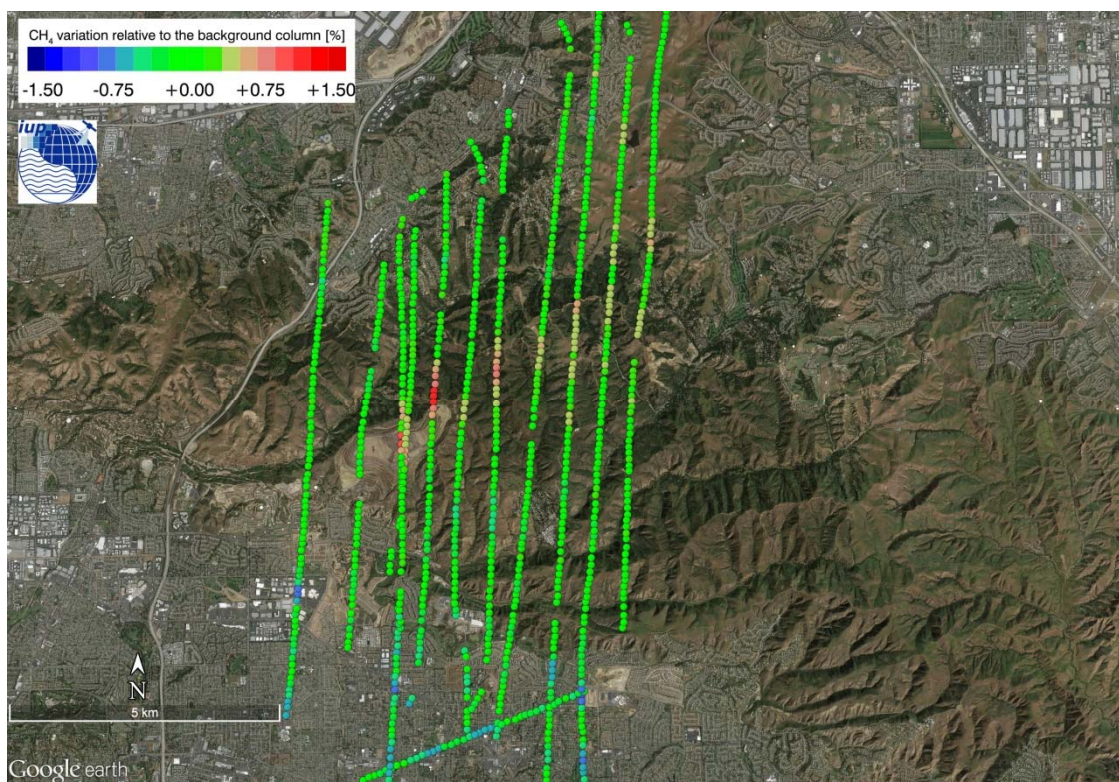


Figure 94: Normalized column averaged dry air mole fraction of  $\text{CH}_4$  of the MAMAP remote sensing sounding of the Olinda Alpha Landfill on 2014-08-28.





COMEX  
Final Report

Version: 2.0  
Doc ID: IUP-COMEX-FR  
Date: 3. July 2016

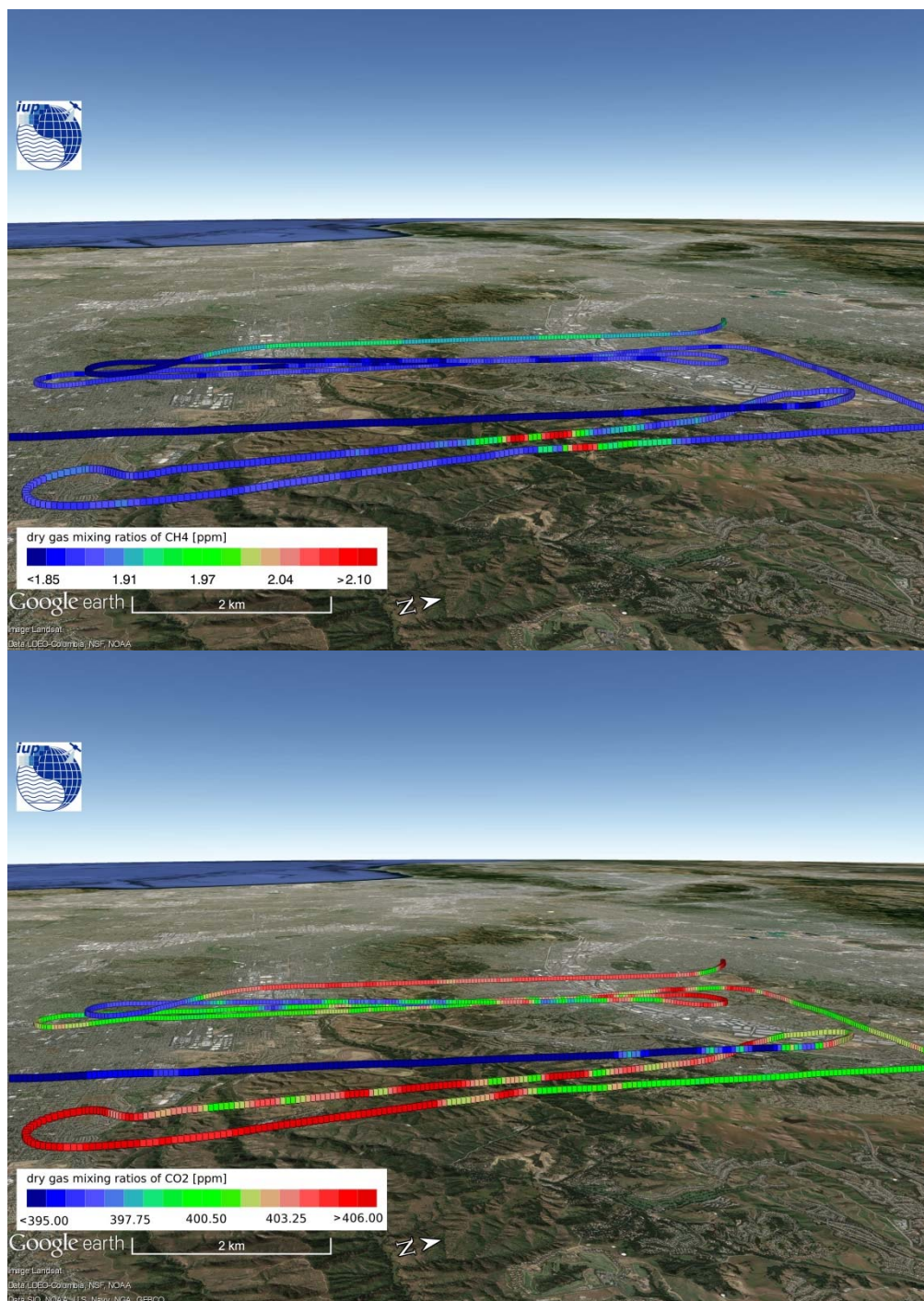


Figure 95: Picarro in-situ measurements of CH<sub>4</sub> (top) and CO<sub>2</sub> (bottom) below remote sensing altitude the Olinda Alpha Landfill on 2014-08-28.

## Flight Day 2014-08-28

**Target:** Puente Hills Landfill (T7)

**Weather conditions:** clear sky

**Other instruments/platforms:** no

**Miscellaneous:**

-

Start	End	Wind	Wind	Approx.	RS	IS in	Spec.	Int.
MAMA	MAMAP	dir.	speed	BLH	alt.	BL	T	time
15:45	16:05	WSW	5 to 6.5 m/s	1400	1467	yes	34°C	80 ms

Table 32: Listed are the start and end local time of the MAMAP remote sensing survey, the wind direction (dir.), the wind speed, the approximate boundary layer height (BLH), the remote sensing (RX) altitude (alt.), whether in-situ (IS) measurements were acquired within the boundary layer (BL), the spectrometer (spec.) temperature (T) and the integration (int.) time of the MAMAP instruments. All altitudes are given in m above mean sea level (mamsl).

**Flight altitude of the in-situ legs:** between 400 and 1150 mamsl

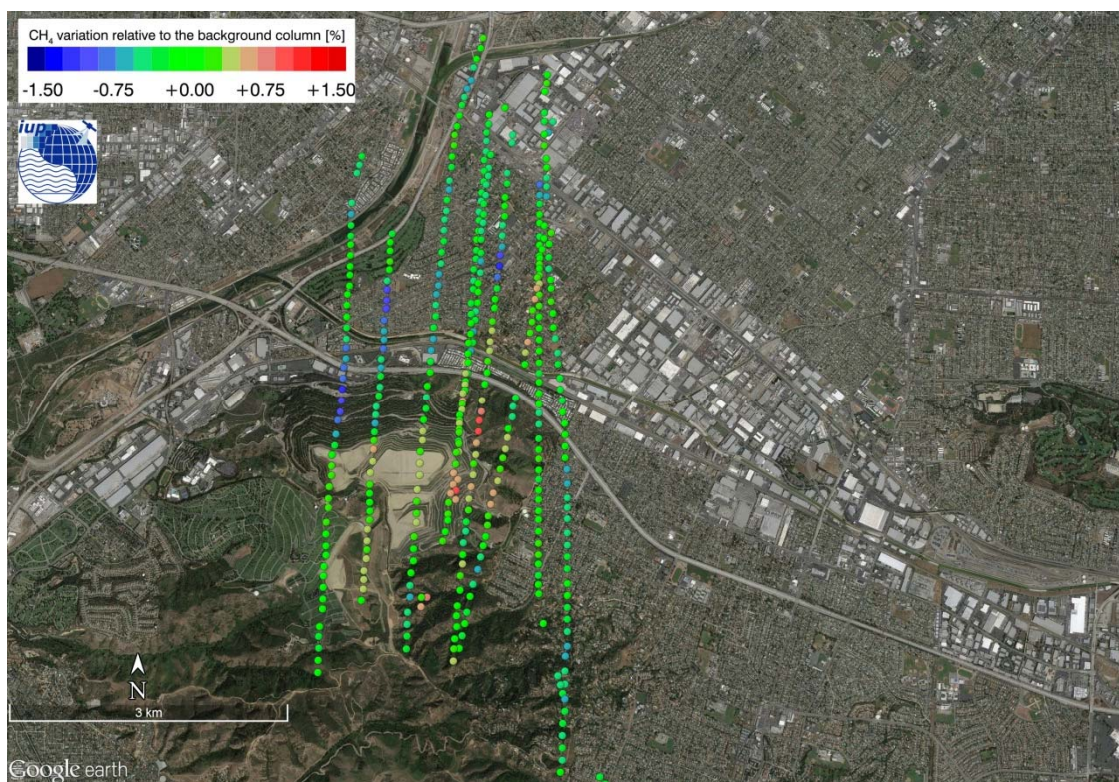


Figure 96: Normalized column averaged dry air mole fraction of  $\text{CH}_4$  of the MAMAP remote sensing sounding of the Puente Hills Landfill on 2014-08-28.





**COMEX**  
**Final Report**

Version: 2.0  
Doc ID: IUP-COMEX-FR  
Date: 3. July 2016

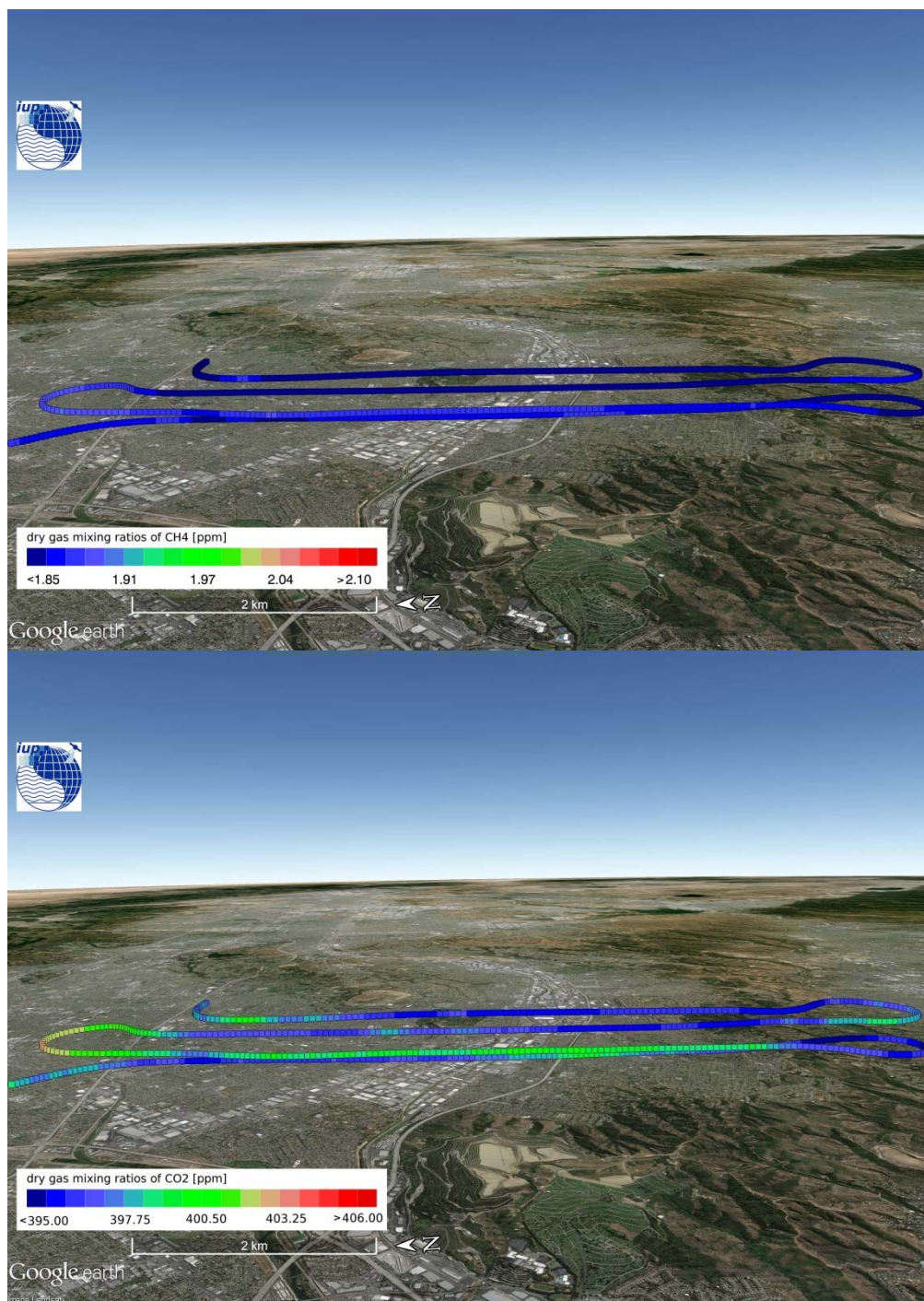


Figure 97: Picarro in-situ measurements of  $\text{CH}_4$  (top) and  $\text{CO}_2$  (bottom) below remote sensing altitude the Puente Hills Landfill on 2014-08-28.



## Flight Day 2014-08-29

**Target:** Los Angeles Basin Survey (T12) (including Carson Refinery (T16) and Tesoro Refinery (T17))

**Weather conditions:** clear sky

**Other instruments/platforms:** AMOG

**Miscellaneous:**

- Second part of the flight (in-situ survey) was aborted due to too low wind speeds and too shallow boundary layer which could not be penetrated over the City due to ATC regulations and restrictions

Start MAMA	End MAMAP	Wind dir.	Wind speed	Approx. BLH	RS alt.	IS in BL	Spec. T	Int. time
11:05	12:25	-	calm	600	2112	yes	34°C	80 ms

Table 33: Listed are the start and end local time of the MAMAP remote sensing survey, the wind direction (dir.), the wind speed, the approximate boundary layer height (BLH), the remote sensing (RX) altitude (alt.), whether in-situ (IS) measurements were acquired within the boundary layer (BL), the spectrometer (spec.) temperature (T) and the integration (int.) time of the MAMAP instruments. All altitudes are given in m above mean sea level (mamsl).

**Flight altitude of the in-situ legs:** between 400 and 600 mamsl

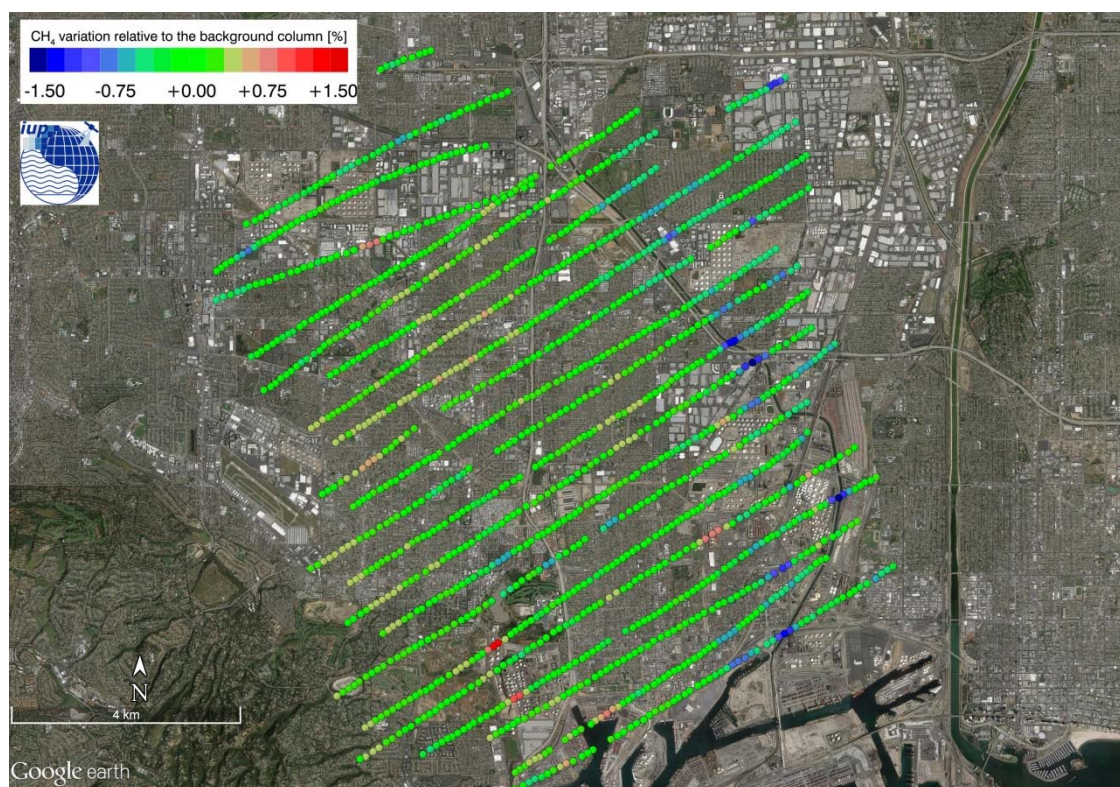


Figure 98: Normalized column averaged dry air mole fraction of  $\text{CH}_4$  of the MAMAP remote sensing sounding of the Carson Refinery and Tesoro Refinery on 2014-08-29.



**COMEX**  
**Final Report**

Version: 2.0  
Doc ID: IUP-COMEX-FR  
Date: 3. July 2016

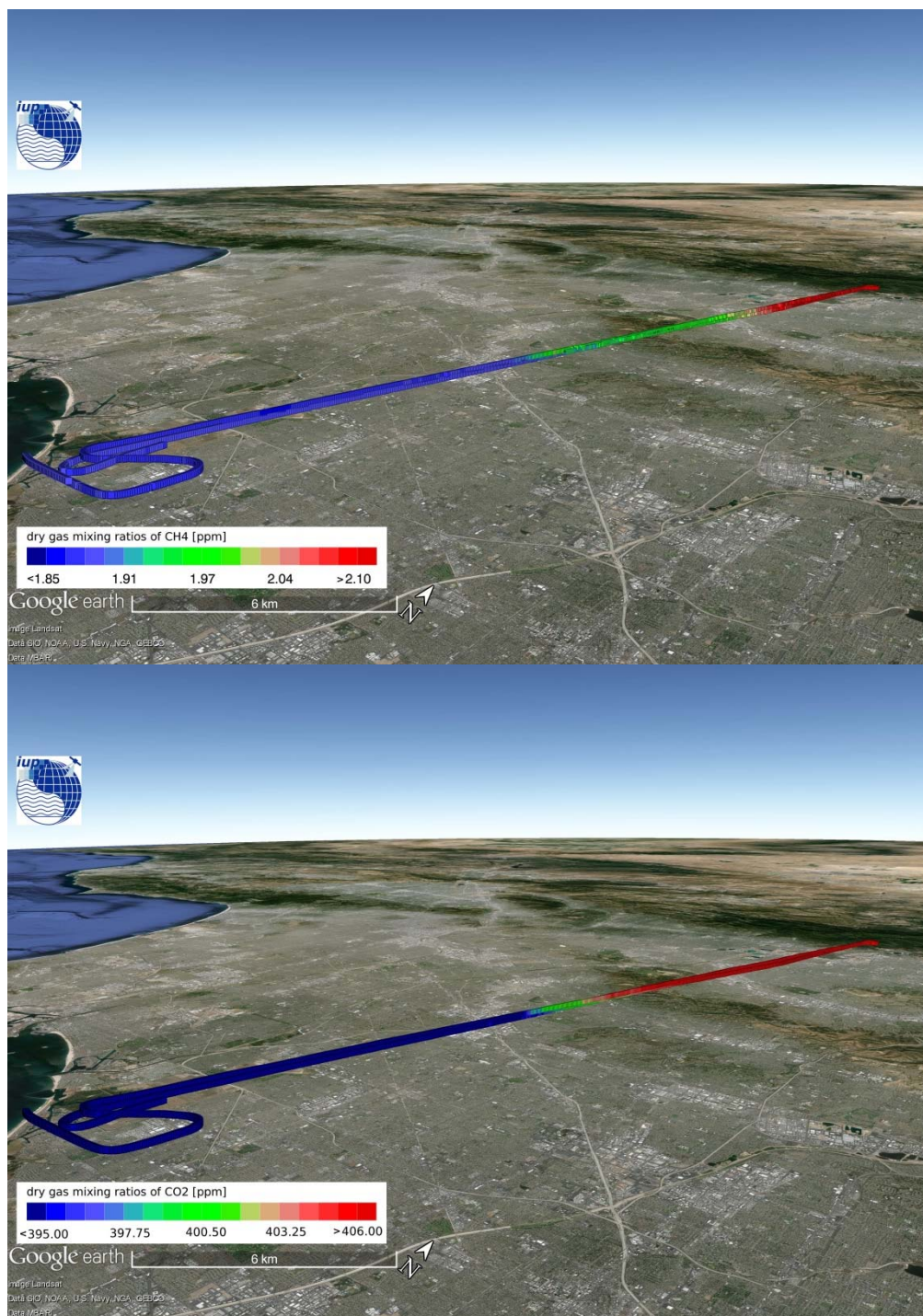


Figure 99: Picarro in-situ measurements of CH<sub>4</sub> (top) and CO<sub>2</sub> (bottom) below remote sensing altitude the Carson Refinery and Tesoro Refinery on 2014-08-29.



## Flight Day 2014-09-01

**Target:** BKK Landfill (T9)

**Weather conditions:** clear sky

**Other instruments/platforms:** AVIRISng

**Miscellaneous:**

-

Start	End	Wind	Wind	Approx.	RS	IS in	Spec.	Int.
MAMA	MAMAP	dir.	speed	BLH	alt.	BL	T	time
14:25	14:55	W	5 to 5.5 m/s	850	1771	no	34°C	80 ms

Table 34: Listed are the start and end local time of the MAMAP remote sensing survey, the wind direction (dir.), the wind speed, the approximate boundary layer height (BLH), the remote sensing (RX) altitude (alt.), whether in-situ (IS) measurements were acquired within the boundary layer (BL), the spectrometer (spec.) temperature (T) and the integration (int.) time of the MAMAP instruments. All altitudes are given in m above mean sea level (mamsl).

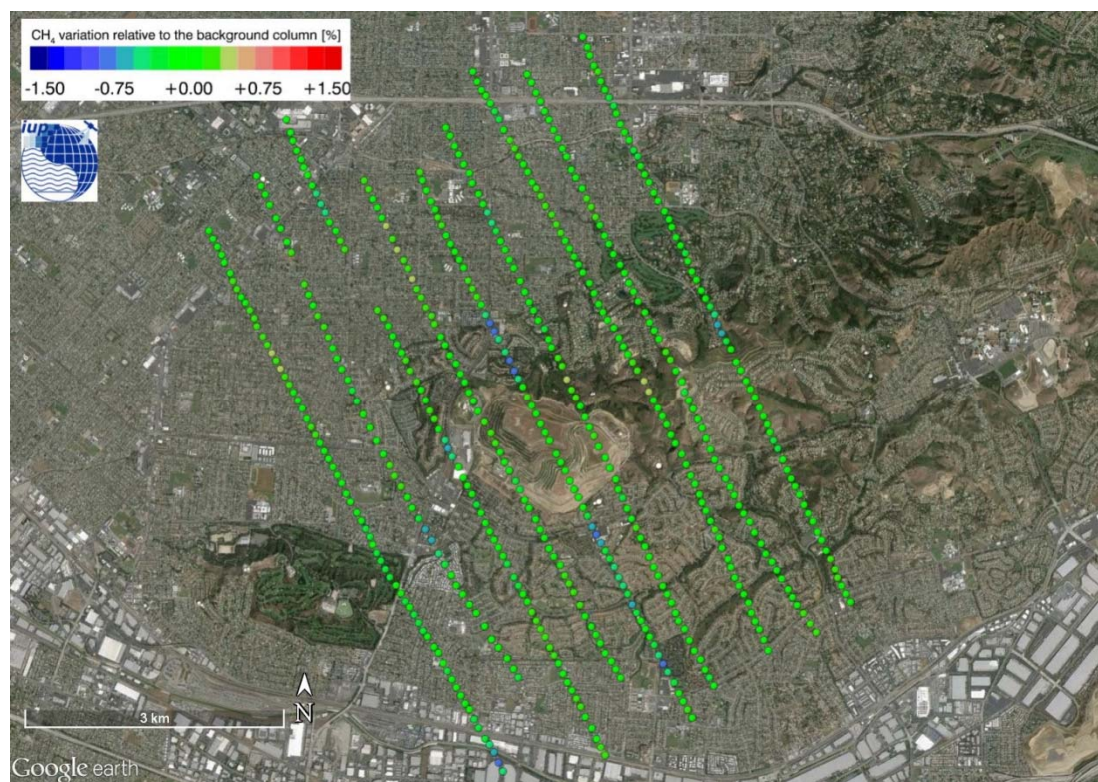


Figure 100: Normalized column averaged dry air mole fraction of  $\text{CH}_4$  of the MAMAP remote sensing sounding of the BKK Landfill on 2014-09-01.



## Flight Day 2014-09-01

**Target:** Olinda Alpha Landfill Landfill (T9)

**Weather conditions:** clear sky

**Other instruments/platforms:** no

**Miscellaneous:**

- For details see Section 9.2.1

Start	End	Wind	Wind	Approx.	RS	IS in	Spec.	Int.
MAMA	MAMAP	dir.	speed	BLH	alt.	BL	T	time
14:55	16:05	SW	4 to 5 m/s	850	1794	yes	34°C	80 ms

*Table 35: Listed are the start and end local time of the MAMAP remote sensing survey, the wind direction (dir.), the wind speed, the approximate boundary layer height (BLH), the remote sensing (RX) altitude (alt.), whether in-situ (IS) measurements were acquired within the boundary layer (BL), the spectrometer (spec.) temperature (T) and the integration (int.) time of the MAMAP instruments. All altitudes are given in m above mean sea level (mamsl).*

### 3D-wind fields along the flight track in the boundary layer for the two downwind walls:

- a) Vertical wind component / vectors:

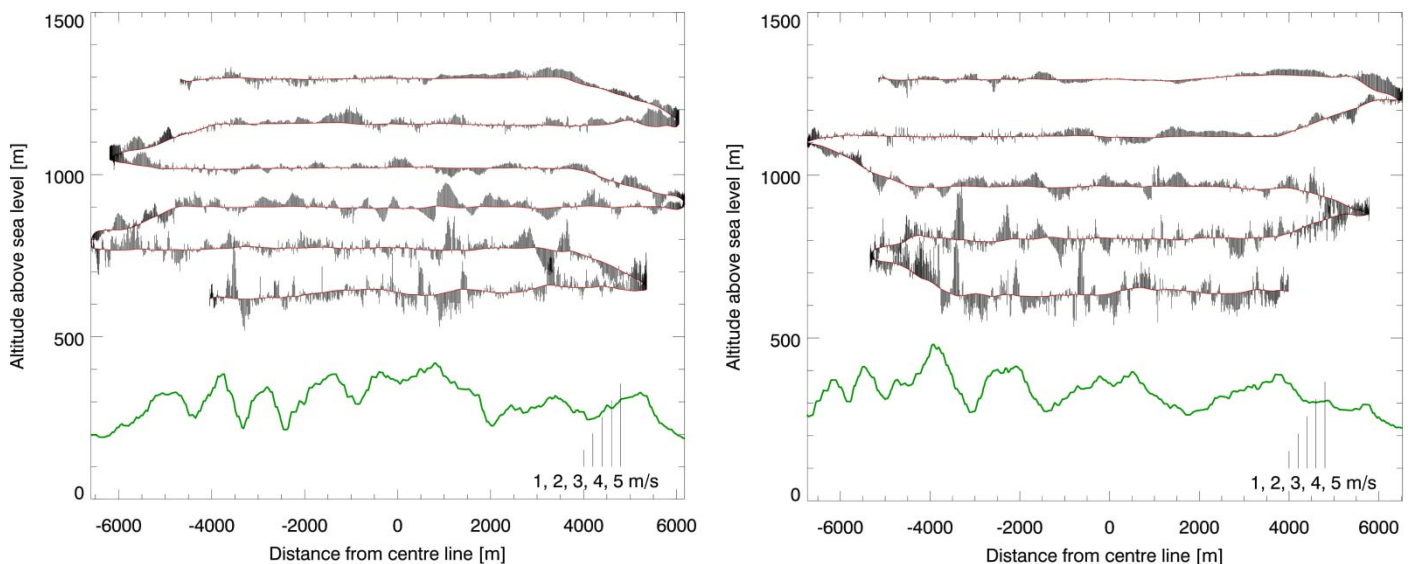


*Figure 101: Shown is the vertical component of the wind field along the flight track measured by the 5-hole turbulence probe of the CIRPAS suite at the Olinda Alpha Landfill on 2014-09-01. The y-axis gives the flight altitude in m amsl and the x-axis gives the distance from the center line (compare to Figure 33). The solid green line depicts the surface elevation (based on the SRTM digital elevation model). Left: First Downwind wall. Right: First Downwind wall.*

b) Horizontal wind component / vectors:

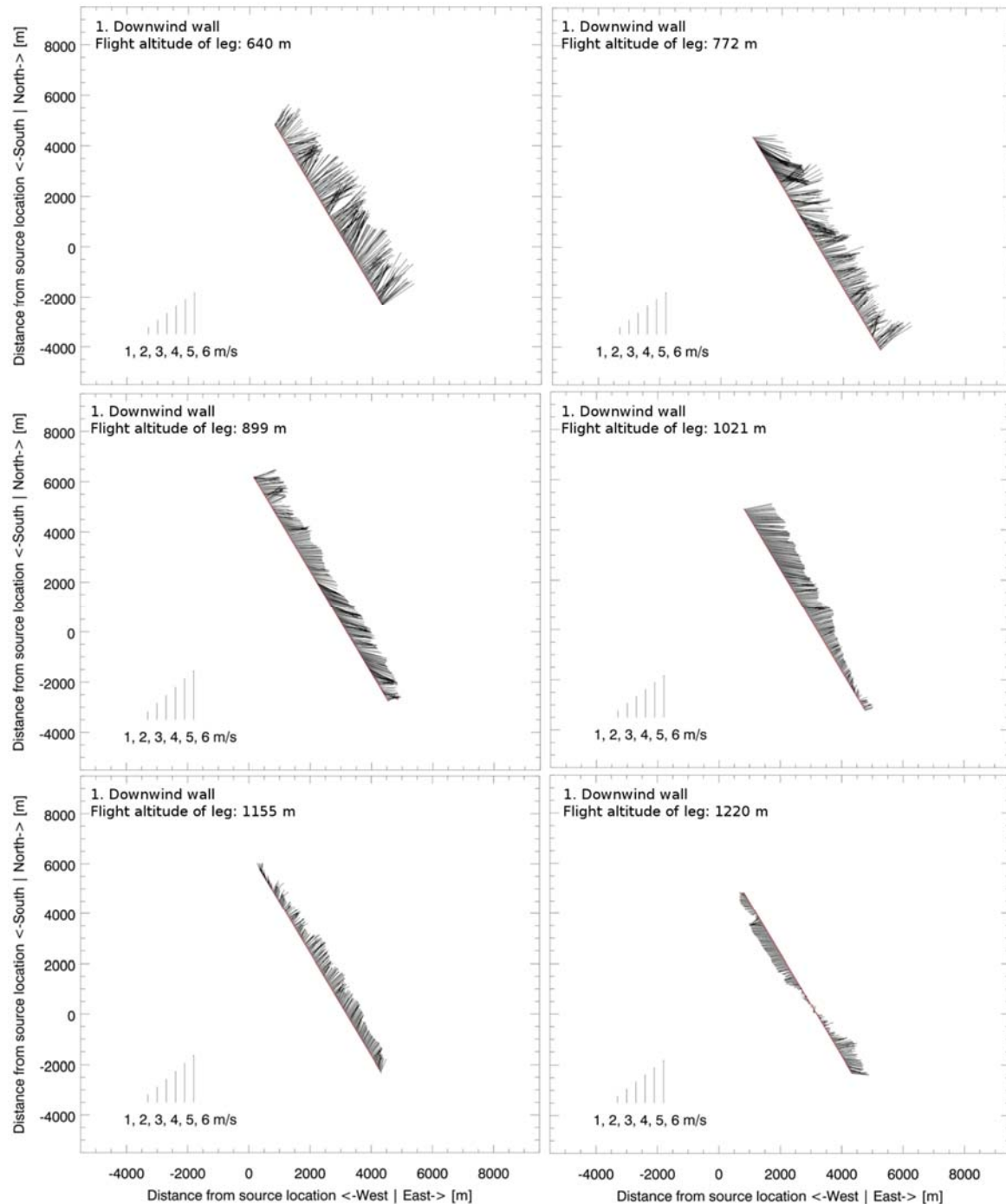


Figure 102: Shown is the horizontal component of the wind field separately plotted for each leg of the first downwind wall at the Olinda Alpha Landfill on 2014-09-01. The upper left plot depicts the lowest flight leg and the bottom right the highest flight leg of that wall. The x- and y-axis give the distance from landfill, which is located at (0,0).

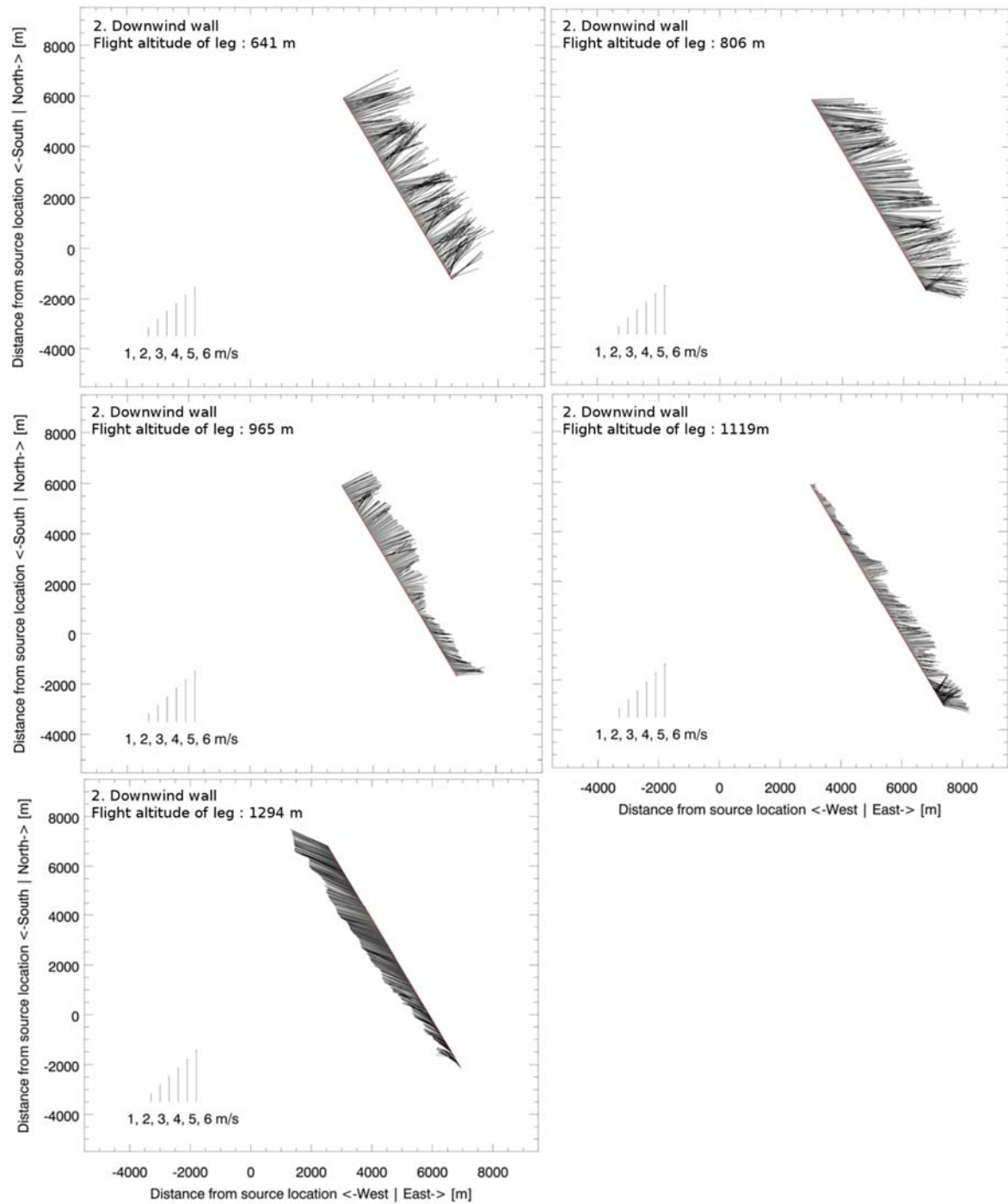


Figure 103: Same as Figure 102 but for the second downwind wall.



## Flight Day 2014-09-02

**Target:** Kern Front and Kern River Oil Field (T1)

**Weather conditions:** clear sky

**Other instruments/platforms:** AVIRISng

**Miscellaneous:**

- Interlace pattern was flown for MAMAP measurements, non-stationary wind conditions

Start MAMA	End MAMAP	Wind dir.	Wind speed	Approx. BLH	RS alt.	IS in BL	Spec. T	Int. time
13:40	16:15	W to NW	2.5 to 4.5 m/s	1500	2111	yes	34°C	80 ms

Table 36: Listed are the start and end local time of the MAMAP remote sensing survey, the wind direction (dir.), the wind speed, the approximate boundary layer height (BLH), the remote sensing (RX) altitude (alt.), whether in-situ (IS) measurements were acquired within the boundary layer (BL), the spectrometer (spec.) temperature (T) and the integration (int.) time of the MAMAP instruments. All altitudes are given in m above mean sea level (mamsl).

**Flight altitude of the in-situ legs:** between 500 and 1300 mamsl

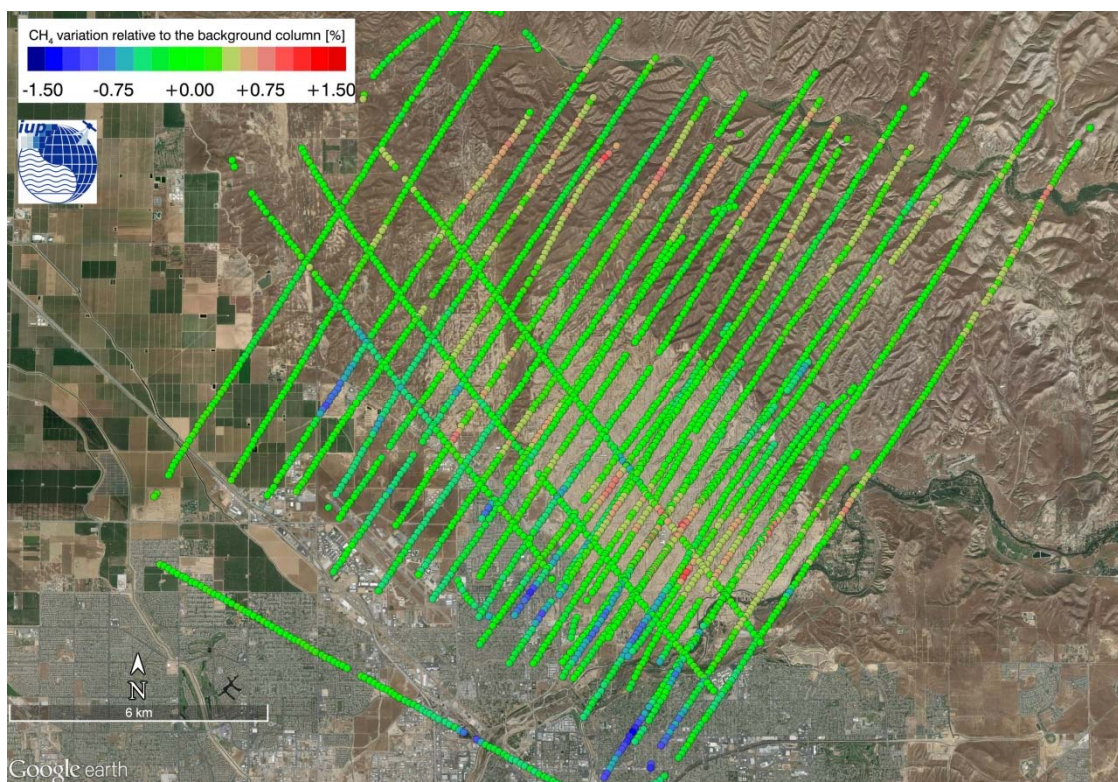


Figure 104: Normalized column averaged dry air mole fraction of CH<sub>4</sub> of the MAMAP remote sensing sounding of the Kern River and Front Oil Field on 2014-09-02.



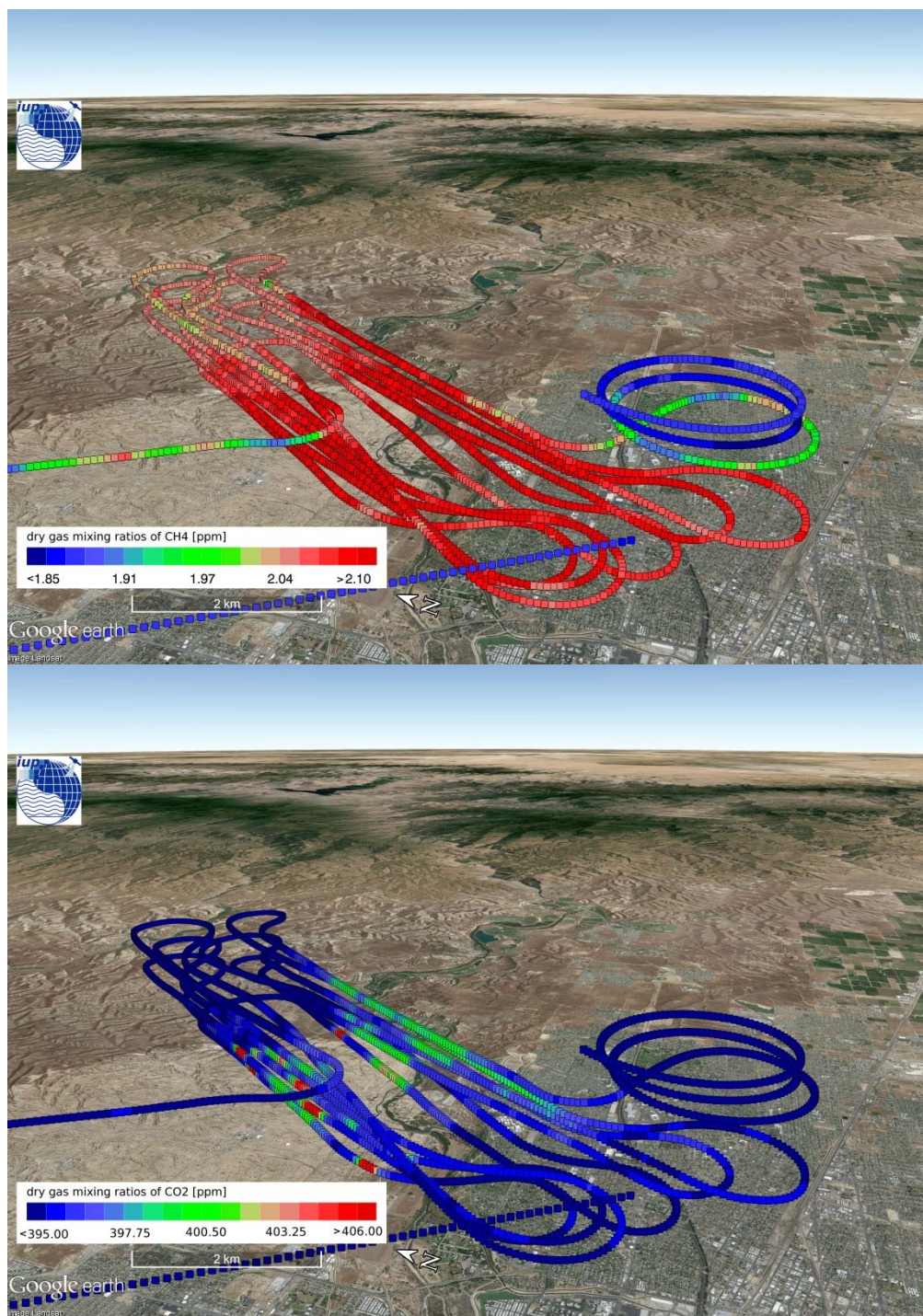


Figure 105: Picarro in-situ measurements of  $\text{CH}_4$  (top) and  $\text{CO}_2$  (bottom) below remote sensing altitude the Kern River and Front Oil Field on 2014-09-02.



## Flight Day 2014-09-03

**Target:** Olinda Alpha Landfill (T9)

**Weather conditions:** clear sky

**Other instruments/platforms:** AVIRISng, AMOG

**Miscellaneous:**

-

Start	End	Wind	Wind	Approx.	RS	IS in	Spec.	Int.
MAMA	MAMAP	dir.	speed	BLH	alt.	BL	T	time
13:25	14:15	WSW	5 to 6 m/s	900	1945	yes	34°C	80 ms

Table 37: Listed are the start and end local time of the MAMAP remote sensing survey, the wind direction (dir.), the wind speed, the approximate boundary layer height (BLH), the remote sensing (RX) altitude (alt.), whether in-situ (IS) measurements were acquired within the boundary layer (BL), the spectrometer (spec.) temperature (T) and the integration (int.) time of the MAMAP instruments. All altitudes are given in m above mean sea level (mamsl).

**Flight altitude of the in-situ legs:** between 690 and 1110 mamsl

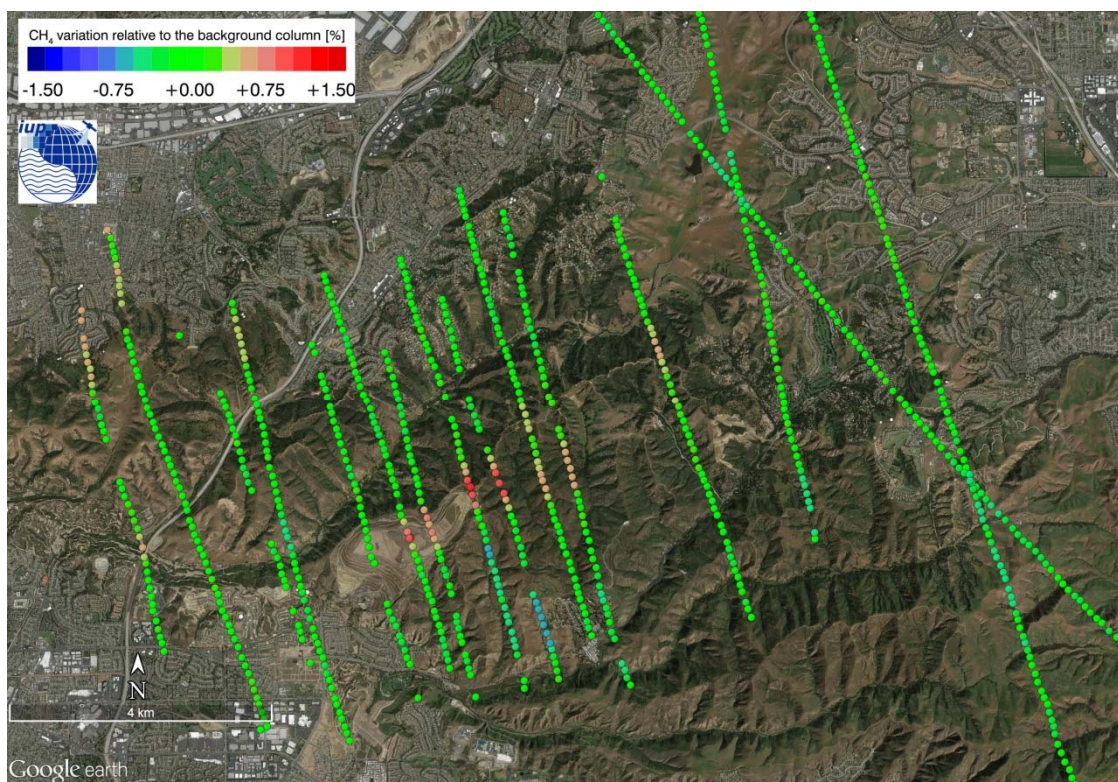


Figure 106: Normalized column averaged dry air mole fraction of  $\text{CH}_4$  of the MAMAP remote sensing sounding of the Olinda Alpha Landfill on 2014-09-03.



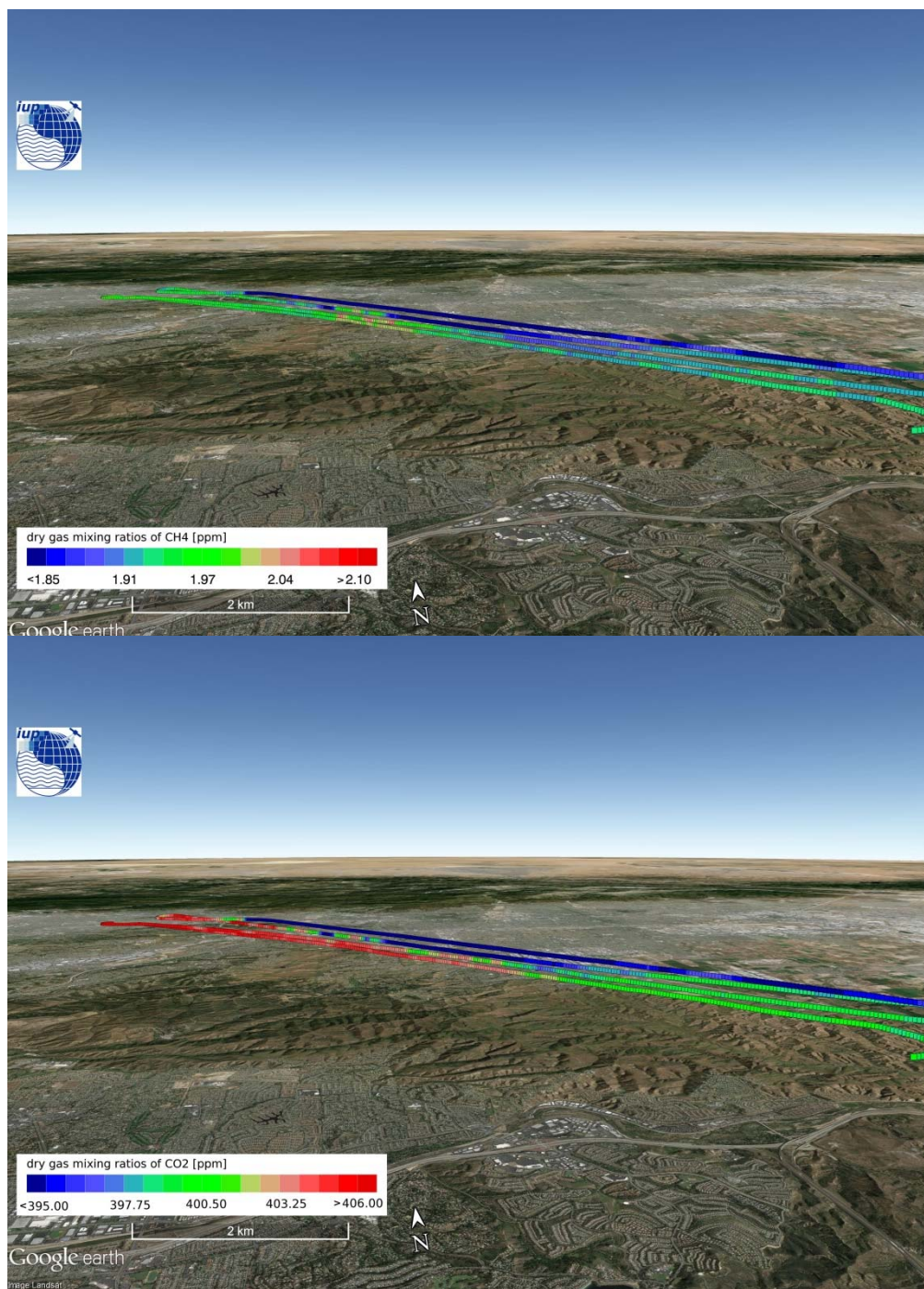


Figure 107: Picarro in-situ measurements of CH<sub>4</sub> (top) and CO<sub>2</sub> (bottom) below remote sensing altitude the Olinda Alpha Landfill on 2014-09-03.

## Flight Day 2014-09-03

**Target:** Chino Cattle Ranch / Feed Lot (T11)

**Weather conditions:** clear sky

**Other instruments/platforms:** AVIRISng, AMOG

**Miscellaneous:**

- Interlace pattern was flown for the MAMAP measurements
- Shutter failure of the MAMAP instrument in the middle of the Chino measurements, but measurements can still be used for analysis

Start MAMA	End MAMAP	Wind dir.	Wind speed	Approx. BLH	RS alt.	IS in BL	Spec. T	Int. time
15:00	17:00	WSW	6 to 7 m/s	700	1778	yes	34°C	80 ms

*Table 38: Listed are the start and end local time of the MAMAP remote sensing survey, the wind direction (dir.), the wind speed, the approximate boundary layer height (BLH), the remote sensing (RX) altitude (alt.), whether in-situ (IS) measurements were acquired within the boundary layer (BL), the spectrometer (spec.) temperature (T) and the integration (int.) time of the MAMAP instruments. All altitudes are given in m above mean sea level (mamsl).*

**Flight altitude of the in-situ legs:** between 640 and 1500 mamsl

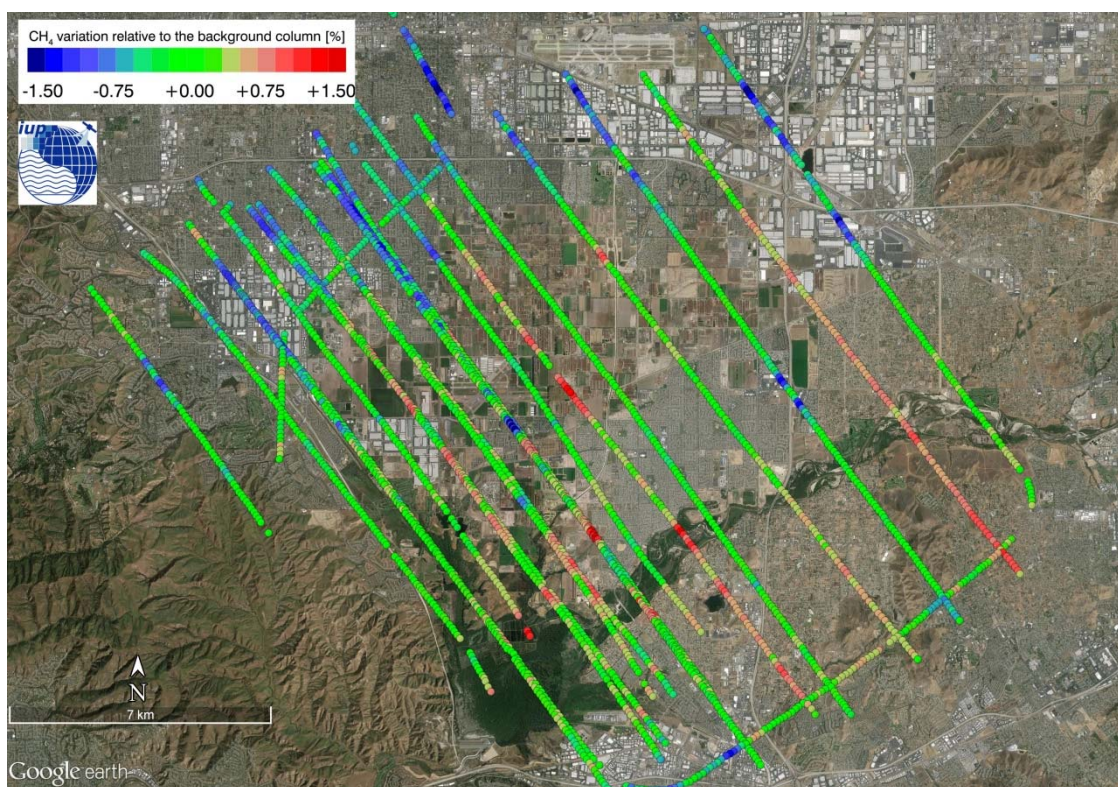


*Figure 108: Normalized column averaged dry air mole fraction of  $\text{CH}_4$  of the MAMAP remote sensing sounding of the Chino Cattle Ranch / Feed Lot on 2014-09-01.*





# COMEX Final Report

Version: 2.0  
Doc ID: IUP-COMEX-FR  
Date: 3. July 2016

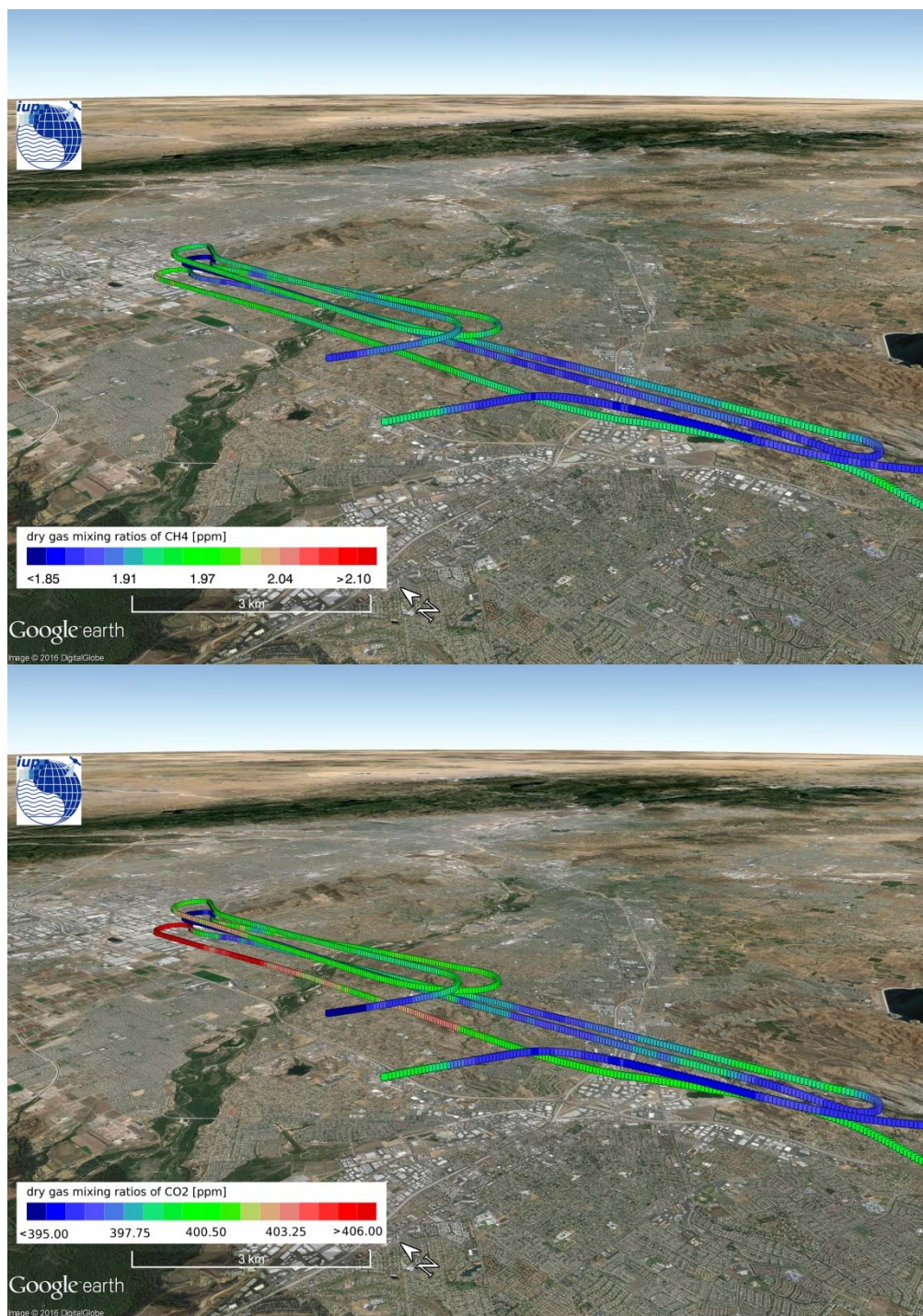


Figure 109: Picarro in-situ measurements of CH<sub>4</sub> (top) and CO<sub>2</sub> (bottom) below remote sensing altitude the Chino Cattle Ranch / Feed Lot on 2014-09-01.



## Flight Day 2014-09-04

**Target:** Kern Front and Kern River Oil Field (T1)

**Weather conditions:** clear sky

**Other instruments/platforms:** AVIRISng, AMOG

**Miscellaneous:**

- Interlace pattern was flown for the MAMAP measurements
- For details see Section 9.3

Start	End	Wind	Wind	Approx.	RS	IS in	Spec.	Int.
MAMA	MAMAP	dir.	speed	BLH	alt.	BL	T	time
13:40	15:50	NW	3.5 to 5.5 m/s	1700	2117	yes	34°C	80 ms

Table 39: Listed are the start and end local time of the MAMAP remote sensing survey, the wind direction (dir.), the wind speed, the approximate boundary layer height (BLH), the remote sensing (RX) altitude (alt.), whether in-situ (IS) measurements were acquired within the boundary layer (BL), the spectrometer (spec.) temperature (T) and the integration (int.) time of the MAMAP instruments. All altitudes are given in m above mean sea level (mamsl).

### 3D-wind fields along the flight track in the boundary layer for the two downwind walls:

a) Vertical wind component / vectors:

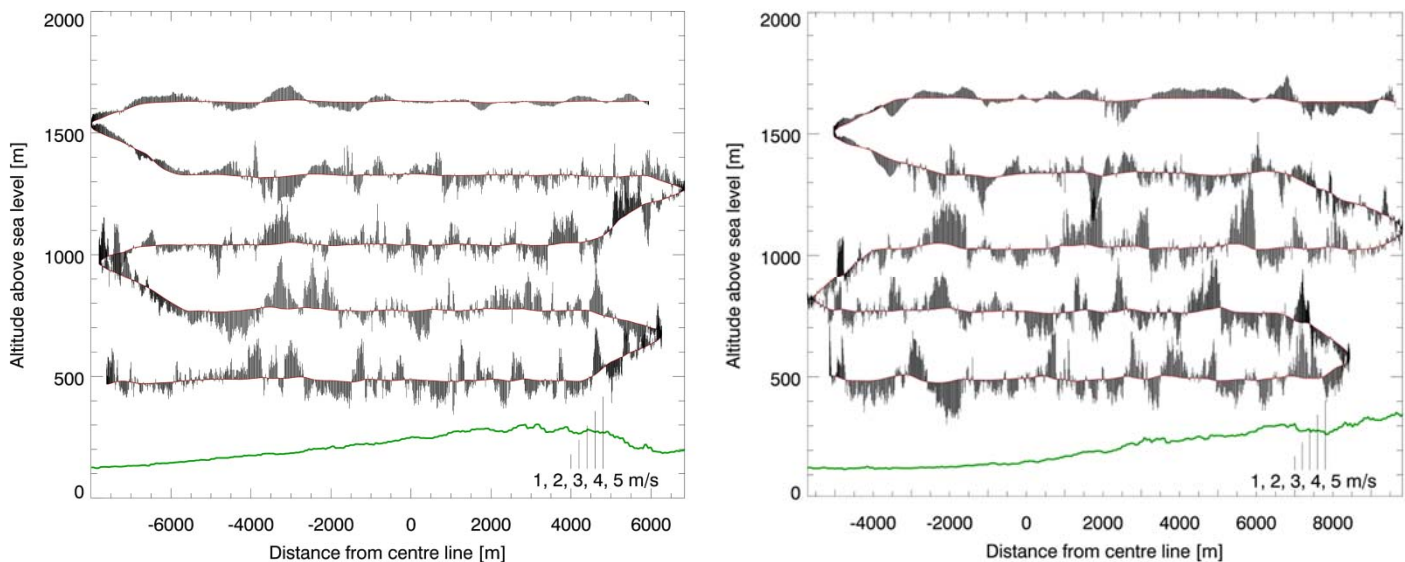


Figure 110: Shown is the vertical component of the wind field along the flight track measured by the 5-hole turbulence probe of the CIRPAS suite at the Kern River and Kern Front Oil Field on 2014-09-04. The y-axis gives the flight altitude in m amsl and the x-axis gives the distance from the center line (compare to Figure 44). The solid green line depicts the surface elevation (based on the SRTM digital elevation model). Left: First Downwind wall. Right: First Downwind wall.

b) Horizontal wind component / vectors:

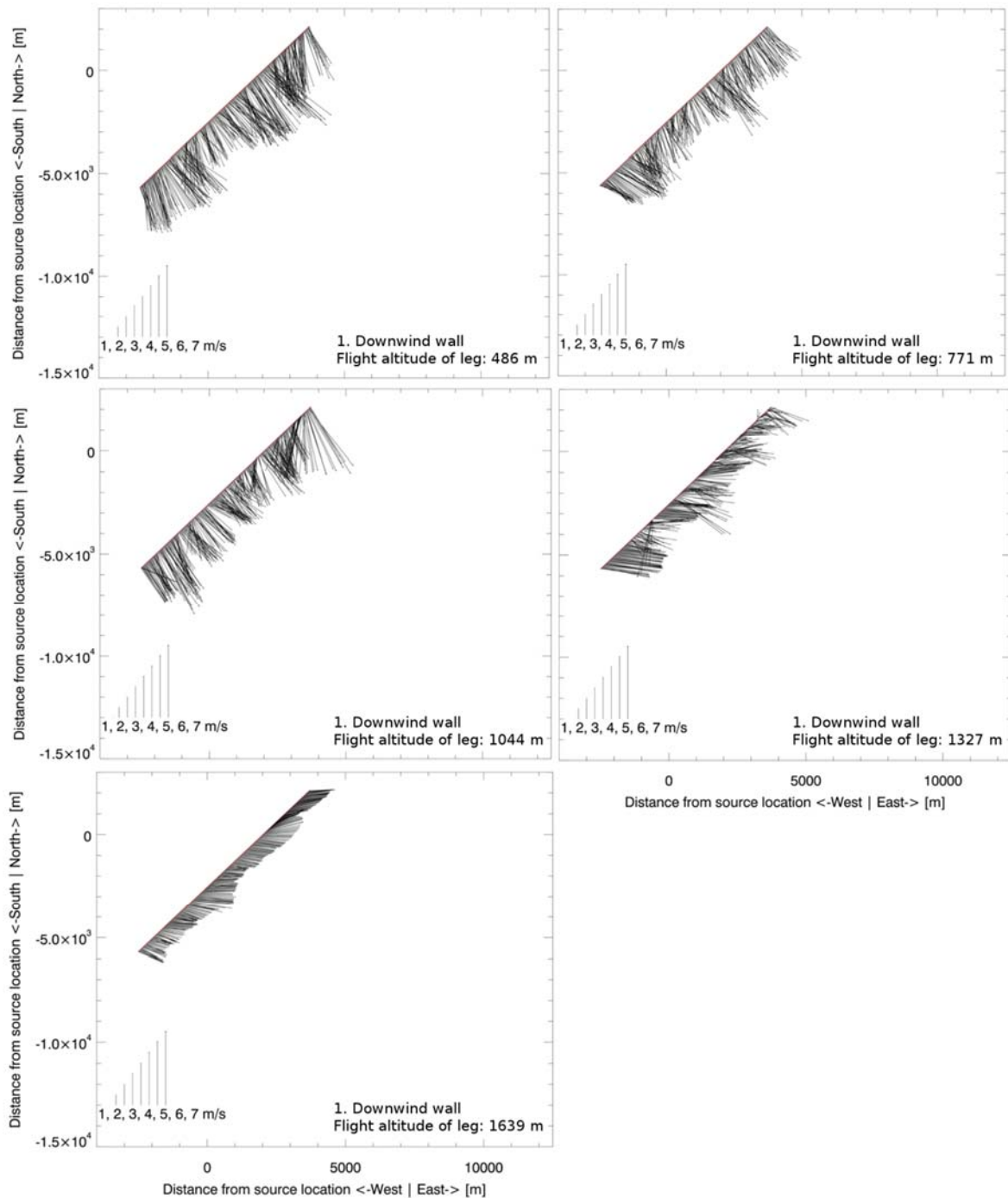


Figure 111: Shown is the horizontal component of the wind field separately plotted for each leg of the first downwind wall at the Kern River and Kern Front Oil Field on 2014-09-04. The upper left plot depicts the lowest flight leg and the bottom left the highest flight leg of that wall. The x- and y-axis give the distance from the source location, which is approximately located in the middle of the third/fourth MAMAP flight track (compare to Figure 40).

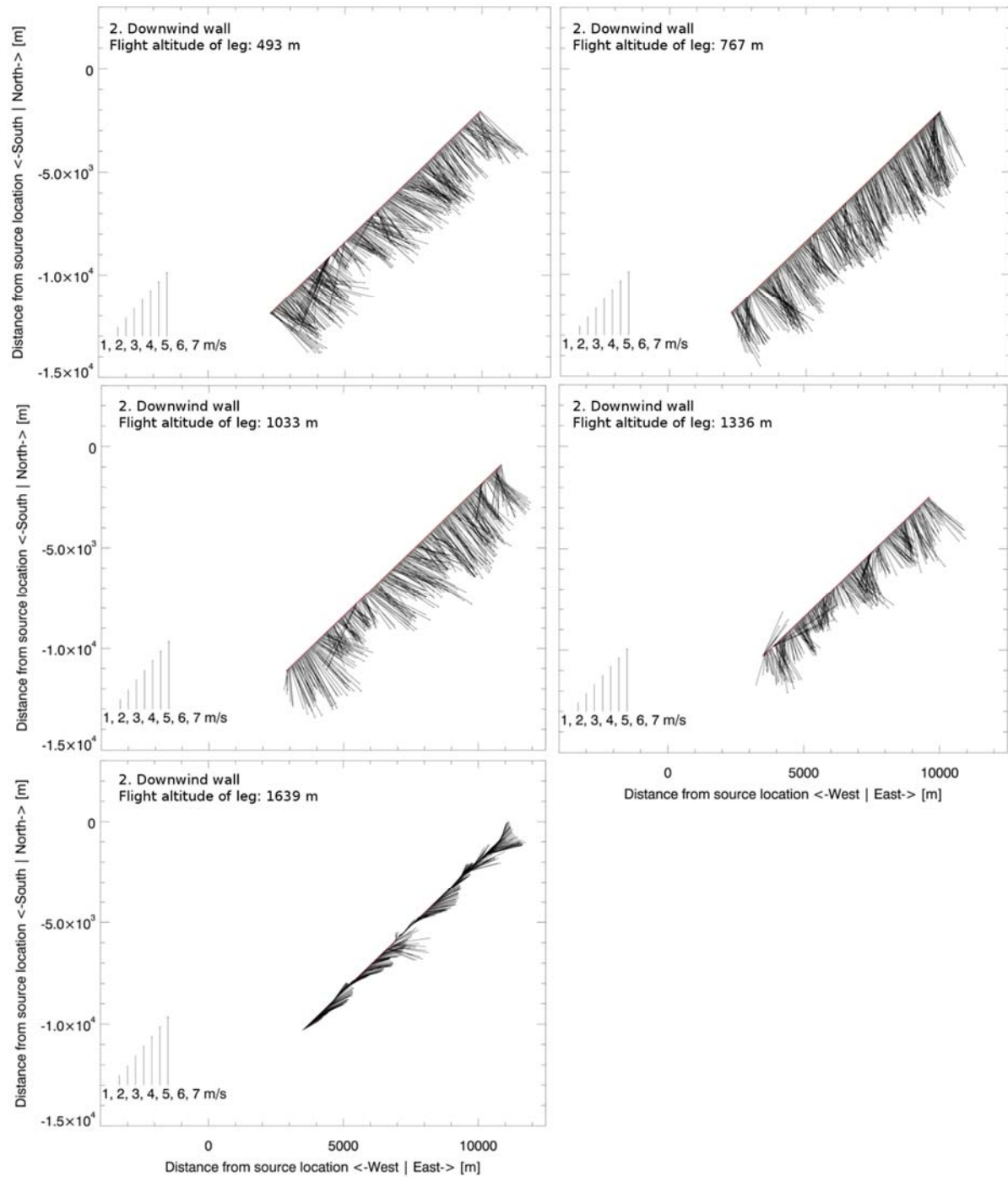


Figure 112: Same as Figure 111 but for the second downwind wall.